



Forschungszentrum Karlsruhe
in der Helmholtz-Gemeinschaft

Wissenschaftliche Berichte
FZKA 6986

SOPRO 2004
International Workshop on
Sorption Processes at
Oxide and Carbonate Mineral
Water Interfaces
Karlsruhe, March 25-26, 2004
Book of extended abstracts

J Lützenkirchen, T. Stumpf, V. Brendler,
B. Bayens, D. Grolimund (Editors)

Institut für Nukleare Entsorgung

Juni 2004

Forschungszentrum Karlsruhe

in der Helmholtz-Gemeinschaft

Wissenschaftliche Berichte

FZKA 6986

SOPRO 2004

**International Workshop on Sorption Processes at
Oxide and Carbonate Mineral Water Interfaces**

Karlsruhe, March 25-26, 2004

Book of extended abstracts

Johannes Lützenkirchen, Thorsten Stumpf, Vinzenz Brendler^a,
Bart Bayens^b, Daniel Grolimund^b (Editors)

Institut für Nukleare Entsorgung

^a Institut für Radiochemie, Forschungszentrum Rossendorf, Dresden

^b Institut für Entsorgung, Paul Scherrer Institut, Villigen, Schweiz

Forschungszentrum Karlsruhe GmbH, Karlsruhe

2004

Impressum der Print-Ausgabe:

**Als Manuskript gedruckt
Für diesen Bericht behalten wir uns alle Rechte vor**

**Forschungszentrum Karlsruhe GmbH
Postfach 3640, 76021 Karlsruhe**

**Mitglied der Hermann von Helmholtz-Gemeinschaft
Deutscher Forschungszentren (HGF)**

ISSN 0947-8620

urn:nbn:de:0005-069867

Zusammenfassung

SOPRO 2004 ist der vierte Workshop in der Reihe der "*Karlsruher Geochemical Workshops*". Der erste Workshop, der 1997 am Forschungszentrum Karlsruhe organisiert wurde, hatte den Titel "Geochemical modelling - radio toxic and chemical toxic substances in natural aquatic systems". Das zweite Treffen wurde 1999 unter dem Thema "Mineral/water interactions close to equilibrium" in Speyer abgehalten. Der dritte Workshop fand 2002 in Karlsruhe statt und beschäftigte sich mit "Modelling of coupled transport reaction processes". **SOPRO 2004** hat Sorptionsprozesse zum Inhalt. Diese sind relevant für die Rückhaltung von Radionukliden bei deren Migration aus einem Endlager für nukleare Abfälle. Der Schwerpunkt der Beiträge liegt auf fundamentalen Arbeiten zur Sorption aus experimenteller und theoretischer Sicht.

Die Absicht von **SOPRO 2004** ist es, ein Forum für die Diskussion von Wissenstand und tatsächlichem Verständnis von Sorptionsprozessen an Mineral Wasser Grenzflächen zu bieten. Der Schwerpunkt liegt bei Oxiden und Carbonaten als sorbierende Festphasen. Der Workshop deckt einen weiten Bereich experimenteller Techniken (klassische Arbeiten, Oberflächenspektroskopie), Modellierungsaspekte (wie Oberflächenkomplexierungsmodelle), theoretische Ansätze (Quantenchemie) und die Entwicklung von Sorptionsdatenbanken auf der Basis dieser Teilaspekte ab.

Der vorliegende Bericht enthält die Zusammenfassungen der Beiträge, die während des Workshops **SOPRO 2004** vorgestellt wurden.

Abstract

SOPRO 2004 is the fourth meeting in the series "*Karlsruher Geochemical Workshops*". The first workshop, held in 1997 at the Forschungszentrum Karlsruhe, was entitled "Geochemical modelling - radio toxic and chemical toxic substances in natural aquatic systems". The second meeting was held in 1999 in Speyer focusing on "Mineral/water interactions close to equilibrium". The third workshop, held in 2002 in Karlsruhe, dealt with "Modelling of coupled transport reaction processes". **SOPRO 2004** is intended to deal with sorption processes. These are for example relevant for retention of radionuclides migrating from nuclear waste repositories. General focus will be on fundamental studies from an experimental and theoretical point of view.

The intention of **SOPRO 2004** is to serve as a possibility to discuss the state of the art and our understanding of sorption processes at mineral water interfaces. Focus will be on oxide and carbonate minerals. The workshop intends to cover a broad range of experimental techniques (classical chemistry studies, surface spectroscopy), modeling aspects (such as surface complexation modeling), theoretical approaches (quantum chemistry) and the synthesis of results in data bases.

The present report includes extended abstracts of the contributions presented at **SOPRO 2004**.

Acknowledgements:

The organisers would like to thank all those who in some way or the other contributed to this workshop. Professor Fanghänel and Dr. Kienzler for their encouragement and interest, Mrs. Schäufele for all she arranged for us, Mrs. Goebel for the excellent cooperation between science and finances, Volker Metz for sharing his know-how from TrePro2002, Silvia Stumpf, Heike Pieper and Maria Marques Fernandes for handling the registration and all the others not explicitly mentioned here.

The organisers would also like to thank the contributors for their co-operation during the making of this report and the participants for the interesting discussions during the workshop.

TABLE OF CONTENTS

RETENTION OF TOXIC SUBSTANCES ON CONSOLIDATED POROUS SYSTEMS. CHARACTERIZATION OF THE STATE OF WATER BY MEANS OF LOW FIELD PROTON NMR AND DETERMINATION OF KD VALUES USING CAPILLARIES <u>E. Alhajji</u> , D. Le Botlan, G. Montavon, B. Grambow.....	1
EXAFS INVESTIGATIONS OF URANIUM(VI) ADSORPTION ON KAOLINITE <u>S. Amayri</u> , T. Reich.....	2
DETECTION OF ADSORBED U(VI) SURFACE SPECIES ON MUSCOVITE BY TRLFS T. Arnold, <u>N. Baumann</u> , V. Brendler, G. Geipel.....	3
COMPUTER MODELLING OF THE STRUCTURE AND REACTIVITY OF CARBONATE MINERALS <u>K. Austen</u> , K. Wright, B. Slater, J. Gale.....	7
INFLUENCE OF TEMPERATURE ON SORPTION OF EUROPIUM ONTO SMECTITE <u>A. Bauer</u> , T. Rabung, F. Claret, T. Schäfer, T. Fanghänel.....	11
INVESTIGATIONS OF URANYL SORPTION ONTO GIBBSITE N. Baumann, <u>V. Brendler</u> , T. Arnold, G. Geipel.....	13
URANYL UPTAKE AT THE CALCITE (104) SINGLE CRYSTAL SURFACE: A P-GIXAFS STUDY <u>D. Bosbach</u> , M.A. Denecke, K. Dardenne, J. Rothe, T. Fanghänel.....	17
THE LINKAGE BETWEEN URANIUM, IRON AND CARBON CYCLING. PROCESSES AT INTERFACES: EVIDENCES FROM COMBINED SOLUTION CHEMICAL AND SPECTROSCOPIC STUDIES J. Bruno, <u>M. Grivé</u> , L. Duro.....	22
THE EFFECTS OF PHOSPHATE ON URANIUM ADSORPTION TO GOETHITE- COATED SAND T. Cheng, <u>M. O. Barnett</u> , E. E. Roden.....	27
LABEL-FREE IN SITU DETECTION OF ADSORPTION PROCESSES BY ACOUSTIC WAVE-BASED SENSORS <u>R. Dahint</u>	30

ERROR CAUSES IN THE DETERMINATION OF THE ACID-BASE REACTIVITY OF OXI-HYDROXIDES M. Duc, <u>G. Lefèvre</u> , M. Fedoroff.....	34
INTERACTION OF TRIVALENT ACTINIDES WITH MINERAL SURFACES: TRLFS STUDIES <u>T. Fanghänel</u> , T. Rabung, T. Stumpf.....	37
SORPTION MECHANISMS AND SORPTION MODELS <u>M. Fedoroff</u> , G. Lefevre, M. Duc, S. Milonjić, C. Neskovic.....	41
FUNCTIONAL SPECIES OF MINERAL / ELECTROLYTE INTERFACES OBSERVED IN SITU BY NONLINEAR VIBRATIONAL SPECTROSCOPY <u>M. Flörsheimer</u> , K. Kruse, R. Klenze, T. Fanghänel.....	46
pH-DEPENDENCE OF URANYL UPTAKE ON QUARTZ:A XPS STUDY <u>A. Froideval</u> , M. Del Nero, R. Barillon, J. Hommet, G. Mignot.....	50
RELATIONSHIP BETWEEN SURFACE STRUCTURE AND ION COMPLEXATION <u>T. Hiemstra</u> , W. H. van Riemsdijk.....	53
PARAMETERS AFFECTING THE pH DEPENDENCE OF SORPTION <u>A.M. Jakobsson</u> , M. Olsson, Y. Albinsson.....	57
TOWARDS A SURFACE COMPLEXATION DATABASE A.M. Jakobsson, <u>J. Lützenkirchen</u>	61
METAL ION SORPTION TO SCHWERTMANNITE PRECIPITATED FROM MINING WASTE LEACHATES J. Jönsson, <u>L. Lövgren</u> , P. Persson.....	65
SORPTION OF ACTINIDES ONTO GRANITE AND ALTERED MATERIAL FROM ÄSPÖ HRL B. Kienzler, <u>J. Römer</u> , D. Schild, W. Bernotat.....	69
INTERACTION PROCESSES OF TETRAVALENT ACTINIDES IN THE SYSTEM HUMIC ACID / QUARTZ SAND / SOLUTION <u>A. Křepelová</u> , J. Mibus, S. Sachs, C. Nebelung, G. Bernhard.....	75
ON STANDARD-STATE CHEMICAL POTENTIALS AND ACTIVITY COEFFICIENTS OF SURFACE SPECIES ON MINERAL-WATER INTERFACES <u>D.A. Kulik</u>	80

USE OF ATTENUATED TOTAL REFLECTION – INFRARED SPECTROSCOPY FOR IN SITU STUDY OF INORGANIC IONS ADSORPTION ON METAL OXY- HYDROXIDES <u>G. Lefèvre, S. Noinville, M. Fédoroff</u>	86
INTEGRATING SORPTION REACTIONS IN A THERMODYNAMIC DATABASE FOR USE IN SPECIATION MODELS <u>C. Lomenech, J. van der Lee</u>	90
THE EFFECT OF PRESSURE ON THE SORPTION OF HEAVY METAL CATIONS ON GOETHITE <u>E. Maćzka, M. Kosmulski</u>	94
INCORPORATION OF TRIVALENT ACTINIDES AND LANTHANIDES IN CALCITE. A TIME RESOLVED LASER FLUORESCENCE SPECTROSCOPY (TRLFS) STUDY <u>M. Marques Fernandes, T. Stumpf, T. Rabung, D. Bosbach, A. Bauer, T. Fanghänel</u>	97
NP SORPTION ONTO CEMENT AND MG(OH) ₂ -MGCL ₂ -BASED BACKFILL MATERIAL IN ALTERED Q-BRINE <u>V. Metz, J. Lützenkirchen, P. Vejmelka, B. Kienzler</u>	101
MODELLING OF ADSORPTION OF REDOX SENSITIVE OXYANIONS ON GIBBSITE <u>M. M. Miedaner, R. Weerasooriya, H.J. Tobschall</u>	108
SELECTED RESULTS OF THE NEA SORPTION FORUM: POTENTIAL AND LIMITATIONS OF THERMODYNAMIC SORPTION MODELS FOR THE DERIVATION OF RADIONUCLIDE K_D VALUES FOR NUCLEAR WASTE DISPOSAL <u>M. Ochs, J.A. Davis, M. Olin, T.E. Payne, C.J. Tweed, M. Askarieh, S. Altmann</u>	110
EU(III) COPRECIPITATION WITH THE TRIOCTAHEDRAL CLAY MINERAL HECTORITE <u>H. Pieper, D. Bosbach, P.J. Panak, K. Dardenne, J. Rothe, M.A. Denecke, T. Fanghänel</u>	114
GALLIUM(III) ADSORPTION ON CARBONATES AND OXIDES: X-RAY ABSORPTION FINE STRUCTURE STUDY AND SURFACE COMPLEXATION MODELING <u>O.S. Pokrovsky, G.S. Pokrovski, J. Schott</u>	119
ADSORPTION AND CO-PRECIPITATION OF METALS AND RADIONUCLIDES AT THE CALCITE-WATER INTERFACE: SPECTROSCOPIC OBSERVATIONS <u>R.J. Reeder</u>	125

CAPABILITY OF SCM AND RES ³ T DATABASE FOR BLIND PREDICTION <u>A. Richter</u> , V. Brendler.....	127
INFLUENCE OF HUMIC ACID ON THE NEPTUNIUM(V) SORPTION ONTO GRANITE AND ITS MINERAL CONSTITUENTS <u>K. Schmeide</u> , G. Bernhard.....	132
CHEMICAL SPECIATION OF ENVIRONMENTALLY SIGNIFICANT HEAVY METALS WITH INORGANIC LIGANDS <u>S. Sjöberg</u>	137
SPECIATION OF CM(III) IN A QUARTZ / SILICIC ACID SYSTEM: INVESTIGATIONS BY TRLFS <u>S. Stumpf</u> , T. Stumpf, T. Fanghänel.....	140
INFLUENCE OF HUMIC ACID ON THE SORPTION OF Eu(III)/Am(III)/Cm(III) ONTO γ -Al ₂ O ₃ - A TIME-RESOLVED LASER FLUORESCENCE SPECTROSCOPY STUDY - X.K. Wang, <u>Th. Rabung</u> , H. Geckeis, P.J. Panak, R. Klenze, T. Fanghänel.....	142
THE 1-PK MECHANISTIC MODELING OF PROTON BINDING ONTO PYRITE <u>R. Weerasooriya</u> , H.J. Tobschall.....	147
THE SURFACE CHEMISTRY OF CARBONATES <u>M. Wolthers</u> , L. Charlet, P. Van Cappellen.....	151

RETENTION OF TOXIC SUBSTANCES ON CONSOLIDATED POROUS SYSTEMS. CHARACTERIZATION OF THE STATE OF WATER BY MEANS OF LOW FIELD PROTON NMR AND DETERMINATION OF K_d VALUES USING CAPILLARIES

E. Alhajji, D. Le Botlan[‡], G. Montavon, B. Grambow

Laboratoire SUBATECH, 4 rue A. Kastler, BP 20722, 44307 Nantes cedex 03, France

[‡]LAIEM, Faculté des sciences et des techniques 2 rue de la Houssinière, BP 92208 F-44322 Nantes CEDEX 3

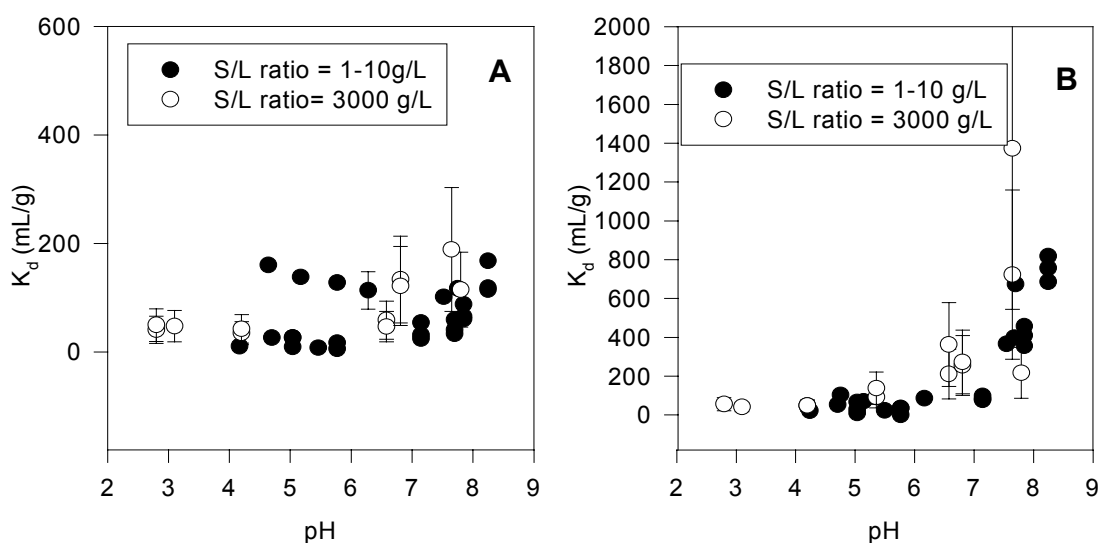
eskander.alhajji@subatech.in2p3.fr

The application of surface complexation models to quantify the retention of toxic substances at water mineral interfaces on consolidated porous systems (high mass / volume ratios) remains a difficult task. The two main difficulties are (i) the definition and quantification of the liquid phase, differentiating between the mobile and immobile water molecules and (ii) the use of the method allowing to measure the K_d values.

The objective of this work is to find a methodology allowing to work in the consolidated state as it is the case actually in the dispersed state with the classical “batch” technique.

To characterize and quantify the states of the water in consolidated systems, low field proton NMR technique is used. The relaxation time of the proton is a direct function of the water mobility. The fundamental question raised here is to make a link between the spectroscopic data characterizing the water molecules (i.e. more or less mobile) and the data needed to model the retention (i.e. external and internal water). In this presentation, the first results obtained with different hydrated samples of non-porous alumina and porous silica (water percentage varying from 0 to 35%) will be presented. They will be compared with those obtained with hydrated illite.

To measure the retention data in the consolidated state, a technique implying capillaries is used. In this presentation, the method will be presented as well as the first results obtained in a consolidated system made of bentonite and Ni (see Figure below).



K_d values obtained by the a batch method in the dispersed and consolidated states as a function of pH for $[Ni]=1.10^{-3}$ (A) and $[Ni]=1.10^{-7}$ mol/L (B).

EXAFS INVESTIGATIONS OF URANIUM(VI) ADSORPTION ON KAOLINITE

Samer Amayri and Tobias Reich

Institut für Kernchemie
Johannes Gutenberg-Universität
Fritz-Strassmann-Weg 2
55128 Mainz
Germany
amayri@mail.kernchemie.uni-mainz.de

For the safety assessment and design of nuclear waste repositories, detailed studies of the migration behavior of uranium and other long-lived radionuclides and actinides in particular are necessary. Sorption on clay minerals such as kaolinite strongly affects the fate and the mobility of radioactive contaminants in the geosphere. Therefore, an atomic level understanding of sorption mechanisms of contaminants on mineral surfaces is of fundamental importance for maintaining environmental quality and assessing the long-term stability of waste repositories. The aim of our investigation was to combine macroscopic studies (batch experiments) of uranium(VI) sorption on kaolinite with spectroscopic techniques such as **Extended X-ray Absorption Fine Structure (EXAFS)** spectroscopy and **X-ray Photoelectron Spectroscopy (XPS)**. We selected the reference kaolinite KGa-1b (Source Clays Repository) to be able to compare the results with those of previous studies [1-4].

EXAFS at the uranium L_{III} -edge was used for determining the structural environment of aqueous uranyl sorbed onto kaolinite. Sorption samples were prepared at total uranium concentrations from 10^{-6} mol/L to 10^{-5} mol/L, 4 g/L kaolinite, pH 3 to 10, presence and absence of ambient CO_2 , and 60-hr equilibration. EXAFS experiments at pH 7 showed a drastic change in the nature of the uranium sorption as function of uranium concentration. As the total uranium concentration decreased by one order of magnitude, the structural order in the equatorial oxygen shell of uranium increased significantly. In addition, clear evidence of U-Al/Si scattering interaction was obtained for the first time. We propose a structural model for the inner-sphere sorption of uranium on kaolinite based on the measured U-O and U-Al/Si distances.

Acknowledgment: This work was supported in part by the Bundesministerium für Wirtschaft und Arbeit under contract No. 02E9653.

References:

- [1] K. Sekine, T.E. Payne, T.D. Waite, J.A. Davis; International Alligator Rivers analogue project (18): Experimental study of uranium adsorption on kaolinite - pH dependence in air-equilibrated system; JAERI-memo 03-036 (1991) 1-14.
- [2] G.D. Redden, J.Li, J. Leckie; Adsorption of U^{VI} and citric acid on goethite, gibbsite, and kaolinite; In Adsorption of Metals by Geomedia (Ed. EA. Jenne) 1998, Academic Press, P. 291-313.
- [3] H.A. Thompson, G.A. Parks, G.E. Brown, Jr.; Structure and composition of uranium^{VI} sorption complexes at the kaolinite-water interface; *ibid*, p. 349-370.
- [4] S.P. Hyun, Y.H. Cho, P.S. Hahn, S.J. Kim; Sorption mechanism of U(VI) on a reference montmorillonite: Binding to the internal and external surfaces; *J. Radioanalyt. Nucl. Chem.* 250 (2001) 55-62.

DETECTION OF ADSORBED U(VI) SURFACE SPECIES ON MUSCOVITE BY TRLFS

T. Arnold, N. Baumann, V. Brendler, G. Geipel
FZ Rossendorf e. V., Institute of Radiochemistry
P.O. Box 510119
D-01314 Dresden
T.Arnold@fz-rossendorf.de

Abstract

Spectroscopic evidence for two adsorbed uranium(VI) surface species on edge surfaces of a muscovite platelet was obtained by Time Resolved Laser-induced Fluorescence Spectroscopy (TRLFS). In contrast, no fluorescence signal was obtained on the basal plane surfaces clearly indicating that U(VI) sorption on muscovite predominantly takes place at the edge surfaces. TRLFS spectra of adsorbed U(VI) surface species on gibbsite are very similar and show that U(VI) sorption on muscovite occurs on aluminol sites of the edge surfaces.

Experimental

TRLFS was used to study the sorption of U(VI) on the sheet silicate muscovite. Muscovite platelets were used as sample specimens to simultaneously investigate the uranium(VI) sorption on basal plane surfaces as well as on edge surfaces. For this purpose, muscovite platelets of approximately 1 cm² and 5 mm height were immersed in 0.1 N NaClO₄ solution, and a pH of about 6.3 was adjusted. The sorption experiment was then conducted as described in /1/. The pH was readjusted every day until it was stable. Then a certain amount uranyl(VI) was added to set the total uranium(VI) concentration in solution to 1×10⁻⁵ M. A contact time of 60 h to ensure complete uranium(VI) sorption was applied. Then the final pH was measured and the uranium concentration in solution was determined by ICP-MS. The results are given in Tab. 1. TRLFS measurements, shown in Fig. 1, in solution, on basal plane surfaces, and on edge surfaces of the muscovite platelets were carried out.

Tab. 1: Uranium(VI) sorption on muscovite platelet in contact with 1×10⁻⁵ M U(VI)

Sample	pH	U(VI) adsorbed on muscovite platelets [%]
Muscovite platelets in contact with 1 × 10 ⁻⁵ M	6.33	72.56

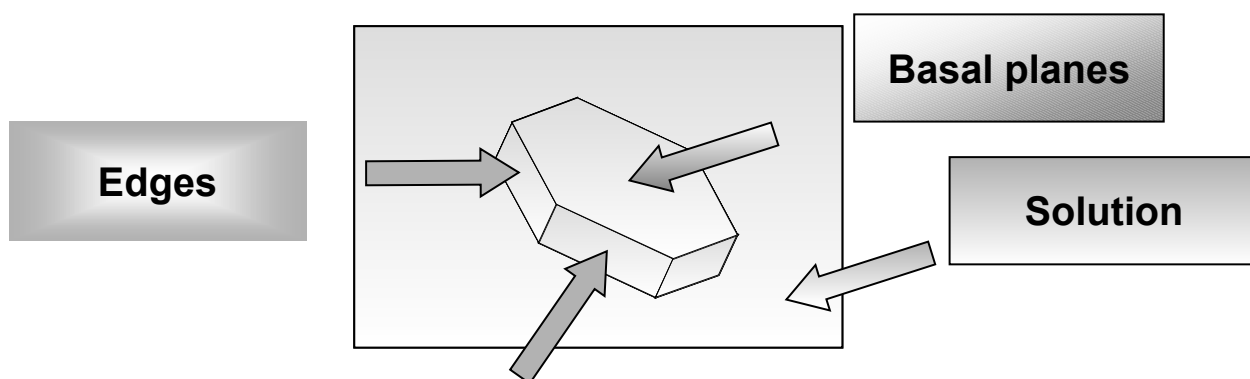


Fig. 1: TRLFS measurements were conducted in the surrounding solution, on the basal plane surfaces, and on the edge surfaces of muscovite platelets.

Results and Discussion

TRLFS Spectra of the solution, in which the platelets were immersed, showed a spectra which is typical for the remaining U(VI) concentration in solution, confirming the results from the ICP-MS analyses. The spectra of the basal plane surfaces showed no U(VI) fluorescence signal at all, clearly indicating that U(VI) does not significantly adsorb on the basal plane surfaces of muscovite. However, Uranium(VI) adsorbs on the edge surfaces of the muscovite platelets. The TRLFS spectrum of the adsorbed U(VI) surface species on muscovite edge surfaces is shown in Fig.2. The spectrum was deconvoluted. It is best described with two surface species with different fluorescence life times. The fluorescence emission spectra of both species are shown in Fig. 3. Species 1 has a fluorescence life time of 1.15 μs and species 2 a distinctively greater one of 9.65 μs . The emission bands and lifetimes of the fluorescence signal of the adsorbed U(VI) edge surface species are shown in Tab. 2.

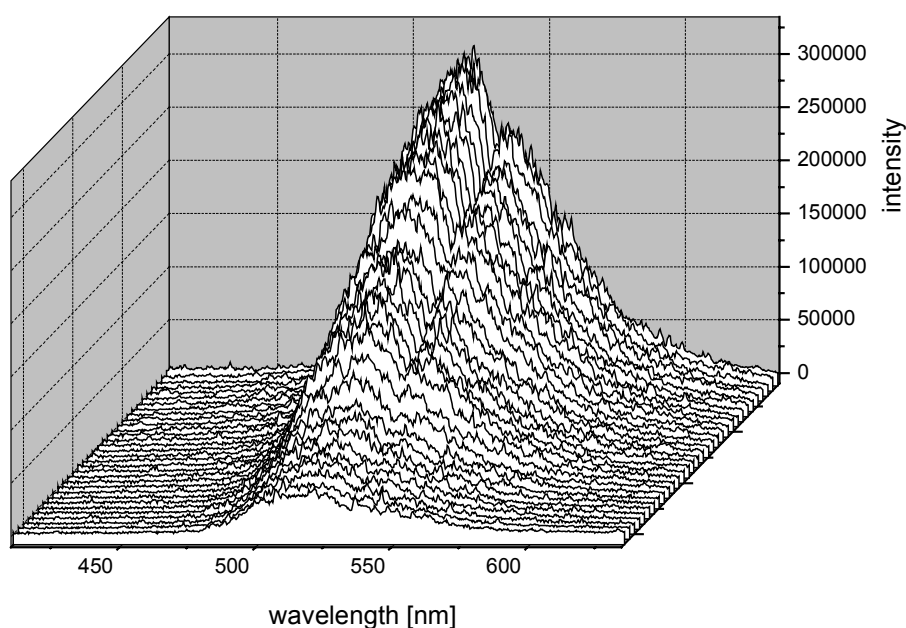


Fig 2: TRLFS of U(VI) sorbed on the edge surfaces of muscovite platelets.

Tab. 2: Life times and emissions bands of the two U(VI) surface species detected on the edge surfaces of muscovite platelets.

Spezies	Lifetimes		Peak Center			
	[ns]					
1	1150 ± 20	502.9	522.1	545.4	569.2	596.4
2	9650 ± 50	502.1	521.7	545.2	569.8	599.4

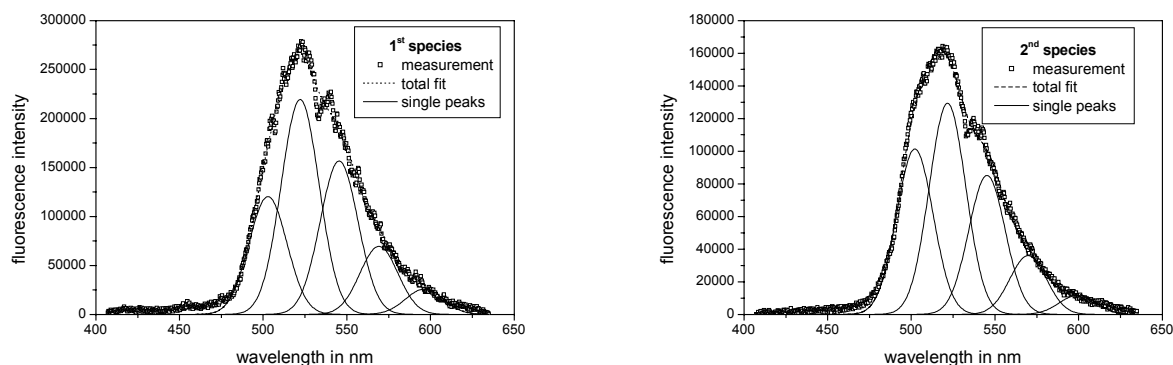


Fig 3: Fluorescence emission spectra of the two adsorbed U(VI) surface species on muscovite edges.

The obtained fluorescence emission bands of both U(VI) surface species are significantly shifted to higher wavelengths when compared with emission bands of aqueous U(VI) species, shown in Tab. 3. This clearly shows that the acquired fluorescence signals are attributed to adsorbed U(VI) surface species and not to aqueous U(VI) complexes.

Since the positions of emission peaks are very similar it can be concluded that the two U(VI) edge surface species on muscovite are quite similar in their chemical environment. They should possess the same number of OH⁻ groups and are probably only distinguished by their number of surrounding water molecules. Our findings show that, in respect to U(VI) sorption reactions on muscovite, the edge surfaces are by far more reactive than the basal plane surfaces. This is in agreement with the growth and dissolution behavior of muscovite.

Tab. 3: Emissions bands of dominant aqueous U(VI) complexes at pH 6.3.

aqueous Species						
UO ₂ ²⁺	472.8	487.9	509.6	532.7	558.6	585.0
(UO ₂) ₂ (OH) ₂ ²⁺	481.3	498.3	519.7	543.4	566.7	602.8
UO ₂ OH ⁺	480.7	497.3	518.4	541.3	566.4	

In addition it was found that TRLFS spectra acquired for adsorbed U(VI) surface species on gibbsite /2/ are very similar. This strongly indicates that U(VI) sorption on muscovite occurs (almost) exclusively on aluminol sites of the edge surfaces.

Acknowledgements

C. Berger is thanked for sample preparation and U. Schaefer for ICP-MS analyses. Financial support through the EU Project ACTAF (Contract No. FIKW-CT-2000-00035) is also gratefully acknowledged.

References:

- /1/ Arnold, T., Zorn, T., Zänker, H., Bernhard, G., Nitsche, H. (2001) Sorption behavior of U(VI) on phyllite: experiments and modeling. *Journal of Contaminant Hydrology* 47, 219-231.
- /2/ Baumann, N., Brendler, V., Arnold, T., Geipel, G. (2004) Investigations of uranyl sorption onto gibbsite (contribution in this report).

COMPUTER MODELLING OF THE STRUCTURE AND REACTIVITY OF CARBONATE MINERALS

Kat Austen^{1,2}, *Kate Wright*^{1,2,3}, *Ben Slater*¹, *Julian Gale*⁴

¹Davy Faraday Research Laboratory, The Royal Institution of Great Britain, 21 Albemarle Street, London, W1S 4BS, UK

²Department of Chemistry, Christopher Ingold Laboratories, University College London, 20 Gordon Street, London, WC1H 0AJ, UK

³Department of Earth Sciences, University College London, Gower Street, London, WC1E 6BT, UK

⁴Nanochemistry Research Institute, Department of Applied Chemistry, Curtin University of Technology, P.O. Box U1987, Perth, WA 6845, Australia

kat@ri.ac.uk, kate@ri.ac.uk, ben@ri.ac.uk, julian@power.curtin.edu.au

Carbonate minerals are important in nature because of their role in controlling the biogeochemical cycle of carbon and their ability to trap potentially toxic metals in the environment. Trace metals, such as iron, aluminium, copper, lead and zinc, undergo processes of co-precipitation, adsorption and surface complexation with carbonate minerals by which their levels in the surrounding aqueous environment are reduced. These attributes have been exploited in many areas; for example, carbonates are commonly used to reduce latent acidity in a number of environments, including mine tailings [1], and the groundwater of pine forests [2]. By so doing the concentration of contaminants is reduced, both by complexation of the pollutants, and by decreasing the level of leaching of metals from the surrounding rock and soil where low pH frees trace elements. Carbonates are also currently used to remove cadmium from industrial by-products [3] and to entrap dye-products in industrial wastewater by adsorption [4].

All the aforementioned processes occur at the mineral surface, and as such a detailed understanding of the mechanisms and energetics of carbonate mineral surfaces is necessary if these attributes are to be further exploited. Dissolution must also be understood in order to create a complete picture of processes at the solid-aqueous solution boundary. It has been noted that the size of carbonate particles affects both dissolution and activity in entrapment of contaminants and reduction of acidity [2], while build-up of precipitates such as iron carbonate on the surface of calcite has been observed to decrease dissolution of the original carbonate [5]. Similarly, it is important to understand the process of precipitation of minerals, and some work has been carried out to investigate the effects of different solutions on the morphology of the precipitating crystals. It has been found that the presence of organic molecules in solution, as well as the concentrations of other elements, affects the crystal shape of calcite [6,7].

On the grounds of natural abundance, the most important of the carbonates are calcite and dolomite, which comprise 90% of the rock forming carbonates [8]. As there has already been considerably more investigation into calcite, this work concentrates on the surface structure and reactivity of dolomite, which has lower symmetry than calcite due to the alternate layers of Mg²⁺ and Ca²⁺ ions. The presence of the magnesium in the structure leads to decreased rates of dissolution. The mechanism for dolomite dissolution has been shown to be via etch-pit evolution and stepwave advancement across the surface [9].

Calcite surfaces have been extensively studied using experimental techniques, such as X-ray photoelectron spectroscopy (XPS) [10] and, most frequently, Atomic Force Microscopy

(AFM) [11]. However, experimental investigation of the surface reactivity of dolomite is more difficult as the reaction rates are slower. A number of methods have been used to model calcite and dolomite. *Ab initio* techniques have been used by Mao [12], and Thackeray [13] among others, to model the CaCO_3 monomer. The Hartree-Fock approach has also been applied to calcite and aragonite crystal structures [14], and also to magnesite [15]. In addition, first principles calculations have been used to examine calcite-magnesite phase diagrams [16]. It has been shown that atomistic techniques are capable of accurately reproducing bulk and surface properties [17-21] of the carbonates, and are useful when studying large crystal systems. Defects in the bulk structure of carbonates have been successfully studied [17, 21]. In particular, there has been some previous modelling of some dolomite surfaces [20, 21], and some work on the solvation of the $(10\bar{1}4)$ surface [21, 22]. The interaction of the calcite $(10\bar{1}4)$ surface with water has been studied with a combination of atomistic simulation methods, electronic structure calculations and molecular dynamics to suggest a model for the dissociation of water on the surface of interest [24].

In this work, interatomic potentials have been used to model the prevalent surfaces of dolomite; the $(10\bar{1}4)$, $(30\bar{3}0)$, $(11\bar{2}0)$ and the (0001) surfaces. Substitutions of divalent impurity cations, Fe^{2+} , Ni^{2+} , Mn^{2+} , Zn^{2+} , Co^{2+} , Cd^{2+} , were carried out on the surfaces in a vacuum. The energetics of these systems have been studied, as were the effects on morphology. Newly developed potentials were used in order to model the behaviour of the carbonate anion accurately at the surface [25]. The surfaces were constructed in the GDIS visualisation package and the calculations carried out using the GULP3.0 code [26]. The $(10\bar{1}4)$ surface was successfully solvated using an empirical potential for water [27], and the effects of the substitution of impurities on this surface evaluated.

The results of impurity substitution on the dry, non-polar surfaces show that the energy of substitution is proportional to the ionic radius of the defect cation [Fig. 1, Fig. 2], whether the substitution site is a calcium site or a magnesium site. We find that the substitution of impurities follows a definite pattern on the dry surfaces. Substitution at calcium sites is energetically favoured over substitution at magnesium sites. Once one calcium site holds a defect, the preferred subsequent substitution site is adjacent to the existing impurity.

Substitution Energy for Ca and Mg sites on Non-Polar Surfaces

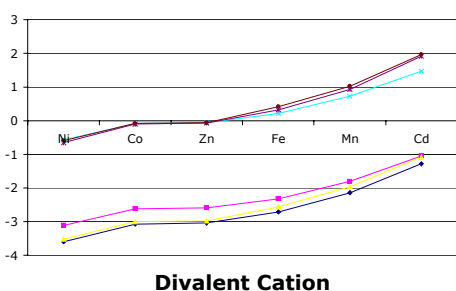


Fig. 1: Substitution energy/ eV vs. cation type

Ionic Radii of Divalent Cations

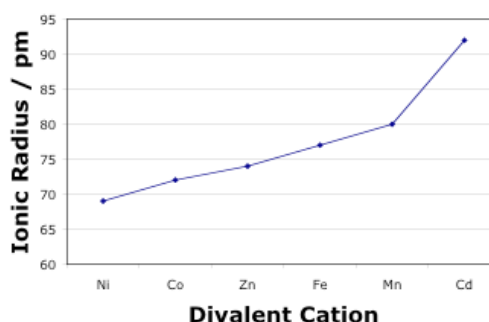


Fig. 2: Ionic radii of relevant divalent cations

The incorporation of the impurities does not affect the relative growth rates of the surfaces and as such has little effect on the morphology, which is that of the cleavage cell of dolomite [Fig. 3]. The prevalent surface in this morphology is the $(10\bar{1}4)$ surface, as expected.

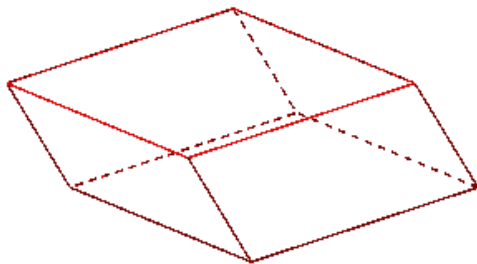


Fig. 3: Morphology of dolomite.

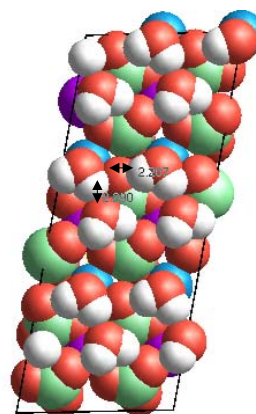


Fig. 4: Dolomite (10 $\bar{1}$ 4) surface with a monolayer of water

The solvation of the (10 $\bar{1}$ 4) surface with a monolayer of water yielded a distinctly ordered arrangement of the water molecules, which form in bands, two molecules thick, along the lines of the cations. Interatomic distances are small enough between the hydrogen on the water and oxygens on both water and carbonate ions to suggest that hydrogen bonding is the cause of the orientation and position of water on the surface [Fig. 4].

The propensity of defect cations to substitute at calcium sites in preference to magnesium sites is contrary to what would be expected from observations in nature. The phenomenon, as it appears from the calculations, appears to be a result of ion size, and is a prediction made on thermodynamic grounds. In order to reconcile the model with experimental observation it is necessary to broaden the scope of the calculations. One aspect of the system that will be addressed is the solvation energy of the relevant ions in solution, which will be done using embedded cluster methods. The residence time of water around the solvated ions will also be of use in investigating kinetic effects on the substitution of impurities onto the surfaces. The co-ordination shell of water around Ca²⁺ and Mg²⁺ ions has already been determined [24], however we plan investigate this for all the ions in our study.

References:

- [1] Al, T.A., C.J. Martin, and D.W. Blowes, *Carbonate-mineral/water interactions in sulfide-rich mine tailings*. *Geochimica et Cosmochimica Acta*, 2000. **64**, (23), 3933-3948.
- [2] Hindar, A. *et al.*, *Effects on stream water chemistry and forest vitality after whole-catchment application of dolomite to a forest ecosystem in southern Norway*. *Forest and Ecology Management*, 2003, **180**, 509-525
- [3] Najafpour, G.D. and S. Rezaei, *Chromium and dolomite removal from rotary filter cake in chrome chemical industries*. *Journal of the Indian Chemical Society*, 2002. **79**, (1), 99-102
- [4] Walker, G.M., *et al.*, *Kinetics of a reactive dye adsorption onto dolomitic sorbents*. *Water Research*, 2003. **37**, (9), 2081-2089
- [5] Brown, J.G. and P.D. Glynn, *Kinetic dissolution of carbonates and Mn oxides in acidic water: measurement of in situ field rates and reactive transport modeling*. *Applied Geochemistry*, 2003. **18**, (8), 1225-1239
- [6] Lakshminarayanan, R. and S. Valiyaveetil, *Influence of silicate anions on the morphology of calcite crystals*. *Crystal Growth & Design*, 2003. **3**, (4), 611-614.
- [7] Colfen, H., *Precipitation of carbonates: recent progress in controlled production of complex shapes*. *Current Opinion in Colloid & Interface Science*, 2003, **8**, (1), 23-31.
- [8] Reeder, R.J. Ch.1, *Reviews in Mineralogy, Series Ed. P.H. Ribbe, Vol.11, Carbonates: Mineralogy and Chemistry*, Mineralogical Society of America, BookCrafters, Inc., Michigan, 1990

- [9] Luttge, A., U. Winkler, and A.C. Lasaga, *Interferometric study of the dolomite dissolution: A new conceptual model for mineral dissolution*. *Geochimica et Cosmochimica Acta*, 2003. **67**, (6), 1099-1116.
- [10] Baer, D.R., et al., *The Interaction of Water and Mn with Surfaces of CaCO_3 - an Xps Study*. *Surface and Interface Analysis*, 1991. **17**, (1), 25-30.
- [11] De Giudici, G., *Surface control vs. diffusion control during calcite dissolution: Dependence of step-edge velocity upon solution pH*. *American Mineralogist*, 2002, **87**, (10), 1279-1285.
- [12] Mao, Y. and P.D. Siders, *Molecular Hartree-Fock model of calcium carbonate*. *Theochem-Journal of Molecular Structure*, 1997, **419**, 173-184.
- [13] Thackeray, D.J. and P.D. Siders, *Molecular-orbital and empirical-potential descriptions of CaCO_3* . *Journal of the Chemical Society-Faraday Transactions*, 1998, **94**, 2653-2661.
- [14] Aquilano, D., et al., *Theoretical equilibrium and growth morphology of CaCO_3 polymorphs .I. Aragonite*. *Journal of Crystal Growth*, 1997. **182**(1-2): p. 168-184.
- [15] Catti, M., et al., *Static Lattice and Electron Properties of MgCO_3 (Magnesite) Calculated by Ab initio Periodic Hartree-Fock Methods*. *Physical Review B*, 1993. **47**, (15), 9189-9198
- [16] Burton, B.P. and A.V. de Walle, *First-principles-based calculations of the CaCO_3 - MgCO_3 and CdCO_3 - MgCO_3 subsolidus phase diagrams*. *Physics and Chemistry of Minerals*, 2003, **30**, (2), 88-97.
- [17] Fisler, D.K., J.D. Gale, and R.T. Cygan, *A shell model for the simulation of rhombohedral carbonate minerals and their point defects*. *American Mineralogist*, 2000. **85**, (1), 217-224.
- [18] Parker, S.C., J.O. Titiloye, and G.W. Watson, *Molecular modelling of carbonate minerals: studies of growth and morphology*. *Philosophical Transactions of the Royal Society of London, A*, 1993. **344**, 37-48.
- [19] de Leeuw, N.H. and S.C. Parker, *Surface structure and morphology of calcium carbonate polymorphs calcite, aragonite, and vaterite: An atomistic approach*. *Journal of Physical Chemistry B*, 1998, **102**, (16), 2914-2922.
- [20] de Leeuw, N.H., *Molecular dynamics simulations of the growth inhibiting effect of Fe^{2+} , Mg^{2+} , Cd^{2+} , and Sr^{2+} on calcite crystal growth*. *Journal of Physical Chemistry B*, 2002. **106**, (20), 5241-5249.
- [21] Wright K., Cygan RT and Slater B, *Impurities and nonstoichiometry in the bulk and on the (10-14) surface of dolomite*. *Geochimica et Cosmochimica Acta*, 2002, **66**, 2541-2546
- [22] de Leeuw, N.H. and S.C. Parker, *Surface-water interactions in the dolomite problem*. *Physical Chemistry Chemical Physics*, 2001. **3**, (15), 3217-3221.
- [23] Wright K., Cygan R.T. and Slater B., *Structure of the (10-14) surfaces of calcite, dolomite and magnesite*. *Physical Chemistry Chemical Physics*, 2001, **3**, 839-844 2001
- [24] Kerisit, S., Parker, S.C. and Harding, J.H., *Atomistic Simulation of the Dissociative Adsorption of Water on Calcite Surfaces*, *J. Phys. Chem. B*, 2003, **107**, 7676-7682
- [25] Rohl AL, Wright K, Gale JD, *Am Miner* 88 921-925 2003 Evidence from surface phonons for the (2x1) reconstruction of the (10-14) surface of calcite from computer simulation
- [26] Gale, J.D. and Rohl, A.L., *The General Utility Lattice Program (GULP)*. *Molecular Simulation*, 2003, **29**, (5), 291-341
- [27] de Leeuw, N.H., *Surface structures, stabilities and growth of magnesian calcites: A computational investigation from the perspective of dolomite formation*. *American Mineralogist*, 2002, **87**, 679-689

INFLUENCE OF TEMPERATURE ON SORPTION OF EUROPIUM ONTO SMECTITE

A. Bauer, T. Rabung, F. Claret, T. Schäfer, T. Fanghänel

Forschungszentrum Karlsruhe
Institute for Nuclear Waste Management
P. O. Box 3640
76021 Karlsruhe
Germany
Bauer@ine.fzk.de

The temperature upon which thermodynamic data used for performance assessment purposes is based is usually 25°C. However, in the near field environment of a spent fuel or vitrified high level waste repository the temperature will remain elevated for a long time period. Thermal calculations (Johnson et al., 2001) have shown that the temperature in the bentonite may attain 70-90°C under saturated conditions for 1000 years after repository closure. According to these calculations temperature then slightly decreases to 40-50°C after about 10000 years, which is the expected life span for the canisters. For the Swedish KBS-3 concept temperatures for the bentonite backfill are calculated to reach up to 80°C at the inner boundary (Ageskog and Jansson, 1999). After 1000 years temperatures are assumed to decrease to 40-55°C. From the above references it is apparent that there may be significant temperature differences for long time periods between thermodynamic standard conditions (i. e. , T= 25°C) and the ones expected in the repositories. Therefore in this study the effect of temperature (20-80°C) on sorption of Eu(III) onto smectite was studied by wet chemistry, time resolved laser fluorescence spectroscopy (TRLFS), scanning transmission X-ray microscopy (STXM) and pyrolysis GC-MS.

The SWy-2 montmorillonite used in this study was purchased from the Source Clay Minerals Repository of the Clay Mineral Society. The < 1 µm size fraction was separated by sedimentation. The material was converted to the homoionic K form by thoroughly washing 10 times with 0.1 M KClO₄. The experiments were carried out at 20°, 60° and 80°C as a function of pH in 0.1 M KClO₄. High density polyethylene Zinsser bottles and quartz cuvettes with a solid/solution ratio of 2.5 g L⁻¹ for the sorption experiments and 0.25 g L⁻¹ for the TRLFS experiments were used. All experiments were performed under argon atmosphere.

The sorption edges for both types of reaction vessels and for any temperature are similar. At low pH the exchangeable sites of smectites, with predominant non-specific adsorption, are mainly occupied by K. Above pH 6 the K_D for Eu(III) increases strongly. XRD measurements showed that the structure of the clay minerals did not change during the course of the experiment. The sorption mechanism of Eu(III) on smectite was studied by TRLFS. The fluorescence emission lifetimes contain information about the coordination sphere of Eu(III). Single component spectra with mono exponential decay behavior are found for all temperatures for both reaction vessels at pH < 4 corresponding to the Eu(III) aquo ion. At higher pH values and higher temperatures a different evolution for the different types of reaction vessels was observed. At 25°C (pH > 6) fluorescence emission lifetime of 190-200 µs were found for the two types of reaction vessels, corresponding to 5 water in the first coordination sphere. At 60 and 80°C (pH > 5) the fluorescence emission lifetime increased significantly in the Zinsser bottles to 800-950 µs indicating a complete loss of water in the first coordination sphere. In the quartz cuvettes under the same conditions a lifetime of 190 µs was measured. DOC, STXM and GC-MS measurements showed a release of organic material

from the Zinsser bottles at higher temperatures. In the presentation possible mechanisms and the relevance for the disposal of nuclear waste will be discussed.

References:

Johnson J. W., Niemeyer M., Klubergans G., Siegel P. (2001) NTB Report 01-04, Wettingen
Ageskog L., Janson P. (1999) SKB Technical report TR-99-02, Stockholm

INVESTIGATIONS OF URANYL SORPTION ONTO GIBBSITE

N. Baumann, V. Brendler, T. Arnold, G. Geipel
FZ Rossendorf, Institute of Radiochemistry
P.O. Box 51 01 19
D-01314 Dresden
V.Brendler@fz-rossendorf.de

Abstract

The sorption of uranium(VI) onto gibbsite was investigated applying conventional batch experiments and time-resolved laser-induced fluorescence spectroscopy. The two uranyl surface species observed in region of sorption (pH 4.5 – 8.5) exhibit very similar fluorescence properties, indicating identical numbers of hydroxyl groups in their first coordination sphere.

Material and characterization

The gibbsite used for this work was a product from Merck: catalogue number 1010931000, name hydrargillite (a synonym for gibbsite), formula $[\text{AlH}_3\text{O}_3 \cdot x \text{H}_2\text{O}]$. For all subsequent experiments gibbsite was used unaltered with no special pre-treatment.

The X-ray diffraction diagrams recorded before and after the sorption experiments confirmed that the investigated mineral was gibbsite and showed that as a result of the uranyl sorption there was no change in mineral structure. The purity of the used gibbsite sample was analysed by energy dispersive XRF and ICP-MS. The used gibbsite has a purity of 99.9 % according to XRF analyses, with traces of CaO (600 ppm) and Fe_2O_3 (250 ppm). These results are similar to the data specified by the manufacturer MERCK. The gibbsite particle size was determined with a laser diffraction device at TU BA Freiberg. The average grain size x_{50} was 12.2 μm , with 95 % of the grains having a size between 0.9 μm and 50 μm . These values are in accordance with the data sheet from the manufacturer. The specific surface area of the gibbsite was determined with a five-point N_2 -BET, yielding 1.5 m^2/g .

Batch experiments of uranyl sorption onto gibbsite as a function of pH

The batch experiments concerning the sorption behaviour of uranyl on gibbsite were carried out at an ionic strength of 0.1 M (adjusted with NaClO_4) and at different pH values with a stepping of 0.5 from 3.5 to 9.5. For each point, 0.5 g gibbsite were weighted in polyethylene tubes, and 40 ml 0.1 M NaClO_4 solution was added. Then the pH was adjusted by NaOH and HClO_4 solutions, controlled over approximately two weeks and readjusted if necessary. Because the sorption experiments were carried out under air atmosphere, it was essential to guarantee equilibrium of CO_2 between air and solution. Therefore, an equivalent amount of NaHCO_3 was added to the samples at pH values equal and higher than 7. Finally, when the pH-value was stable, uranium was added as $\text{UO}_2(\text{ClO}_4)_2$ solution, giving a total concentration of uranium in the gibbsite suspension of 10^{-5} M. After uranium was added, the pH-value was readjusted again.

After a contact time in the overhead shaker of 2 days gibbsite was separated by centrifugation. The concentration of uranium in the separated solution was measured by ICP-MS. The amount of adsorbed uranium on gibbsite was calculated from the following equation:

$$U_{\text{ads}} = U_{\text{total}} - U_{\text{solution}} - U_{\text{wall}}$$

The resulting sorption curve indicates a maximum sorption between pH 5.5 and 7.5 (Fig. 1). In a following step, the gibbsite separated by centrifugation was re-suspended in 40 mL of a solution with pH and ionic strength being identical to the original solution. This ascertained that only fluorescence signals caused from originally sorbed uranium would be detectable,

eliminating the dissolved uranium fraction. TRLIF spectra were recorded of this gibbsite suspension, at permanent stirring.

Also, the re-distribution of fluorescent U(VI) species between solid and liquid phase after the first centrifugation was negligible. To verify that, after the first TRLIF measurement gibbsite was separated again from the solution. The resulting solutions did not show any TRLIF signals clearly documenting the absence of fluorescent uranium species above the detection limit of 10^{-7} M U(VI).

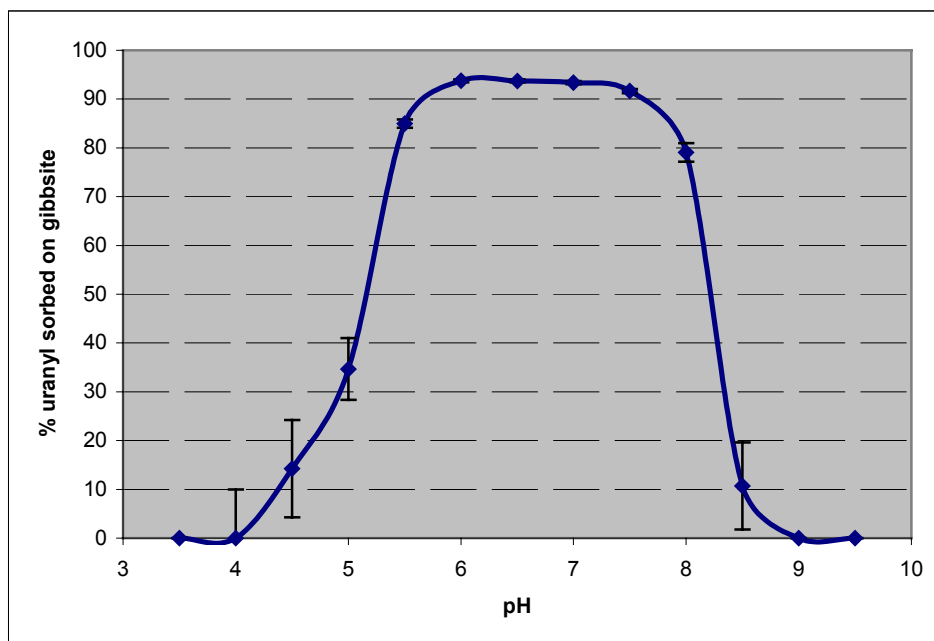


Fig. 1: Uranium sorbed on gibbsite vs. pH value (Batch experiments)

TRLIF (Time Resolved Laser-Induced Fluorescence) spectroscopy investigations
The TRLFS system consists of a Nd:YAG diode laser with subsequent 4th harmonic generation. This wavelength (266 nm) was used for the excitation of the samples. The emitted fluorescence radiation was focussed into a spectrograph and the resulting spectra were measured by a diode array (701 intensified diodes). The gate width (exposure time) is variable from 5 ns to 2 ms. Here, 5 μ s were used. The delay time after the excitation laser pulse ranges from 0 ns to 6500 ns. Every spectrum was measured three times, and for each spectrum 100 laser shots were averaged. 31 spectra at different delay times were collected totally for one time-resolved spectrum.

Results and discussion

Fig. 2 presents a compilation of fluorescence spectra at the shortest delay time at different pH-values. The peak at 532 nm is the laser-dispersions peak (2nd order of excitation radiation at 266 nm). Distinct peaks of the U(VI) fluorescence are around 500 and 520 nm, a smaller peak is at about 540 nm, and a little shoulder occurs near 560 nm.

The evaluation of the spectroscopic data was performed with Origin 6.01 software (Origin Lab Inc.). Based on the TRLIF spectra at different delay times the fluorescence decay function was determined. For that purpose, the complete fluorescence spectra for each time step were integrated, excluding the wavelength range between 525 and 540 nm influenced by the laser dispersion peak. The integrated curve was then fitted to a sum of exponential decay terms. The best approximation gave a bi-exponential decay function:

$$y = y_0 + A_1 e^{-(x-x_0)/t_1} + A_2 e^{-(x-x_0)/t_2}$$

yielding two fluorescence decay times. Mono-decay functions gave significant worse fittings, whereas fits for three-exponential decays did not converge.

The results of the fluorescence lifetime determinations are summarized in table 1. There, t_1 and t_2 are the calculated lifetimes from the short and the long-lived species, respectively, with errors, r^2 is the correlation coefficient of the fluorescence lifetime fit.

Tab. 1: Fluorescence lifetimes of the uranium(VI) species sorbed on gibbsite.

pH	t_1 / ns	t_2 / ns	r^2
5	210 ± 7	5200 ± 330	0.998
5.5	260 ± 6	7800 ± 200	0.998
6	370 ± 2	5700 ± 40	0.998
6.5	320 ± 12	5200 ± 220	0.998
7	300 ± 11	4600 ± 250	0.998
7.5	420 ± 15	5900 ± 280	0.999
8	380 ± 4	6500 ± 50	0.999
8.5	440 ± 7	7800 ± 100	0.998

As can be seen from Fig. 2, the relative fluorescence signal intensities as function of the pH are similar to the sorption curve given in Fig. 1: high intensity in the neutral range, lower intensities in more acid or base regions.

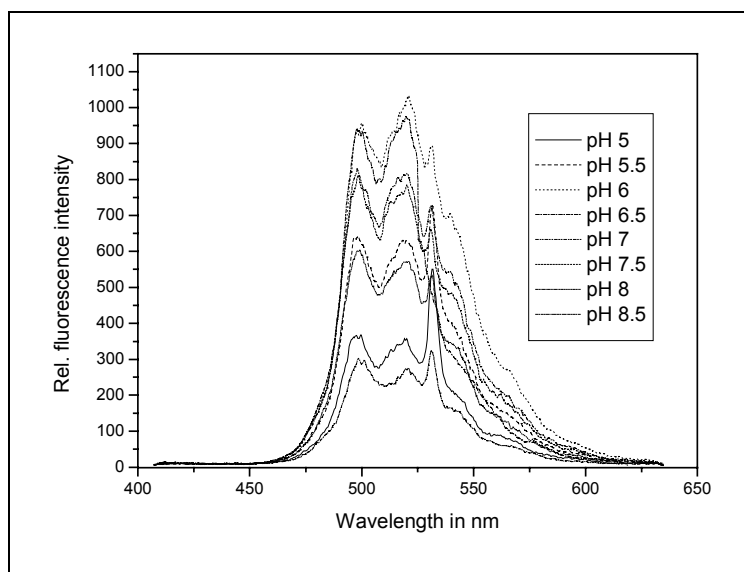


Fig. 2: Compilation of fluorescence spectra at the shortest delay time at different pH-values

From Fig. 2 and table 2 it becomes also obvious, that the peak maxima differ slightly at varying pH, but do not show systematic shifts. The same holds for the long-lived species, c.f. Fig. 3 and table 3. The two uranium surface species are therefore assumed to have very similar first coordination spheres throughout the investigated pH range, namely identical numbers of hydroxyl groups. Their different fluorescence decay time indicate, however, differences in their respective water content.

Tab. 2: Wavelengths of peak maxima positions in nm at a delay time of 0 ns

pH	Positions of the fluorescence maxima in nm			
5	497	522	539.6	565.5
5.5	497.4	521	539.3	561.7
6	499.4	523.1	539.1	556.7
6.5	495.1	519.3	547.1	554.7
7	498.7	519.8	546.7	556.1
7.5	500.1	519.3	549.3	558.8
8	497.9	523.3	541.3	556.5
8.5	499.5	521.8	538.4	547.9

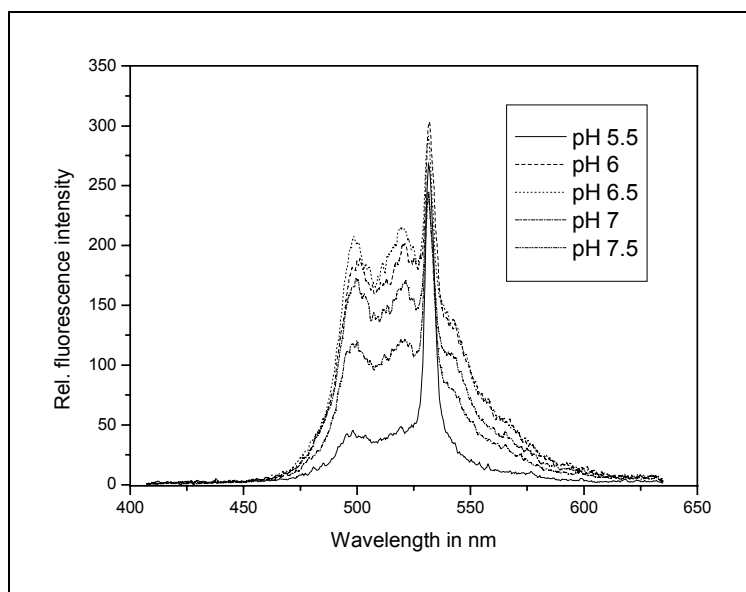


Fig. 3: Compilation of spectra recorded at time 3000 ns after excitation

Tab. 3: Wavelengths of peak maxima positions in nm at a delay time of 3000 ns

pH	Positions of the fluorescence maxima in nm			
5.5	501	520.5		
6	501	522.2	541.3	
6.5	499.2	520.7	540.7	555.6
7	499.2	521.4	540.6	560.2
7.5	500.5	522.3	540.8	553.6

Acknowledgement

Financial support by the European Commission under contract No. FIKW-CT-2000-00035 (ACTAF Project) is gratefully acknowledged.

URANYL UPTAKE AT THE CALCITE (104) SINGLE CRYSTAL SURFACE: A P-GIXAFS STUDY

Dirk Bosbach, Melissa A. Denecke, Kathy Dardenne, Jörg Rothe, Thomas Fanghänel

Forschungszentrum Karlsruhe
Institut für Nukleare Entsorgung (INE)
P.O. Box 3640
D-76021 Karlsruhe
Germany
Bosbach@ine.fzk.de

The mobility of U(VI) under (oxidizing) near surface conditions is ultimately linked with its interaction with mineral surfaces. Calcite is a very common mineral in soil systems as well as in clay, which is considered as a potential host formation for the geological disposal of high level nuclear waste in many countries. Adsorption and (co)precipitation of U(VI) with calcite therefore represent a key reaction mechanisms (Fig. 1). A sound understanding of these reactions requires fundamental knowledge of the surface sorbed U(VI) species including geometry and preferential sorption sites, using surface sensitive spectroscopic as well as high resolution microscopic techniques..

AFM observations clearly show that the nanotopography of calcite (104) surfaces exposed to an aqueous solution is build up of atomically flat terraces and molecular steps with a step height of 0.304 nm (Fig. 2). Due to the distinct nanotopography, various sorption sites for U(VI) occur. Since adsorption can be considered as a precursor to incorporation, one would expect coprecipitation also be affected by this heterogeneity. In particular the reactivity of edges of molecular steps, which are considered as the most important surface sites for crystal growth and coprecipitation, need to be considered. At the (104) surface of calcite, the carbonate groups exhibit a characteristic tilt angle, which results in molecular step edges with an acute and obtuse angle parallel to the [-441] and [48-1] (Fig. 1). The incorporation of many trace metals and radionuclides including U(VI) occurs preferentially at one of these step edges (Paquette & Reeder, 1995, Reeder et al., 2000, Reeder et al., 2001).

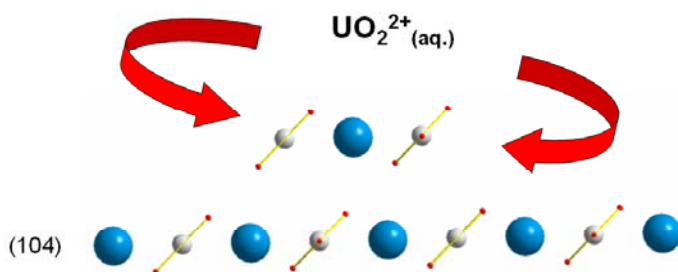


Figure 1: Cross-sectional view of the (104) calcite surface structure.

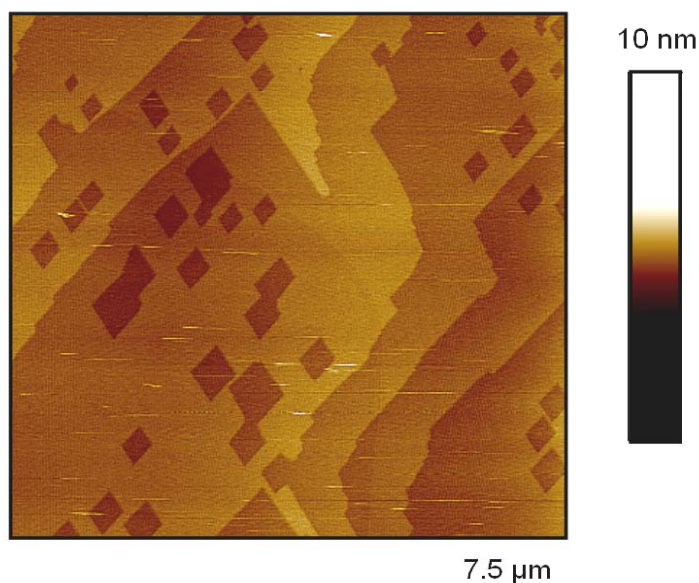


Figure 2: AFM image of a Calcite (104) surface exposed to a saturated aqueous solution at pH 8.3. Monomolecular steps with a height of 3.04 Å are mostly associated with rhombohedral etch-pits.

Polarized dependent grazing incidence XAFS (P-GIXAFS) measurements of U(VI) sorbed onto a freshly cleaved (10-14) surface of a natural calcite sample were performed. The investigation was aimed at determining if preferential adsorption occurs at one of two types of angled molecular step edges, associated with the $[-441]-$ and $[48-1]-$ and with the $[-441]+$ and $[48-1]+$ steps. Investigations by other groups report a differential incorporation of uranyl cations between two symmetrically non-equivalent vicinal surfaces associated with growth at these + and - steps during calcite single crystal growth (Reeder et al., 2000, Reeder et al., 2001). The question arises if site-selective sorption affects step selective incorporation. To ascertain if site-selective sorption occurs, two P-GIXAFS U L3 edge spectra of uranyl sorbed onto (10-14) CaCO_3 with ϵ oriented approximately parallel to the $[-441]-$ and to the $[48-1]+$ directions are recorded. The spectra are designated SO_0 and SO_270, respectively.

P-GIXAFS measurements were performed at the HASYLAB X1 experimental station. Si(111) crystals are used in the double-crystal monochromator (DCM) in pseudo-channel cut mode. The energy of the beam is calibrated against the first derivative in the XANES spectrum of a Pt foil, defined as 11564.0 eV. Spectra are recorded with the sample surface oriented with respect to the impinging beam at an incident angle (θ_i) of 100 mdeg. Samples are mounted and held in place with carbon paste (Leit-C, Plano, Münster, Germany) in a circular, domed cell with Kapton windows (for incident and reflected beam) and a window on top of the cell, normal to the sample plane, for registering the fluorescent signal using a Canberra LEGe 5-element solid state detector, mounted above it. The incoming intensity is measured using 50:50 Ar:N₂ in the ionization chamber. The samples are in a humid atmosphere to keep them moist during measurement.

The measured k^2 -weighted U L3 edge P-GIXAFS and their corresponding Fourier transforms (FT) are depicted in fig. 3. Because the calculated aqueous U speciation of the alkaline uranyl solution used to prepare the sorption sample (pH 8.3, $[\text{U}] = 1.3 \cdot 10^{-4}$ M) is dominated by $\text{UO}_2(\text{CO}_3)_3^{4-}$, we compare the EXAFS for the uranyl sorbed calcite with that for an aqueous tricarbonato uranium(VI) solution species ($\text{UO}_2(\text{CO}_3)_3^{4-}$) shown in fig. 4. In order to correctly

model the $\text{UO}_2(\text{CO}_3)_3^{4-}$ spectrum, multiple-scattering (MS) to the distal oxygen (*Odis*) along the U-C-*Odis* path must be included. Path analysis reveals this MS path to be responsible for the ‘triplet’ structure between k 6.5 and 8.5 \AA^{-1} . This oscillatory fingerprint of the $\text{UO}_2(\text{CO}_3)_3^{4-}$ EXAFS is missing in the EXAFS of the uranyl sorbed calcite in fig. 3. We conclude that the calcite surface sorbed uranyl species is not simply a tricarbonato species. Studies of uranyl incorporated into calcite report loss or partial loss of three carbonato ligands (Kelly et al., 2003, Reeder et al. 2001). This seems also the case for the calcite sorbed species here.

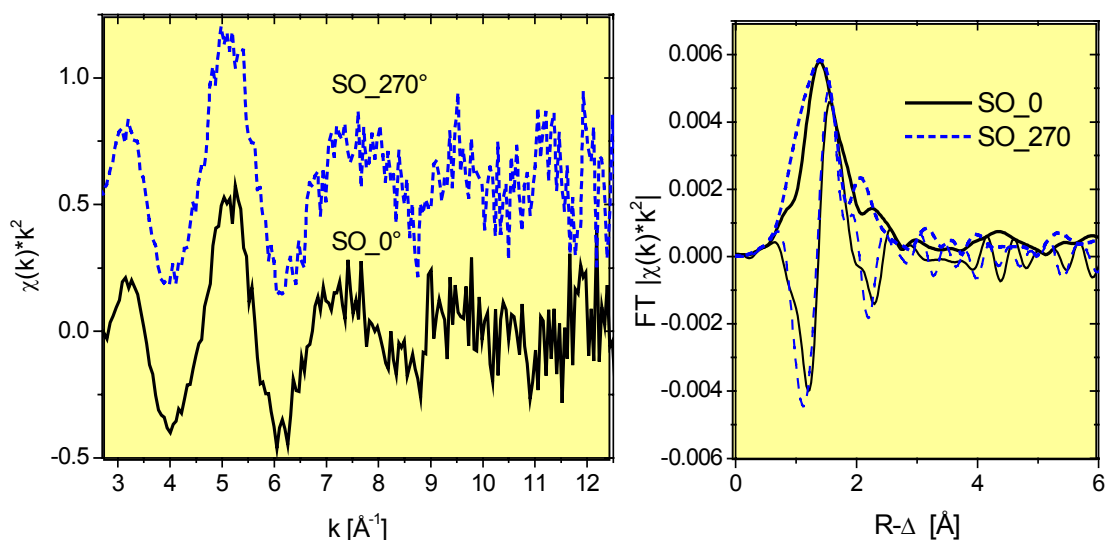


Figure 3: U L3 P-GIXAFS (left) and corresponding Fourier transforms (right) for uranyl sorbed (10-14) calcite surface measured at angles with ϵ being approximately parallel to the $[-441]-$ and $[48-1]_+$ directions (designated SO_0 and SO_270).

Qualitative examination of the spectra in fig. 3 reveals the amplitude of the U-O ax shell in both spectra to have similar amplitudes. However, the U-O eq signal in the SO_0 spectrum is significantly different than in the SO_270 spectrum. There are two possible explanations for this apparent non-variance in $\Theta(\text{U-O}ax)$ with ϵ . Either the linear $[\text{O}=\text{U}=\text{O}]^{2+}$ units are perpendicular to ϵ or they are oriented at a small constant ‘tilt’ relative to ϵ in both the SO_0 and SO_270 spectra. That $\Theta(\text{U-O}eq)$ is observed to change with relative orientation of ϵ to the + and - steps may infer that the coordination of U(VI) in its equatorial plane is significantly asymmetric. That uranyl appears to be oriented perpendicular (or at a constant tilt) to the (10-14) surface and that the equatorial coordination shows asymmetry in these measurements with the beam incident to + and - steps may result from preferential sorption of uranyl cations onto one of the steps. To test this hypothesis, the spectra are fit to the EXAFS equation considering the polarization dependency of the EXAFS amplitude. This is done by introducing an effective coordination number (N_{eff}), which is related to the actual coordination number (N) by $N_{\text{eff}} = \frac{1}{2}N(1+3\cos^2\Theta)$ (Hudson et al., 1996), where Θ is the angle between the bond axis and ϵ . The independent variables $\Theta(\text{U-O}ax)$ and $\Theta(\text{U-O}eq)$ are included in the fit to describe the angle between ϵ and the $[\text{O}=\text{U}=\text{O}]^{2+}$ unit and between ϵ and the equatorial plane. N is 2 for the axial oxygen atoms, O ax . Fits using N of both 4 and 5 for equatorial oxygen atoms, O eq , are performed. Results of these fits are listed in Table 1.

By comparing the fit results with the atomic arrangement of atoms on the (10-41) calcite surface, we conclude that uranyl cations sorb at equivalent crystal Ca-positions with monodentate coordination to carbonate groups. However, because a C atom is observed at a ~ 2.9 Å distance, the sorbed uranyl cation must retain one bidentate carbonate ligand. As inferred from our qualitative interpretation of the spectra, fits show the uranyl cations are at a near constant tilt to the (10-14) surface. This suggests that binding is likely on terrace steps and not parallel to the (10-14) surface. The values for $\Theta(\text{U-O}_{eq})$ of 145° and 177° indicate that crystal lattice oxygen atoms lying perpendicular to the b axis cannot be involved in O_{eq} binding. The experimental $\Theta(\text{U-O}_{eq})$ values are within 7° of those expected for monodentate binding to calcite carbonate O atoms above and below the (10-14) plane for $S0_0$ (141°) and binding to carbonate O atoms lying in the (10-14) plane (180°) for $S0_270$. From the possible sites on the $[-441]_-$ and $[48-1]_+$ steps, only a $[-441]_-$ attachment would lead to the observed change in the C atom intensity. In summary, results of these P-GIXAFS measurements suggest preferred uranyl binding to a $[-441]_-$ face (acute angle step).

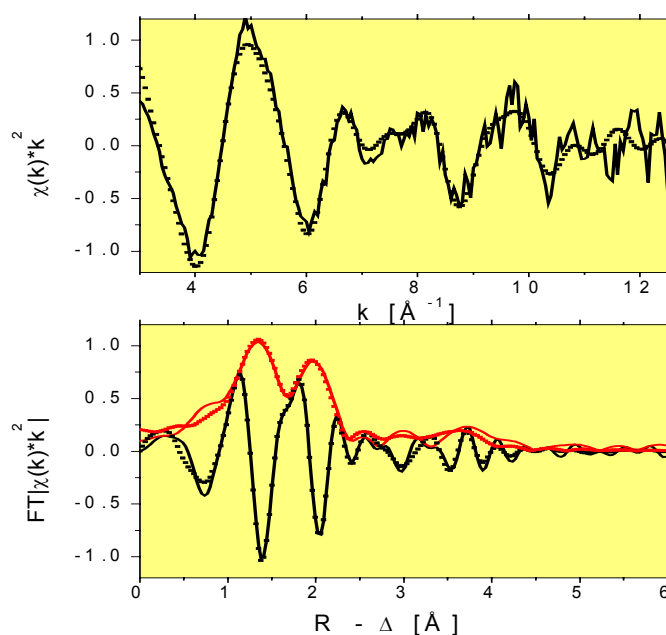


Figure 2: U L3 EXAFS (top) and corresponding Fourier transforms (bottom) for an aqueous $\text{UO}_2(\text{CO}_3)_3^{4-}$ solution. Continuous lines are the experimental data; symbols represent a theoretical model of the data including multiple-scattering (U-Oax-U-Oax and U-C-Odis) paths.

Spectrum	Shell	N_{eff}^*	R [Å]	σ^2 [Å ²]	ΔE_0 [eV]	Θ [deg]
<i>Fit to SO_0</i>						
A	Oax	2.2	1.81	0.008		52
	Oeq	7.2	2.32	0.024	0.0	142
	C	1.5	2.90	0.004		-
B	Oax	2.2	1.82	0.008		51
	Oeq	6.3	2.33	0.024	2.2	148
	C	1.5	2.96	0.004		-
<i>Fit to and SO_270</i>						
A	Oax	2.5	1.78	0.008		45
	Oeq	10.0	2.31	0.035	-2.7	176
	C	2.4	2.88	0.004		-
B	Oax	2.3	1.78	0.007		48
	Oeq	8.0	2.31	0.030	-2.3	179
	C	1.6	2.87	0.001		-

Calculated from the variable Θ with $N(\text{Oeq})=5$ for results listed in rows **A** and $N(\text{Oeq})=4$ for **B**.

Table 1: Metric parameters from fits to the U L3 EXAFS of the uranyl loaded (10-41) calcite surface described in the text.

References:

- Paquette, J., Reeder, R.J., Relationship between surface-structure, growth mechanisms and trace-element incorporation in calcite, *Geochim. Cosmochim. Acta*, 59, 735-749 (1995).
- Reeder RJ, Nugent M, Lamble GM, Tait CD, Morris DE, Uranyl incorporation into calcite and aragonite: XAFS and luminescence studies *Environ. Sci. Technol.* 34, 638 (2000)
- Reeder, R.J., Nugent, M., Tait, C.D., Morris, D.E., Heald, S.M., Beck, K.M., Hess, W.P., Lanzirrotti, A., *Geochim. Cosmochim. Acta* 65, 3491 (2001).
- Kelly, S., Newville, M.G., Cheng, L., Kemner, K.M., Sutton, S.R., Fenter, P., Sturchio, N.C., Spötl, C., *Environ. Sci. Technol.* 37, 1284 (2003).
- Hudson, E. A., Allen, P. G., Terminello, L. J., Denecke, M. A., Reich, T., *Phys. Rev. B* 54, 156 (1996).

THE LINKAGE BETWEEN URANIUM, IRON AND CARBON CYCLING. PROCESSES AT INTERFACES: EVIDENCES FROM COMBINED SOLUTION CHEMICAL AND SPECTROSCOPIC STUDIES

Jordi Bruno, Mireia Grivé and Lara Duro

Enviros Spain
Pg. Rubí, 29-31
08197- Valldoreix, Barcelona
Spain
jbruno@enviros.biz

Abstract

Interfacial processes have a critical role in many reactions and phenomena in the environment, including mineral weathering, particle stability in surface waters, transport of chemical species and element cycling in natural environments. In order to predict the environmental impact of human activities such as uranium mining and radioactive waste disposal, it is necessary to understand the migration of actinides, uranium among them, in the environment. Iron oxides and oxyhydroxides are ubiquitous in nature and they are of particular interest due to their large capacity to sorb radionuclides onto their surface. The Fe and U cycles are also linked to the carbon one and aqueous carbonate plays a major role in the transport of radionuclides due to its high affinity to form complexes with hexavalent uranium. On the other hand, dissolved carbonate can compete for the sorption sites of the iron oxides, promoting the dissolution of these oxides and consequently increasing the mobility of the associated radionuclides in natural systems. Our understanding of how radionuclides impact the environment is dependent on our ability to measure chemical reactions at environmental interfaces.

Introduction

The presence of radionuclides in soils and waters due to nuclear waste management facilities and uranium mining tailings is a problem of major environmental concern. The mobility of these radionuclides in oxic groundwaters is linked to the iron cycle and controlled by geochemical processes such as adsorption on major mineral surfaces and precipitation/dissolution. In this context, iron oxides and oxyhydroxides are of particular importance due to the fact that they are ubiquitous in nature and to their large capacity to sorb radionuclides, hexavalent uranium among them. The iron and uranium cycles are linked to the carbon one since aqueous carbonate plays a major role in the transport of radionuclides due to its high affinity to form complexes with some radionuclides, specially with uranium. Furthermore, dissolved carbonate can compete for the sorption sites of the iron oxides, promoting the dissolution of these oxides and consequently increasing the mobility of the associated radionuclides in natural systems.

The ability to develop adequate models for predicting the fate of inorganic contaminants in surface environments is highly dependent on accurate knowledge of the distribution of these constituents between the solid and solution phases and ultimately on the capability to provide molecular-level information on chemical species distributions in both of these phases. Most of the information we have about interactions of cations or anions at mineral/water interfaces

comes from macroscopic measurements. In the last years, efforts to quantify observed sorption reactions at solid/liquid interfaces by means of surface complexation models have been developed. However, it is very difficult to precisely study these sorption reactions without spectroscopic evidence, mainly due to the uncertainty in the definition of the nature of the surface species formed.

Objectives

Our main objective in this work is to characterize the bonding environments of uranium onto oxide surfaces and to study the most probable mechanism of uptake of these metals in carbonated solutions. We have mainly studied three different systems: 1) the effect of carbonate on the dissolution of iron oxides since they are representative of one of the most widespread oxides in nature behaving as a sink of trace metals, 2) the effect of carbonate on schoepite, which is one of the main secondary phases of uranium forming under oxidizing conditions, and 3) given that the formation and dissolution of Fe minerals can imply the incorporation of U into these Fe oxide structures or the sorption of U onto these newly formed minerals, we have studied the effect of carbonate on a mixed Fe(III) and U(VI) solid phase.

In this work we will show the outcome of the use of combined information gathered from thermodynamic and kinetic macroscopic studies with information from EXAFS spectroscopy. The coupling of such different studies will help us both qualitative and quantitative to characterize bonding environments of uranium onto Fe-oxide surfaces and to study the most probable mechanism of uptake of these metals in carbonated solutions

Experimental procedures

We prepared a 2-line ferrihydrite according to the method described by Cornell and Schwertmann (1992), a co-precipitate of iron (III) and U(VI) and a metaschoepite synthesized as described in Bruno and Sandino (1989). Characterization of the solids was made with X-ray diffraction and by SEM analysis.

During solubility measurements, we measured the metal concentrations in equilibrium with the corresponding solid at given pH and $p\text{CO}_2$ values. The $p\text{CO}_2$ was kept constant by flushing CO_2/N_2 gas mixtures of the appropriate composition. The attainment of equilibrium was monitored by measuring the variation of hydrogen ion concentration with time. We assumed that equilibrium was obtained when the potential of the glass electrode remained constant within 0.2 mV (equivalent to 0.006 pH units) for 24 hours.

Kinetic experiments were performed in a continuous flow column and the behaviour of the system was controlled by measuring the dependence of the metal concentration at the output as a function of the flow, for a certain constant pH, $p\text{CO}_2$ condition. The solid sample was placed in the column and was let to react with the flowing solution at a certain $p\text{CO}_2$, pH condition. The output metal concentrations at constant flow were monitored until steady state was reached, i.e. until the glass electrode potential at the outlet remained constant within 0.1-0.2 mV. Samples were taken and analysed after assuring the absence of particulate in the samples by filtering with 0.02 μm porous membrane filters.

Spectroscopic measurements were made with dry samples at room temperature at the ROSSendorf BeamLine (ROBL) at the European Synchrotron Radiation Facility (ESRF) in Grenoble, and processes using EXAFSPAK software (George and Pickering (2000)). Phase and amplitude functions were obtained from FEFF8 calculations (Zabinsky et al., 1995).

Results and discussion

We will show some of the results obtained from both macroscopic and microscopic studies, which have helped us to have an idea of the linkage between uranium, iron and carbon cycling processes at interfaces.

It is because of the importance of Fe (III) in many geochemical processes occurring in natural systems, that there is a strong need for reliable thermodynamic data on Fe(III) aqueous species. Despite the attention that has been already devoted to Fe(III) aqueous speciation, the thermodynamics of some species are not yet well known, particularly in the pH range of natural waters. The presence of ligands such as carbonate that might form soluble complexes with Fe(III) could enhance the solubility of the solid. In fact, complexation of iron (III) by carbonates in natural systems has not been sufficiently addressed in the available literature. For this reason we have conducted solubility measurements of some iron oxides and hydroxides under different pCO₂ and, after proving the increase of different iron oxides under carbonate solutions, we proposed the formation of two different Fe(III)-CO₃ aqueous species not described before, FeOHCO₃ (aq) and Fe(CO₃)₃³⁻, as the responsible of the increase of iron (III) concentrations in such systems (Figure 1) (Bruno et al., 1992, Bruno and Duro (2000) and Grivé et al.,2003).

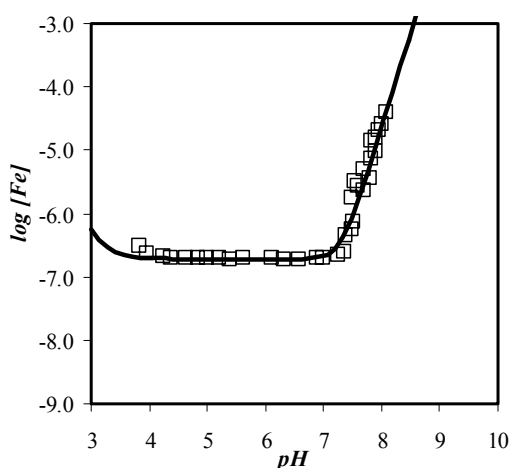


Figure 1. Plot of the measured iron concentrations (symbols) in equilibrium with ferrihydrite under at a pCO₂=0.3 atm. Solubility (line) calculated by assuming the formation of FeOHCO₃ (aq) and Fe(CO₃)₃³⁻. (Data from Grivé et al., 2003).

Kinetic data have been obtained for the dissolution of ferrihydrite, schoepite as well as of a co-precipitate of U(VI) and Fe(III) in bicarbonate solutions. Figure 2 show the kinetic data obtained for the co-precipitate in the form of log rate as a function of log[HCO₃⁻] for experiments performed at pCO₂ 0.97, 0.3 and 0.01 atm. The obtained empirical rate equation for the dissolution of the co-precipitate, normalized to the specific surface area of the solid, is as follows:

$$rate = k_1 \times [HCO_3^-]^{0.74} \quad (\text{mol} \cdot \text{m}^{-2} \cdot \text{h}^{-1}) \quad (1)$$

with $k_1 = 2.09 \cdot 10^{-8} \text{ h}^{-1}$. The fractional order of bicarbonate-promoted dissolution in that system (see Figure 2), suggests a surface control of the rate of dissolution of this solid phase.

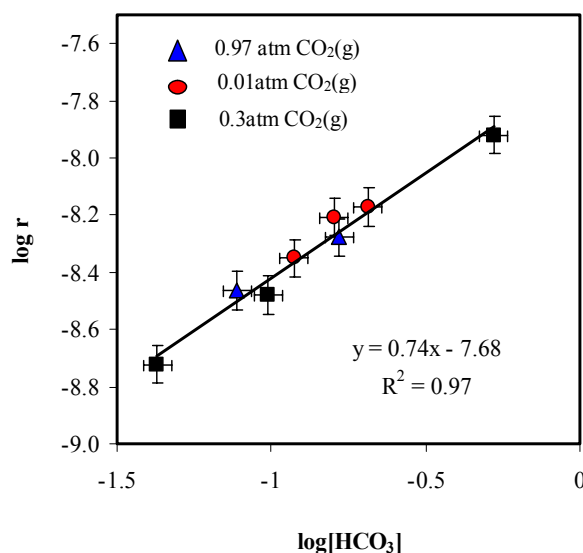


Figure 2. Plot of the logarithm of the rate of dissolution of a co-precipitate of U(VI) and Fe(III) as a function of the logarithm of the concentration of bicarbonate in dissolution. Experiments undertaken under three different pCO₂(g).

In order to characterize and to get more information from the superficial complex coordinated to the surface of each different solid studied here, we have used X-ray absorption spectroscopy (XAS) as a direct molecular probe. This technique has provided us both qualitative and quantitative information about the oxidation states, coordination environments, and short-range order of metal ions, including metal-oxygen or metal-carbon bond distances and coordination numbers.

When schoepite is under a constant pCO₂ tends to dissolve as results of the high affinity of carbonate and uranium to form aqueous carbonate uranyl complexes. EXAFS measurements of carbonate on the surface of schoepite suggest that U(VI) carbonato-schoepite ternary complexes occur and are important species responsible for the dissolution of the secondary solid phase to form aqueous carbonate uranium species. The quantification of its dissolution is fundamental to assess for example, the environmental impact of DU in conflict zones.

Conclusions

1. -The dissolution of ferrihydrite, schoepite and a co-precipitate of Fe(III) and U(VI) is affected both thermodynamically and kinetically by the carbonate system.
2. -The rate of dissolution of ferrihydrite, schoepite and a co-precipitate of Fe(III) and U(VI) is enhanced in bicarbonate solutions although in different degree depending on the solid studied, and the kinetics of dissolution seem to be surface controlled and bicarbonate promoted in all cases.

The combination of macroscopic and microscopic studies is very helpful to have a deeper understanding of the mechanism of uptake/release of trace metals by iron oxihydroxides under carbonated waters commonly found in natural environments and of the implications of these findings in natural environments.

References:

Bruno, J., Stumm, W., Wersin, P. and Brandberg (1992). On the influence of carbonate in mineral dissolution. I. The thermodynamics and kinetics of hematite dissolution in bicarbonate solutions at T= 25°C. *Geochim. Cosmochim. Acta.*, 56, 1139-1147.

Bruno, J.; Sandino (1989). The solubility of amorphous and crystalline schoepite in neutral to alkaline aqueous solutions. *Mat. Res. Symp. Proc. Vol.*, 127, 871-877

Bruno, J. and Duro, L. (2000). Reply to W, Hummel's com. ment on and correction to "On the influence of carbonate in mineral dissolution:1. The thermodynamics and kinetics of hematite dissolution in bicarbonate solutions at T=25°C, by Jordi Bruno, W.Stumm, P.Wersin and F. Brandberg. *Geochim. Cosmochim. Acta*, 64: 2173-2176.

George, G.N. and Pickering, J. (2000). A suite of computer for analysis of x-ray absorption spectra.

Grivé, M., Duro, L., Bruno, J. and de Pablo, J. (2003). The thermodynamics of ferrihydrite dissolution in bicarbonate solutions at T=25°C. Effect of the colloid/polynuclear species. Migration'03, Spetember 21-26, 2003. Gyeongju, Korea

Schwertmann, U. I Cornell, R.M. (1991). *Iron oxides in the laboratory*. VCH, Weinheim, 137pp.

Zabinsky, S.I., Rehr, J.J., Ankudinov, A., Albers, R. C. and Eller, M. J. (1995) Multiple Scattering Calculations of X-ray Absorption Spectra. *Phys. Rev. B* 52, 2995

THE EFFECTS OF PHOSPHATE ON URANIUM ADSORPTION TO GOETHITE-COATED SAND

Tao Cheng[†], Mark O. Barnett,*[†] and Eric E. Roden[‡]

Department of Civil Engineering, 238 Harbert Engineering Center, Auburn University, Auburn, AL 36849 USA, and Department of Biological Sciences, A122 Beville Bldg 7th Ave, University of Alabama, Tuscaloosa, AL 35487-0206 USA

* Corresponding author phone: +1 (334) 844-6291; fax: +1 (334) 844-6290
barnettm@eng.auburn.edu

[†] Auburn University.

[‡] University of Alabama.

Introduction

The purpose of this investigation is to describe the effects of phosphate on U(VI) adsorption onto Fe-coated subsurface materials based on our experimental data. Previously, Barnett *et al.* (2002) reported that a model independently developed to describe U(VI) adsorption to synthetic ferrihydrite can be successfully applied to predict U(VI) adsorption to heterogeneous, iron oxide-containing subsurface media. In this investigation we used goethite-coated sand to mimic natural Fe-coated subsurface materials. U(VI) adsorption onto goethite-coated sand is studied in batch experiments as a function of pH in systems closed to the atmosphere, in the presence and absence of added phosphate. A surface complexation model (SCM) is used to model the data under a range of conditions.

Experiments

Batch adsorption experiments were conducted at room temperature (~298 K) in 40-mL polycarbonate centrifuge tubes on goethite-coated sand. The samples were bubbled with N₂(g) to expel CO₂(g), and then air-tight caps were used to minimize the exchange of CO₂(g) with the atmosphere. After shaking for 48 hours, which had been established as adequate to reach equilibrium, the samples were removed from the shaker and centrifuged. The samples were opened, and the pH, aqueous phosphate and U(VI) concentrations were measured.

Modeling

All the surface complexation reactions included in our model are listed in Table 1. The reactions include acid/base properties of goethite surface (Nilsson *et al.*, 1992), phosphate surface complexation reactions (Nilsson *et al.*, 1992), and a U(VI) surface complexation reaction. A ternary surface complex involving both uranyl ion and phosphate is also required to correctly model U(VI) adsorption in the presence of phosphate. The aqueous reactions in our model include U(VI) complexation reactions with water and phosphate and the disassociation of water and phosphate acid. The aqueous U(VI) and phosphate reactions and their equilibrium constants are from Grenthe *et al.* (1992) and corrected for ionic strength.

Results

In the absence of U(VI), phosphate strongly adsorbs to the goethite-coated sand, and the extent of adsorption decreases with increasing pH (not shown). Adsorption of phosphate is

predicted by the model of Nilsson *et al.* (1992). An optimal value of 3.23 sites/nm² is used as the total surface site density. The model prediction agrees well with our experimental data for a range of solid solution ratio, pH, and total phosphate concentration so it is adopted in our model to calculate phosphate adsorption.

In the absence of phosphate, the percentage of U(VI) adsorbed increases sharply with increasing pH (Figure 1, 2). Higher solid/solution ratio shifts the pH edge to left, indicating more U(VI) adsorption at the same pH due to a higher concentration of available surface sites. U(VI) adsorption in the absence of phosphate is modeled using the U(VI) surface complexation reaction and stability constant in Table 1. The stability constant of U(VI) adsorption onto goethite surface is determined to be log K = - 4.66 by FITEQL 4.0. The model gives a reasonable fit and prediction of the experimental data (Figure 1, 2, long dash lines).

The addition of phosphate greatly increases U(VI) adsorption in the low pH range, shifting the pH edge to the left (Figure 1, 2). Payne *et al.* (1996) reported increased U(VI) adsorption onto ferrihydrite in the presence of 10⁻⁴ M phosphate in low pH range of 3.0 to 6.0. A ternary surface complex in the form of >FeLM is required to correctly model U(VI) adsorption in the presence of phosphate. The stoichiometry of the purposed ternary species is listed in Table 1. The stability constant of the ternary surface complex is obtained as log K = 10.60 by FITEQL 4.0. At a solid/solution ratio of 33.3 g/L, the shape of the pH edge predicted by the model is in agreement with the experimental results for the whole pH range (Figure 1). At a solid/solution ratio of 3.33 g/L, the model correctly predicts the pH edge for both total phosphate concentrations in the range of pH < 7.0, and indicates the pH edge for those two phosphate concentrations will overlap, which agrees with our experimental data (Figure 2). At pH > 7.0, the model predicts some decrease in U(VI) adsorption, however, the model fails to generate the shape of the experimental adsorption edge at pH > 7. The disparity between model prediction and experimental data at high pH is attributed to the under-estimation of the formation of aqueous U(VI)-phosphate species in the current database. Surface speciation calculation by our model also indicates the formation of the ternary surface complex is highly pH-dependent. At low pH, the dominant U(VI) surface species is the ternary surface complex, as pH increases, binary U(VI) surface complex becomes dominant.

Table 1. Surface complexation reactions of the model (T = 298 K, I = 0.1 M, constant capacitance model (CCM) with a specific capacitance of 1.28 F/m²)

	log K
Acid/base Properties of Goethite Surface	
>FeOH + H ⁺ ↔ >FeOH ₂ ⁺	7.47
>FeOH ↔ >FeO ⁻ + H ⁺	-9.51
Phosphate Surface Complexation Reactions	
>FeOH + H ₂ P O ₄ ⁻ + H ⁺ ↔ >FePO ₄ H ₂ + H ₂ O	12.68
>FeOH + H ₂ P O ₄ ⁻ ↔ >FePO ₄ H ⁻ + H ₂ O	7.93
>FeOH + H ₂ P O ₄ ⁻ ↔ >FeP O ₄ ²⁻ + H ⁺ + H ₂ O	2.16
U(VI) Surface Complexation Reaction	
>Fe(OH) ₂ + UO ₂ ²⁺ ↔ (>FeO ₂)UO ₂ ⁰ + 2H ⁺	-4.66
U(VI)-phosphate Surface Complexation Reaction	
>FeOH + UO ₂ ²⁺ + H ₂ PO ₄ ⁻ ↔ >FePO ₄ UO ₂ + H ₂ O + H ⁺	10.60

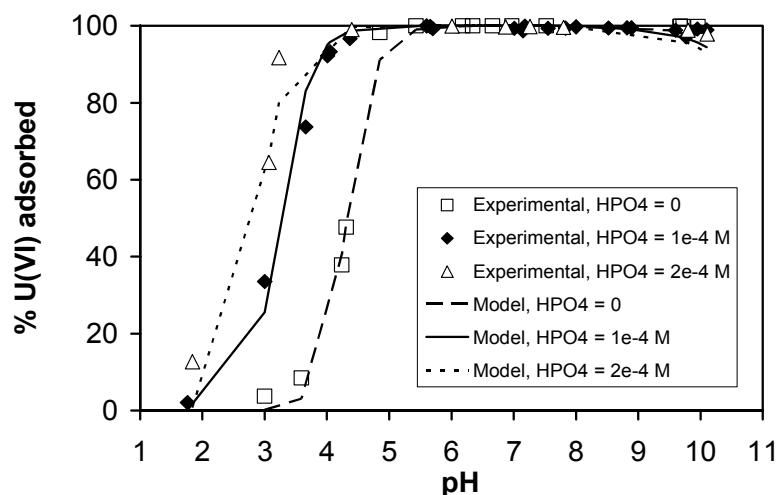


Figure 1. Adsorption of $5 \cdot 10^{-6}$ M U(VI) onto goethite-coated sand at solid/solution ratio of 33.3 g/L in the absence of phosphate (open squares) and at phosphate concentration of 10^{-4} M (filled diamonds) and $2 \cdot 10^{-4}$ M (open triangles). $I = 0.1$ M, $K = \sim 298$ K. The lines are model prediction.

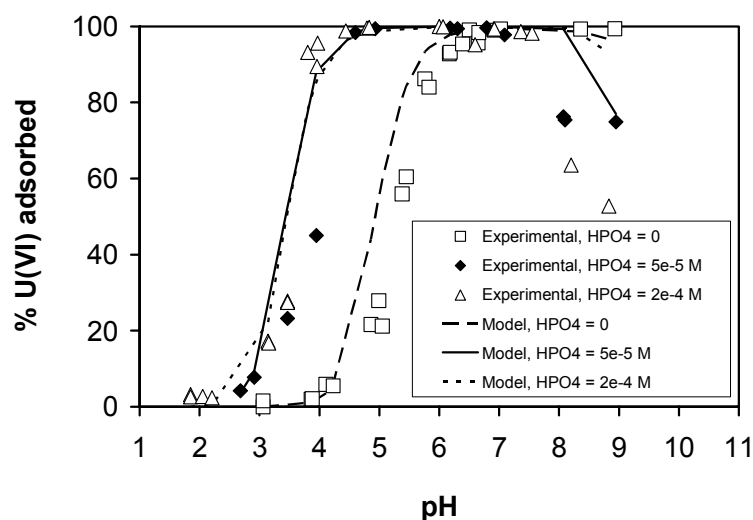


Figure 2. Adsorption of $5 \cdot 10^{-6}$ M U(VI) onto goethite-coated sand at solid/solution ratio of 3.33 g/L in the absence of phosphate (open squares) and at phosphate concentration of $5 \cdot 10^{-5}$ M (filled diamonds) and $2 \cdot 10^{-4}$ M (open triangles). $I = 0.1$ M, $K = \sim 298$ K. The lines are model prediction.

References:

- Barnett, M. O., P. M. Jardine, *et al.* (2002). "U(VI) Adsorption to Heterogeneous Subsurface Media: Application of a Surface Complexation Model." Environmental Science and Technology **36**: 937-942.
- Grenthe, I. (1992). Chemical Thermodynamics of Uranium. Elsevier Science, New York, NY.
- Nilsson, N., L. Lovgren, *et al.* (1992). "Phosphate Complexation at the Surface of Goethite." Chemical Speciation and Bioavailability **4**(4): 121-130.
- Payne, T. E., J. A. Davis, *et al.* (1996). "Uranium Adsorption on Ferrihydrite - Effects of Phosphate and Humic Acid." Radiochimica Acta **74**: 239-243.

LABEL-FREE *IN SITU* DETECTION OF ADSORPTION PROCESSES BY ACOUSTIC WAVE-BASED SENSORS

Reiner Dahint

Angewandte Physikalische Chemie
Universität Heidelberg
Reiner.Dahint@urz.uni-heidelberg.de

In recent years, the growing demand for medical and environmental diagnostic tools has stimulated the investigation of new sensor concepts for liquid phase analysis. Particularly, the accurate identification of (bio)chemical species, and their interaction with both natural and artificial surfaces have been a major topic of interest. Although well-established analytical techniques have proven to be highly sensitive and selective – such as radio immunoassays (RIA) and enzyme-linked immunosorbent assays (ELISA) in case of biomolecules – they often involve time-consuming multi-stage processes (Fig. 1). Thus, they are not suitable for on-line monitoring and the direct determination of adsorption kinetics. Moreover, in case of label-based detection methods, it has to be guaranteed that the introduction of marker molecules does not significantly change the properties of the system under study. In contrast, (bio)chemical sensors facilitate the *in situ* detection of dissolved molecules in real time, and can be used for the study of both specific interactions and non-specific adsorption processes.

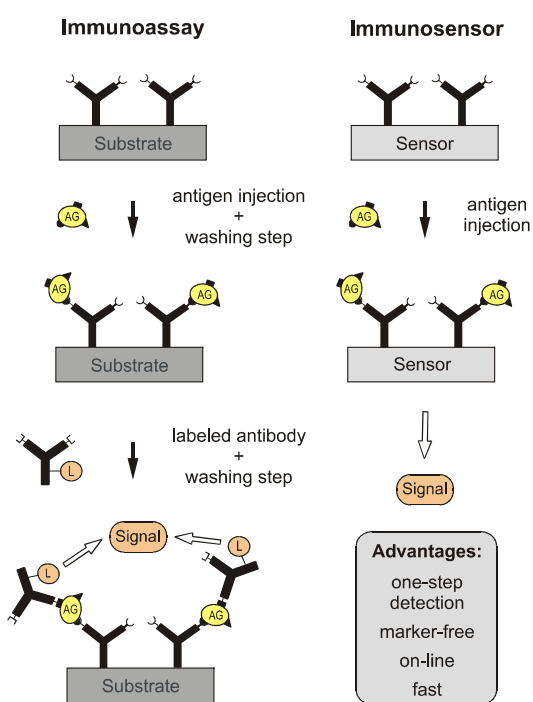


Fig. 1: Comparison of a traditional sandwich immunoassay and an immunosensor, i.e. a sensor for the specific detection of biomolecules. Both technologies involve the same surface chemistry. However, while the immunoassay requires several incubation and washing steps as well as the use of labeled molecules, the immunosensor facilitates a one-step detection of marker-free analytes.

In the picture, “AG” (abbreviation for antigen) denotes the target species captured by the immobilized receptors (usually surface bound antibodies). “L” indicates the label of the added secondary antibody, which binds to another surface marker of the analyte, and is crucial for the detection process.

Present approaches to the development of (bio)chemical sensors include optical fiber technology, surface plasmon resonance (SPR), and electrochemistry. Over the past decade, there has also been a great deal of interest in the development of acoustic wave-based liquid sensors. Promising features of these devices are their robustness, their compatibility with integrated circuits, the opportunity to realize low-cost sensors in miniature packages and their high surface sensitivity. For example, the penetration depth of a 300 MHz shear horizontally (SH) polarized acoustic wave into an adjacent aqueous solution is only about 30 nm and, thus, almost one order of magnitude shorter than the decay length in optical techniques utilizing He/Ne light sources. Such way, bulk liquid effects on sensor response can be drastically reduced. However, detection in liquid environments has proven to be difficult due to various

reasons ranging from the type of acoustic wave used to the sensor coating. A major problem in device design is, e.g., the damping of the acoustic wave upon liquid contact: only acoustic waves with surface-parallel polarization will propagate along the solid/liquid interface without suffering excessive losses.

A number of acoustic wave devices have been investigated for liquid-phase (bio)chemical sensors (Fig. 2), such as thickness shear mode (TSM) resonators, SH polarized acoustic plate modes (APMs), surface acoustic waves (SAWs) with exclusively SH particle displacements, lamb (or flexural plate) waves, and Love waves. Among the various types of acoustic wave sensors, APM devices offer the opportunity to strictly separate the sensor electrodes from the sensing surface, thus, avoiding any corrosion problems, facilitating surface derivatization and enhancing device stability.

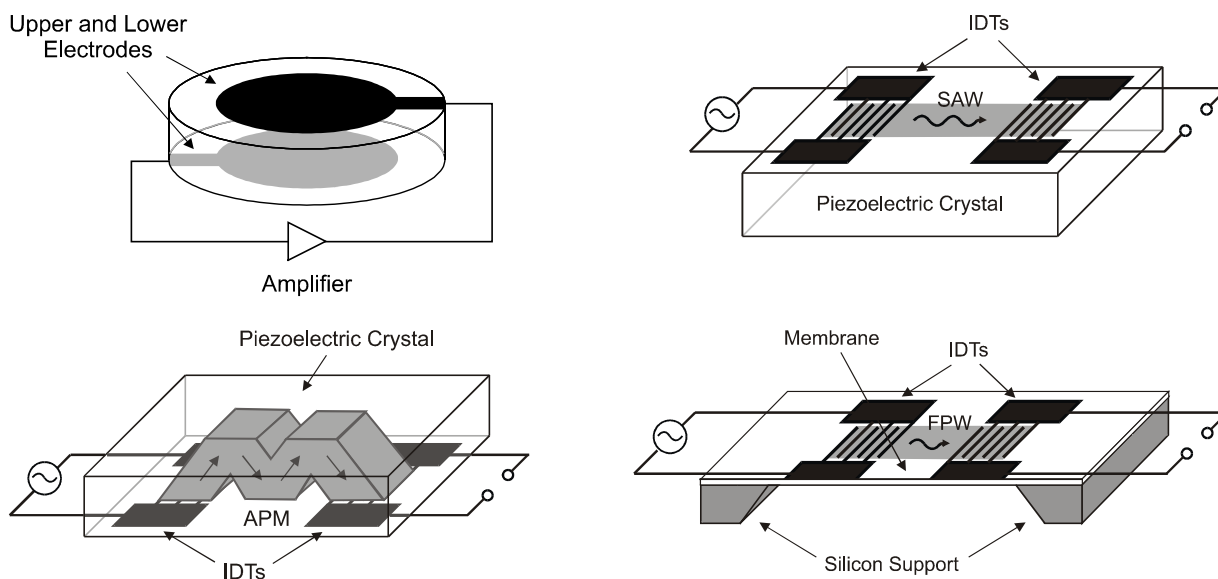


Fig. 2: Different types of acoustic wave-based sensors (schematic): Thickness shear mode (TSM) resonator (upper left), surface acoustic wave (SAW) device (upper right), acoustic plate mode (APM) device (lower left), and flexural plate wave (FPW) device (lower right).

The different mechanisms of interaction used in acoustic wave sensors fall into two major categories: *mechanical effects*, which are based on mass accumulation at the sensing surface and/or changes in the viscoelastic material properties, and *acoustoelectric interactions*, which are due to changes in the electric and/or dielectric material constants. Although recent research in acoustic wave-based liquid sensors indicates that experimental situations exist, where viscoelastic effects significantly contribute to the response of the device, it is widely accepted that mass loading is one of the primary interaction mechanism in molecule detection. The selection of an appropriate sensor platform for protein detection will, therefore, mainly be based on mass sensitivity considerations and handling aspects. Fig. 3 compares the mass sensitivity of the different sensor configurations as a function of device frequency.

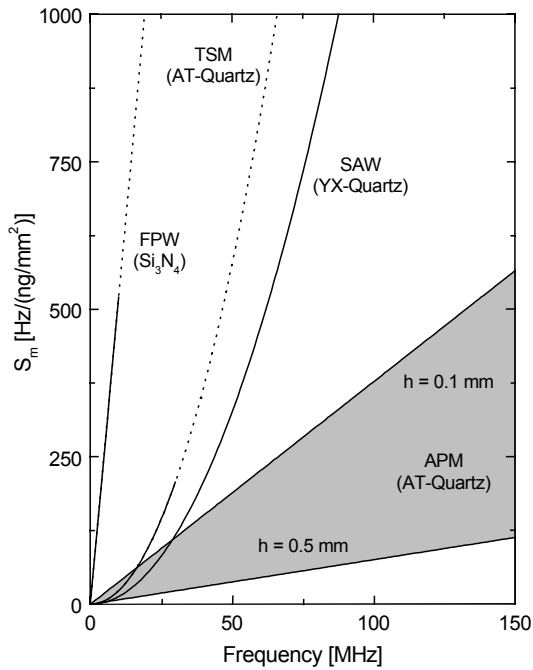


Fig. 3: Mass sensitivity of different acoustic wave-based sensors. Dotted lines indicate a frequency range, which is usually not accessible for this specific type of device. h denotes the plate thickness of the APM device.

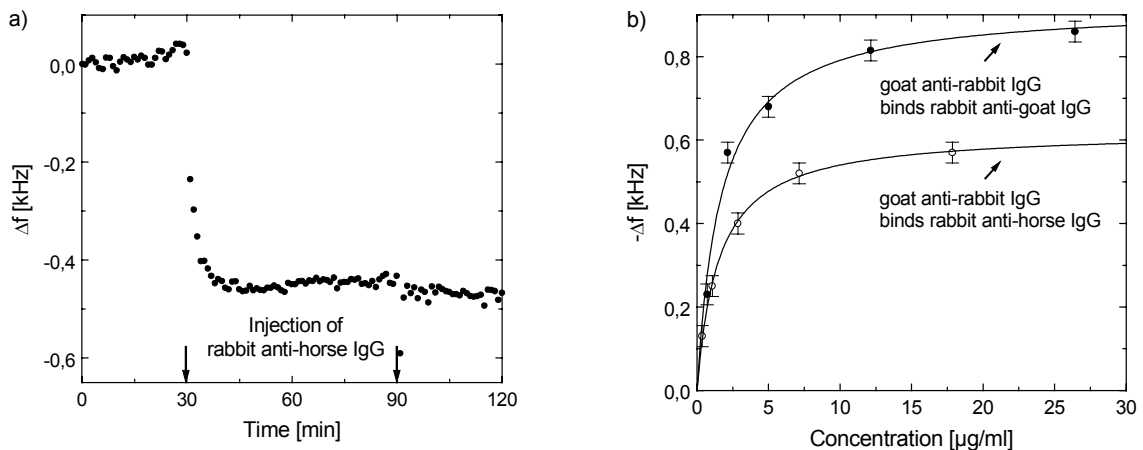


Fig. 4: Response of a 150 MHz APM sensor on 0.5 mm ZX-LiNbO₃ towards antigen/antibody reactions. a) Rapid detection of rabbit anti-horse IgG binding to immobilized goat anti-rabbit IgG. b) Sensor response as a function of antigen concentration for two antigen/antibody systems with different binding ability.

In order to evaluate the potential of APM sensors for the specific detection of biomolecules, receptors have been covalently immobilized on the sensing surface via aminosilane and glutaraldehyde. A dual delay line configuration was used, in which a reference line serves to correct the sensor response for spurious effects such as changes in the bulk liquid properties, non-specific protein adsorption and temperature variations. Fig. 4 shows the *in situ* detection of the binding process in real time, as well as the obtained steady state values for different concentrations of analyte in solution. From the latter curves, the respective binding constants can be derived. It has been demonstrated that specific molecule detection is also possible in complex liquid environments such as human plasma.

Non-specific protein adsorption is another important topic in biomedical technology. While specific adsorption processes are used to detect target molecules in solution, non-specific protein adsorption is one of the major effects that limit the accuracy of these analytical methods. Non-specific protein/surface interactions are also crucial in the development of

medical products such as catheters, prostheses and contact lenses, as they determine the biocompatibility of synthetic coatings in contact with biological fluids. Fig. 5 shows the detection of non-specific fibrinogen adsorption on hydrophobic, methyl-terminated surfaces. From the measured adsorption kinetics at different fibrinogen concentrations, the time constants for both adsorption and unfolding of the proteins have been determined.

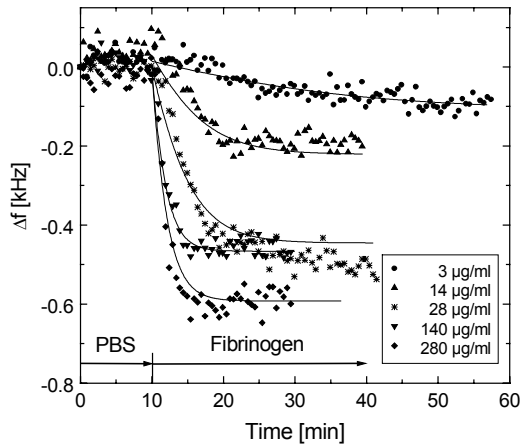


Fig. 5: Adsorption of fibrinogen at methyl-terminated surfaces is monitored for different concentrations of protein. A protein resistant sensor line coated with hexa(ethylene glycol) serves as an internal reference. It is observed that the steady state frequency shifts strongly depend on protein concentration. From the adsorption kinetics, the time constants for adsorption and unfolding of the proteins have been derived.

In summary, the investigations demonstrate that acoustic wave-based sensors are promising tools for the *in situ* detection of specific and non-specific adsorption processes. As direct, single-step analytical techniques they are intrinsically fast, facilitate real time measurements and abstain from the introduction of marker molecules, which may have a major impact on the behavior of the (bio)chemical system under study. Moreover, they are versatile detection methods, which may be applied to a variety of problems by adjusting the specific surface chemistry used, and provide the opportunity to implement miniaturized sensor systems.

ERROR CAUSES IN THE DETERMINATION OF THE ACID-BASE REACTIVITY OF OXI-HYDROXIDES

M. Duc, G. Lefèvre and M. Fedoroff

Centre d'Etudes de Chimie Métallurgique
C. N. R. S.
15, rue Georges Urbain
94407 Vitry
France
fedoroff@glvt-cnrs.fr

Introduction

The long term safety of radioactive waste depositories is based on the sorption of radionuclides from underground water onto engineered and natural barriers. For a quantitative prediction of the migration in such barriers, we need accurate sorption data. Models should be in agreement with the sorption mechanism. Surface complexation is the most often used model for oxides and hydroxides. In fact, there are several types of surface complexation models such as 1-pK and 2-pK monosite, 1-pK and 2-pK multisite, pK-distribution models. Furthermore, there are several ways to describe the distribution of the electrostatic potential in the vicinity of the solid surface (CCM, DLM, BSM, TLM,...). However, all these models are based on the acid-base properties of superficial hydroxide or oxide groups of the solid. It is necessary to determine the surface charge versus pH (titration curves), the point of zero charge (pzc), the surface density of sites active towards protons and hydroxides in aqueous solutions, the acid-base constants of these sites. These parameters are then used for calculating the sorption constants of ions other than protons and hydroxide ions. It is therefore important to determine these parameters very accurately.

A comparison of acid-base parameters published in the literature shows a large scatter for the "same" oxides [1,2]. Several causes could explain this scatter. One reason is the use of different models, each electrostatic models leading to different values of site density and constants. However, titration curves and pzc are independent of the model chosen. Another reason may be uncontrolled differences in the composition and purity of oxides. Finally, other causes could be found in the titration procedure, in the solubility and the stability of the solid. In order to understand more about the acid-base properties of oxides and about the origin of the discrepancies between measurements, we have performed a systematic experimental study of several parameters: titration procedure, kinetics of the sorption and desorption of protons during titration, solubility of the solid, evolution of the solid with time, influence of impurities. Finally, we have evaluated the consequences of these factors on modeling and determining the acid-base parameters.

Titration procedure

Several parameters, such as the nature of electrodes, methods of standardization, problem of salt release from the electrode, problem of pH measurement in a suspension, method of "blank" deduction, have been studied. All these parameters have a more or less pronounced effect on the results, but their optimization limits the errors, especially if compared to other causes of error.

Kinetics of titration

As an example, we show the variation of pH after an addition of acid during titration of a suspension of alumina, silica or goethite (Fig. 1). The delay to obtain an equilibrium value depends on the solid and is connected to several factors such as its porosity. For this type of alumina, a delay of 1 hour is needed after each addition, otherwise the pH and calculated

surface charge do not correspond to equilibrium values. Modeling kinetic curves showed that after a fast step of proton uptake, a slower, more or less important and diffusion controlled step takes place. The effective diffusion coefficients (from 10^{-20} to 10^{-12} $\text{m}^2 \cdot \text{s}^{-1}$) depend on the porosity of the solid.

Solubility of the solid

Species dissolved in solution may react with other ions present in this solution and lead to precipitation, either in the bulk of the solution, or on the surface of the solid. Even if precipitation does not take place, dissolution has an effect on the pH during titration experiments and, hence, on the calculated surface charge. A correction for dissolution must be applied, taking into account the speciation of dissolved species. In the case of the titration of γ -alumina (Fig. 2) [3], the surface charge not corrected for dissolution seems to increase continuously with increasing H^+ concentration in solution. After correction, Q_{cor} achieves a maximum, which corresponds to the surface density of active sites.

In the case of hydroxyapatite, this problem is much more important. A non negligible solubility takes place in a large pH range. Furthermore, solubility is incongruent: the Ca/P and Na/P ratios in the solution are not equal to these ratios in the solid, and vary with pH. The effect on surface charge calculation is so strong, that its correction leads to very large errors on the corrected surface charge.

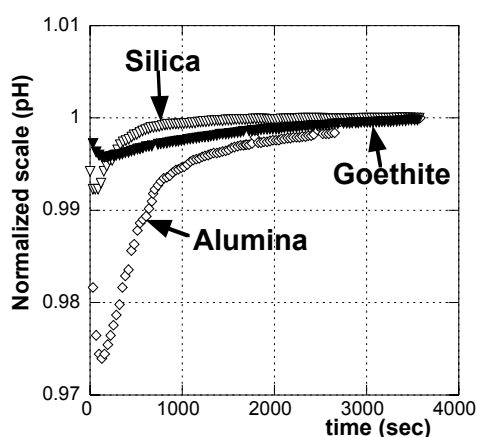


Fig. 1 Kinetics of proton sorption during titration of γ -alumina, silica and goethite by a nitric acid solution. Variation of pH (normalized scale) versus time after addition of an aliquot of acid.

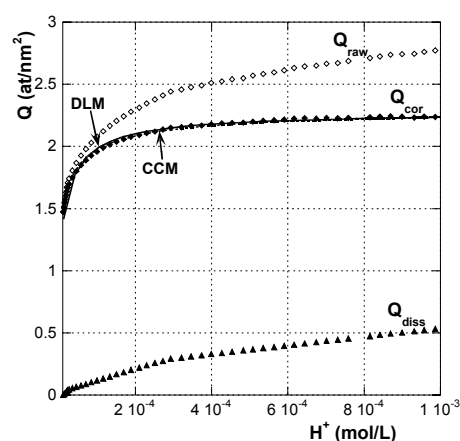


Fig. 2 Apparent surface charge of γ -alumina without solubility correction Q_{raw} , after solubility correction Q_{cor} and contribution of solubility to surface charge Q_{diss} versus H^+ concentration with fitting by the constant capacitance (CCM) and diffuse layer (DLM) models

Evolution of the solid

It is well known from geological processes, that mineral species are subject to alteration, dissolution, recrystallization. However, the quantitative impact of such processes on the long term efficiency of sorption barriers is difficult to estimate, although some information can be deduced from thermodynamic data on the stability of minerals and through exchange of knowledge between chemists and geologists.

An example is the large decrease of the density of active sites when γ -alumina is kept in water (Fig. 3) [4]. Investigation by X-ray diffraction, scanning electron microscopy (SEM), TGA and DTA showed that this modification of surface reactivity is induced by a transformation of γ -alumina into bayerite ($\text{Al}(\text{OH})_3$).

Influence of impurities

Impurities and, especially, surface contaminations, can hide the "intrinsic" surface reactivity of a solid. We show on Fig. 4 the influence of a washing procedure, including treatments by acid and basic solutions, on the titration curves of goethite and hematite. Impurities and removed elements were determined by ICP-OES. This procedure removes species such as carbonates and sulfates, shifts the titration curves and, hence, the calculated surface charge and the pzc. Sorption and desorption processes of impurities lead also to hystereses in the titration curves.

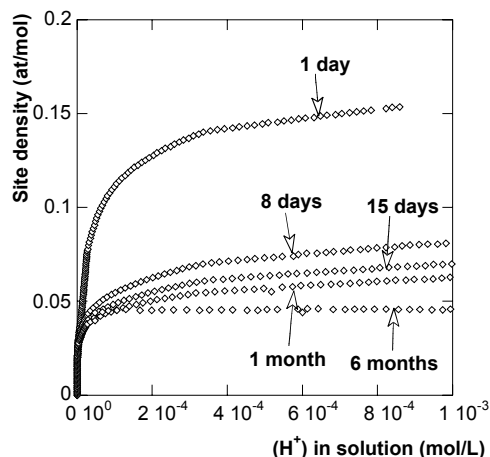


Fig. 3 Variation of the density of sorption sites on γ -alumina versus (H^+) activity in water, for several times of treatment in water

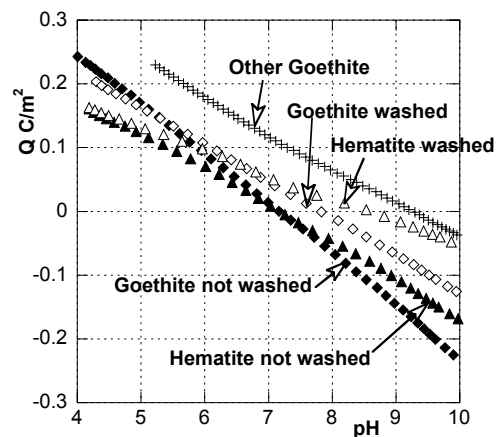


Fig. 4 Influence of washing on surface charge Q versus pH for goethite and hematite

Conclusion

All these effects can completely hide the real acid-base properties of a solid and, consequently, give an erroneous interpretation of the sorption of species other than protons and hydroxide ions. They have large effects on pzc, site density, acid-base constants. As an example, the presence of impurities can shift the pzc by several units. Therefore, use of pure solids with well known composition and structure, together with a systematic and careful control of all these effects is required before trying to determine the "intrinsic" acid-base parameters.

References:

- [1] M. Kosmulski, Colloids and Surfaces A: Physicochem. Eng. Aspects 222, 113 (2003)
- [2] V. Brendler, RES³T – Rossendorf Expert System for Surface and Sorption Thermodynamics (2003)
- [3] G. Lefevre, M. Duc, M. Fedoroff, J. Colloid Interface Sci., 269, 274 (2004)
- [4] G. Lefevre, M. Duc, P. Lepeut, R. Caplain, M. Fedoroff, Langmuir, 18, 7530 (2002).

INTERACTION OF TRIVALENT ACTINIDES WITH MINERAL SURFACES: TRLFS STUDIES

T. Fanghänel, T. Rabung and T. Stumpf

Institut für Nukleare Entsorgung
Forschungszentrum Karlsruhe
Germany

For the long-term performance assessment of nuclear waste repositories, knowledge concerning the interactions of actinide ions with mineral surfaces is imperative. The mobility of released radionuclides is strongly dependent on the sorption/desorption processes at mineral surfaces. Therefore, it is necessary to characterise the surface species formed and to elucidate the reaction mechanisms involved. Insight into the sorption mechanisms and identification of surface species is of cardinal importance for a reliable predictive modeling of sorption reactions. Time resolved laser fluorescence spectroscopy (TRLFS) allows due to its high fluorescence yield speciation studies of Cm(III) in the nanomolar concentration range. Exemplary the results of TRLFS studies for the interaction of Cm(III) with three different minerals are presented.

Sorption of Cm(III) onto γ -alumina

The sorption of Cm(III) onto γ -Al₂O₃ is investigated by time-resolved laser fluorescence spectroscopy (TRLFS) at a constant ionic strength of 0.1 M NaClO₄. Sorption experiments are carried out in a glove box under argon atmosphere in the pH range between 3.5 and 13 and at a Cm(III) concentration of 2.5×10^{-7} mol/L. Fig. 1 shows the evolution of the TRLFS spectra with increasing pH. Spectra are normalized to the same peak area. A red shift of the Cm(III) fluorescence emission band indicates the formation of inner-sphere surface complexes up to pH=13.2.

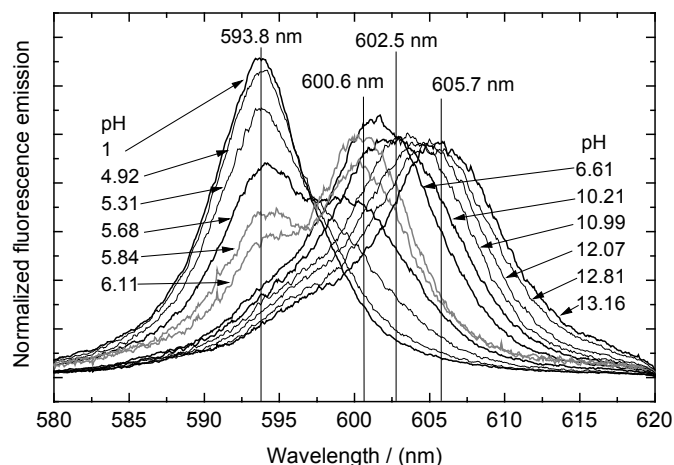


Fig. 1: Fluorescence emission spectra of 2.5×10^{-7} mol/L Cm(III) in 0.57 g/L aqueous γ -Al₂O₃ suspension (0.1 M NaClO₄) at various pH; spectra are scaled to the same peak area.

Three different surface-sorbed Cm(III) species are identified by their emission spectra with peak maxima at 600.6 nm, 602.5 nm, and 605.7 nm appearing at different pH regions. No change in the time dependence of the emission decay can be observed for the three sorbed species (constant lifetimes of 110 μ s). Inner-sphere monodentate complexation is assumed for

the first complex: $[\equiv\text{Al-O-Cm}]^{2+}(\text{H}_2\text{O})_5$. The other two surface-sorbed species dominant at higher pH are attributed to consecutive hydrolysis of the monodentate complex. The results of the pH dependent species distribution obtained from peak deconvolution of emission spectra are correlated with the results of earlier Eu(III)/Am(III) sorption experiments and with the aqueous Cm(III) speciation. A first attempt to the thermodynamic modeling of the experimental data over the whole pH range is included and the possible influence of a modification of the alumina surface with pH is discussed.

Sorption of Cm(III) onto clay minerals

The evolution of the fluorescence emission spectra of $3 \cdot 10^{-7}$ mol/L Cm(III) with 0.25 g/L smectite in aqueous suspension at various pH shows at $\text{pH} \leq 4.6$ only the signal of the Cm(III) aquo ion. At $\text{pH} \geq 5.24$, the intensity of the 593.8 nm peak decreases and two other peaks appear with maxima at 598.8 nm ($\text{pH} \geq 5.24$) and 603.3 nm (for $\text{pH} \geq 7.15$). Comparable evolution is observed for the kaolinite suspension. It is remarkable that, in case of smectite and kaolinite, the spectra of the sorbed Cm(III) species at low pH (≤ 5) show no difference to spectra of the Cm(III) aquo ion. This observation indicates that at pH values ≤ 5 the sorbed Cm(III) ion retains its hydration sphere. Such a sorption process suggests outer-sphere complex formation on the interlayer sites.

The red shift of the fluorescence emission of Cm(III) at higher pH (> 5) in the smectite suspension is caused by a change in the ligand field of the Cm(III) ion and indicates inner-sphere complex formation. A peak deconvolution was carried out to resolve the individual species from the composite fluorescence emission spectra at $\text{pH} \geq 5$. Three different species have been identified. In addition to the Cm(III) aquo ion, two different inner-sphere Cm(III) surface complexes are formed. All measured spectra have been deconvoluted using pure component spectra with peak maxima at 598.8 nm and 603.3 nm. The results are illustrated in Fig. 2.

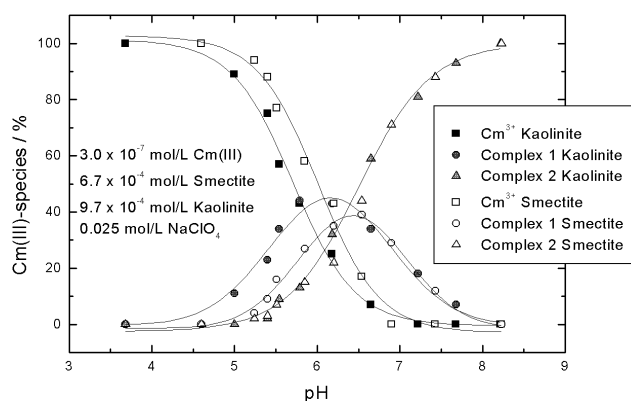


Fig. 2: Speciation plot of the Cm(III)/clay system.

The fluorescence emission lifetime of Cm(III) in the clay suspensions at various pH was determined. In both cases at $\text{pH} \leq 5$, the number of water molecules in the first co-ordination shell of the Cm(III) was found to be 9. This proves that the outer-sphere complex has not only the same fluorescence emission spectrum as the Cm(III) aquo ion, but also the same number of water molecules in the first co-ordination shell of curium. The fluorescence lifetimes of the formed kaolinite, smectite and γ -alumina inner-sphere complexes are very similar. The lifetime of 110 ± 7 μs corresponds to five water molecules in the first co-ordination shell of the sorbed Cm(III).

Interaction of Cm(III) with calcite

Selected fluorescence emission spectra of Cm(III) (8.9×10^{-8} mol/L) in calcite suspension (1.0 g/L) measured at different contact times are presented in Fig. 3.

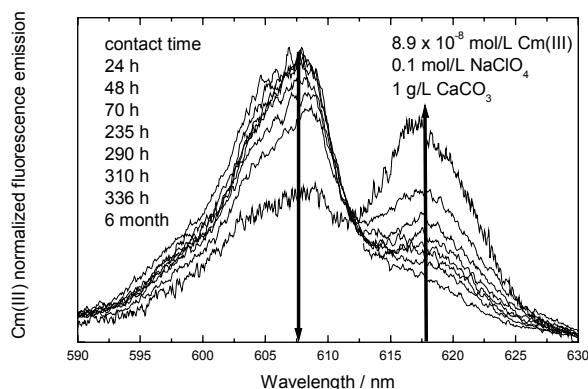


Fig. 3: Fluorescence emission spectra of Cm(III) in aqueous calcite suspension at various contact times; spectra are scaled to the same peak area.

All spectra show two peak maxima at 607.5 nm and 618.0 nm. These two emission bands can be assigned to two different Cm(III)/calcite species. With increasing contact time the fluorescence intensity of the first species decreases and the intensity of the second species increases. The spectrum of this first sorption complex in the calcite system is very similar to the spectrum of the Cm(III) tetracarbonato complex in solution. However, the formation of $\text{Cm}(\text{CO}_3)_4^{5-}$ can be ruled out under the present conditions. The formation of detectable amounts of the tetracarbonato complex in solution requires orders of magnitude higher carbonate concentration ($\log[\text{CO}_3^{2-}] > -2$) as present in the calcite suspension. As both species, the first Cm(III)/calcite sorption species and the Cm(III) tetracarbonato complex in solution, show almost identical emission bands we conclude that the ligand field and hence the first coordination sphere should be very similar in both species. The unusual extraordinary red shift of the fluorescence emission of the second Cm/calcite complex with a peak maximum at 618.0 nm indicates a considerable large change of the ligand field of the actinide ion which could be caused by a change in the coordination number of Cm(III).

In Fig. 4 the fluorescence intensity (in logarithmic scale) is plotted as a function of the delay time. The relaxation follows a bi-exponential decay law.

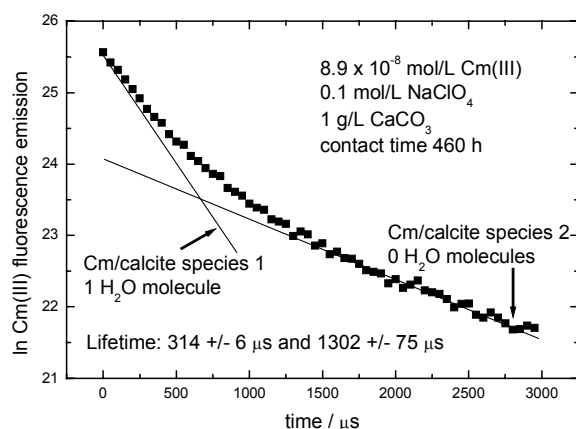


Fig. 4: Time dependency of the fluorescence emission decay of Cm(III) in aqueous calcite suspension.

For the first Cm(III) sorption species a lifetime of $\tau = 314 \pm 6 \mu\text{s}$ and for the second species $\tau = 1302 \pm 75 \mu\text{s}$ have been determined. The second value is very close to the calculated radiative lifetime for Cm(III). Hence, the excited state is not quenched by OH vibrations. Applying the linear correlation between the decay rate $k_{\text{obs}} [\text{ms}^{-1}]$ (reciprocal lifetime of the excited state) and the number of water molecules in the first coordination sphere of the Cm(III) species

$$n(\text{H}_2\text{O}) = 0.65k_{\text{obs}} - 0.88$$

it follows, that the first species contains one water molecule in the first coordination sphere, while the second species has lost its complete hydration sphere. This is a clear indication for the incorporation of the Cm(III) into the bulk structure of the calcite lattice. This spectroscopic investigation reveals for the first time the spontaneous incorporation of an actinide into a mineral in the trace concentration range and underline the high potential of the speciation method TRLFS.

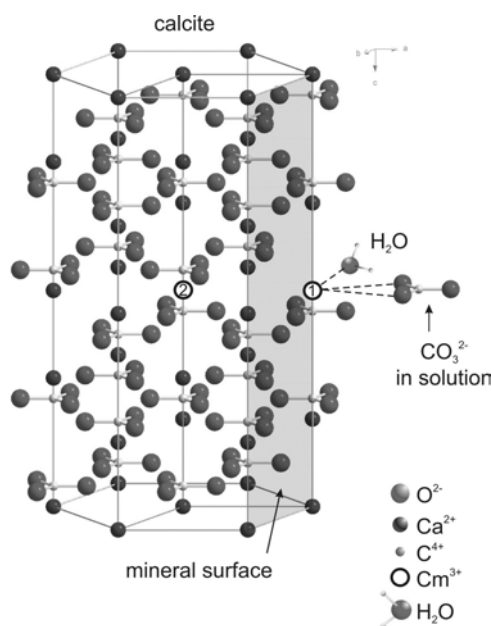


Fig. 5: Schematic diagram of the structure of Cm(III)/calcite incorporation species.

References:

- T. Stumpf, T. Rabung, R. Klenze, H. Geckeis, J. I. Kim: A spectroscopic study of the Cm(III) sorption onto γ -Alumina, *J. Colloid Interface Sci.*, 238, 219, (2001)
- T. Stumpf, A. Bauer, F. Coppin, J. I. Kim: *Time-Resolved Laser Fluorescence Spectroscopy (TRLFS) Study of the Sorption of Cm(III) onto Smectite and Kaolinite*, *Environ. Sci. Technol.*, 35, 3691, (2001)
- T. Stumpf, T. Fanghänel: A Time-Resolved Laser Fluorescence Spectroscopy (TRLFS) Study of the Interaction of Trivalent Actinides (Cm(III)) with Calcite. *J. Colloid Interface Sci.*, 249, 119 (2002)
- T. Kimura, G. R., Choppin: Luminescence Study on Determination of the Hydration Number of Cm(III). *J. Alloys Comp.*, 213/214, 313 (1994).

SORPTION MECHANISMS AND SORPTION MODELS

M. Fedoroff¹, G. Lefevre¹, M. Duc¹, S. Milonjić², C. Neskovic¹

¹ Centre d'Etudes de Chimie Métallurgique, C. N. R. S.
15, rue Georges Urbain, 94407 Vitry, France

² Vinča Institute of Nuclear Sciences, P.O. box 522, 11001 Beograd, Serbia and Montenegro
fedoroff@glvt-cnrs.fr

Introduction

Sorption at the solid-liquid interfaces play a major role in many phenomena and technologies: chemical separations, catalysis, biological processes, transport of toxic and radioactive species in surface and underground waters. The long term safety of radioactive waste repositories is based on artificial and natural barriers, intended to sorb radionuclides after the moment when the storage matrixes and containers will be corroded. Predictions on the efficiency of sorption for more than 10^6 years have to be done in order to demonstrate the safety of such depositories, what is a goal never encountered in the history of sciences and technology.

For all these purposes, and, especially for the long term prediction, acquiring of sorption data constitutes only a first step of studies. Modeling based on a very good knowledge of sorption mechanisms is needed. In this review, we shall examine the main approaches and models used to quantify sorption processes, including results taken from the literature and from our own studies. We shall compare sorption models and examine their adequacy with sorption mechanisms. The cited references are only a few examples of the numerous articles published in that field.

Distribution coefficients

A first approach to quantify sorption processes is the use of the "distribution coefficient", generally noted K_d or R_d , which is the ratio of the concentration of the element in the solid phase to its concentration in the aqueous phase, K_d representing an equilibrium value for some authors. K_d is used in the calculation of the migration of an element through the retardation factor R , which is the ratio of the velocity of water to the velocity of the element through the same volume [1,2]. K_d data bases have been constituted for use in transport calculations [3].

However, K_d values depend very much on the experimental conditions: temperature, concentration of the element, pH, influence of complexing agents and competing elements, kinetics. Therefore, extrapolation of K_d values to scales larger than those of laboratory experiments, especially to natural systems, may be hazardous.

Empirical linear or non linear expressions of the concentration of competing elements have been proposed for the calculation of K_d [4]. However, these expressions are valid only for certain experimental conditions.

Sorption isotherms

An isotherm represents the variation of the concentration of the element in the solid phase, or the variation of K_d , versus the equilibrium concentration of the element in the aqueous solution, at a constant temperature. An equilibrium of sorption is supposed to be achieved, but apparent isotherms are often used. Isotherms are fitted by several mathematical models, which have some theoretical bases, but are often used as empirical ones. Among the most used

models are the Langmuir isotherm [5], derived from the sorption of gas molecules on a solid, whose sites have equal sorption energy, the Dubinin-Radushkevitch isotherm [6] and the Freundlich isotherm [7], both with non homogeneous sorption sites. We shall give examples of fitting sorption data by these isotherms.

Although sorption isotherms include the influence of element concentration, they depend on many other parameters and are generally used as empirical models.

Sorption models

In order to quantify more accurately sorption data, several models have been developed. They are based on hypotheses on the sorption mechanisms and suppose that thermodynamic equilibrium is achieved. Theoretically, they are able to predict K_d values of an element taking into account competing elements and complexing agents.

Ion exchange model

This model is based on the mass-action law, quantifying the exchange of ions between the solid and the solution. No hypotheses have to be done on the real mechanisms at the atomic scale.

The problem arising in calculating the thermodynamic exchange constant is that the activity coefficients in the solid phase cannot be calculated a priori. Therefore, a "corrected selectivity coefficient" K_c is defined, from which the activity coefficients in the solid phase are excluded. K_c may be almost constant in some cases, but, generally, it varies when the concentration in the solid is increasing. The thermodynamic constant, the variations of the activity coefficients in the solid and the free energy can be calculated from the Gaines-Thomas equation [8].

We shall indicate how to interpret the variation of K_c with the concentration in the solid, by considering the partition function $Q = \sum_j \exp\left(\frac{-E_j}{kT}\right) = \exp\left(\frac{-G}{RT}\right)$ where E_j is the energy of each level in the solid and G the free energy [9].

As an example, the variation of $\ln(K_c)$ with the Sr^{2+} concentration in polyantimonic acid $\text{H}_2\text{Sb}_2\text{O}_6$ [10] shows first a constant value and then a linear decrease (Fig. 1), corresponding to the successive substitution of two types of sites in the solid.

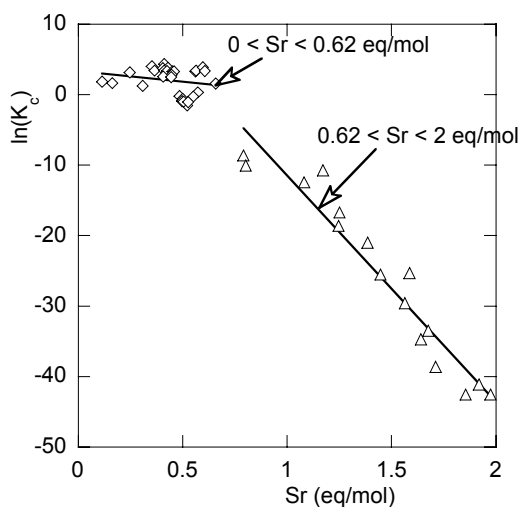


Fig. 1. Variation of $\ln(K_c)$ versus Sr^{2+} concentration in polyantimonic acid, with successive occupation of two different sites

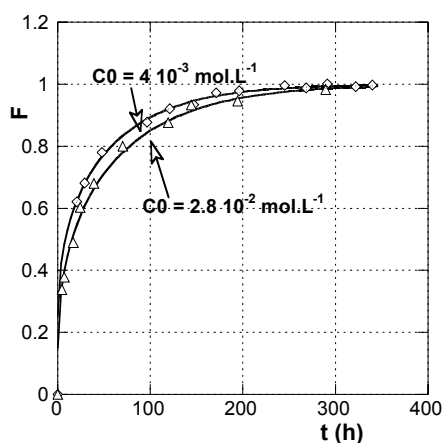


Fig. 2 Kinetics of Sr^{2+} sorption on polyantimonic acid. Variation of the achievement factor F versus time for two initial concentrations C_0 of Sr, with fitting by a diffusion law

Surface complexation models

These models were developed for oxyhydroxides. They are based on the acid-base properties of superficial hydroxide groups of these solids. Several types of such models were developed: the monosite 2-pK and 1-pM models, the multisite 1-pK model, the pK-distribution model.

We shall compare these models and their consequences on the quantification of sorption. The "monosite 2-pK model" [11] assumes that the surface is covered by one type of hydroxide groups with amphoteric properties, leading to two equilibria with protons. The 1-pK "Multisite complexation model" or "Music" [12], considers that the surface presents several families of oxide and hydroxide sites, each one with a specific acidity constant pK. However, each type of site cannot be amphoteric (1-pK model), but the occurrence of several families of sites may confer an amphoteric property to the surface. Another feature of this model is the fact that the charge of a site may be fractional.

Whatever the model, the determination of acid-base and sorption parameters (point of zero charge, acid-base and sorption constants, density of active sites) presents several experimental and theoretical difficulties. Many error causes occur in the measurement of the "surface charge", but the main theoretical difficulty results from electrostatic interactions in the vicinity of the surface. Several models, based on the electric potential distribution near to the surface have been proposed (constant capacitance model, diffuse layer model, basic Stern model, triple layer model,..). These models use a certain number of parameters, which are fitted from experimental sorption data together with sorption constants.

Finally, several different ways of modeling can be proposed for the same experimental system, sometimes with different types of surface complexes for the sorbed elements.

Evaluation of sorption mechanisms and sorption models

Do models represent the true sorption mechanisms? If not, what is the validity of such models when using them far from laboratory conditions, especially for radioactive wastes repositories, where prediction must be valid for more than million of years and applied to natural systems?

To insure a safe extrapolation of models, it is necessary to know as better as possible the real sorption mechanisms. We must use methods able to localize the sorbed elements, determine the nature of their species and types of bindings. This goal can only be achieved by using a multidisciplinary approach, with several different methods which bring complementary results.

Several factors should to be considered, when applying this strategy: kinetics, solubility, stability of solids, speciation of elements, role of colloids and bacteria.

We have applied this multidisciplinary approach to several solids. For hydroxyapatites, [13,14], the main feature is that the sorption mechanisms depend strongly on the element: ion exchange with more or less limited diffusion for Cd^{2+} and SeO_3^{2-} , formation of new solid phases for Pb^{2+} and UO_2^{2+} . Equilibrium is not achieved in many cases. Thus, the classical models described above cannot be used.

In the case of hexacyanoferrates [15,16], depending on the composition and structure of the solid and on the composition of solution, the main sorption processes are ion exchange, incorporation of ion pairs or formation of new solid phases. Kinetics controls very often the process. Here also, the classical models cannot be applied.

For a large number of oxy-hydroxides, the general principles of surface complexation on superficial OH sites can be applied, but, as already noted, the determination of the real sorption mechanisms and of the true thermodynamic constants present some difficulties.

Above developed models suppose that equilibrium is achieved. In fact, kinetic effects play an important role in sorption chemistry. Kinetics may be modeled by considering the process controlling the sorption mechanism, such as: diffusion in the superficial liquid layer, adsorption/desorption, diffusion in the solid, ion exchange, formation of a new superficial solid phase, diffusion in a new-formed superficial phase.

We show the kinetics of the sorption of Sr^{2+} on polyantimonic acid [10] (Fig. 2), for which more than ten days are needed to achieve equilibrium. The kinetic curves can be fitted according to a diffusion in the crystal structure.

Comparison of models

We have performed a systematic comparison of models, including ion-exchange, by fitting a set of experimental titration data. We present a comparison of results on goethite (Table 1). Several models can fit the experimental data, but a choice cannot be easily made from the differences between the experimental and fitted values. The resulting parameters may vary considerably from one method to the other. As an example, note the variation of the surface site density.

Conclusion

Progress has been obtained in the past years in the knowledge of sorption processes, but this progress has induced new problems for finding appropriate quantitative models. Next steps will certainly be studies on high-purity solids with known surface orientations, use of better electrostatic models with parameters determined independently from sorption measurements, models with realistic surface electron density taking into account surface reconstruction.

Table 1 Examples of comparison of models used to fit a set of titration data for washed goethite: calculated intrinsic constants pK^+ and pK^- , surface site density, capacitance and pzc

Models and methods	pK^+	pK^-	Sites at/nm ²	Cap. C/m ²	PZC
Ion exchange	11.8	9.08	1.8 Imp		
2-pK monosite					
Graphical method (basic pH)		8.87	1.8 Imp	3.8	
NWLS (basic pH)		8.85	1.6	1.6	
Graphical method (acid pH)	6.92		1.8 Imp	3.5	
NWLS (acid pH)	6.94		1.8	1.5	
NWLS on H ⁺	6.92	9.19	3.9	1.2	8.05
WLS on pH	6.92	8.68	1.5	1.7	7.80
FITEQL	6.96	8.85	1.8	1.5	7.91
1-pK multisite SuOH ^{1/2-} /SuOH ₂ ^{1/2+}					
WLS on H ⁺	7.79		6.6	1.1	7.79
NWLS on H ⁺	7.77		13	1.1	7.77

WLS: weighted last squares, NWLS: not weighted last squares

Imp: imposed, FITEQL is a commercial computer code

References:

- [1] R. J. Serne, A. B. Muller, "A perspective on adsorption of radionuclides onto geologic media", in "the geological disposal of high level radioactive wastes", Brookins, D. G. Edit., Theophrastus Pub., Athens (1987).
- [2] M. Ochs, M. Boonekamp, H. Wanner, H. Sato, M. Yui, Radiochim. Acta, 82, 437 (1998).
- [3] M. J. Stenhouse, J. Pöttinger, Radiochim. Acta 66/67, 267 (1994).
- [4] D. D. Holstetler, R. J. Serne, A. J. Baldwin, G. M. Petrie, "Status report on sorption information retrieval systems", PNL-3528, Pacific Northwest Lab. Richland, Washington, USA (1980).
- [5] D. Langmuir, J. Am. Chem. Soc., 40, 1361 (1918).
- [6] M. M. Dubinin, L. V. Radushkevich, Proc. Acad. Sci, Phys. Chem. USSR, 55, 331 (1947).
- [7] H. Freundlich, "Colloid and Capillary Chemistry", Methuen, London, England (1926).
- [8] G. L. Gaines, H. Thomas, J. Chem. Phys. 21, 214 (1953).
- [9] R. M. Barrer, J. D. Falconer, Proc. Roy. Soc. 236A, 227 (1956).
- [10] S. Zouad, J. Jeanjean, C. Loos-Neskovic, M. Fedoroff, J. Solid State Chem. 98, 1 (1992).
- [11] W. Stumm, "Chemistry of the Solid-Water Interface", Wiley-Interscience (1992).
- [12] T. Hiemstra, W. H. Van Riemsdijk, G. H. Bolt, J. Colloid Interface Sci. 133, 91 (1989).
- [13] M. Fedoroff, J. Jeanjean, J. C. Rouchaud, L. Mazerolles, P. Trocellier, P. Maireles-Torres, D. J. Jones, Solid State Sciences, 1, 71 (1999).
- [14] F. Monteil-Rivera, M. Fedoroff, J. Jeanjean, L. Minel, M. G. Barthes, J. Dumonceau, J. Colloid and Interface Sci., 221(2), 291 (2000).
- [15] C. Loos-Neskovic, M. Fedoroff, Solvent Extraction and Ion Exchange, 7, 131 (1989).
- [16] S. Ayrault, B. Jimenez, E. Garnier, M. Fedoroff, D. J. Jones, C. Loos-Neskovic, J. Solid State Chem. 141, 475 (1998).

FUNCTIONAL SPECIES OF MINERAL / ELECTROLYTE INTERFACES

OBSERVED IN SITU BY NONLINEAR VIBRATIONAL SPECTROSCOPY

M. Flörsheimer, K. Kruse, R. Klenze, Th. Fanghänel

Forschungszentrum Karlsruhe
Institut für Nukleare Entsorgung
Karlsruhe
Germany
florshg@ine.fzk.de

The reactivity and the adsorption/desorption properties of mineral/electrolyte interfaces are controlled by the functional species of the mineral surfaces. The identification of these groups and the measurement of their stability constants is essential for the quantitative understanding of mineral/electrolyte interaction in the aquifer. So far, however, it was difficult to obtain chemical in situ information with interface selectivity. We thus introduce a novel approach for speciation measurements. We apply vibrational sum frequency (SF) spectroscopy^{1,2} to sapphire ($\alpha\text{-Al}_2\text{O}_3$) single crystal surfaces under water between pH 4 and 12.

In the nonlinear optical experiment of sum frequency generation, a sample is illuminated with intense light from two lasers at frequencies ω_1 and ω_2 . Due to the high intensities, photons from the two beams can couple to the sample at the same time in order to generate photons at the sum frequency $\omega_{SF} = \omega_1 + \omega_2$. An SF signal can always be generated at a surface or an interface. In the bulk of media which exhibit certain point groups, however, SF generation is symmetry forbidden. In particular centrosymmetric matter such as the bulk of a liquid does not provide SF light in the electric dipole approximation. Also, no signal originates from the bulk of, for example, a sapphire crystal (point group $\bar{3}m$). As a result, we can obtain SF light selectively from the interface between sapphire and water.

Additionally chemical analytical information can be obtained. To this end, a laser system is applied that provides one beam of coherent light at a fixed wavelength (532 nm) and another beam whose wavelength is tunable to the infrared (IR) absorption bands of the functional species at the interface. If the wavelength is within an absorption band resonance enhancement of the SF intensity occurs. From the quantitative measurement of the SF intensities the interface concentrations of the individual species can be obtained. From the polarization state of the SF signal as a function of the incident polarizations, the orientation of the species can be calculated.

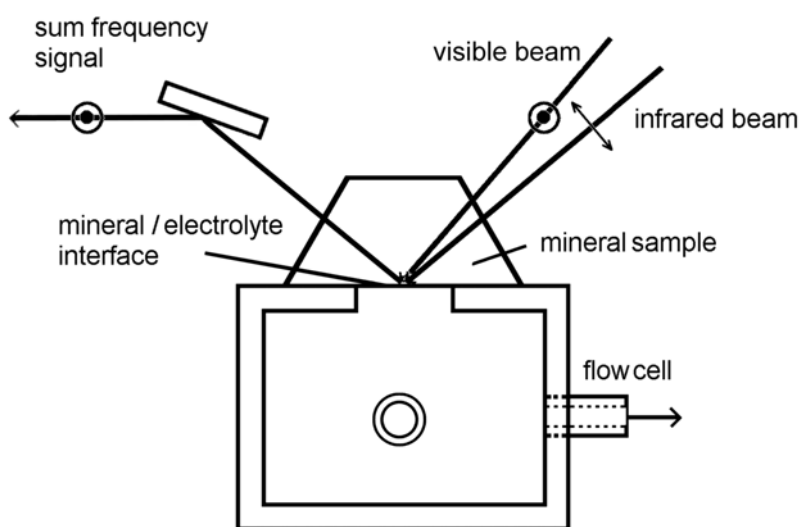


Fig. 1
Scheme of the sum
frequency experiment,
top view

A scheme of our experiment is shown in Figure 1. The sapphire crystal is applied in the form of a Dove prism whose hypotenuse face is cut in a well-defined crystallographic orientation. The specimens were obtained from Kyburz AG, Safnern, Switzerland. The hypotenuse face is pressed against the wall of a Teflon flow cell. In the wall, there is a drill hole so that contact between the mineral surface and the electrolyte occurs. The two laser beams are applied to the interface under total internal reflection conditions. In our first experiments, we tuned the IR laser over the spectral region in which the O-H stretching bands are expected. Since the other laser provides visible light the SF signal occurs also in the visible spectrum and can be measured with a photomultiplier. The laser system and the detection equipment were obtained from Euroscan, Namur, Belgium. The experiment and the laser are operated in a home-built argon chamber. The polarization state of the incident and the detected light can be altered. The spectrum of Figure 2 was obtained by using the polarization combination shown in Fig. 1 (SF signal *s*-polarized, visible beam *s*-polarized, IR beam *p*-polarized). As electrolyte, we used Millipore water whose pH was varied by applying NaOH or HCl. In the experiment of Fig. 2, the pH was 12.0 as measured with a Ross electrode. The crystal surface was *C*-cut. In the experiment, the signal depends on the optical nonlinearities of the interface and on its Fresnel factors.³ The latter do not provide information on the surface speciation. Due to their frequency dependence, however, they influence the spectra considerably. We thus correct the measured spectra for this effect by normalizing the raw data with the Fresnel factors. In the spectrum of Fig. 2, the square root of the corrected SF intensity $I^{(SF)}$ is given as a function of the IR wavenumber $\tilde{\nu}$. The deconvolution of the corrected spectrum provides seven bands which are also shown in Fig. 2. We modeled the bands as Lorentzian lines (homogeneous linewidths of 22 cm^{-1})⁴ which are inhomogeneously broadened according to Gaussian functions. The two bands at 3112 and 3215 cm^{-1} , which are well-known from various aquatic interfaces, are due to the polar ordered water film directly near the interface. The other five bands originate from up to five aluminol species or from specifically bound water molecules. This surprisingly high number of species could not be detected in recent studies.⁵ The dominating peak at 3693 cm^{-1} among these five bands, we attribute to an OH species bridging two⁶⁻⁹ aluminium atoms.

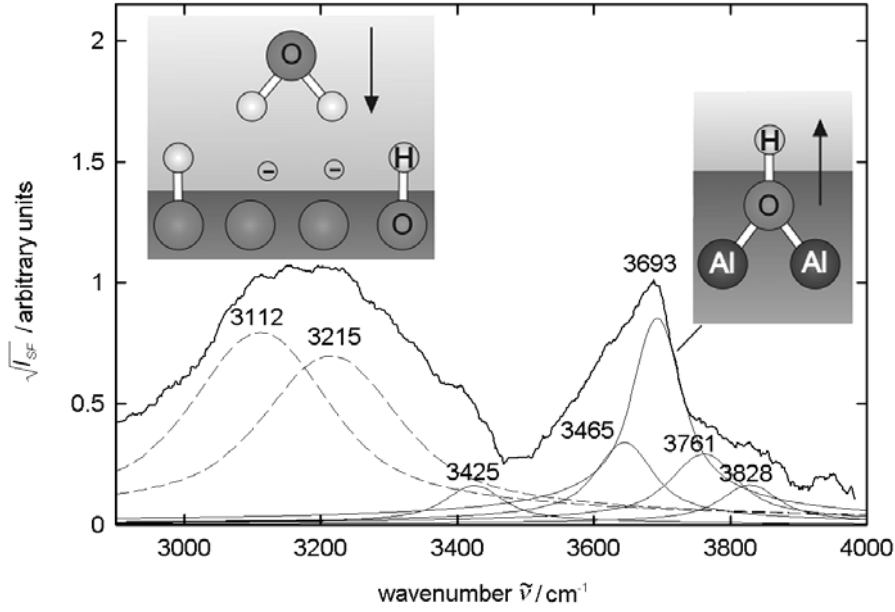


Fig. 2
Sum frequency spectrum of sapphire (001) surface under water at pH 12 together with result of deconvolution and interpretation. The two arrows indicate the dipoles of the polar ordered water film near the interface and the dipole of the OH group bridging two Al atoms.

For the complete interpretation of Fig. 2, it is important to realize that an SF spectrum cannot be considered as a simple addition of the intensities from the individual bands. Due to the coherence of the SF light, we have to consider the *interference* of the signal contributions from the individual species. The spectrum $I^{(SF)}(\tilde{\nu})$ is given by

$$\sqrt{I^{(SF)}(\tilde{\nu})} \propto \left| \sum_{species} d_{eff}(\tilde{\nu}, species) \right| \quad (1)$$

with d_{eff} an effective susceptibility. This quantity describes the nonlinear optical properties of a species at an interface. It is different for different kinds of species and depends also on the IR wavenumber. The effective susceptibilities are complex quantities with magnitude and phase. The seven individual bands in Fig. 2 give the *magnitudes* of the corresponding seven effective susceptibilities as a function of the IR wavenumber.

In order to obtain the *phases* of the effective susceptibilities we have to know that the phases in a second-order optical experiment depend on the polar orientation of the species which generate the light. The signal phases from two species, whose polar orientation is opposite, differ by 180° at their resonance maxima. Parallel species exhibit identical phases at their resonance maxima. In general, an SF spectrum is thus the result of partially constructive and partially destructive interference of signal contributions from the different species. The addition of the complex nonlinearities in Eq. (1) takes account of this interference phenomenon.

We have taken advantage of Eq. (1) already when we decomposed the spectrum in Fig. 2 into the individual bands. We obtained a phase difference of 180° at the maxima near 3112 and 3215 cm^{-1} (polar water film) relative to the phases at the other maxima. This result is indicated in Fig. 2 by using broken lines for the two bands of the polar water film. We can assume that the OH dipole of the aluminol species with the peak maximum at 3693 cm^{-1} points into the aquatic phase. The dipoles of the polar ordered water film thus point to the interface. This result agrees with our expectation for the interface at high pH.

In first series of experiments in which we altered the pH between 4 and 12 we observed that the positions of most of the bands do not change. This is a strong, additional argument for our interpretation of the spectrum in Fig. 2 with seven bands. These bands are not due to arbitrary assumptions but represent real species. Additionally we observed that the susceptibilities of the different bands and thus the concentrations of the corresponding species depend differently on the pH of the electrolyte as we could expect.

In conclusion, we have shown that SF generation can be used to probe the speciation of the functional species of mineral surfaces in situ under electrolyte with interface selectivity. First results show that rich information at the molecular level can be expected.

References:

- [1] Shen Y.R. (1989) *Nature* **357**, 519
- [2] Richmond G.L. (2002) *Chem. Rev.* **102**, 2693
- [3] Mizrahi V., Sipe J.E. (1988) *J. Opt. Soc. Am. B* **5**, 660
- [4] Morita A., Hynes J.T. (2000) *Chem. Phys.* **258**, 371
- [5] Yeganeh M.S., Dougal S.M., Pink H.S. (1999) *Phys. Rev. Lett.* **83**, 1179
- [6] Digne M., Sautet P., Raybaud P., Euzen P., Toulhoat H. (2002) *J. Catal.* **211**, 1
- [7] Barrón V., Torrent J. (1996) *J. Colloid Interface Sci.* **177**, 407
- [8] Busca G., Lorenzelli V., Sanchez Escribano V., Guidetti R. (1991) *J. Catal.* **131**, 167
- [9] Hass K.C., Schneider W.F., Curioni A., Andreoni W. (2000) *J. Phys. Chem. B* **104**, 5527

pH-DEPENDENCE OF URANYL UPTAKE ON QUARTZ : A XPS STUDY

A. Froideval¹, M. Del Nero¹, R. Barillon¹, J. Hommet² and G. Mignot³

¹Institut de Recherches Subatomiques, UMR 7500, Strasbourg, France.

²Institut de Physique et Chimie des Matériaux de Strasbourg, GSI, Strasbourg, France.

³Commissariat à l'Energie Atomique, DAM / RCE, Bruyères-le-Chatel, France.

annick.froideval@ires.in2p3.fr, mireille.delnero@ires.in2p3.fr,
remi.barillon@ires.in2p3.fr, jean.hommet@ipcms.u-strasbg.fr, g.mignot@hemispheres.fr

Introduction

Uranium release in ground- and drinking water is of concern at several U-contaminated areas in the world. U mining and reprocessing has led to large amounts of U-rich soils, sediments or mine tailings, which are a local source for water contamination in specific environments. Predicting the transport of uranium in the near-field of highly U-contaminated sites is thus critically needed. It requires detailed knowledge on both sorption and precipitation processes of uranyl occurring at high concentrations of U(VI) in the aqueous phase.

In this work, we aimed at gaining insights into the pH-dependence of the « uranyl components » – such as uranyl surface species, (surface-) precipitates – formed on a quartz fraction equilibrated with concentrated uranyl solutions i.e. under conditions favouring aqueous polynuclear species and / or formation of U(VI)-colloids or $\text{UO}_2(\text{OH})_2$ precipitates. X-ray Photoelectron Spectroscopy (XPS) was used to distinguish between different type of uranyl ions on the quartz fractions and thus to assess whether distinct uranyl « components » contribute to a pH-dependent U(VI) uptake. The U 4f spectra were interpreted in terms of coordination environments of the uranyl ions in the components, on a basis of EXAFS data published in the literature on sorbing uranyl species. Our study provides valuable insights into the uranyl sorption complexes / (surface-) precipitates governing a pH-dependence of U(VI) uptake in a poorly sorbing medium. XPS is a surface technique which provides direct chemical and structural information on ions in or on minerals. The energy of the emitted photoelectron for a given atom in an XPS spectrum is indeed related to its coordination environment. Different bonding environments can induce binding energy shifts. Many studies have already shown that XPS is a valuable tool for studying chemical speciation of several sorbing ions, including U(VI) (1, 2).

Experimental and analytical procedure

Batch experiments were carried out to prepare the U(VI)-containing quartz fractions to be analysed by XPS. We measured the partitioning of U(VI) between a quartz fraction, a colloidal phase and an aqueous phase at 298 K under a CO_2 -free atmosphere. The initial aqueous uranyl concentrations are 10 μM , 50 μM and 100 μM . The quartz / solution ratio of the samples is equal to 25 g / L. The ionic strength (I.S.) of the solution is kept at a value of 0.1 M using a NaNO_3 electrolyte solution. The parameter under investigation is the final solution pH ($5 < \text{pH}_F < 8$).

The specific surface area of the quartz used is low ($< 0.1 \text{ m}^2/\text{g}$) and may be taken as representative of the surface area of primary minerals which may immobilize U(VI) in rocks. Due to the weak sorptive properties of quartz and to our high aqueous U(VI) concentrations, particular attention was paid to detect a possible formation of colloids or a precipitation of schoepite-type minerals in our experiments. So, (meta-) schoepite was synthesized and its XPS spectrum was recorded and taken as an uranium(VI) oxide hydrate reference.

In order to gain insights into the coordination environments of sorbed / precipitated uranyl ions in the quartz fraction, we recorded the U 4f XPS spectra of the U(VI)-containing quartz samples (

Figure 1). All the spectra, including the metaschoepite ones, were shifted to reposition the Si 2p peak at a binding energy value of 103.5 eV.

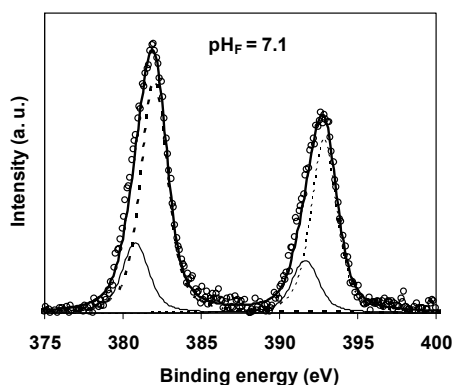


Figure 1 : U 4f XPS spectrum of a U(VI)-containing quartz sample recorded at pH 7.1 and its fitting curve showing a contribution of two components for uranyl ions (dashed line: “component I” or metaschoepite-like component; solid line: “component II”) from Froideval et al., 2003 (3). Experimental sample conditions: $[\text{U}]_i = 100 \mu\text{M}$, I.S. = 0.1 M NaNO_3 electrolyte solution, N_2 -atmosphere, 298 K.

Interpretation of the U 4f XPS binding energies in terms of U(VI) coordination environment

- Because all uranyl ions in metaschoepite display a single coordination environment (4), a single component was used to fit the U 4f peaks of our synthetic metaschoepite. The U 4f lines were found to be positioned at 382.0 eV for U 4f_{7/2} and at 392.85 eV for U 4f_{5/2}.
- The U 4f XPS spectra of the U(VI)-containing quartz samples could not be fitted by assuming a unique single component for uranyl ions, which suggested convoluted signals.

The U4f XPS spectra allowed to identify unambiguously the presence of two uranyl components. A high binding energy component, whose relative proportion increases with pH, exhibits the U 4f lines characteristics of our synthetic metaschoepite. A second uranyl component exhibits binding energies for the U 4f core levels at values significantly lower ($\Delta E_b = 1.2 \text{ eV}$; U 4f line at 380.8 eV for U 4f_{7/2} and at 391.65 eV for U 4f_{5/2}) than for metaschoepite. This evidences the presence of uranyl ions having a coordination environment significantly different from that of uranyl ions in U(VI) oxide hydrates. The high binding energy component is interpreted as a component having an U(VI) oxide hydrate character, either as polynuclear surface oligomers and/or as amorphous schoepite-like (surface) precipitates. Its pH-dependence suggests that a binding of polynuclear species at quartz surfaces and/or a formation of amorphous schoepite-like (surface) precipitates is favoured when increasing a proportion of aqueous polynuclear species (pH increase). The second component may be attributed to monomeric uranyl surface complexes on the basis of EXAFS data on uranyl surface complexes (5-7). A finding of two uranyl components on our quartz

fractions suggests anyway that the uranyl surface speciation on silica minerals is not uniquely controlled by the aqueous uranyl speciation.

Conclusions

Our XPS analyses allowed to identify unambiguously the presence of two pH-dependent uranyl components on a quartz fraction equilibrated with concentrated uranyl solutions over a pH range 5-8. An important contribution of our XPS study is to identify unambiguously the presence of a component in which the U(VI) coordination environment differs significantly from that of uranyl ions in U(VI) oxide hydrates, at pH values where aqueous polynuclear species/uranyl colloids predominate in solution. A valuable information is that the U 4f binding energies of such species are positioned at values significantly lower than those obtained for metaschoepite. Such a position may be consistent with EXAFS data published on the coordination environment of uranyl ions in monomeric uranyl surface complexes. Such species were reported to form on various minerals brought in contact with acidic solutions (5-7) or at the surface of Fe- or Al-oxyhydroxides in contact with near-neutral solutions (7). Our XPS results suggest that pH-dependent monomeric surface complexes may also form at a high surface coverage on silica minerals, together with polynuclear surface oligomers and / or schoepite-like (surface) precipitates.

Our study shows that XPS is a powerful tool for evidencing the coexistence of uranyl ions having very distinct coordination environments and for providing valuable qualitative and quantitative information on the uranyl « surface speciation ». XPS analyses can thus be complementary to EXAFS studies by offering a possibility to discriminate unambiguously between several kind of surface species / precipitates on a mineral.

References:

- (1) Drot, R., Simoni, E., Alnot, M., and Ehrhardt, J. J., *J. Colloid Interface Sci.* **205**, 410 (1998).
- (2) Van den Berghe, S., Laval, J. -P., Gaudreau, B., Terryn, H., and Verwerft, M., *J. Nucl. Mater.* **277**, 28 (2000).
- (3) Froideval, A., Del Nero, M., Barillon, R., Hommet, J. and Mignot, G., *J. Colloid Interface Sci.* **266**, 221 (2003).
- (4) Weller, M. T., Light, M. E., and Gelbrich, T., *Acta Cryst.* **B56**, 577 (2000).
- (5) Waite, T. D., Davis, J. A., Payne, T. E., Waychunas, G. A., and Xu, N., *Geochim. Cosmochim. Acta* **58**, 5465 (1994).
- (6) Reich, T., Moll, H., Arnold, T., Denecke, M. A., Hennig, C., Geipel, G., Bernhard, G., Nitsche, H., Allen, P. G., Bucher, J. J., Edelstein, N. M., and Shuh, D. K., *J. Electron Spectrosc. Relat. Phenom.* **96**, 237 (1998).
- (7) Bargar, J. R., Reitmeyer, R., Lenhart, J. J., and Davis, J. A., *Geochim. Cosmochim. Acta* **64**, 2737 (2000)

RELATIONSHIP BETWEEN SURFACE STRUCTURE AND ION COMPLEXATION

Tjisse Hiemstra, Willem H. van Riemsdijk

Department of Soil Quality,
Wageningen University
P.O. Box 8005
6700 EC Wageningen
The Netherlands.
tjisse.hiemstra@wur.nl

Introduction

Metal (hydr)oxide surfaces are widely studied because of their capability to interact with cations and anions. Oxide surfaces are amphoteric, being either negatively, zero or positively charged. The primary charge of metal (hydr)oxides is variable and depends on the conditions in solution (pH, ionic strength). Surface charge is very important since it is regulating the binding characteristics of ions via electrostatic double layer properties, as founded in the double layer theories of Gouy, Chapman, Stern and Graham.

Charge and structure

The interaction of ions with a mineral surface strongly depends on the location of the ions in the electrostatic double layer profile. Fokkink et al. (1) showed that the precise location of the ion charge is a key factor in the co-adsorption or co-desorption of protons in case of ion adsorption. An ion which is closer to the surface has a larger interaction and a higher co-ad(de)sorption of protons. This effect of location of charge is very important since co-adsorption/desorption of protons is thermodynamically related to the pH dependency of ion adsorption, as shown by Perona and Leckie (2). The conclusion is that the location of the ion charge in the electrostatic double layer profile and the pH dependency of adsorption must be tightly connected.

Charge distribution and complex structure

Surface complexation models (SCM) of the first generation locate the charge of innersphere complexes at one electrostatic position (surface), treating an ion as a point charge. Structural differences of innersphere surface complexes can not easily be introduced in these point charge models. Let us consider the microstructure of an innersphere surface complex of two divalent ions, selenite SeO_3^{2-} and selenate SeO_4^{2-} (Fig.1). Fig.1 illustrates that only part of the adsorbing ion is incorporated in the surface.

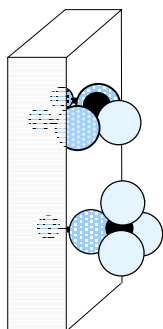
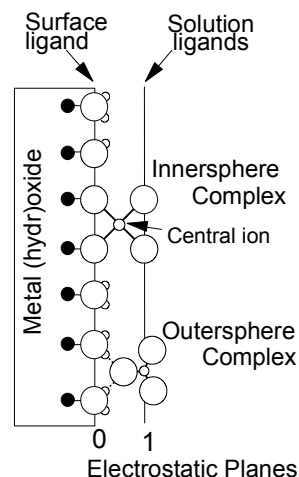


Fig.1. The selenite Se(IV)O_3 surface complex (upper) has two oxygens common with the surface and one oxygen protruding to the solution. Two-third of the Se(IV) charge is used to neutralise the two surface ligands.

The innersphere selenate Se(VI)O_4 surface complex (lower) has only one ligand common with the surface. The other three ligands are solution directed. One-fourth of the Se(VI) charge is used to neutralise the surface ligand.

A considerable part of the surface complex with corresponding charge is located at a larger distance from the surface. To account for this phenomenon, the charge distribution (CD) model has been developed (3). In the CD model, the charge of the adsorbed ion is distributed over the ligands. In turn, the ligands are distributed over the electrostatic planes based on the structure of the surface complex (Fig.2).

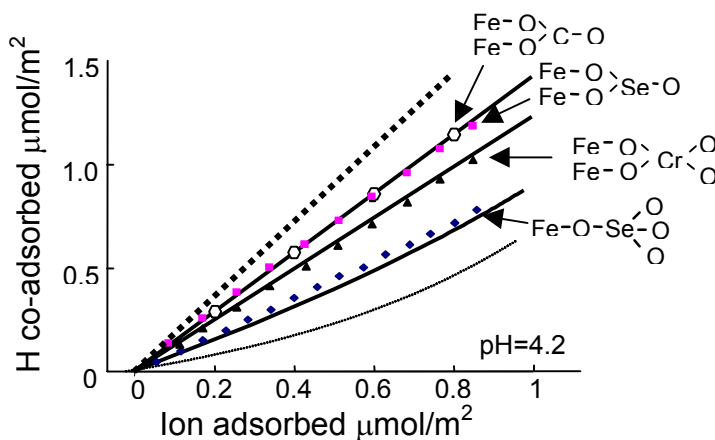
Fig.2. A schematic representation of a metal (hydr)oxide surface with protonated surface oxygens, innersphere complex formation and outersphere complex formation. The charge of protonated surface oxygens originates from the coordinating metal ion(s) of the solid and adsorbed proton(s). In case of an innersphere surface complex, also part of the charge of the central ion contributes to the neutralisation of the (common) surface oxygen. The charge of the central ion in the innersphere complex is also partly used to contribute to the neutralisation of the ligands that are solution oriented, as depicted. The mean location of the charge of the outersphere complexes is at the outer electrostatic plane. A model with two electrostatic planes is called a Basic Stern (BS) model.



Bidentate and monodentate complexation

For many surface complexes of oxyanions, the CD can be assessed, in a first approach, from the structure of the surface complex. For instance, it has been shown (4, 5) that the main differences in proton co-adsorption for a series of divalent oxyanions, including SO_4^{2-} , SeO_4^{2-} , CrO_4^{2-} , WO_4^{2-} (CN=4) and CO_3^{2-} and SeO_3^{2-} (CN=3) are due to differences in distribution of ligands in the interface. These differences result from structural differences like binding mode (monodentate vs. bidentates) and overall coordination numbers (CN). In case of bidentate formation of SeO_3^{2-} or CO_3^{2-} about 2/3 of the ligands *with corresponding charge* is present at the surface, whereas in case of monodentate complex formation of SeO_4^{2-} and SO_4^{2-} only 1/4 of the ligands and corresponding charge is present in the surface plane. CrO_4 has an intermediate position since here half of the charged ligands is present in the surface. The variation in charge distribution leads to a different interaction of the divalent ions with the protons bound at the surface. This is illustrated in Fig.3.

Fig.3. The co-adsorption of protons due to the binding of CO_3^{2-} , SeO_3^{2-} , CrO_4^{2-} and SeO_4^{2-} on goethite in 0.01 M NaNO_3 at pH=4.2. The dotted lines indicate the expected co-adsorption in case all ion charge (-2) is present at the surface or in the 1-plane (BS approach), yielding a very high and a low co-adsorption respectively. The full lines are calculated assuming a Pauling distribution of charge of the central ion over the coordinating ligands, leading to a surface charge attribution of respectively 67, 50 and 25 % of the anion charge (-2). Data for SeO_3^{2-} , CrO_4^{2-} , and SeO_4^{2-} are of Rietra et al. (6). Data for CO_3^{2-} are generated from the data of Villalobos and Leckie (7).



Consistency principle and pH dependency

The H- co-adsorption χ is thermodynamically related to the pH dependency, according to (6, 8):

$$\left(\frac{\partial \log C_t}{\partial \text{pH}}\right)_{\Gamma_i} = \left(\frac{\partial \Gamma_H}{\partial \Gamma_i} - n\right)_{\text{pH}} = (\chi - n)_{\text{pH}} \quad [1]$$

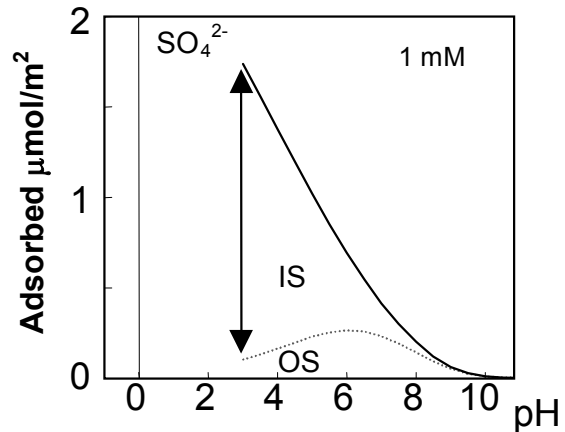
in which $\partial \log C_t / \partial \text{pH}$ is the change of the logarithm of the overall ion concentration C_t with a change of pH at a constant ion loading Γ_i . The expression says that this change is equal to the change in H adsorption (Γ_H) due to adsorption of ion i at the surface (Γ_i) for a given pH after correction for the mean number (n) of protons present at the ion in solution at that pH.

Combination of the consistency principle and the above relation between surface complex structure and proton co(de)sorption, shows that pH dependency and complex structure are coupled.

Inner- and outer-sphere complexation

Besides innersphere complexation some ions like Ca^{2+} , Sr^{2+} , SO_4^{2-} and SeO_4^{2-} , also exhibit outersphere complexation. The contribution as function of pH and loading of these complexes is regulated by electrostatics and therefore related to the interface structure and the location of the ions in it. Since outersphere ions are located at a larger distance, a smaller interaction with the protonated surface exists, which implies that the co-ad(de)sorption is less. As a result, the species with the highest pH dependency of adsorption will dominate when the adsorption increases at change of pH. An example is given in Fig.4.

Fig.4. The adsorption in a SO_4^{2-} -goethite at an ion concentration of 0.001 M in 0.1 M NaNO_3 (full line). The contribution of outersphere complexes (os) is given as dotted line. The difference between both lines gives the contribution of innersphere (is) complexes. Parameters are taken from Rietra et al. (5).

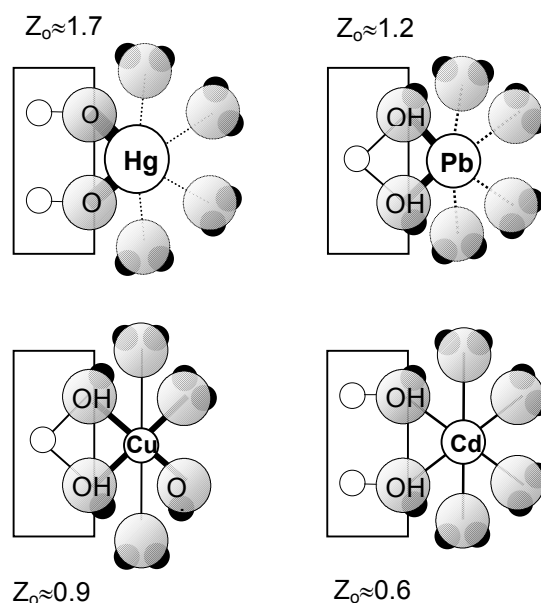


Asymmetrical charge distribution

Recently, it has been shown for goethite that the coordination environment of some heavy metal ions like Hg^{2+} (9) and Pb^{2+} (10) will change drastically upon adsorption, in contrast to an ion like Cd^{2+} (11). In case of Hg^{2+} , a highly asymmetrical surface complex is formed. The Hg^{2+} ion forms two strong bonds (bidentate complex) (9) with the surface oxygens and no or very weak bonds with outer ligands (H_2O). In terms of the CD-MUSIC model approach, it is expected that formation of very strong Hg-O bonds with the surface leads to a situation in which most of the ion charge should be attributed to the surface. Indeed, the observed charge attribution of the surface (derived from applying the CD-model to

adsorption data) is high ($Z_o \approx 1.7$). This differs from an ion with a symmetrical coordination environment, e.g. Cd^{2+} (11,12). In a symmetrical coordination environment, the Pauling rule for charge distribution can be applied. In case of bidentate formation, this leads for the Cd^{2+} surface complex to a predicted charge distribution in which only about 1/3 of the Cd^{2+} charge is attributed to the surface (13). The remaining part of the ion charge (2/3) is present at the outer H_2O ligands at some distance from the surface. The modelled charge distribution (CD-MUSIC model) is in line with this prediction ($Z_o \approx 0.6$). Also other ions distribute their charge asymmetrically in surface complexes. This is known for e.g. Cu(II) , Pb(II) , UO_2^{+2} and NpO_2^{+} . The CD values of these complexes, calculated from adsorption data, agree with the expected CD based on the experimental structure of the complexes.

Fig.5. The surface complexes of Hg, Pb, Cu and Cd present on goethite. The Hg ion is highly distorted in the coordination environment. It attributes so much charge to the surface ligands that no proton can be retained on the common ligand. The asymmetry prevents hydrolysis of the loosely bound water molecules. Asymmetry is less strong in the Pb surface structure. The common ligand can remain a hydroxyl. The asymmetry causes longer Pb-OH₂ bonds, which suppress hydrolysis of those ligands. The distortion of Cu is symmetrical. This leads to a relatively high charge attribution to both surface and solution ligands of the equatorial plane and enables hydroxylation of the solution oriented ligands, which is strongly stimulated by the repulsive charge of the surface on the H. The attribution to the surface ligands is not high enough to cause deprotonation of these ligands in the pH range studied. The Cd environment is entirely symmetrical. The bond valence to each ligand is relatively low, preventing hydrolysis in the major pH range.



References:

- 1 Fokkink, L.G.J., De Keizer, A., Lyklema, J. *J. Colloid Interf. Sci.* 118, 454 (1987)
- 2 Perona, M.J., Leckie, J.O. *J. Colloid Interf. Sci.* 106, 65 (1985)
- 3 Hiemstra, T., Van Riemsdijk, W.H. *J. Colloid Interf. Sci.* 179, 488 (1996a)
- 4 Rietra, R.P.J.J., Hiemstra, T., Van Riemsdijk, W.H. *Geochim. Cosmochim. Acta.* 63, 3009 (1999a)
- 5 Rietra, R.P.J.J., Hiemstra, T., Van Riemsdijk, W.H. *J. Colloid Interf. Sci.* 240, 384 (2001b)
- 6 Rietra, R.P.J.J., Hiemstra, T., Van Riemsdijk, W.H. *J. Colloid Interf. Sci.* 229, 199 (2000a)
- 7 Villalobos, M., Leckie, J.O. *Geochim. Cosmochim. Acta.* 64, 3787 (2000)
- 8 Hiemstra, T., Van Riemsdijk, W.H. in "Encyclopaedia of Surface and Colloid Science", 1: Marcel Dekker, Inc.: New York, USA, 3773, 2002;
- 9 Collins, C.R., Sherman, D.M., Ragnarsdottir, K.V. *J. Colloid Interf. Sci.* 219, 345 (1999a)
- 10 Bargar, J.R., Brown, G.E., Jr., Parks, G.A. *Geochim. Cosmochim. Acta.* 61, 2639 (1997b)
- 11 Randall, S.R., Sherman, D.M., Ragnarsdottir, K.V. *Geochim. Cosmochim. Acta.* 63, 2971 (1999)
- 12 Spadini, L., Manceau, A., Schindler, P.W., Charlet, L. *J. Colloid Interf. Sci.* 168, 73 (1994)
- 13 Venema, P., Hiemstra, T., Van Riemsdijk, W.H. *J. Colloid Interf. Sci.* 183, 515 (1996b)

PARAMETERS AFFECTING THE PH DEPENDENCE OF SORPTION

Anna-Maria Jakobsson, Mattias Olsson and Yngve Albinsson

Nuclear Chemistry

Department of Materials and Surface Chemistry

Chalmers University of Technology

SE-412 96 Göteborg

Sweden

miaj@chem.chalmers.se

Introduction

Surface complexation is dependent on several phenomena and parameters. Quantification of these dependencies is an important contributant to understanding and increasing the precision of surface complexation modeling. An attempt has been done to clarify what factors affect the pH dependence of the experimentally observed cation distribution coefficient. A derivation of an expression for the relationship between the distribution coefficient and pH has been done to relate separate parameters to the experimentally observed sorption curve. A complete derivation was done for a 1-pK Constant Capacitance model with a mono-dentate complex formed. It will be extended to more cases eventually.

Having this derivation done makes it rather easy to do a sensitivity analysis in an ordered fashion to investigate what factors are more or less important with regard to the impact on the distribution, and why. This is valuable information since it is well known that for example hydrolysis constants are often associated with massive uncertainties.

The relationship between distribution and pH

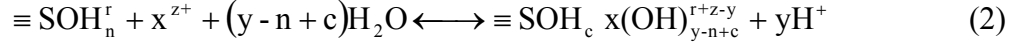
The distribution coefficient with respect to surface area, K_a , which can be determined experimentally, is related to the equilibrium constant of the surface complexation reaction. A relationship between the K_a , the apparent equilibrium constant for the surface complexation, K^{app} , and the pH can be derived for only one surface complex formed as follows.

The distribution coefficient is defined as:

$$K_a = \frac{([\text{surface complex}] + [\text{surface layer}])}{[x]_{\text{total}}} \cdot \frac{S_{\text{mol}}}{[=SOH_{\text{tot}}]} \quad (1)$$

where x is the sorbing species, brackets denote concentration, $[=SOH_{\text{tot}}]$ is the total concentration of surface sites, and S_{mol} is the site density in mole sites per area. After an impact analysis, the surface layer concentration is regarded as negligible.

The general surface complexation reaction considered here is:



where $\equiv \text{SOH}_n^r$ is some type of surface site of charge r , x^{z+} is a sorbing cation, y is the number of protons released in the reaction and $\equiv \text{SOH}_c x(\text{OH})_{y-n+c}^{r+z-y}$ is the surface complex formed. The equilibrium constant, K_x , for the reaction is:

$$K_x = \frac{\left\{ \equiv \text{SOH}_c x(\text{OH})_{y-n+c}^{r+z-y} \right\} \left\{ \text{H}_{i\text{-plane}}^+ \right\}^y}{\left\{ \equiv \text{SOH}_n^r \right\} \left\{ x_{i\text{-plane}}^{z+} \right\}} \quad (3)$$

where the i -plane is the plane at which the reaction occurs. The planes are defined by the electric double layer model used.

The equilibrium constant for the surface complexation constant is expressed as an apparent constant, referring to the bulk concentrations. There will be no difference in activity (or concentration) at the surface compared to the bulk according to a non-electrostatic model (NEM), since the effect of the potential on the ion distribution is neglected. By expressing the surface complexation constant as an apparent constant, the resulting relationships will hold for the electrostatic models as well. However, for these, the apparent constants will not be constant but will vary with pH and degree of sorption.

From a mass balance the total concentration of the sorbing species in the aqueous phase, $[X^{z+}]_{\text{totalaq}}$, is :

$$[X^{z+}]_{\text{totalaq}} = \frac{-b \pm \sqrt{b^2 + 4K_x^{\text{app}} [X]_{\text{tot}} \left\{ \text{H}^+ \right\}^y \alpha_X \alpha'_{\text{SOH}}}}{2K_x^{\text{app}}} \quad (4)$$

where

$$b = K_x^{\text{app}} \left([\text{SOH}]_{\text{tot}} - [x]_{\text{tot}} \right) + \left\{ \text{H}^+ \right\}^y \alpha_X \alpha'_{\text{SOH}} \quad (5)$$

$$2 - \text{pK} : \alpha'_{\text{SOH}} = \alpha'_{\text{SOH}2-\text{pK}} = 1 + K_{\text{sa}1}^{\text{app}} \left\{ \text{H}^+ \right\} + \frac{K_{\text{sa}2}^{\text{app}}}{\left\{ \text{H}^+ \right\}} \quad (6)$$

$$1 - \text{pK} : \alpha'_{\text{SOH}} = \alpha'_{\text{SOH}1-\text{pK}} = 1 + K_{\text{sa}}^{\text{app}} \left\{ \text{H}^+ \right\} \quad (7)$$

and

$$\alpha_X = \left(1 + \frac{\beta_{x1} \gamma_x}{\left\{ \text{H}^+ \right\} \gamma_{x(\text{OH})}} + \frac{\beta_{x2} \gamma_x}{\left\{ \text{H}^+ \right\}^2 \gamma_{x(\text{OH})2}} + \frac{\beta_{x3} \gamma_x}{\left\{ \text{H}^+ \right\}^3 \gamma_{x(\text{OH})3}} + \dots \right) \quad (8)$$

$\beta_{x1}, \beta_{x2}, \dots$ are the hydrolysis constants. Other complexing agents can easily be included in (7). It is assumed that no polynuclear complexes are formed. The only unknown pH dependent factor in equation 4 is potential difference between the surface and the aqueous phase; ψ .

The distribution can be calculated from

$$K_a = \frac{[X]_{\text{tot}} - [X]_{\text{totaq}}}{[X]_{\text{totaq}}} * \frac{V}{A} \quad (9)$$

The sensitivity of K_a

Expressing the derivative of (9) with regard to pH is the first step in investigating the impact of the terms on the slope of the log K_a versus pH function:

$$\frac{\partial \log K_a}{\partial \text{pH}} = h * \left(\left(\frac{(1 - \alpha'_{\text{SOH}})}{\alpha'_{\text{SOH}}} - y \right) + \frac{\partial \ln \alpha_x}{\ln(10) \partial \text{pH}} + \frac{\partial \Psi}{\partial \text{pH}} \left(\frac{F}{RT \ln(10)} \right) \left((z - y) + \frac{(1 - \alpha'_{\text{SOH}})}{\alpha'_{\text{SOH}}} \right) \right) \quad (10)$$

where

$$\frac{\partial \ln(\alpha_x)}{\partial \text{pH}} = \frac{\left(\frac{\beta_{x1} \gamma_x}{\{H^+\} \gamma_{x(OH)}} + \frac{2\beta_{x2} \gamma_x}{\{H^+\}^2 \gamma_{x(OH)2}} + \frac{3\beta_{x3} \gamma_x}{\{H^+\}^3 \gamma_{x(OH)3}} + \dots \right)}{\ln(10) * \alpha_x} \quad (11)$$

and

$$h = \frac{\left(\left(\frac{[SOH]_{\text{tot}}}{[X]_{\text{tot}}} \right) - \left(\frac{[X]_{\text{tot}} - [X]_{\text{totaq}}}{[X]_{\text{tot}}} \right) \right)}{\left(\frac{([X]_{\text{tot}} - [X]_{\text{totaq}})}{[X]_{\text{tot}}} \right)^2 - \left(\frac{[SOH]_{\text{tot}}}{[X]_{\text{tot}}} \right)} \quad (12)$$

How the potential difference between the surface and bulk aqueous phase depends on pH depends on the electric double layer model used and also on the charge of the cation. From equation (10) the relative contributions of the different pH dependent factors can be found.

Generally the first hydrolysis constant is well known but with an increasing degree uncertainty for the higher constants. This is clear especially for the tetravalent metals where the third and fourth hydrolysis constants are almost always missing or poorly determined.

Hydrolysis constants is only one group of parameters of those that make up the distribution coefficient. The others are: the surface site density, the surface acidity constants, the concentration of the sorbing cation, the constants pertaining to the different EDL models

(the values of the capacitance(s) and dielectric constant) and the conceptual model used. All these have an effect on which reaction best fits the data, i.e. the number of protons released in the reaction (y). In addition, these parameters are interdependent, and the alteration of one will affect the others in that they must fit the sorption and the titration data.

Including an electrostatic model

If the electrostatic models are to be applied in an analysis, there is a need for a relationship between the equilibrium constant and the apparent equilibrium constant of the surface reaction. Such a relationship is derived below for the 1-pK constant capacitance model. The constant capacitance model does not commonly distinguish between inner and outer sphere complexes. In this derivation, however, inner sphere complexes are included and assumed to be formed at the inner surface. For an inner sphere complex, the charge will depend on the concentration of the cation sorbed onto the solid. That concentration will be significant at high surface loading.

$$\Psi = \frac{F}{CA} \left(\frac{0.5(\alpha'_{\text{SOH1-pK}} - 2)([\text{SOH}]_{\text{tot}} - ([x]_{\text{tot}} - [x]_{\text{totaq}}))}{\alpha'_{\text{SOH1-pK}}} + (z - y)([x]_{\text{tot}} - [x]_{\text{totaq}}) \right) \quad (13)$$

where C is the capacitance, F is faradays constant, and A is the surface area per volume (m^2/L). $[x]_{\text{totaq}}$ and $\alpha'_{\text{SOH1-pK}}$ are a function of pH and Ψ , and the equation has to be solved iteratively. It can be seen from this relationship that the surface site density, the capacitance, the surface area, the charge of the cation and the number of protons released in the reaction will determine how large the contribution of the electrostatic term will be for the system.

Discussion

Issue number one: We sought out to further understand what parameters affect the distribution of a species between the solid and the aqueous phase. A simple relationship was derived. This can be useful in understanding how the choice of electrostatic model will affect the outcome of the interpretation of the surface complex formed on the surface and the distribution between the phases.

Issue number two (arisen from the previous point): Even for a simplified system with only one surface reaction all parameters will be coupled. In order to solve this problem sorption data (giving data for distribution) and spectroscopic data (possibly revealing the surface reaction) are needed for the same system. Above all a method is needed for explicitly determining the electrostatic contribution. How that can be done is still a fairly open question.

TOWARDS A SURFACE COMPLEXATION DATABASE

Anna-Maria Jakobsson

Nuclear Chemistry, Department of Materials and Surface Chemistry
Chalmers University of Technology
SE-412 96 Göteborg, Sweden
miaj@chem.chalmers.se

Johannes Lützenkirchen

Institut für Nukleare Entsorgung
Forschungszentrum Karlsruhe
Postfach 3640
DE-76021 Karlsruhe, Germany

Abstract

Whereas for aqueous solutions widely accepted thermodynamic databases exist, extensive databases for sorption processes are based on compilations of K_d -values, although surface complexation theory allows a straightforward extension of the principles applied to aqueous solutions. Unfortunately, surface complexation databases are scarce. A pathway towards such a database is proposed, which encompasses the critical evaluation of mineral specific raw-data based on available collections of references. A major task is the elaboration of reasonable quality control criteria for the experimental raw-data. Accepted raw-data are digitized and stored in a database. From the raw-data input files for a parameter estimation code may be created. These may be modeled with a self-consistent surface complexation model.

Based on an analysis of the currently available surface complexation models, the 1-pK basic Stern model with charge distribution might be considered for first applications due to its relative simplicity and simultaneous ability to incorporate molecular level information. Aqueous speciation is suggested based on the SIT approach which is currently used for major database development by NEA and IUPAC.

Introduction

Sorption reactions are considered important in many fields. In the context of nuclear waste storage sorption is considered the major retention process in radionuclide migration. However, there is a huge gap between the knowledge on sorption processes and their treatment in reactive transport calculations. While dramatic effects of pH or solution composition on the retention of solutes have been demonstrated experimentally, the K_d concept used in the reactive transport codes involves a constant distribution factor irrespective of the pH or solution composition. Surface complexation models provide a platform that can in principle take such changes into account.

At present enormous progress is made in establishing thermodynamic databases for the speciation of radionuclides in aqueous solution and solid phases by NEA. Similar initiatives

are taken by IUPAC for heavy metals. Both organizations recommend the specific ion interaction theory (SIT) for calculating activity coefficients. For solutions an agreement exists on the treatment of correcting for ionic strength variation.

In principle, surface complexation models are an extension of the aqueous speciation schemes to adsorption reactions at functional groups of mineral surfaces. However, the treatment of electrostatics in surface complexation theory is a matter of debate and no agreement has been reached in many respects. Besides, these drawbacks from the point of view of modelling, there is a need to implement criteria for the evaluation of data quality.

Proposed Procedures

Different steps are required towards the establishment of accepted surface complexation databases. First, in a model independent step published data are collected and evaluated. Data include mineral surface charge and metal, ligand adsorption data. Thus and for the sake of comparison available data for different sorbates and sorbents we propose a primary database where the relevant **raw** data from experiments are collected. We see three different main uses for this first data collection:

1. For adjusting the surface complexation approach. First, the observations may define the minimum requirements of a model (i.e. what needs to be described). Second, different models and consistent approaches may be tried on a large collection of data sets.
2. Gaining a better understanding for the experimental parameters that govern sorption patterns.
3. Identification of areas that need more investigations (and areas that do not need to be further investigated).

This primary, model-independent data base needs to be continuously updated. In a second step the quality of the data is to be evaluated. It is necessary to decide which of the collected data should actually be used in modeling. At present no procedures are available that allow quality control. The problem is visualized on figure 1, which shows a collection of measured points of zero charge for the iron oxyhydroxide goethite. Although for goethite points of zero charge of about 9.3 are now widely obtained by a variety of groups, the majority of data is clearly below this value. Scatter of this important surface chemical property is not expected to be less for other important model sorbents.

Once there is consensus on the acid-base properties of a certain mineral these data define the fixed acid-base sub-model for adsorption studies involving cations or anions or both simultaneously. For all systems where spectroscopy data are available these should be included in order to make the database as comprehensive as possible.

As a summary the following systems have to be included:

- pure minerals acid base properties
- cation, anion adsorption data
- data on ternary systems

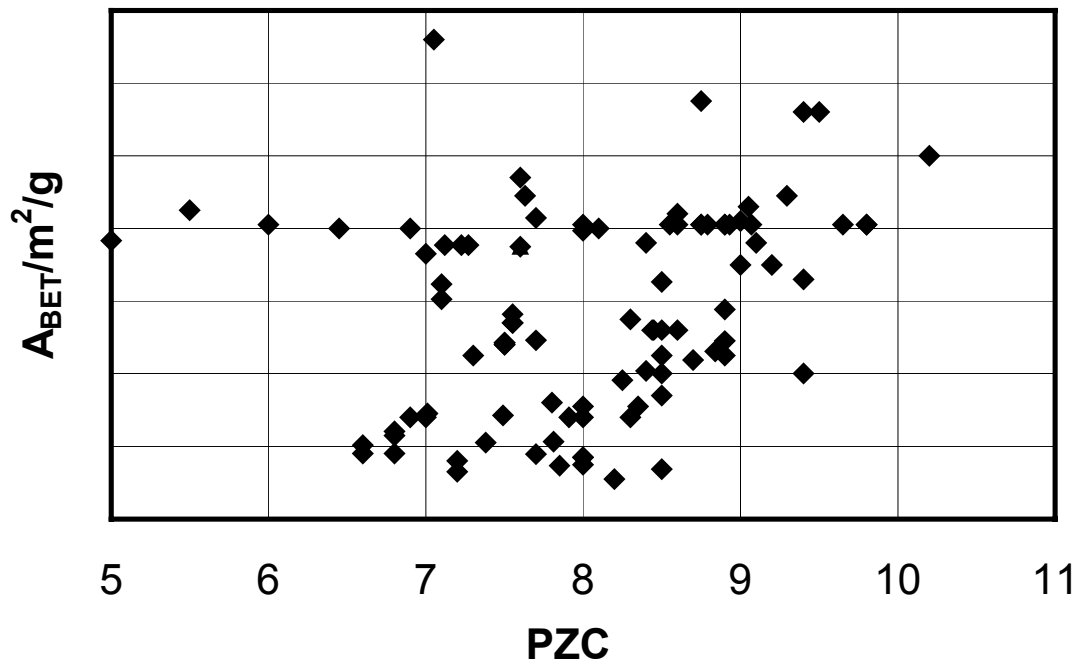


Figure 1: Points of zero charge (PZC) and specific surface area (A_{BET}) for goethite samples as published in the literature (J. Lützenkirchen, in preparation).

Starting from the collection of experimental data to be used, standard procedures for evaluation of surface complexation parameters should be developed and suggested. At present, there is no consensus on which model to use. We suggest that the first model attempt is based on a 1-pK, charge distribution, basic Stern model, since it has been shown to allow

- good fits to experimental data
- include spectroscopic data in the interpretation of macroscopic data
- parameterization that allows treatment of mixed oxide and electrolyte systems

Since all the input-data files are to be stored in the secondary database, it is easy to test different currently applied models for the sake of model comparison, to apply new models, and to include new information on surface speciation. The suggested structure is open so that adjustments in model components or additions of data sets (raw experimental data) and complementary information (spectroscopy) should be possible. The procedures are summarized schematically in Figure 2.

Summary

The database development procedure is proposed to occur along the following pathway:

- Experimental raw data collection from existing compilations of literature references (primary data base of experimental raw data)
- Development of data quality criteria

- Selection of data corresponding to the criteria (selected data from primary data base to be used for parameter optimization)
- Selection of a first model and application to the selected data
- Application of selected model to selected data (secondary data base of optimization input files)
- Construction of the final surface complexation database (including recommended parameters)

The actual modeling procedure is proposed as follows:

- Fix solution speciation and activity coefficient approach (SIT) and the surface complexation model components.
- Model acid-base properties of solids.
- Model adsorption data (anions, cations, ternary systems).
- Use constraints from spectroscopy whenever possible.

In the future the chosen options should allow:

- Continuous updating of surface complexation parameters (with new data)
- Continuous updating of models
- Identification of lacks in the databases

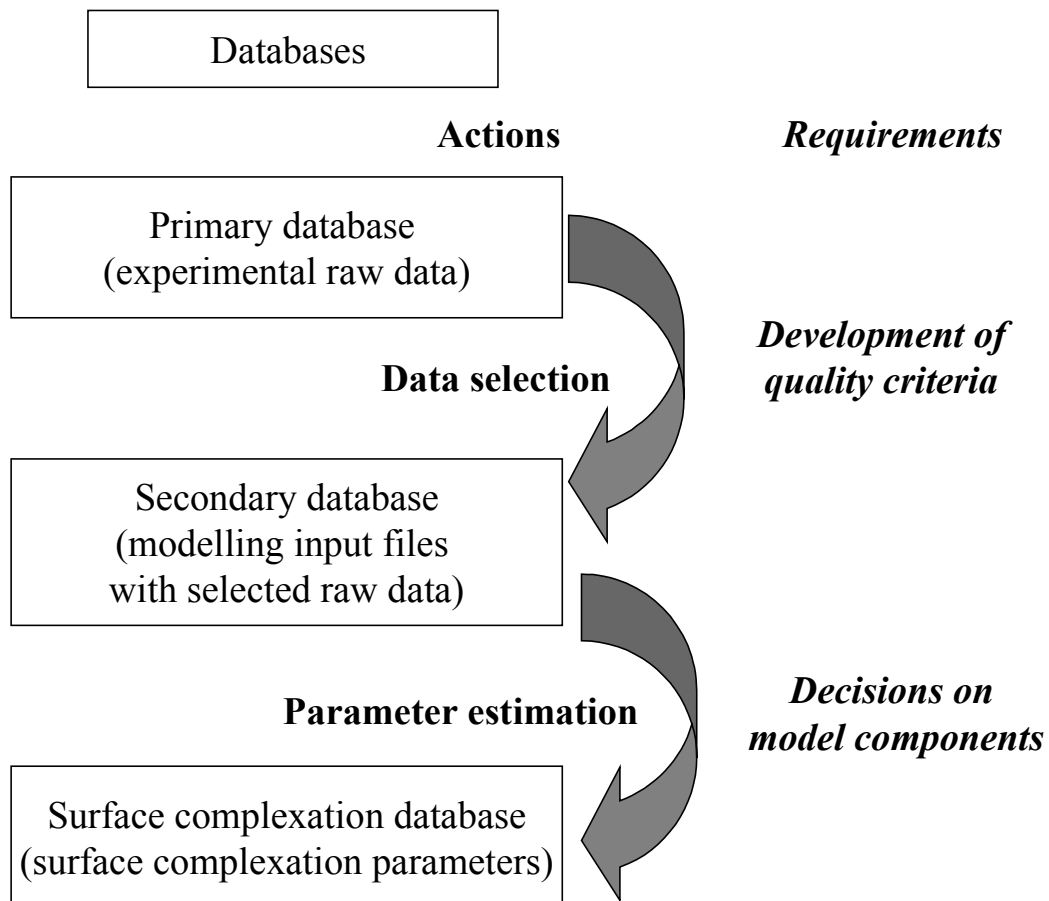


Figure 2: Summary of the proposed procedure towards the development of a surface complexation database.

METAL ION SORPTION TO SCHWERTMANNITE PRECIPITATED FROM MINING WASTE LEACHATES

Jörgen Jönsson, Lars Lövgren, and Per Persson

Department of Chemistry
Inorganic chemistry
Umeå University
Umeå, Sweden
lars.lovgren@chem.umu.se

Introduction

Heavy metals in metal-laden leachates from sulphidic mining waste, often referred to as acid mine drainage (AMD), may be significantly attenuated by formation of secondary solid phases under oxidising conditions. Secondary minerals, above all phases containing ferric iron, can serve as primary adsorbing phases for elements released by weathering processes. Depending on geochemical conditions different iron containing solid phases may be formed by ferrous iron oxidation. At very low pH jarosite ($\text{K,Na,H}_3\text{O}[\text{Fe}_3(\text{OH})_6(\text{SO}_4)_2]$) is commonly formed. In the range $2.8 < \text{pH} < 4.5$, a common pH range for AMD, the most frequently formed solid phase is schwertmannite ($\text{Fe}_8\text{O}_8(\text{OH})_6\text{SO}_4$) (Bigham et al., 1996). Formation of Fe oxyhydroxides without structural sulphate, such as ferrihydrite ($\text{Fe}_2\text{O}_3 \cdot 1.8 \text{H}_2\text{O}$), lepidocrocite ($\gamma\text{-FeOOH}$) and goethite ($\alpha\text{-FeOOH}$) is limited to near neutral and neutral conditions. However, sulphate containing phases have been found to be metastable and are eventually transformed into thermodynamically stable goethite (Jönsson, 2003). The kinetics of this phase transformation depends on both pH and temperature.

The main objectives of the present work have been to study the adsorption of Cu(II) and Cd(II) to schwertmannite as a function of pH, and to characterise surface species formed at different pH on a molecular level. An experimental approach has been used where batch adsorption experiments as a function of pH and total metal ion concentration have been combined with synchrotron-based EXAFS measurements. As schwertmannite is unstable with respect to goethite, in many cases the results obtained have been compared with analogous experiments using goethite as the adsorbent. The present study forms part of the thesis work by Jönsson (2003).

Materials and Methods

The material studied was sampled on top of a till covered tailings deposit at the Kristineberg mine, northern Sweden in June 1998. The pH of the pore water was 3.05. To remove dissolved ions from the pore water and adsorbed metals from the surface, the sample was repeatedly washed with 1 mM nitric acid. The washing procedure also removed many of the larger detrital particles originally present in the material. The remaining solid was dried at 40°C for 3 days, ground in an agate mortar and dried at 40°C for about 10 days until constant weight and stored dry.

The elemental composition of the precipitates was determined after homogenisation by SGAB Analytica AB, Luleå using ICP-AES, and ICP-MS. The elemental analysis gave the composition $\text{Fe}_8\text{O}_8(\text{OH})_{5.02}(\text{SO}_4)_{1.49} \cdot 1.05 \text{H}_2\text{O}$, Table 1. Based on results from a study of Bigham et al. (1990) it was assumed that SO_4^{2-} exceeding $\text{S/Fe}=1/8$ was residing at the

surface rather than as part of the bulk structure. In the current study the SO_4^{2-} exceeding $\text{S/Fe}=1/8$ was 33% of the total amount SO_4^{2-} . Hence, 1/3 of the SO_4^{2-} is estimated to be adsorbed to the mineral surface.

Table 1: Elemental composition of schwertmannite. Elements in $\mu\text{mol g}^{-1}$, H_2O and LOI in weight-% of dry weight.

Fe	8 700	Na	29	Zn	0.15	Zr	0.034	Mn	<0.46	Nb	<0.06
S	1 600	Mg	11	Ba	0.12	Co	0.006	W	<0.32	Mo	<0.06
C	580	P	6.8	La	0.094	Ni	0.004	Cr	<0.19	Sc	<0.02
Si	340	As	2.8	Pb	0.081	Cd	0.0002	Sn	<0.17	Hg	<0.0002
Al	56	V	0.74	Sr	0.068	N	<35	Cu	<0.16	LOI	35.6
K	37	Ti	0.53	Y	0.056	Ca	<18	Be	<0.07	H_2O	20.7

The X-ray powder-diffractogram (Figure 1) resembles those reported for schwertmannite (Cornell and Schwertmann, 1996).

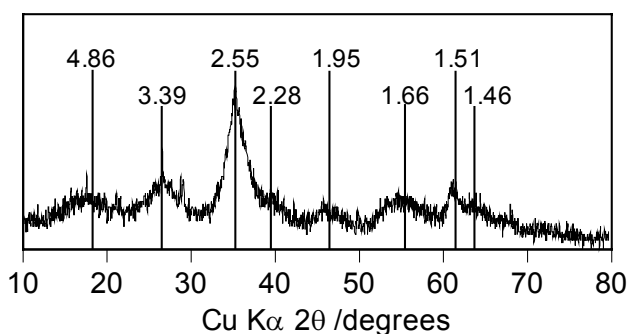


Figure 1: XRD patterns for schwertmannite. The peak positions for schwertmannite (PDF 47-1775) are given as vertical lines.

In a separate study it was shown by XRD measurements that the precipitates were during aging at pH 6 and 9 transformed from schwertmannite to goethite ($\alpha\text{-FeOOH}$), which resulted in an increased specific surface area (Jönsson et al., 2003). At both pH the measured BET area increased within 6 h from $42.9 \text{ m}^2 \text{ g}^{-1}$ to $\geq 180 \text{ m}^2 \text{ g}^{-1}$. However, at pH 9 the surface area decreased comparatively rapid and levelled out at ca. $100 \text{ m}^2 \text{ g}^{-1}$ after approximately one year. The decrease in surface area was significantly slower at pH 6, but at the end of the study ($t = 514$ days) the surface area was approaching the value for the pH 9 sample.

Uptake experiments. The uptake of Cu(II) and Cd(II) to schwertmannite was investigated in a series of batch experiments within the range $3 < \text{pH} < 7$. Metal ion solutions were added to suspensions of schwertmannite (solid concentration: 1 g/dm^3) in $0.1 \text{ mol/dm}^3 \text{ NaNO}_3$ ionic medium. pH in subsamples was adjusted by additions of base. After 48 h of equilibration at 25°C the samples were centrifuged and the aqueous metal ion concentration was measured using Atomic Absorption Spectrometry.

To determine the adsorption capacity of schwertmannite, the uptake of Cd(II) was studied at a pH fixed at a value where the sorption of Cd to well-defined iron oxyhydroxides is known to be almost complete, i.e., pH 7.5 (Palmqvist et al, 1997). Volumes of a Cd solution were added in increments to a suspension of the schwertmannite, and pH was controlled using a pH-stat equipment. The concentration of Cd remaining in solution was determined by atomic absorption spectrometry (AAS) after phase separation by centrifugation.

Structural characterisation of surface species. Cu(II) and Cd(II) K-edge EXAFS data were collected in fluorescence mode at the Stanford Synchrotron Radiation Laboratory, California on beam line 4-1. Data reduction was performed with EXAFSPAK (George and Pickering, 1995) and WinXAS (Ressler, 1998).

Results and discussion

The uptake of metal ions showed a strong pH-dependence, with increased adsorption at high pH. The adsorption edges for Cu and Pb are very similar. Results from experiments with Cu(II) are shown in figure 2. This sorption behaviour is close to what can be predicted by model calculations invoking models for surface complexation based on laboratory studies of metal sorption onto well-defined Fe oxyhydroxides, e.g. goethite (α -FeOOH) (Palmqvist et al., 1997).

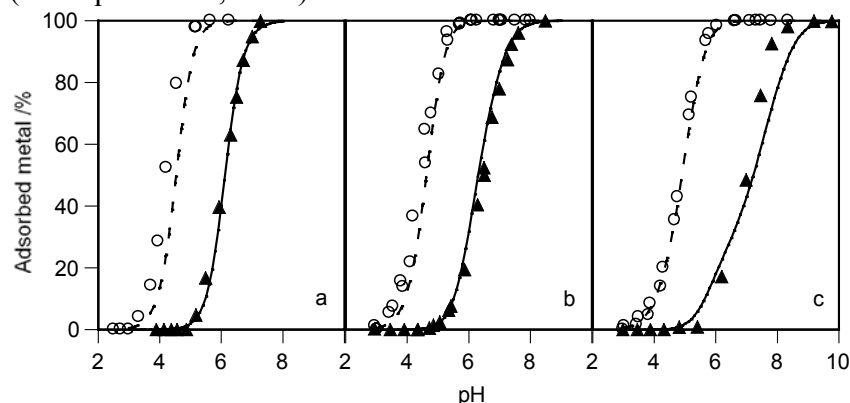


Figure 2: Adsorbed fractions of Cu(II) (\circ) and Cd(II) (\blacktriangle) to schwertmannite as a function of pH with metal/schwertmannite ratios of a) 0.057, b) 0.52 and c) $2.6 \mu\text{mol m}^{-2}$. The model lines are calculated for Cu(II) (dashed) and Cd(II) (solid) adsorption to goethite in the absence of sulphate (data from Palmqvist *et al.*, 1997).

A density of active surface sites of ca. $3 \mu\text{mol m}^{-2}$ was determined from adsorption isotherms obtained from the experiment in which Cd(II) was added to a schwertmannite suspension at pH 7.5. This value is rather similar to the surface site density of crystalline goethite (Lützenkirchen et al, 2002).

Cu(II) EXAFS spectra were collected for samples in the pH range 5-8 with the Cu(II)/schwertmannite ratios 0.52 and $2.6 \mu\text{mol m}^{-2}$ after 1 h and 1 month for the lower ratio and after 1 month for the higher ratio. The general appearance of the Fourier transforms for all data sets is similar with three peaks, representing three shells of atoms at distances of $\sim 2, 3$ and 4 \AA . The EXAFS spectra indicate that two Cu(II) surface species exist in the Cu(II)-schwertmannite system. One is a ternary type B surface complex ($\equiv\text{Fe-SO}_4\text{-Cu}$). However, the increasing Cu-S and Cu-Cu coordination numbers with increasing pH suggest that the initial surface complex is converted into a precipitate-like phase. In the

other surface complex, Cu(II) is directly coordinating to the surface in a bridging bidentate mode ($(\equiv\text{FeO})_2\text{Cu}$). The ageing of the samples suggests that schwertmannite is partly transformed to goethite and that the surface species form at a goethite surface instead of forming at a schwertmannite surface. An alternative interpretation is that adsorbed Cu(II) stabilises the schwertmannite surface and thereby prevents transformation.

In the case of Cd(II) EXAFS spectra were collected for samples in the pH range 6.6-10 with two different Cd(II)/schwertmannite ratios (0.52 and $2.6 \mu\text{mol m}^{-2}$) after 1 month. The results from the Cd(II)-schwertmannite system are similar to the results obtained in the Cu(II)-schwertmannite system. Two different surface species are suggested for both systems and precipitate-like phases form as pH increases. In the Cd(II) system the question whether adsorption occurs to a goethite or a schwertmannite surface is even more justified as the transformation to goethite accelerates as pH increases.

Acknowledgments

This study forms part of the research program Mitigation of the Environmental Impact of Mining Waste (MiMi), which is financed by The Foundation for Environmental Strategic Research (MISTRA).

References:

- Bigham, J.M., Schwertmann, U., Carlson, L. and Murad, E. (1990) A poorly crystallized oxyhydroxysulfate of iron formed by bacterial oxidation of Fe(II) in acid mine waters. *Geochim. Cosmochim. Acta* **54**, 2743-2758.
- Bigham, J.M., Carlson, L. and Murad, E. (1994) Schwertmannite, a new iron oxyhydroxysulphate from Pyhäsalmi, Finland, other localities. *Mineral. Mag.*, **58**, 641-664.
- Cornell, R.M. and Schwertmann, U. (1996) *The iron oxides*, VCH, Weinheim.
- George, G.N. and Pickering, I.J. (1995) *EXAFSPAK*, Stanford Synchrotron Radiation Laboratory, Stanford.
- Jönsson, J. (2003) *Phase transformation and surface chemistry of secondary iron minerals formed from acid mine drainage*. Doctoral thesis, Umeå University.
- Jönsson, J., Persson, P., Sjöberg, S. and Lövgren, L. (2003) Schwertmannite precipitated from acid mine drainage: Phase transformation, sulphate release and surface properties. Submitted to *Appl. Geochem.*
- Lützenkirchen J, Boily JF, Lövgren L, Sjöberg S. (2002) Limitations of the potentiometric titration technique in determining the proton active site density of goethite surfaces. *Geochim. Cosmochim. Acta.* **66**, 3389-3396.
- Nordstrom, D.K. and Alpers, C.N. (1999): Geochemistry of acid mine waters. In: *The environmental geochemistry of mineral deposits. Part A: Processes, techniques and health issues*. Society of Economic Geologists, Inc., Littleton.
- Palmqvist, U., Ahlberg, E., Lövgren, L., Sjöberg, S. (1997) *In situ* voltammetric determinations of metal ions in goethite suspensions: Single metal ion systems. *J. Colloid Interface Sci.* **196**, 254-266.
- Ressler, T. (1998) WinXAS: a program for X-ray absorption spectroscopy data analysis under MS-Windows. *J. Synch. Rad.*, **5**, 118-122.

SORPTION OF ACTINIDES ONTO GRANITE AND ALTERED MATERIAL FROM ÄSPÖ HRL

Bernhard Kienzler, Jürgen Römer, Dieter Schild and Walter Bernotat

Institut für Nukleare Entsorgung
Forschungszentrum Karlsruhe GmbH
D-76021 Karlsruhe, GERMANY
Kienzler@ine.fzk.de

Abstract

Within the scope of a bilateral cooperation between Svensk Kärnbränslehantering AB (SKB) and Forschungszentrum Karlsruhe, Institut für Nukleare Entsorgung (FZK-INE), actinide migration experiments with Pu, Am, and Np are conducted at the Äspö Hard Rock Laboratory. Migration experiments are complemented by batch experiments providing detailed information on the relevant retention processes for actinides onto granite and altered fracture material. α -Autoradiography and XPS were used to quantify local sorption properties of the rock samples. It is shown that Np is retained by reduction to Np(IV) in the presence of Fe(II) minerals. Sorption of U correlates with Fe oxide phases. The sorption coefficient for Pu is significantly higher compared to Np or U. Pu retention takes place on a multitude of minerals.

Introduction

The Äspö Hard Rock Laboratory (HRL) was established in Sweden in a granite rock formation for in-situ testing of disposal techniques and for investigations concerning migration and sorption of radionuclides [1]. Groundwater flow through fractures in crystalline host rocks may cause migration of radionuclides from the repository. Within the scope of a bilateral cooperation between Svensk Kärnbränslehantering AB (SKB) and Forschungszentrum Karlsruhe, Institut für Nukleare Entsorgung (FZK-INE), actinide migration experiments with Pu, Am, and Np are conducted at the Äspö Hard Rock Laboratory. The same type of migration experiments were performed in laboratory at FZK-INE and at Äspö HRL. To guarantee most realistic undisturbed conditions typical for a deep underground repository, experiments are performed in the CHEMLAB 2 probe [2]. To understand findings of the migration experiments, series of laboratory experiments are conducted. Batch experiments provide information on the sorption behavior of the different solids present at Äspö HRL [3].

Materials

Groundwater: For laboratory investigations, Äspö groundwater was used, which was extracted from the drill hole SA 2600. The groundwater composition is given in ref. [4]. Major cations were Na^+ and Ca^{2+} , the dominant anion was Cl^- (with 0.09, 0.04 and

0.2 mol dm⁻³). Ionic strength was 0.24 molal. The laboratory experiments were performed in a glove box under a 99% Ar, 1% CO₂ atmosphere at room temperature (22±1°C). pH was 7.2 and Eh was between 112 to -50 mV (Ingold Pt-4805 against Ag/AgCl, corrected with respect to hydrogen electrode). Fe could not be measured in the groundwater used in laboratory (SA 2600). Fe-hydroxides had been precipitated during the transport to Germany.

Rock samples from Äspö: Sorption experiments in laboratory were performed onto samples provided as slices (1.5cm × 1.5cm, grinded and polished) of freshly broken Äspö rock and of altered material (weathered fracture filling, untreated, selected planar samples). The solids were characterized and analyzed by scanning electron microscopy (SEM-EDS) and XRD. Element mappings of granite and altered material in a fracture are presented in ref. [5]. The granite showed fine grained Fe-oxides /oxyhydroxides. X-ray diffraction showed that chlorite is a main constituent in the altered fracture material.

Radionuclides: For batch experiments, actinide spiked groundwater SA 2600 was prepared (according to ref [6]) using the actinides ²³⁸Pu, ²³⁷Np and ²³³U. Concentrations applied were 1×10⁻⁹ mol dm⁻³ (7.5×10⁵ Bq dm⁻³) for ²³⁸Pu, 1×10⁻⁴ mol dm⁻³ (5×10⁵ Bq dm⁻³) for ²³⁷Np and 1×10⁻⁵ mol dm⁻³ (8.4×10⁵ Bq dm⁻³) for ²³³U. The pH measured in the different spike solutions were 6.9 to 7.1.

Methods

The rock samples were pre-equilibrated with Äspö groundwater [3] for about 2 weeks in a glovebox at anoxic conditions (99% Ar, 1% CO₂). The atmospheric oxygen concentrations were kept less than 10 ppm. After equilibration, the slices were immersed in actinide spiked Äspö groundwater. The exposure periods varied between 1 hour and 14 days. After exposure, the slices were scanned by means of an optical scanner using a resolution of 600×600 pixel per inch. The radioactivity retained on each slice was measured by spatially resolved autoradiography (Cyclone Phosphor Scanner, Packard BioScience) at same resolution. By calibration of α-autoradiography of a rock sample with respect to α-spectroscopy, the absolute activity on the slices was obtained. Composition and area distribution of the mineral phases in the slices was determined by SEM-EDS. Retained Np was dissolved from some slices and by means of TTA extraction, the oxidation state of initially pentavalent Np could be detected.

XPS is used for identification of chemical valence states of Np and Fe on the surface. A transfer vessel was used to move samples from the glovebox to the XPS spectrometer (PHI model 5600ci) avoiding air contact. High-resolution scans of elemental lines were recorded by use of monochromatic Al K_α X-ray excitation (1486.6 eV) and 11.75 eV pass energy of the hemispherical capacitor analyzer which yields a full-width-at-half-maximum (FWHM) of the Ag 4d_{5/2} line of 0.60 eV. XPS maps are acquired by use of Mg K_α (1253.6 eV) X-rays. The binding energy scale of the spectrometer was calibrated by Cu 2p_{3/2}, Ag 3d_{5/2}, and Au 4f_{7/2} lines of pure and Ar⁺ sputter cleaned metal foils.

Results and Discussion

Sorption onto natural material: For comparison of sorption between the different actinides the sorption coefficient K_s is calculated by

$$K_s = \frac{\text{activity on the surface (Bq cm}^{-2}\text{)}}{\text{activity in the solution (Bq cm}^{-3}\text{)}}$$

K_s (cm)	freshly broken granite	altered material
^{238}Pu	2.50	1.30
^{237}Np	0.16	0.16
^{233}U	0.026	0.018

Tab. 1: Sorption coefficient of actinides on Äspö materials after 14 days of immersion

Results of sorption experiments onto freshly broken granite and onto altered material are given in Table 1. Significant differences of K_s are observed between the actinides, but only slight differences between freshly broken granite and altered materials. The time dependence of sorption within the period under investigation is similar for Pu and U. In contrast Np shows fast sorption onto altered material and retarded sorption onto granite (Fig. 1). Fig. 2 shows the optical scan, α -autoradiogram and elemental map of iron for a slice consisting of altered material exposed to U-solution. The optical scan shows differently colored phases. Black areas indicate mainly epidote or chlorite in line with measured Fe abundance. Light colored areas are identified as feldspar and quartz. The α -autoradiogram correlates well with the measured Fe distribution. Maxima of retained U coincide with local enrichments of Fe oxides. Np shows similar sorption features as U for altered and fresh granite and is also correlated to Fe bearing minerals. In contrast, Pu has a significant higher sorption coefficient but α -autoradiography shows no correlation with the Fe distribution. Pu is retained inhomogeneously onto the surfaces, but correlation with the element distributions of K, Ca, Si, Al or Mg is not observed.

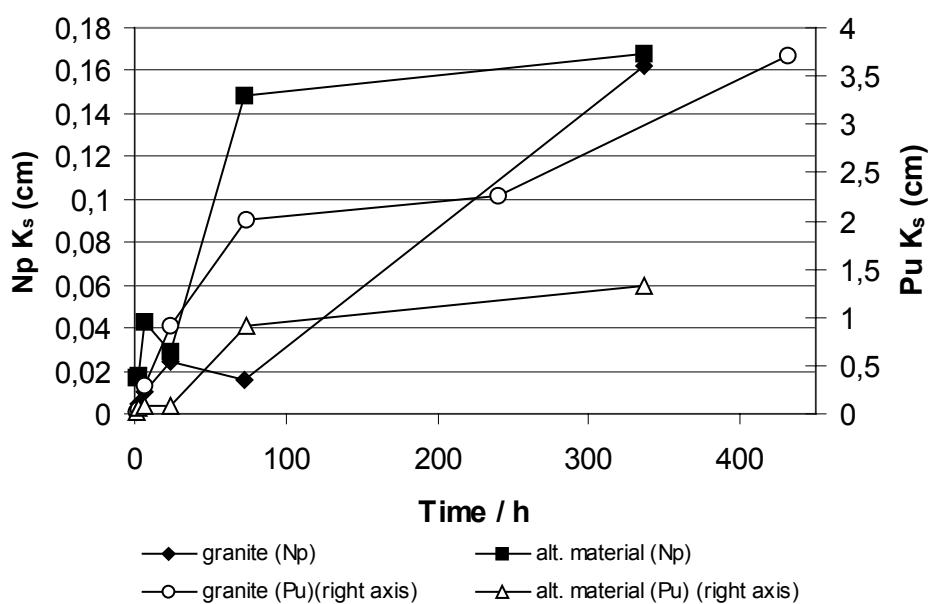


Fig. 1: Sorption coefficient of Np and Pu onto granite and altered material

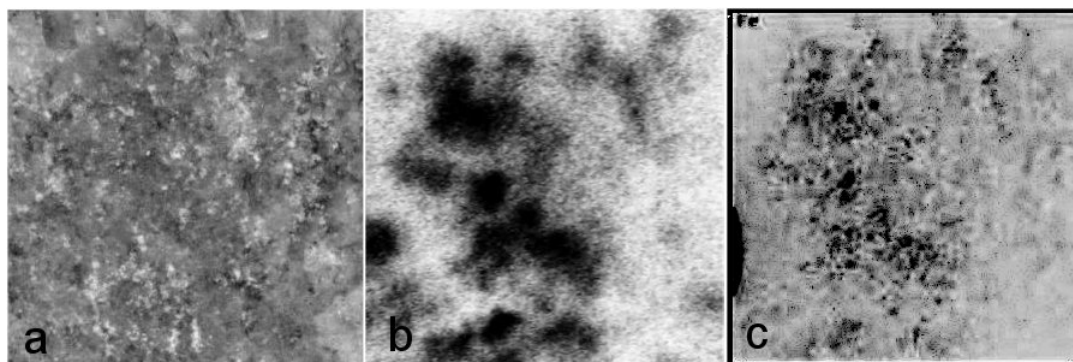


Fig. 2: Optical scan (a), α -autoradiography(b), and Fe distribution (c) of altered material exposed to U spiked solution.

Speciation of retained actinides: XPS was used for identification of chemical valence states of redox sensitive elements on the surface, such as Np and iron. Analyses of various areas on the samples indicated correlation of Np(IV) with the presence of Fe(II). More than 80 % of Np could be assigned to the tetravalent state which is confirmed by TTA extraction method. XPS mapping of a (2 x 2) mm² area of granite immersed for 14 days in Np spiked solution showed correlation between Fe(II) and Np(IV) (Fig. 3). Concentrations of ²³⁸Pu are too low for this kind of investigations. Reduction of U(VI) to U(IV) retained on crushed high-FeO olivine rock was reported by Rodrigues at al. using XPS [7]. Due to groundwater composition used for our experiments, U concentration in the spiked solution was by one order of magnitude lower. This fact and limited sorption of U (Tab. 1) prevented detection of U by XPS.

Conclusions

Following conclusions can be drawn from this study:

- Np is retained onto granite and altered materials by reduction to Np(IV) in presence of Fe(II) minerals. This finding is in line with the results of other authors [8].
- Pu sorption takes place on a multitude of minerals. Specific sorption processes cannot yet be presented. However, the sorption coefficient is significantly higher compared to Np or U in agreement with migration experiments [3].
- Strongest sorption of U is correlated with Fe oxide phases.

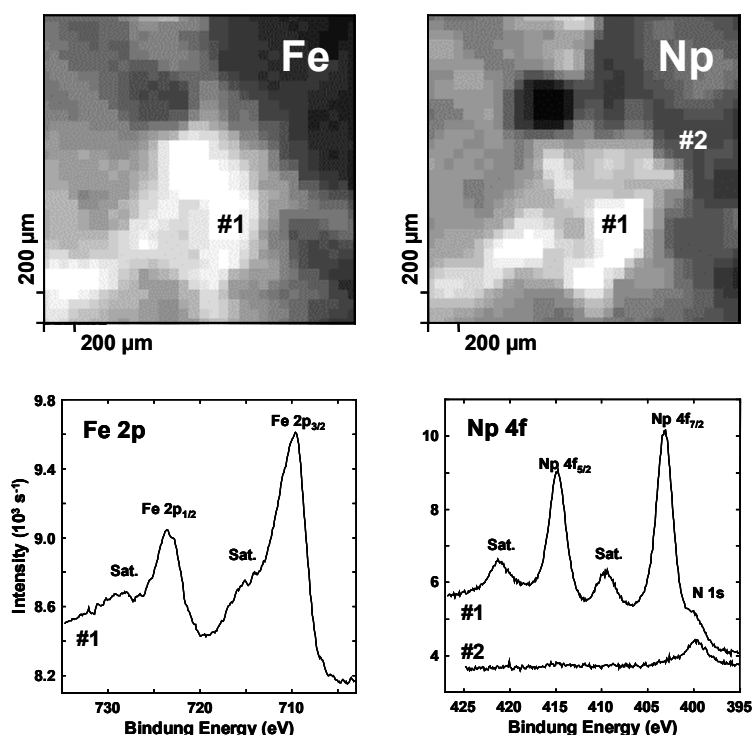


Fig. 3: XPS maps of a 2mm × 2mm area of granite immersed for 14 days in Np spiked solution (bright plotted areas correspond to enhanced atomic concentrations). Curve #1 and #2 are measured at the locations indicated in the maps

Acknowledgment

The present work was performed within the Project Agreement for collaboration on certain experiments related to disposal of radioactive waste in the Äspö Hard Rock Laboratory (HRL) between the German Bundesministerium für Wirtschaft und Arbeit (BMWA) and the Svensk Kärnbränslehantering AB (SKB).

References:

1. Bäckblom, G.: The Äspö hard rock laboratory - a step towards the Swedish final repository for high-level radioactive waste. *Tunnelling and Underground Space Technology* **4** (1991) 463-467.
2. Jansson, M.; Erikson, T. E.: CHEMLAB In-Situ Diffusion Experiments Using Radioactive Tracers. *Radiochim. Acta* **82** (1998) 153-156.

3. Kienzler, B.; Römer, J.; Vejmelka, P.; Jansson, M.; Eriksen, T. E.; Spahiu, K.: Actinide Migration in Granite Fractures: Comparison between In-Situ and Laboratory Results. *Mat. Res. Soc. Symp. Proc.* Vol. **757** (2003) 523-528.
4. Kienzler, B.; Vejmelka, P.; Römer, J.; Fanghänel, E.; Jansson, M.; Eriksen, T. E.; Wikberg, P.: Swedish-German actinide migration experiment at Äspö hard rock laboratory. *J. Cont. Hydrol.* **61** (2003) 219– 233.
5. Römer, J.; Kienzler, B.; Vejmelka, P.; Soballa, E.; Görtzen, A.; Fuß, M.: Actinide migration experiment in the HRL ÄSPÖ, Sweden: Results of laboratory and in-situ experiments (Part II). Forschungszentrum Karlsruhe, FZKA 6770 (2002).
6. Vejmelka, P.; Kienzler, B.; Römer, J.; Marquardt, C.M.; Soballa, E.; Geyer, F.; Kisely, T.; Heathman, D.: Actinide migration experiment in the HRL ÄSPÖ, Sweden: Results of laboratory and in-situ experiments (Part I). Forschungszentrum Karlsruhe, FZKA 6652 (2001).
7. Rodrigues, E.; El Aamrani, F.Z.; Giménez, J.; Casas, I.; Torrero, M.E.; de Pablo, J.; Duro, L.; Hellmuth, K.-H.: Surface characterization of olivine-rock by X-ray photoelectron spectroscopy (XPS): Leaching and U(VI)-sorption experiments. *Mat. Res. Soc. Symp. Proc.* Vol. **506** (1998) 321-327.
8. Nakata, K.; Nagasaki, S.; Tanaka, S.; Sakamoto, Y.; Tanaka, T.; Ogawa H.: Sorption and reduction of neptunium(V) on the surface of iron oxides. *Radiochim. Acta* **90** (2002) 665-669.

INTERACTION PROCESSES OF TETRAVALENT ACTINIDES IN THE SYSTEM HUMIC ACID / QUARTZ SAND / SOLUTION

A. Křepelová, J. Mibus, S. Sachs, C. Nebelung, G. Bernhard

Forschungszentrum Rossendorf e.V.
Institute of Radiochemistry
P.O. Box 510119
D-01314 Dresden
Germany
a.krepelova@fz-rossendorf.de

Introduction

Studies on the migration behavior of radioactive and non-radioactive toxic substances are of high importance for the reliable long-term risk assessment of potential underground nuclear waste repositories. Depending on the prevailing geochemical conditions different materials and processes can influence the behavior of such pollutants in natural aquifer systems. Therefore, knowledge on these processes and materials is indispensable for the trustworthy modeling of the migration of radioactive and toxic metal ions, e.g., actinide ions, in the nature.

Besides inorganic ligands humic acids (HA), organic macromolecules ubiquitous found in natural environments, play an important role in the interaction processes of actinide ions. HA are soluble in the pH range of natural waters and possess the ability for complex and colloid formation. In addition to that, HA are characterized by redox properties, which can influence the oxidation state of metal ions. Due to these properties HA can affect the speciation of metal ions, e.g., actinide ions, and therefore, their migration in the environment. The colloidal behavior of HA together with their high complexing ability for metal ions may cause an effective transport mechanism for actinides. Under reducing conditions, as prevalent in deep underground environments, e.g., in deep groundwaters (Kim, 1986), actinides can occur in the tetravalent oxidation state, which then dominates their speciation and migration.

In the present work the influence of HA on the interaction of tetravalent actinides onto quartz sand was investigated in batch and column experiments. HA can affect the sorption of actinides onto mineral surface as a complexing ligand for cations in solutions, and as an adsorbent by modifying the properties of the mineral surface.

Batch experiments were performed with Th(IV) as stable tetravalent actinide element. Column experiments were carried out with uranium which is less stable in the tetravalent state under laboratory conditions. Results of the U(IV) migration were compared to the U(VI) migration.

Materials and methods

A marine fine sand, Gaussian distributed in particle size, with a mean grain diameter of 153 μm from Heerlen, Netherlands, was chosen for its chemical purity (0.3 % Al, 0.02 % Ti, 0.02 % Fe). Prior to use, the quartz sand was washed with Milli-Q water and annealed for 6 hours at 700 °C.

The HA interactions in the quartz sand system were studied applying synthetic HA type M42 (Pompe et al., 1998) and ^{14}C -labeled synthetic HA type M42 (2.38 MBq/g, Pompe et al., 2001). Both, the unlabeled and the ^{14}C -labeled synthetic HA show comparable properties (Pompe et al., 2001). Their functional and structural characteristics are also comparable to natural HA.

All experiments were performed at room temperature under inert gas conditions (N_2), in a 0.1 M NaClO_4 background electrolyte solution, which was degassed for the column experiments. The quartz sand was equilibrated with the solution over a period of 3 – 4 weeks.

Batch experiments

Three kinds of batch experiments were performed: HA sorption on quartz sand in the absence of Th(IV), Th(IV) sorption onto quartz sand in the absence of HA, and Th(IV) sorption in the presence of HA. In the last case, Th(IV) and HA were simultaneously added to the preconditioned mineral. The final concentrations of Th(IV) and HA were $1.2 \cdot 10^{-8}$ M and 20 mg/L, respectively. The solid solution ratio was 5 mg/L. The pH values were adjusted in the range from pH 3 to pH 7.5. The samples were shaken for 4 days to reach the equilibration. After shaking and short sedimentation of mineral particles, the supernatants of single samples were filtered using Minisart N membranes (Sartorius) with a pore size of 450 nm. The filtrates were analyzed by liquid scintillation counting (LSC) for the final HA concentration and by ICP-MS for the final Th(IV) concentration. The amount of Th(IV)/HA adsorbed on the surface mineral was calculated as the difference between the initial Th(IV)/HA concentration and the sum of the amounts of Th(IV)/HA remaining in solution and Th(IV)/HA adsorbed onto the vial walls (for the details see Sachs et al., 2003).

Column experiments

Columns 250 mm in length and 50 mm in diameter, tightly packed with quartz sand were used. Continuous pulse injection was applied. The tracer impulse was followed by a multiple elution of the column with 0.1 M NaClO_4 (pH 7.5). The Darcy velocity was $(3.6 \pm 0.5) \cdot 10^{-6} \text{ ms}^{-1}$. For the determination of the hydraulic and transport parameters of the columns, tritiated water (HTO) was used as conservative tracer. The effective pore volume was determined to 178.2 ± 3.8 mL. Each experiment was studied in a separate column in order to avoid mutual interferences. Concentrations of the reactive substances are listed below in Tab. 1. U(IV) was prepared by electrochemical reduction. Redox speciation was proven by TTA (4,4,4-trifluoro-1-(2-thienyl)-1,3-butanedione) solvent extraction. Breakthrough curves (BTC) of HTO, HA and U were measured by fraction analysis using LSC for HTO, ^{14}C and ^{234}U , and ICP-MS for ^{238}U . The LSC spectra were deconvoluted to determine the activity contribution of ^{232}U and its daughter nuclides contained as traces in ^{234}U .

Results and discussion

HA and Th(IV) sorption (Fig. 1)

The sorption of HA on quartz sand depends on pH. The HA sorption decreases with increasing pH value. The results show that about 70 % of HA are sorbed onto quartz sand at pH 3. However, partial precipitation of HA on the surface at pH 3 can not be ruled out. At $\text{pH} \geq 7$ no HA adsorption was detected.

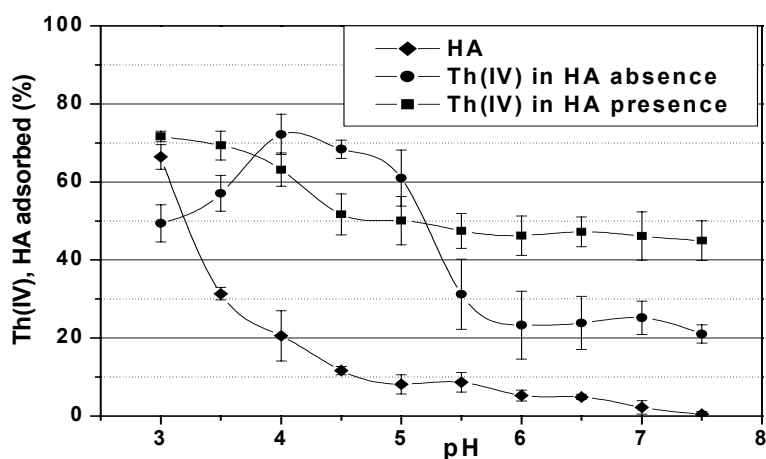


Fig. 1: Th(IV) and HA sorption onto quartz sand. (Th(IV) adsorption in the absence of HA at $\text{pH} > 5$ is influenced by wall sorption).

These results correspond to the properties of quartz sand and HA in solution. Quartz has a low point of zero charge - PZC: 2.0 (Schmeide et al., 2000), which results in predominantly negatively charged surfacespecies ($> \text{SiO}^-$) in the pH range studied. At $\text{pH} > 7$ carboxyl groups of HA are deprotonated, resulting in a negative charge of the HA. Due to electrostatic repulsion no HA is sorbed onto the negatively charged surface of quartz sand, which explains the observed sorption behavior. In the pH range between pH 3 and pH 4, the sorption of Th(IV) on quartz sand in the presence of HA seems to be slightly higher compared to the HA - free system which can be explained by additional binding sites from HA. From pH 4 to pH 5 dissolved HA leads to a decrease of Th(IV) uptake compared to the system free of HA due to formation of dissolved Th(IV)-humate complexes. In the range of $\text{pH} > 5$, the sorption of Th(IV) in the absence of HA is weak due to the high Th(IV) sorption onto the vial walls which competes with Th(IV) sorption on the quartz sand surface. Thus, it is not comparable with the sorption in the presence of HA.

Migration of U(IV)/U(VI) and HA

The retardation factors (R_f , Tab. 1) for HA indicate that there is no significant interaction between HA and quartz sand. R_f is the ratio of effluent pore volume at tracer breakthrough and the effective pore volume. The tracer recovery for HA in the eluate (R_{eluate} , Tab. 1) points to irreversible filtration effects. R_{eluate} is the ratio of eluted and input tracer quantity. The U(VI) migration in the absence of HA (Fig. 2a) is characterized by a kinetically controlled strong retardation which is reflected in the shape of the BTC and the $R_f > 1$. The

low U(VI) recovery is ascribed to sorption processes. However, in HA presence the U(VI) transport is accelerated and the recovery is increased (Fig. 2a). Both, HA and U(VI), exhibit slightly different R_f and R_{eluate} values caused by association/dissociation processes in the system HA-U(VI)-quartz sand. Considering the results reported in Artinger et al., 2002, it can be assumed that these processes are kinetically controlled.

Tab. 1: Experimental conditions and results.

Exp.	HA (mg/L)	U (mol/L)	Species	R_f	R_{eluate}
1	49.9	-	HA	1.02 ± 0.02	0.91 ± 0.01
2	50.3	-	HA	1.02 ± 0.02	0.92 ± 0.01
3	-	$1.1 \cdot 10^{-5}$	U(VI)	2.09 ± 0.10	0.43 ± 0.02
4	49.9	$1.0 \cdot 10^{-5}$	HA	1.05 ± 0.02	0.85 ± 0.01
			U(VI)	1.19 ± 0.02	0.80 ± 0.01
5	50.0	$1.0 \cdot 10^{-6}$	HA	1.04 ± 0.02	0.90 ± 0.01
			U(VI)	1.11 ± 0.02	0.90 ± 0.06
			U(IV)	1.07 ± 0.02	0.66 ± 0.05

The portion of U(IV) and U(VI) in the starting solution amounts to 8 % and 92 %, respectively. This ratio was stable over the duration of the experiments and was also found in the effluent solutions, thus indicating that no oxidation occurred in the column. Fig. 2b shows the BTC for HA, U(IV), and U(VI). As with the case of U(IV), the association/dissociation reactions control the transport behavior in presence of HA ($R_f > 1$). In the Exp. 5 R_{eluate} of U(VI) and HA agree very well. This fact refers to a HA bound U(VI) transport. The lower U(IV) recovery points to a stronger interaction with the quartz sand and thus to a more distinct immobilization. Nevertheless, there are strong indications that HA has a mobilizing effect on the U(IV) transport.

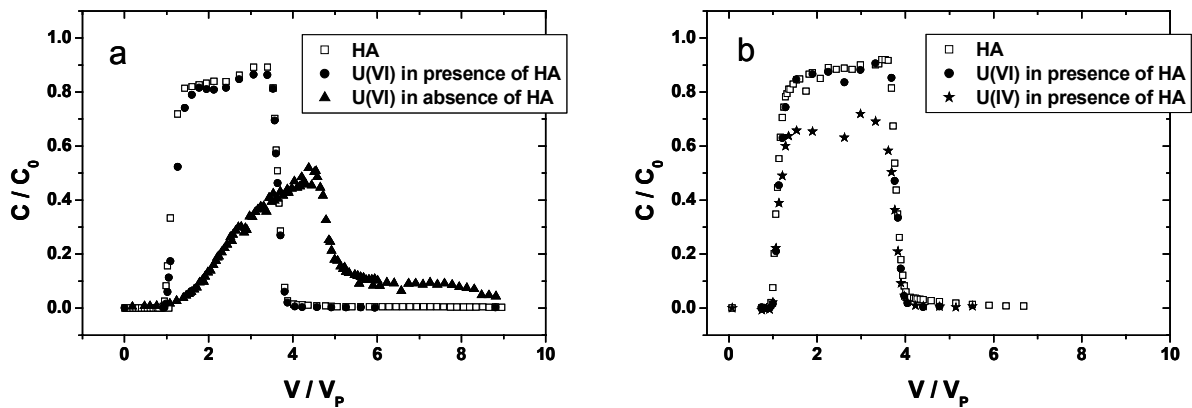


Fig. 2: Breakthrough curves of HA and U. a) U(VI), b) U(IV)/(VI)

C : measured and C_0 : initial concentration.

V : effluent volume, V_p : effective pore volume.

Conclusions

HA shows a pH-dependent influence on the Th(IV) sorption onto quartz sand. At $pH < 4$ HA may immobilize Th(IV) due to HA sorption and/or precipitation onto the surface. Between $pH 4$ and $pH 5$ the Th(IV) sorption is decreased in the presence of HA which can

be attributed to the formation of dissolved Th(IV)-humate complexes. For higher pH values a comparable effect is assumed.

From the column experiments it can be concluded that HA affects the migration of both U(IV) and U(VI). In the presence of HA U(VI) is significantly mobilized. A similar effect is supposed for U(IV). This is in accordance with the results of the batch experiments.

Acknowledgements

This work was financially supported by the Bundesministerium für Wirtschaft und Arbeit under contract No. 02E9299. We thank V. Brendler for the thermodynamic calculations, J. Tutschku for the electrochemical reduction of uranium(VI), and U. Schaefer for ICP-MS measurements. The authors gratefully acknowledge S. Brockmann, R. Ruske, and M. Meyer for their technical assistance.

References:

- Artinger, R., Rabung, T., Kim, J.I., Sachs, S., Schmeide, K., Heise, K.H., Bernhard, G., Nitsche, H.: Humic Colloid-borne Migration of Uranium in Sand Columns. *J. Contam. Hydr.* 58, p. 1-12 (2002)
- Kim, J.I.: Chemical Behaviour of Transuranic Elements in Natural Aquatic Systems. In: *Handbook on the Physics and Chemistry of the Actinides* (Freeman, A.J., Keller, C., eds.). Elsevier Science Publishers B.V., p. 413 – 455 (1986)
- Pompe, S., Brachmann, A., Bubner, M., Geipel, G., Heise K.H., Bernhard, G., Nitsche, H.: Determination and Comparison of Uranyl Complexation Constants with Natural and Synthetic Humic Acids. *Radiochim. Acta* 82, p. 89 – 95 (1998)
- Pompe, S., Bubner, M., Meyer, M., Nicolai, R., Heise, K.H., Bernhard, G.: Synthesis of ¹⁴C-Labeled and Unlabeled Synthetic Humic Acid Type M42. In Th. Fanghänel (ed.), *FZR-318, Annual Report 2000*: Forschungszentrum Rossendorf, Institute of Radiochemistry, Rossendorf, Germany (2001)
- Sachs, S., Schmeide, K., Brendler, V., Křepelová, A., Mibus, J., Geipel, G., Heise, K.H., Bernhard, G.: Investigation of the Complexation and the Migration of Actinides and Non-Radioactive Substances with Humic Acids under Geogenic Conditions. Complexation of Humic Acids with Actinides in the Oxidation State IV Th, U, Np. Final Report, BMWA Project No. 02E9299, Rossendorf (2003)
- Schmeide, K., Pompe, S., Bubner, M., Heise, K.H., Bernhard, G., Nitsche, H.: Uranium(VI) sorption onto phyllite and selected minerals in the presence of humic acid. *Radiochim. Acta* 88, p. 723 – 728 (2000)

ON STANDARD-STATE CHEMICAL POTENTIALS AND ACTIVITY COEFFICIENTS OF SURFACE SPECIES ON MINERAL-WATER INTERFACES

Dmitrii A. Kulik

Waste Management Laboratory

Paul Scherrer Institute

CH-5232 Villigen PSI

Switzerland

dmitrii.kulik@psi.ch

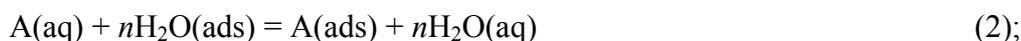
Introduction

Compilation of an internally consistent chemical thermodynamic data base for surface species remains a challenge because, first of all, the experimental K_d values must be converted into standard chemical potentials μ° or equilibrium constants $\ln K = -\Delta_r \mu^\circ / (RT)$ comparable between all mineral surfaces, and consistent with that of solids, gases, liquids and aqueous species. Required conventions on standard and reference states for adsorbed chemical species are missing; it is not clear how to convert μ° or K between various already proposed standard states. Until major disagreements are sorted out, the unified adsorption thermodynamic database will loom as an unreachable dream. This contribution is aimed at exploring the sources of disagreements, and identifying feasible ways to reach the missing conventions.

The (electro)chemical potential μ_j for any j -th component of any phase in the system is:

$$\mu_j = \mu_j^\circ + RT \ln(C_j \cdot \gamma_j) + F \cdot z_j \Psi \quad (1)$$

(the surface tension term omitted; other symbols explained below). Adsorption on mineral-water interface can be seen in the simplest case as an equilibrium partitioning of a component A between the bulk solution (aq) and a surface “interphase” (ads), with concomitant displacement of n water molecules forming a “pure interphase” [3]:



$$\ln K = \ln \{A(\text{ads})\} + n \ln \{H_2O(\text{aq})\} - \ln \{A(\text{aq})\} - n \ln \{H_2O(\text{ads})\} \quad (3),$$

where braces $\{ \}$ denote activities a_j as

$$\ln a_j = (\mu_j - \mu_j^\circ) / (RT) \quad (4).$$

In order to define the activity-concentration relationships, standard μ_j° values, and to describe adsorption at arbitrary states of interest using eqns (1) - (4), several things must be established:

1. Scale, in which concentration of surface species C_j is expressed.
2. Standard states of surface species and the “surface solvent” to determine μ_j° values.
3. Reference states, where $(\mu_j - \mu_j^\circ) / (RT)$ equals $\ln C_j$.

4. Activity coefficient terms γ_j of surface complexes and of “surface solvent” or “sites”.
5. Coulombic correction terms $Fz_j\Psi$ for surface species of charge z_j .

By now, some agreement exists only about expressing the electrical potential Ψ in Coulombic correction terms (5.) as a function of EDL structure and surface plane charge densities σ (in $\text{C}\cdot\text{m}^{-2}$) in an electrostatic model of choice (CCM, BSM, TLM etc. [4]). Such models imply that the total surface area A_T of the sorbent is known. As Ψ has no thermodynamic significance [10], the reference state must be defined at $\Psi = 0$, meaning that Coulombic terms correct C_j as exponential activity coefficient terms [7]. However, there is still a lot of confusion regarding items 1. to 4. common to all surface complexation models (SCM), either electrostatic or not.

Thermodynamic Concentration

In LMA codes (PHREEQC, FITEQL) and related literature, surface complexes are handled in molar ($\text{mol}\cdot\text{L}^{-1}$) or molal ($\text{mol}\cdot(\text{kgH}_2\text{O})^{-1}$) concentrations, just as aqueous complexes, but subject to additional mole-balance constraints for the total concentration of surface sites C_{TS} ($\text{mol}\cdot\text{L}^{-1}$ or molal), and, optionally, to Coulombic terms. The input value C_{TS} is usually obtained as $C_{TS} = \Gamma_T \cdot A_s \cdot C_s$, where A_s is the specific surface area of the solid ($\text{m}^2\cdot\text{g}^{-1}$), C_s is the solid concentration ($\text{g}\cdot\text{L}^{-1}$) in the system, and Γ_T is a total site density ($\text{mol}\cdot\text{m}^{-2}$) that refers to the actual solid surface. C_{TS} values are often treated as fitting parameters, especially in non-electrostatic SCMs [13]. In experiments, C_s is usually fixed and A_s is measured; thus, fitting C_{TS} is equivalent to adjusting the Γ_T value, which can be also estimated from crystallographic data [8] or found from adsorption measurements [5,12].

A natural way to express concentration of a j -th surface species is $C_j = \Gamma_j / \Gamma_o$, where Γ_j is the actual density and Γ_o ($\text{mol}\cdot\text{m}^{-2}$) is the *reference density at standard state* [9] common to all mineral surfaces; thus defined C_j can exceed unity. If adsorption occurs in a monolayer of H_2O molecules attached to oxide surfaces at density $0.95\cdot 10^{-5}$ to $3.31\cdot 10^{-5}$ (mean $2.37\cdot 10^{-5}$) $\text{mol}\cdot\text{m}^{-2}$ [12] then our proposed value $\Gamma_o = 2 \cdot 10^{-5} \text{ mol}\cdot\text{m}^{-2}$ [9] appears reasonable and practical. Other suggestions for the “standard site density” ranged from $0.384\cdot 10^{-5} \text{ mol}\cdot\text{m}^{-2}$ [5,7] to $1.66\cdot 10^{-5} \text{ mol}\cdot\text{m}^{-2}$ (or $10\cdot 10^{18} \text{ sites}\cdot\text{m}^{-2}$) [11].

In interpretation of gas-solid and liquid-solid adsorption isotherms, a *surface coverage fraction* $\theta_j = \Gamma_j / \Gamma_T$ is traditionally used. Clearly, $\theta_j \leq 1$ and $\theta_j = C_j$ only when $\Gamma_T = \Gamma_o$.

Note that the Γ_o parameter is *not the same quantity* as the total density parameter Γ_T , which, in turn, is not equivalent to the maximum density Γ_{max} related to physically limited availability of reactive sites. Hence, the common practice of setting $\Gamma_T = \Gamma_{max}$ and putting the mole balance constraint on top of it leads to inconsistencies and losses of information.

Standard States

Standard states must be defined in order to obtain μ_j^o from μ_j (see eqn 1) and relate μ_j to concentration C_j in a convenient way, allowing comparisons with different systems of interest [1]. For adsorbed species, various standard states have been proposed in the past - mainly in interpretation of adsorption isotherms [3]. Being a matter of convention (not

reached yet!), neither of suggested approaches was incorrect, as long as the standard states were uniquely defined and thermodynamic quantities involved in equations (1) to (4) were referred to them. Unfortunately, more often, the standard states were not clearly defined, or the defined states were non-unique. Thus, questions about convenience and rationality of choice of standard states still have to be asked. The answers depend on our research objectives – either an understanding a single experiment, or a compilation of the consistent thermodynamic data base. Screening of the literature unveils 3 approaches, where standard states for surface species are:

- (1) borrowed from those of aqueous electrolyte species [7], as in FITEQL, PHREEQC codes;
- (2) expressed via coverage fraction θ , convenient for interpretation of adsorption isotherms;
- (3) defined by combining states of the sorbent, its surface (sites), and the bulk solution phase.

Approach (1) was criticized [9] because of its non-uniqueness. If a 1.0 M standard state is chosen then infinitely many systems can contain 1 M of a surface species, but at different concentration C_s and specific surface A_s of solid sorbent, leading to different “standard” densities $\Gamma_T^{(0)}$. Conversely, equilibrium constants for surface reactions based on 1.0 M standard state depend on properties of the solid, such as site densities [9,11] and also surface areas [11].

Approach (2). Conway et al. [3] investigated standard states chosen such that the Langmuir (L) hyperbolic term $\theta/(1-\theta)$ turns into unity, i.e. $\theta_o = 0.5$ would be good in L isotherms for gas-on-solid adsorption. However, for adsorption on solid-aqueous interfaces (eqn 2) described e.g. by the Flory-Huggins isotherm $\theta e^{1-n}/(1-\theta)^n$, θ_o will depend on n . A more convenient choice, independent of n and similar to “pure substance” standard states for solids or liquids, is a “full coverage” standard state: $\theta_o = 1$ for A(ads) and $1-\theta_o = 1$ for H₂O(ads) [3]. Because the quantity $\theta_j = \Gamma_j/\Gamma_T$ is scaled to the total density Γ_T and not to Γ_o , the “surface coverage based” standard states are also non-unique: related adsorption constants refer to the actual total density and are not directly comparable between surfaces having different Γ_T .

Approach (3) overcomes this non-uniqueness by defining “full-coverage” standard states of surface species (other than water-solvent) at fixed (site) density Γ_o (in mol·m⁻²) and specific surface area (A_s^o in m²·mol⁻¹) common to all solids [9,11]. For convenience, mole amounts of the sorbent X_s^o ; of surface species x_o ; and of solvent in the bulk solution X_w^o can be also fixed, making the standard concentration equal to unity [9]. This standard state (at defined T and P) is unique; it leads to μ^o and K values comparable between all mineral-water interfaces and consistent with those of aqueous species. Instead of fixing X_s^o , x_o and X_w^o , it has been proposed alternatively to include the actual sorbent molarity C_s (in g·L⁻¹) into the standard state for surface complexes, and also to use a different standard state (full coverage at actual Γ_T , A_s and C_s) for the ≡SOH sites [11]. Thus, definitions [9] and [11] are not fully compatible.

Activities and Reference States

Choice of the standard state also determines the activity of surface species at the actual state of interest (eqn 1). To relate activity and concentration, the *reference state* must also be defined. As reference states are usually not considered in papers dealing with L or similar adsorption isotherms, functions like $\theta e^{1-n}/(1-\theta)^n$ comprise a blend of concentration and activity coefficient, which are difficult to separate. In computer-aided LMA speciation models, the hypothetical “infinite dilution” reference states at $\Psi = 0$ were implicitly borrowed from aqueous species together with 1.0 M (or 1.0 *m*) standard states.

For mineral-water interfaces, it is advantageous to take the reference state for “surface water” or “sites” as a “full coverage” or “pure surface” (leading to Raoult’s mixing behavior) [3,6,9,11]. For other adsorbed species, a different reference state of hypothetical “infinite surface dilution” at $\Psi = 0$ conveniently applies (leading to Henry’s mixing behavior). Thus, upon dilution of the bulk aqueous electrolyte, both reference states are approached simultaneously.

The 2p*K* intrinsic constants K^{int} for surface complexation reactions like $\equiv\text{SOH}^0 = \equiv\text{SO}^- + \text{H}^+$ involve activity of neutral $\equiv\text{SOH}$ groups (“sites” or “surface solvent”) that can be assumed constant [9]. The reason is that the chemical potential of “surface solvent” is determined by that of the bulk water, always present in great excess. The assumption $\{\equiv\text{SOH}\} \approx \text{const}$ also explains how K^{int} depend on $\Gamma_T^{(0)}$ and how to convert K^{int} into K [9]. An alternative idea is that the activity of the $\equiv\text{SOH}$ site is proportional to its concentration [7,11]. Another discrepancy...

Activity Coefficients

Convenient choice of reference states makes consideration of non-Coulombic activity coefficients γ_s possible for surface species – perhaps, the most obscure and confusing topic so far. This problem has been traditionally circumvented by assuming γ_s to approach unity or cancel out in LMA expressions [5,7,11]. Activity coefficients were also rarely associated with L-type isotherms, probably because the hyperbolic L function $\theta/(1-\theta)$ can be derived either from statistical thermodynamic reasoning or from the mole balance for a site-binding reaction $\equiv\text{S} + \text{A}(\text{aq}) = \equiv\text{SA}(\text{ads})$ at fixed total concentration of sites C_{TS} . One can also assume that the L isotherm represents the simplest “ideal” behavior to which more complex isotherms can be compared, and deviations can be expressed in γ_s terms.

In GEM SCMs [9], instead of one (Γ_T), two density parameters are involved: Γ_o that scales thermodynamic concentration C_j to a common reference level at standard state, and Γ_{max} - a non-thermodynamic limiting density of available binding sites. Γ_{max} is a mineral surface specific parameter; it may also be adsorbate specific. There is no other place for Γ_{max} than the activity coefficient term in eqn (1). In GEM SCMs that have mole balance constraints for total amounts of chemical elements and charge but not for “surface sites”, the problem of activity coefficients had to be resolved.

As a simple practical solution replacing the Γ_T -based mole balance constraint, a *surface activity term* (SAT) Ξ has been introduced in place of γ_j (eqn 1) as a truncated L function as $\Xi = \theta_{SAT}/(1 - \theta_{SAT}) \geq 1$ [9], where $\theta_{SAT} = \Gamma_j / \Gamma_{max}$ is the real surface coverage fraction. In a “diluted” surface layer, $\theta_{SAT} < 0.5$, $\ln \Xi = 0$, and (at $\Psi \approx 0$) adsorption occurs close to the reference state, in a “linear region”, where $[A(ads)] \approx K \cdot [A(aq)]$. Upon increasing activity of the aqueous counterpart in the bulk solution, in the high coverage region $\theta_{SAT} > 0.5$, the SAT term maintains the density Γ_j of a strongly adsorbing species below the physical limit Γ_{max} . Another SAT expression was introduced in GEM approach for the constant-activity “surface solvent” $>O_{0.5}H^0$ species [9] to account for its displacement or consumption upon increasing coverage by surface complexes. The SAT non-ideality corrections work fine in GEM, reproducing also the model titration curves made for the same system with a LMA SCM code [9]; there are also drawbacks. The L function is mathematically stiff: if $\theta_{SAT} \rightarrow 1$ then $\Xi \rightarrow \infty$ and this sometimes causes numerical convergence difficulties in the GEM algorithm at large values of $\Xi > 100$. The L isotherm has been also found unsatisfactory for the multilayer-, “multidentate” adsorption, or that involving lateral interactions between adsorbed molecules, where the BET, Flory-Huggins or other quasi-chemical isotherms may be more appropriate [2,3].

Conclusions

To make the compilation of the internally consistent thermodynamic database for adsorbed species feasible, the following questions still have to be addressed and resolved.

1. Concentration: $C_j = \Gamma_j / \Gamma_o$ is recommended; a convention on Γ_o value is needed ($2 \cdot 10^{-5} \text{ mol} \cdot \text{m}^{-2}$?). Usage of coverage fraction $\theta_j = \Gamma_j / \Gamma_T$ leads to inconsistent μ^o values.
2. Standard states: combined “full coverage” states (Approach 3) are most convenient. What parameters of A_o , Γ_o , C_o , X_o , x_o should be fixed for all mineral surfaces? At which values? The same or different for surface complexes and $\equiv\text{SOH}$ “solvent”?
3. Reference states and activities: Asymmetric states - “pure surface” for “surface solvent” or $>\text{SOH}$ sites, and “infinite dilution” at $\Psi=0$ for surface complexes – are most convenient. Is the activity of “surface solvent” or $>\text{SOH}$ sites constant or proportional to molarity? What are correct conversions between K^{int} , K and μ^o for different $\Gamma_T^{(o)}$?
4. Activity coefficient: The “Truncated L-type” SAT is not yet rigorous and versatile enough; more theoretical work is necessary. How to *derive* SAT corresponding to L, Flory-Huggins, and other isotherms? At what conditions the SAT may be ignored?
5. Coulombic terms: the generic Stern-Graham EDL model is more or less accepted; what is thermodynamically the “best” implementation for amphoteric oxide surfaces (TLM, BSM, MUSIC,...)? Is such EDL model necessary for permanent-charge surfaces?

Acknowledgment

Partial financial support from Nagra (Wettingen) is gratefully appreciated.

References:

- [1] Anderson G.M. and Crerar D.A. (1993): *Thermodynamics in Geochemistry*. Oxford, N.Y.
- [2] Benjamin M. (2002): - *Environ. Sci. Technol.* **36**, 307-313.
- [3] Conway B.E. et al. (1974): - *Electrochim. Acta* **19**, 455-460.
- [4] Lützenkirchen J. (2002): - *Encyclopedia of surface and colloid science*. Dekker, N.Y., 5028-5046.
- [5] Davis J.A. and Kent D.B. (1990): - *Rev. Mineral.* **23**, 177-260.
- [6] Dugger D.L. et al. (1964): - *J. Phys. Chem.* **68**, 757-760.
- [7] Dzombak D.A. and Morel F.M.M. (1990): *Surface complexation modeling*. Wiley, N.Y.
- [8] Koretsky C.M. et al. (1998): - *Amer. J. Sci.* **298**, 349-428.
- [9] Kulik D.A. (2002): - *Amer. J. Sci.* **302**, 349-428; - *Radiochim. Acta* **90**, 815-832.
- [10] Sposito G. (1983): - *J. Colloid Interf. Sci.* **91**, 329-340.
- [11] Sverjensky D.A. (2003): - *Geoch. Cosmoch. Acta* **67**, 17-28.
- [12] Tamura H. et al. (2001): - *J. Colloid Interf. Sci.* **243**, 202-207.
- [13] Westall J.C. (1995): - *Mat. Res. Soc. Symp. Proc.* **353**, 937-950.

USE OF ATTENUATED TOTAL REFLECTION – INFRARED SPECTROSCOPY FOR *IN SITU* STUDY OF INORGANIC IONS ADSORPTION ON METAL OXY-HYDROXIDES

G. Lefèvre¹, S. Noinville² and M. Fédoroff³

¹ CECM – CNRS UPR 2801; 15, Rue Georges Urbain, F-94407 Vitry/Seine (France)

² LADIR – CNRS UMR 7075; 2-8, Rue Henri Dunant, F-94320 Thiais (France)

³ ENSCP - Laboratoire d'Electrochimie et de Chimie Analytique - CNRS UMR 7575

11, Rue Pierre et Marie Curie, F-75231 Paris Cedex 05 (France)

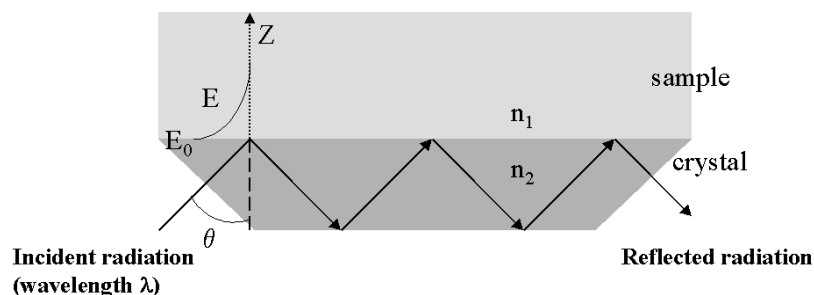
lefevre@glvt-cnrs.fr

Introduction

The long-term safety of radioactive waste depositories is based on the sorption of radionuclides on engineered and natural barriers. In order to predict the safety of such depositories, the extrapolation of sorption data measured on reference systems at the laboratory scale, to real systems and over a very long time is needed. This prediction must be performed through models based on physico-chemical processes as close as possible to the real ones.

The structure of surface complexes is an important data when determining thermodynamic surface complexation constants. Differentiating between inner- (IS) and outer-sphere (OS) complexes has been often made by observing the effect of ionic strength on the quantity of sorbed ions. However, this method has been questioned, pointing out the need of spectroscopic methods to solve this problem [1]. The fitting of experimental data, as the sorbed fraction of ions versus pH, has been used to determine both the surface inner-sphere complex structure (typically monodentate or bidentate) and the thermodynamic complexation constant. However, due to the number of adjustable parameters (site density, acidity constants, surface complexation constants, electrostatic parameters,...), such a method often led to several sets of surface complexes, what makes spectroscopic results of invaluable help for determining the nature of surface complexes.

Due to its ability to probe chemical bonds, infrared spectroscopy has been applied for years to sorption studies. The first studies made use of invasive sampling techniques on dried samples. Since ions might be coordinated differently on dried and wet surfaces, *in-situ* FTIR measurements in the presence of water should be preferred. The problem of the strong IR absorption by water has been solved by using attenuated total reflection (ATR), able to probe a short depth of sample by the evanescent wave existing in a lower index refraction medium (water) in contact with a more dense medium in which an IR radiation is propagating (see figure below).



This presentation will address the current state of knowledge in the use of ATR-IR to determine surface complexes between inorganic ions and oxides/hydroxides surfaces [2] together with our recent results.

Field of application

Due to the principle of IR spectroscopy, only polyatomic ions have been probed by this method whose vibration bands are detected between 1500 cm^{-1} (carbonate) and ca. 800 cm^{-1} (selenate) (see table below). The transmission threshold of the crystal material determines the lowest wavenumbers which can be measured, so the use of materials with high thresholds (Ge for example) prevents from studying “heavy” oxoanions, since the stretching vibrations reach low wavenumbers for heavy elements (as illustrated by the comparison between SO_4^{2-} and SeO_4^{2-}).

IR absorption bands for some free and sorbed oxanions (systems in presence of water)

species*	Infrared active band (cm^{-1}) ** ([2] and references herein)			
	1000	1200	1400	
SO_4^{2-}		1100		
HSO_4^-	890	1050	1195	
Sulfate on hematite	975	1060	1130	
Sulfate on goethite	975	1055	1135	
ClO_4^-		1105		
Perchlorate on TiO_2		1104		
CO_3^{2-}	885	1065		1385
HCO_3^-	845	1010	1310	1360
Carbonate on γ alumina	----	----	1390	1510
Carbonate on HFO		1070	1335	1410
Carbonate on hematite			1350	1500
Carbonate on goethite	----	----	1335	1490
SeO_4^{2-}	870			
Selenate on goethite	820	850	880	
Selenate on HFO	885	895		
$\text{UO}_2(\text{OH})^+ \#$	960			
Uranyl on hematite ##	910			

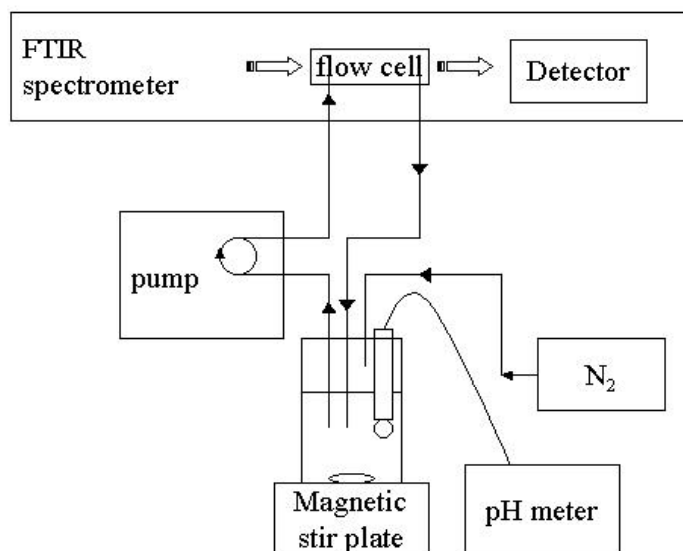
* HFO = amorphous ferric oxide, ** range where absorption bands of the solid phases prevent the detection of sorbed species is dotted, # Quilès and Burneau [5], ## our work

The symmetry of the ions is lowered when they are sorbed onto a mineral surface via an inner-sphere complex, leading to a peak split of ca. 150 cm^{-1} for carbonate and sulfate for example. On the other hand, the outer-sphere sorption, as illustrated by perchlorate ions, has a low impact on ion symmetry and, hence, on IR absorption band if compared to the free ion. For sulfate ions, the characterization of the ν_3 split and the structure of the IR band may help to determine the structure of the surface complex, *i.e.* monodentate or bidentate.

Cells and methods of solid deposition

Two methods were used to bring particulate matter into contact with the crystal: (1) spreading a concentrated suspension or a paste on the crystal or (2) coating by colloidal particles to form a film stable toward stirring or flowing of the solution in direct contact. For the first method, the equilibrium of the system solid/solution is reached by a classical batch experiment, then the suspensions are centrifugated to obtain a suspension with a high mass/volume ratio. In order to increase the surface probed by the evanescent light, the coating of the crystal with a stable layer of colloidal oxy-hydroxides particles can be performed [3]. Other methods have been developed to obtain an oxide layer on an ATR substrate, based on sol-gel techniques [4].

Once the modified ATR crystal has been prepared, it is generally placed into a flow cell (see experimental apparatus below), allowing to rapidly obtain pH envelopes and adsorption isotherms, with time-resolved possibilities.



Results

We have applied this method to the sorption of sulfate, carbonate and uranyl ions on colloidal hematite prepared by hydrolysis of iron chloride (particles diam. 25 nm). A special cell was designed in order to increase sensitivity by multiplying reflexions and allow *in-situ* study of kinetics, reversibility, isotherms, influence of pH and ionic strength.

We showed that the status of sorbed sulfate complexes is not as simple as could be deduced from previous studies and depends on several factors, including the methods of deposition of hematite. For uranyl ions sorbed on hematite, the spectra obtained in presence of water is close to the spectra obtained on dry samples, indicating that the drying process does not change the surface complex of uranyl. The high shift of $\nu_a(\text{UO}_2)$ (50 cm^{-1}) between free and sorbed uranyl ion indicates a strong binding of the anion.

The spectra of sorbed ions have been recorded with dissolved concentration as low as $1 \mu\text{M}$. Thus, ATR-IR can be used not only as a tool for speciation but also as a sensitive sensor for several elements [4].

Conclusion

ATR-IR is a very useful technique for the knowledge of sorption mechanisms of several inorganic ions, differentiating between OS and IS for example. Interpretation of the spectra to obtain information on IS complexation is more complex due to the different possibilities of spectra decomposition. This step is especially complex for ions able to sorb with several different geometries (phosphate for example). Better interpretation can be performed by using reference compounds and comparing with other spectroscopic methods. However, this method has several advantages suitable for the current problems in the sorption field: an in situ analysis, a high sensitivity to surface complexes, and the possibility of time-resolved study. For five years, less than 20 articles have mentioned the use of ATR-FTIR to study the sorption of inorganic ions onto oxy-hydroxides amongst dozens of studies in this field. It illustrates the recentness of this technique and the possibilities of future developments [2].

References:

- [1] K.F. Hayes, A.L. Roe, G.E. Brown, K.O. Hodgson, J.O. Leckie, and G.A. Parks, *In situ X-ray absorption study of surface complexes: selenium oxyanions on $\alpha\text{-FeOOH}$* , Science **238** (1987) 783.
- [2] G. Lefèvre, *In Situ Fourier-transform infrared spectroscopy studies of inorganic ions adsorption on metal oxides and hydroxides*, Advances in Colloid and Interface Science, in press
- [3] S.H. Hug, *In situ Fourier transform infrared measurements of sulfate adsorption on hematite in aqueous solutions*, J. Colloid Interface Sci. **188** (1997) 415.
- [4] M. Janotta, M. Karlowatz, F. Vogt and B. Mizaikoff, *Sol-gel based mid-infrared evanescent wave sensors for detection of organophosphate pesticides in aqueous solution*, Anal. Chim. Acta **496** (2003) 339
- [5] F. Quilès and A. Burneau, *Infrared and Raman spectra of uranyl(VI) oxo-hydroxo complexes in acid aqueous solutions: a chemometric study*, Vib. Spectrosc. **23** (2000) 231

INTEGRATING SORPTION REACTIONS IN A THERMODYNAMIC DATABASE FOR USE IN SPECIATION MODELS

Claire Lomenech and Jan van der Lee

Ecole des Mines de Paris, CIG

35, rue Saint-Honoré

77305 Fontainebleau Cedex

France

Claire.Lomenech@ensmp.fr, Jan.vanderLee@ensmp.fr

Introduction

The importance to take into account sorption processes when modelling the migration of ions in the subsurface is widely recognized by the scientific community. So far, however, most thermodynamic databases integrate very few sorption data, despite the growing number of sorption studies published in the last decades. Lack of consensus on the underlying concepts of the sorption process and limited possibilities of speciation codes to handle sophisticated sorption models are the major reasons. Only the database developed by Dzombak and Morelⁱ, for a single mineral and the diffuse layer model, is directly available to the users of a few speciation codes, for example, MINTEQA2ⁱⁱ or CHESSⁱⁱⁱ. Fortunately, considerable efforts are currently made to gather and analyse the available sorption data^{iv,v}, but no sorption database is at present directly available to the users of speciation codes. Integrating sorption reactions in a thermodynamic database for speciation models is one of the main objectives of the CTDTP project which has recently been presented to the scientific community^{vi}. As a first step, the project focused on a subset of relatively simple (hydr)oxides, for which surface complexation models (SCM) give a satisfactory description of the sorption properties.

Description of the initial methodology

The main problem associated with the integration of sorption constants in a thermodynamic database is probably the loss of internal consistency. Indeed, surface complexation constants depend on the surface parameters (site density, surface capacitances, protonation and deprotonation equilibrium constants) used during the data-fitting process. The surface parameters were then defined for each solid in the database, prior to the integration of literature sorption constants. Two types of criteria have been considered to define the surface parameters (site density, surface capacitances and surface acidity constants): scientific criteria, based on a critical review of the published data, and pragmatic criteria. Surface parameters used on a large number of systems have been preferred, in order to integrate an important number of consistent sorption constants. Supplementary criteria have been applied for the selection of the sorption equilibria and their constants. Especially, a strong preference has been given to mechanisms supported by structural data (spectroscopic data, or theoretical calculations) when they exist. Indeed, the correct choice of the reaction mechanism is of crucial importance : the quantitative results of predictive modelling will strongly depend on the precise definition of the surface species.

The proposed methodology is illustrated by the example of the selection of a site density value for goethite. Measured and calculated site densities collected in the literature are summarized by Figure 1a. First, some values were not included on the basis of scientific criteria. For example, data corresponding to samples with a low $\text{pH}_{z.p.c.}$ value were rejected since it has been shown that this results from CO_2 contamination^{xii}. Accordingly, different groups of values were obtained (Fig. 2b). Significantly more sorption data exist in the literature, based on site densities obtained from potentiometric titrations. In order to integrate a large amount of data in the base, and since there is no general agreement in the scientific community concerning site density values, we preferred to use the average of the values determined by potentiometric titrations. This choice is purely pragmatic, to ensure consistency with the literature sorption constants integrated in the base. This last treatment leads to a value of $(2.6 \pm 0.3) \mu\text{mol}/\text{m}^2$. Note that this value may evolve with the base, and should only be considered as a starting point for the first phase of the project.

The “pragmatic” methodology developed in the first part of this paper has been used to define the surface parameters of 9 solids: goethite, ferrihydrite, hematite, magnetite, silica, quartz, corundum, γ -alumina and kaolinite. The final result is a sorption database containing 330 sorption equilibrium constants, determined with the three more widely employed SCM: the constant capacitance model (CCM), the diffuse layer model (DLM) and the triple layer model (TLM).

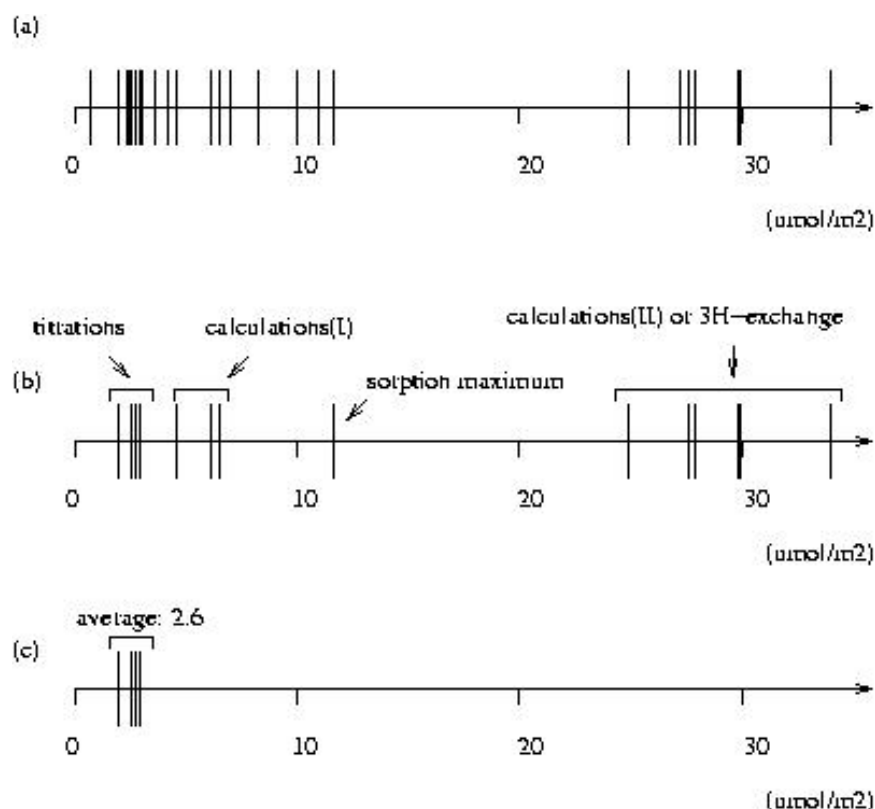


Figure 1 : Selection of a site density value for goethite. (a) Collected literature data.

(b) Scientific selection. (c) Pragmatic selection and retained value.

Titration refers to acid/base titrations, calculations (I) and (II) to calculations based on crystallography, considering a fraction of the hydroxyl groups as reactive (I) or all the hydroxyl groups (II).

Discussion and perspectives

Some fundamental problems are encountered if one wants to create a highly consistent sorption database. These main theoretical problems are summarized below and will be discussed in the second part of this contribution. Some possible answers will be proposed, as a starting point for a discussion with other sorption experts.

Some authors recently pointed out that surface complexation models do not really have an unambiguous thermodynamic basis^{vii,viii}. For example, the definition of the standard state for surface species is not clear. Indeed, the standard state for surface species is classically defined at a concentration of 1 molar, at zero surface charge and zero surface potentialⁱ. The problem is that this can correspond to several states: different site densities (expressed in mol/g of solid) combined with different solid concentrations (in g/L) can, indeed, lead to a concentration of 1 molar for surface species; it has been then proposed that a reference surface site density should be part of the definition of the standard state in order to ensure the consistency of a thermodynamic database for surface complexes^{vii}. Davis and Kent^{ix} had already proposed to set the site density at the same value for all minerals, in order to achieve consistency in a sorption thermodynamic database. Other authors have also proposed different standard states, for example corresponding to a complete coverage of the surface sites^x.

Another problem lies in the definition of sorption equilibrium constants involving several sorption sites, for example for a reaction leading to the formation of a bidentate surface complex. Should there be an exponent of 2 for the concentration of surface sites in the mass action law? Here again, the interpretations diverge between different authors : although many authors choose to set the exponent to 2, as for a solution equilibrium, this approach seems questionable, as pointed out first by Yeasted and Morel^{xi} who proposed to set the exponent to 1, treating the behaviour of surface sites more like the one of a chelating ligand in solution.

Besides these fundamental questions on the thermodynamic basis itself of SCM, one of the main problems is the choice of the best surface complexation model for the creation of a sorption database : either 1- or 2-pK, with one site type or a multisite approach, with which description for the electrostatic term? For example, some authors have pointed out that the widely used DLM, successfully applied to sorption of a wide range of sorbates onto ferrihydriteⁱ, gives much poorer results than the CCM or the TLM to model goethite potentiometric titration data^{xii}. However, this model has been yet the only one to be applied to achieve consistent surface complexation modelling on ferrihydrite in the early nineties¹, and this approach has been recently followed to model sorption of a large range of sorbates on manganese oxide^{xiii}.

Solving such problems in the development of a sorption database would mean a complete remodelling of the existing experimental data, instead of using published literature values. Thus, this approach is beyond the scope of the first phase of this project and represents a very important amount of work, integrating some fundamental work on the theoretical basis of sorption models, the careful selection of datasets, and the parallel development of modelling tools associated with the base. Nevertheless, we believe that such an approach

has to be initiated from the beginning of the project, even if the pragmatic methodology proposed in the first part of this presentation is retained for the constitution of an operational database. The proposed model and theoretical assumptions are not yet fixed for the second phase of the project. In this sense, this presentation is also meant as a call for a participation of other sorption experts to the CTDp project^{xiv}.

References:

-
- ⁱ D.A. Dzombak, F.M.M. Morel, *Surface complexation modeling. Hydrous ferric oxide*, John Wiley and sons, Inc., New York (1990)
- ⁱⁱ J.D. Allison, D.S. Brown, K.J. Novo-Gradac, *MINTEQA2/PRODEF2: A geochemical assessment model for environmental systems. Version 3.0 user's manual*, USEPA Report No. EPA/600/3-91/021, Athens, Georgia (1991)
- ⁱⁱⁱ J. van der Lee, *Thermodynamical and mathematical concepts of CHESS*, Tech. Report LHM/RD/98/39, CIG, Ecole des Mines de Paris, Fontainebleau, France (1998)
- ^{iv} J.A. Davis, M. Ochs, M. Olin, T.E. Payne, C.J. Tweed, *NEA sorption project. Phase II - TDT Report*, OECD/NEA (2001)
- ^v V. Brendler, A. Vahle, T. Arnold, G. Bernhard, T. Fanghänel, "RES³T-Rosendorf expert system for surface and sorption thermodynamics", *J. Contam. Hydrol.*, vol. 61, pp. 281-291 (2003)
- ^{vi} J. van der Lee, C. Lomenech, "Towards a common thermodynamic database for speciation models", Migration'03, Gyeongju, South Korea, 21-26 September 2003, proceeding submitted to *Radiochim. Acta*
- ^{vii} D.A. Kulik, "Sorption modelling by Gibbs energy minimization: Towards a uniform thermodynamic database for surface complexes of radionuclides", *Radiochim. Acta*, vol. 90, pp.815-832 (2002)
- ^{viii} D.A. Sverjensky, "Standard states for the activities of mineral surface sites and species", *Geochim. Cosmochim. Acta*, vol. 67, n° 1, pp. 17-28 (2003)
- ^{ix} J.A. Davis, D.B. Kent, *Surface complexation modeling in aqueous geochemistry*, in "Reviews in Mineralogy", vol. 23, chapter 5, pp. 177-260 (1990)
- ^x D.L. Parkhurst, C.A.J. Appelo, *User's guide to PHREEQC version 2*, W-R I Report 99-4259, USGS, Denver (1999)
- ^{xi} J.G. Yeasted, F.M.M. Morel, personal communication cited by J.A. Davis, J.O. Leckie, in "Surface ionisation and complexation at the oxide/water interface. 3. Adsorption of anions. *J. Colloid Interface Sci.*, vol. 74, n° 1, pp. 32-43 (1980)
- ^{xii} D.G. Lumsdon, L.J. Evans, "Surface complexation model parameters for goethite (α -FeOOH)", *J. Colloid Interface Sci.*, vol. 164, pp. 119-125 (1994)
- ^{xiii} J.W. Tonkin, L.S. Balistrieri, J.W. Murray, "Modeling sorption of divalent metal cations on hydrous manganese oxide using the diffuse double layer model", *Applied Geochem.*, vol. 19, pp. 29-53 (2004)
- ^{xiv} See: <http://ctdp.ensmp.fr> for more information.

THE EFFECT OF PRESSURE ON THE SORPTION OF HEAVY METAL CATIONS ON GOETHITE

Edward Mączka and Marek Kosmulski

Department of Electrochemistry
Lublin University of Technology
Lublin, Poland
KOSMULSK@hermes.umcs.lublin.pl

The effect of pressure on the chemical equilibria in condensed phases is negligible unless the pressure exceeds 10^7 Pa. Therefore the equilibrium constants of reactions in condensed phases determined at atmospheric pressure apply over a wide pressure range, and usually there is no need to consider the pressure effect at all. On the other hand, the pressures $>10^7$ Pa often induce a substantial effect, which can be quantified by the following equation:

$$\Delta V^\circ = - RT \frac{d \ln K}{dp} \quad (1)$$

where ΔV° is the standard volume of reaction at atmospheric pressure. One typical example of practical importance where the pressure effect matters is deep ocean, namely, the average depth in the ocean is about 3800 m, and the corresponding pressure is 3.8×10^7 Pa. We are particularly interested in the fate of heavy metals in deep ocean. Apparently the equilibrium constants of precipitation/sorption reactions obtained at atmospheric pressure are not relevant to the conditions in deep ocean.

Direct study of precipitation/sorption reactions at pressures $>10^7$ Pa is technically difficult. It is much easier to experimentally determine K at atmospheric pressure, then determine ΔV° in a dilatometric experiment and finally calculate the equilibrium constant at elevated pressure from Eq. (1). At pressures on the order of 10^8 Pa (corresponding to the deepest ocean trench) the second derivative ($d^2\Delta V^\circ/dp^2$) is negligible.

The dilatometric effects of solution reactions involving heavy metals were extensively studied in the 1950s and 1960s. The standard volumes of metal cations in aqueous solution are negative. This is because the specific density of the hydration water is much higher than that of bulk water. Thus, precipitation of heavy metal hydroxides induces release of water from the hydration shell, and consequently the system expands. Since the dilatometric effect is positive, the increase in pressure induces the decrease in the equilibrium constant of precipitation reactions (Eq.1).

The pressure effect on adsorption of heavy metal cations was first addressed in 1980s by Hachiya et al. who designed the pressure jump technique to study the kinetics of adsorption. Their studies were not aimed at calculation of equilibrium constants at elevated pressures, but they directly demonstrated that the pressure effect does exist. Very recently Yamaguchi and Okazaki measured the dilatometric effect of adsorption of Pb and Cu on amorphous hydrous iron oxide. Their results can be used to calculate the pressure effect.

The main concern of the present authors about the choice of amorphous hydrous iron oxide as the model system is its spontaneous crystallization (which may induce a dilatometric effect). Therefore we used another model system, namely, synthetic goethite. Synthetic goethite of controlled and reproducible morphology can be easily obtained in kilogram-

amounts. Unfortunately the specific surface area of synthetic goethite is lower by an order of magnitude than that of amorphous hydrous iron oxide.

The uptake of heavy metals in the K_d -pH coordinates is illustrated in Fig. 1-6.

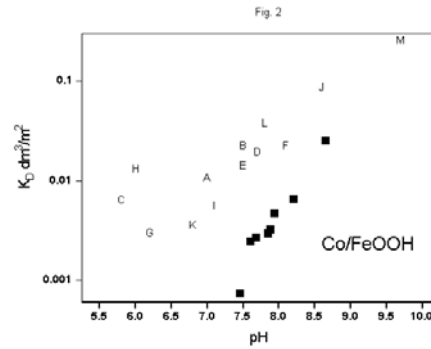
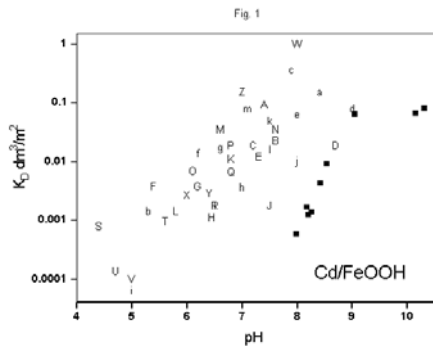


Fig. 1 Uptake of Cd on goethite. Letters - from the literature, black squares - this study.

Fig. 2 Uptake of Co on goethite. Letters - from the literature, black squares - this study.

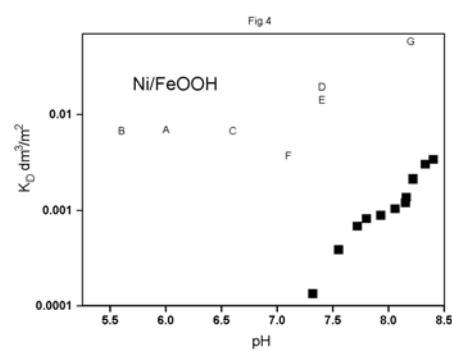
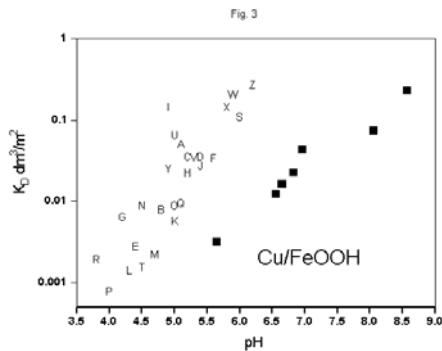


Fig. 3 Uptake of Cu on goethite. Letters - from the literature, black squares - this study.

Fig. 4 Uptake of Ni on goethite. Letters - from the literature, black squares - this study.

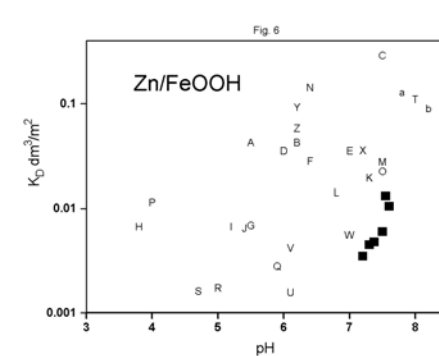
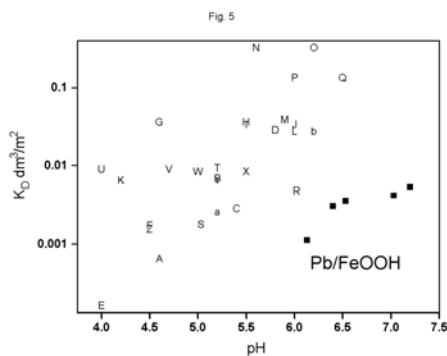


Fig. 5 Uptake of Pb on goethite. Letters - from the literature, black squares - this study.

Fig. 6 Uptake of Zn on goethite. Letters - from the literature, black squares - this study.

The K_d obtained in the present study are lower than most results reported in the literature due to relatively high initial concentration of the heavy metal cations ($> 10^{-3} \text{ mol dm}^{-3}$), which was necessary to bring about a measurable dilatometric effect, and to short equilibration time (the system reached constant volume in less than 2 h). The dilatometric effect was roughly proportional to the amount of heavy metal adsorbed. The dilatometric results were rather scattered (Fig. 7), and there was hardly any correlation between ΔV and the experimental conditions (pH, initial concentration of heavy metal cations). On the other hand, the uptake (pH) curves were smooth, and the pH_{50} (the pH value, at which 50% of metal cations is adsorbed under certain experimental conditions) shows almost perfect linear correlation with the first hydrolysis constant of metal cations (Fig.8).

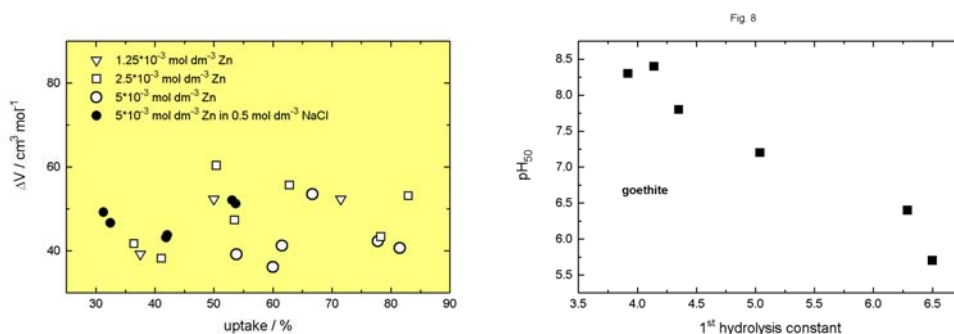


Fig. 7 Specific volume of adsorption of Zn on goethite for various initial Zn-concentrations.

Fig. 8 The correlation between pH_{50} and the first hydrolysis constant.

The specific volume of sorption of divalent metal cations on goethite of about $30 \text{ cm}^3/\text{mol}$ was found (the ΔV for Zn shown in Fig. 7 was substantially higher than for other metal cations). The effect of pH and inert electrolyte (up to $0.5 \text{ mol dm}^{-3} \text{ NaCl}$) on the results of dilatometric experiments was rather insignificant. The specific volume of precipitation of hydroxides of divalent heavy metals is about $60 \text{ cm}^3/\text{mol}$. Since the dilatometric effects are chiefly due to the difference in specific density between the hydration water on the one hand and bulk water on the other, the present results can be used to estimate the degree of dehydration in the adsorption process. Our results suggest that metal cations adsorbed on goethite loose about $\frac{1}{2}$ of their hydration water, and this roughly matches the degree of dehydration calculated from X-ray absorption spectroscopy.

References:

- Kosmulski, M. *Chemical Properties of Material Surfaces*; Marcel Dekker: New York, 2001.
- Yamaguchi, N.U.; Okazaki, M. *J. Colloid Interf. Sci.* 2002, **249**, 489-491.
- Kosmulski, M.; Mączka, E. *Colloids Surf. A*, 2003, **223**, 195-199; *Langmuir*, 2004, **20**, 2320-2323.

INCORPORATION OF TRIVALENT ACTINIDES AND LANTHANIDES IN CALCITE. A TIME RESOLVED LASER FLUORESCENCE SPECTROSCOPY (TRLFS) STUDY

M. Marques Fernandes, T. Stumpf, T. Rabung, D. Bosbach, A. Bauer and T. Fanghänel
Forschungszentrum Karlsruhe
Institut für Nukleare Entsorgung
P.O. Box 3640
76021 Karlsruhe
Germany
maria.marques@ine.fzk.de

Introduction

Although incorporation of radionuclides into the bulk structure of mineral phases represents a very important retardation process, very little is known about the reaction mechanism and about the structure of the involved incorporated species. Carbonates are among the most important secondary alteration products formed during the degradation of cement in radioactive waste repositories. Previous studies have shown that divalent and trivalent metal ions like Mg^{2+} [1], [2], Cd^{2+} [3], [4] and Rare Earth Elements (REE) [5], [6] in presence of calcite are efficiently removed from the aqueous phase.

An important point for incorporation of foreign ions into a crystal structure is the similarity of the ionic radii of the cation in the bulk structure and of the substituting element. The size of trivalent actinide and lanthanide ions are close to that of Ca^{2+} . Another important question for any heterovalent substitution is the charge compensation mechanism. In an Eu^{3+} /calcite co-precipitation study, Stipp et al. [7] proposed the substitution of Ca^{2+} by $EuOH^{2+}$. Structural parameters of REE [8] and Nd^{3+} [9] incorporated into the calcite lattice were obtained by using extended X-ray absorption fine structure spectroscopy (EXAFS). The studies show that the local oxygen coordination of the incorporated ions change from six fold to seven fold with increasing ionic radius of the lanthanide ions.

The aim of this study was to identify the Cm/calcite incorporation mechanism (charge compensation) and to characterize the involved species. Structural information of Cm(III) incorporated in calcite was obtained by using Time Resolved Laser Fluorescence Spectroscopy (TRLFS). From fluorescence emission lifetime measurements one can calculate the number of H_2O/OH^- molecules in the first coordination sphere of the actinide ion. Cm(III) was used as a representative for trivalent actinides and lanthanides because of its high fluorescence spectroscopy sensitivity which enables speciation studies in the nanomol concentration range [10]. The method TRLFS was used to investigate the sorption process of Cm(III) onto calcite in batch experiments [11]. To study the incorporation mechanism in detail, homogeneous Cm doped calcites were synthesized.

Experimental

The Cm doped calcite crystals were grown by using a Stirred-Flow-Through Reactor (Fig.1). Flow-Through Reactors are useful because they allow crystal growth under constant and controlled conditions (saturation state, pH, ionic strength).

Three input solutions (Ca_2ClO_4 , $\text{NaHCO}_3/\text{Na}_2\text{CO}_3$ and a Curium-248 ($t_{1/2}=3.4 \times 10^5$) containing keep the concentrations of the precipitating and co-precipitating components constant.

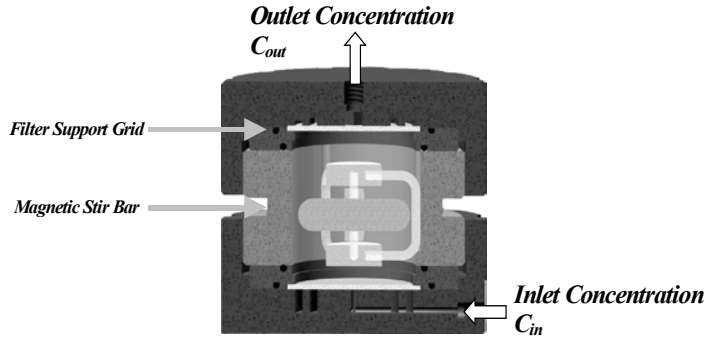


Fig.1. Stirred Flow-Through Reactor

The reactor has an internal volume of 45 ml. Input solutions enter and left the reactor through a hydrofoil Teflon membrane. A grained ($\leq 32 \mu\text{m}$) natural calcite was used as seed crystals for the calcite precipitation. The specific surface area measured by the N_2BET method was found to be $4 \text{ m}^2\text{g}^{-1}$. The seed suspension in the reactor was continuously stirred by a magnetic Teflon bar. Concentration of calcium, sodium and curium were controlled by using ICP mass spectroscopy. The precipitation experiment was done at a constant temperature of $25 \pm 0.5^\circ\text{C}$.

The co-precipitation reaction was:



The calcium and curium concentrations were analyzed periodically to verify that the steady state of the reaction was reached and to calculate the precipitation rate. The calcite precipitation rate was calculated by using the equation:

$$R (\mu\text{mol} \cdot \text{m}^{-2} \cdot \text{min}^{-1}) = \frac{F}{S v_i W_{seed}} \Delta C_i$$

ΔC : Ca^{2+} /or $\text{Cm}^{3+}/\text{Gd}^{3+}$ concentration difference between input and reacting solution

F: solution addition rate (lmin^{-1})

S: specific reactive surface area (m^2g^{-1})

W_{seed} : mass of calcite seeds (g)

v_i : molar fraction of foreign metal ion ($\text{Cm}^{3+}/\text{Gd}^{3+}$) in the calcite overgrowth.

Each co-precipitation experiment was conducted over a week. Two homogenous Cm doped calcites were synthesized with different trivalent metal ion concentrations of 0.5 nM Cm^{3+} (calcite1) and of 500 nM M^{3+} (0.5 nM Cm^{3+} and 499.5 nM Gd^{3+}) (calcite2). The growth rate of the calcites varied with metal ion concentration [12] from $0.75 \mu\text{molm}^{-2}\text{min}^{-1}$ to $1.35 \mu\text{molm}^{-2}\text{min}^{-1}$.

X-ray diffraction of the doped calcites shows the reflections of pure calcite. No other phases were detected.

Spectroscopic characterization of the Cm co-precipitated calcite samples

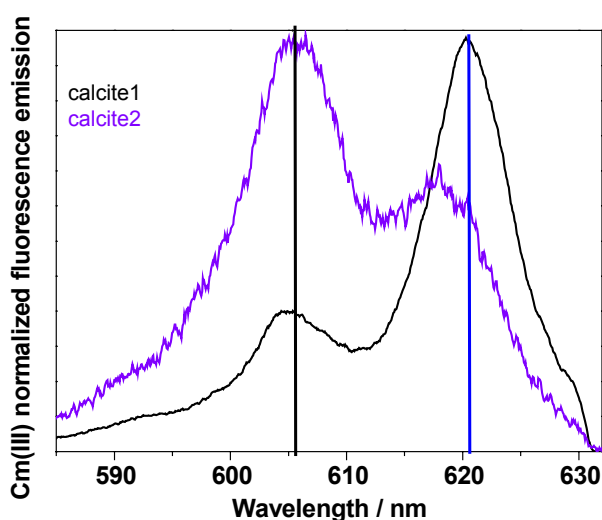


Fig.2. Fluorescence emission spectra of Cm(III) in calcite

Selected fluorescence emission spectra of the two Cm(III) doped calcites are presented in Fig.2. Both spectra show, two emission bands at 605.5 nm (1) and 620.3 nm (2), which can be assigned to two different Cm/calcite species. These peak maxima are quite similar to the peak positions of the Cm(III) species identified by Stumpf and Fanghänel (2002) during Cm/calcite batch experiments. In contrast to the emission maxima of Cm(III) species sorbed onto mineral surfaces (γ -alumina, kaolinite and smectite (603.3 nm), and silica (604.9 nm))[13] [14], the emission maximum of the first Cm(III)/calcite species appears at a higher wavelength (605.5 nm). The extreme red shift of the emission spectrum of the second Cm/calcite species with peak maximum at 620.3 nm is a clear indication for a change in the ligand field of Cm(III), which can be attributed to a reduction in the coordination number of Cm(III).

The proportion of the Cm/calcite species with a peak maximum at 605.5 nm increases with increasing trivalent metal ion concentration [M^{3+}] of the doped calcites.

Fluorescence decay measurements of Cm(III)

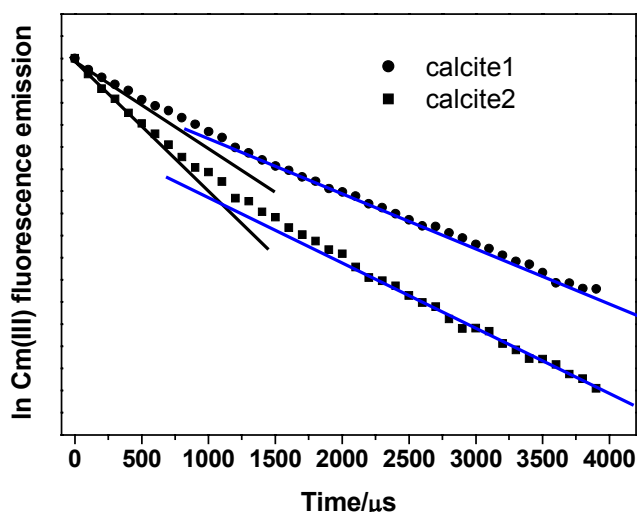


Fig.3. Time dependency of the fluorescence emission decay of Cm(III) in calcite (solid).

Fluorescence emission lifetime measurements give information about the hydration status of the identified Cm(III) species. By varying the delay time the ratio of the fluorescence intensities of the two Cm(III)/calcite species changes. With increasing delay time the fluorescence signal with the peak maximum at 605.5 nm decreases while the relative intensity of the peak of the Cm(III) species at 620.3 nm increases. This indicates that the two Cm(III)/calcite species have different lifetimes. In Fig. 3 the fluorescence intensities are plotted as a function of the delay time. The emission decay follows a bi-exponential decay law. Two different lifetimes of $\tau_1=350 \mu\text{s}$ and for the second species $\tau_2=2167 \mu\text{s}$ were calculated. According to the equation postulated by Kimura et al.[15], a lifetime of 2167 μs indicates the total loss of the hydration sphere. A lifetime of 350 μs can be attributed to a Cm species with one water or OH⁻ molecule in the first coordination sphere.

The long lifetime and the extreme red shift of the Cm(III)/calcite species with peak maximum at 620.3 nm are a clear indication for the incorporation of Cm into the calcite bulk structure by replacing Ca²⁺. A peak maximum at 605.5 nm and a emission lifetime of 350 μs can be attributed to an incorporated CmOH species. This suggestion has to be verified by further investigations.

References:

1. Mucci, A. and Morse, J. W., *Geochim. Cosmochim. Acta* **47**, 217 (1983).
2. Dromgoole, E. L. and Walter, L. M., *Chem. Geol.* **81**, 311 (1990).
3. Stipp, S. L., Hochella, Jr., M. F., Parks, G. A. and Leckie, J. O., *Geochim. Cosmochim. Acta* **56**, 1941 (1992).
4. Curti, E., *Appl. Geochem.* **14**, 433 (1999).
5. Zhong, S. J., Mucci, A., *Geochim. Cosmochim. Acta* **59**, 443 (1995).
6. Piriou, B., Fedoroff, M., Jean, J., and Bercis, L., *J. Colloid Interface Sci.* **194**, 440 (1997).
7. Stipp, S. L. S, Lakshatanov, L. Z., Jensen, J. T., Baker, J. A., *J. Contaminant Hydrol.* **61**, 33 (2003).
8. Elzinga, E. J., Reeder, R. J., Withers, S. H., Peale, R. E., Mason, R. A., Beck, K. M., Hess, W. P., *Geochim. Cosmochim. Acta* **66**, 2875 (2002).
9. Withers, S. H., Peale, R. E., Schulte, A. F., Braunstein, G., Beck, K. M., Hess, W. P., Reeder, R. J., *Phys. Chem. Minerals* **30**, 440 (2003).
10. Fanghänel, T., Weger, H. T., Könnecke, T., Neck, V., Paviet-Hartmann, P., Steinle, E., and Kim, J.I., *Radiochim. Acta* **82**, 47 (1998).
11. Stumpf, T., Fanghänel, T., *J. Colloid Interface Sci.* **249**, 119(2002).
12. Terjesen, S. G., Erga, O., Thorsen, G. and Ve, A., *Chem. Eng. Sci.* **14**, 277(1961).
13. Stumpf, T., Rabung, T., Klenze, R., et al., *J. Colloid. Interface Sci.* **238**, 219(2001).
14. Stumpf, T., Bauer, A., Coppin, F., Kim, J.I., *Environ. Sci. Technol.* **35**, 3691 (2001).
15. Kimura, T. and Choppin, G. R., *J. Alloys. Comp.* **213/214**, 313 (1994).

Np SORPTION ONTO CEMENT AND Mg(OH)₂-MgCl₂-BASED BACKFILL MATERIAL IN ALTERED Q-BRINE

Volker Metz, Johannes Lützenkirchen, Peter Vejmelka and Bernhard Kienzler

Institut für Nukleare Entsorgung (INE)

Forschungszentrum Karlsruhe

P.O.Box 3640

D-76021 Karlsruhe

Germany

Volker@ine.fzk.de

Introduction

Retention of actinides such as Np in the near field is critical for the long-term disposal and storage of radioactive waste in geological salt deposits. Portland cement and potential backfill material may have the capability to retard actinide migration through sorption processes. However, the effectiveness of the backfill material and cement (and their corrosion products, respectively) in concentrated MgCl₂-NaCl solutions is not known. No models are available to evaluate sorption processes for such conditions based on thermodynamic data. In the present communication we report on results of site specific sorption experiments for the Asse mine.

The Asse mine is situated in a diapir of Zechstein salt deposits. The salt mine operated for production of halite and potash. After termination of potash mining, low- and intermediate-level radioactive waste was emplaced in 13 of the excavated rooms in a depth of about 750, 725 and 511 m below surface ground. The salt mine was used thereafter as an underground research laboratory to develop technologies for disposal of high-level radioactive waste. Since termination of research in 1995, numerous excavated rooms, where no radioactive waste was emplaced, are being backfilled with crushed salt. Leaking of ca. 10 m³ d⁻¹ NaCl- and CaSO₄-rich brine into the mine is observed for several years now. The leaking is considered in the closure concept of the mine. In the present closure concept, systematic filling of the Asse mine with crushed rock salt and a MgCl₂-rich solution, e.g. Q-brine, is planned. Recently, the use of a Mg(OH)₂-MgCl₂-based material, so called *Mg-depot*, was proposed for backfilling of the emplacement rooms of the Asse mine (Schüßler et al., 2001). As described in a forthcoming publication of the authors (Metz et al., 2004), the *Mg-depot* provides favorable chemical conditions with respect to actinide solubility. Currently there is a strong interest if the *Mg-depot* or brucite, one of its main constituent, provides considerable sorption capacity with respect to actinides.

Methods and materials

Preconditioning of the studied brine/solid systems

The equilibrium concentration of Np is studied in the binary system Q-brine/cement and the ternary systems Q-brine/cement/*Mg-depot* and Q-brine/cement/iron. The chemical compositions of Q-brine, cement (ordinary Portland cement, type PZ35) and *Mg-depot* are given in Table 1. Iron powder (Merck #103815, p.a., 10 µm grain size) is used for the experiments in the Q-brine/cement/iron system. Experiments are carried out in a glove box

under Argon flow at room temperature ($pO_2 < 5$ ppm, $pCO_2 < 5$ ppm). The binary and ternary systems are equilibrated within 160 days. Approaching equilibrium is monitored by probing compositions of both the altered solution and the altered solid. Aqueous cation and anion concentrations are analyzed by ICP-AES (Perkin Elmer, Plasma 400) and ion chromatography (Dionex, DX300), respectively. Combination pH electrodes (type ROSS, Orion), freshly calibrated against dilute standard pH buffers (Merck), were used to determine the molal H^+ concentration pH_c . The derivation of the pH_c values from measured pH_{exp} is described elsewhere (Altmaier et al., 2003). The solids are characterized by XRD (Bruker AXS D8) and SEM-EDX (Figure 1). Using the EQ3/6 software package (LLNL, 1997; Wolery, 1992) and an extended Pitzer-Harvie-Møller-Weare data base (Harvie et al., 1984; Pitzer, 1987), equilibrium compositions of the studied binary and ternary systems are calculated. Since there is a lack of reliable Pitzer coefficients for aqueous Fe species in concentrated $MgCl_2$ -solutions, speciation of Fe is not calculated. An excellent agreement is found between experimental and calculated results regarding the interaction of the backfill material and cement in the studied brines, demonstrating the achievement of brine/solid equilibrium. Compositions of the equilibrated solutions of the systems Q-brine/cement, Q-brine/cement/*Mg-depot* and Q-brine/cement/iron are quite similar. An average composition of the equilibrated brine is given in Table 1. The measured Eh_{exp} varies between -145 mV in system Q-brine/cement/iron and $+70$ mV in system Q-brine/cement. During the Np sorption experiments described below, pH_c and Eh values do not differ significantly from the initial values given in Table 1.

Table 1: Compositions of initial Q-brine, Q-brine equilibrated with the solids, cement product (water to cement ratio, $W/C = 0.4$) and $Mg(OH)_2$ - $MgCl_2$ -based backfill material (*Mg-depot*).

aqueous constituent	initial Q-brine (mol (kg H ₂ O) ⁻¹)	equilibrated brine (average) (mol (kg H ₂ O) ⁻¹)	solid constituent	cement product (mol (kg solid) ⁻¹)	<i>Mg-depot</i> (mol (kg solid) ⁻¹)
H ₄ SiO ₄	0	0	Si	2.38	0.2
Al ³⁺	0	0	Al	1.4	0
Mg ²⁺	4.2	4.0	Fe	0.45	0
Ca ²⁺	0	0.2	Mg	0.27	6.6
Na ⁺	0.4	0.4	Ca	8.15	0.4
K ⁺	0.5	0.4	Na	0	4.3
Cl ⁻	9.0	8.9	K	0	0
SO ₄ ²⁻	0.2	0.003	Cl	0	5.6
			S	0.22	0
Eh_{exp} (mV)	-100	-135 to +70	O	32.77	29.5
pH_c	7.3	8.9	H	35.04	44.9

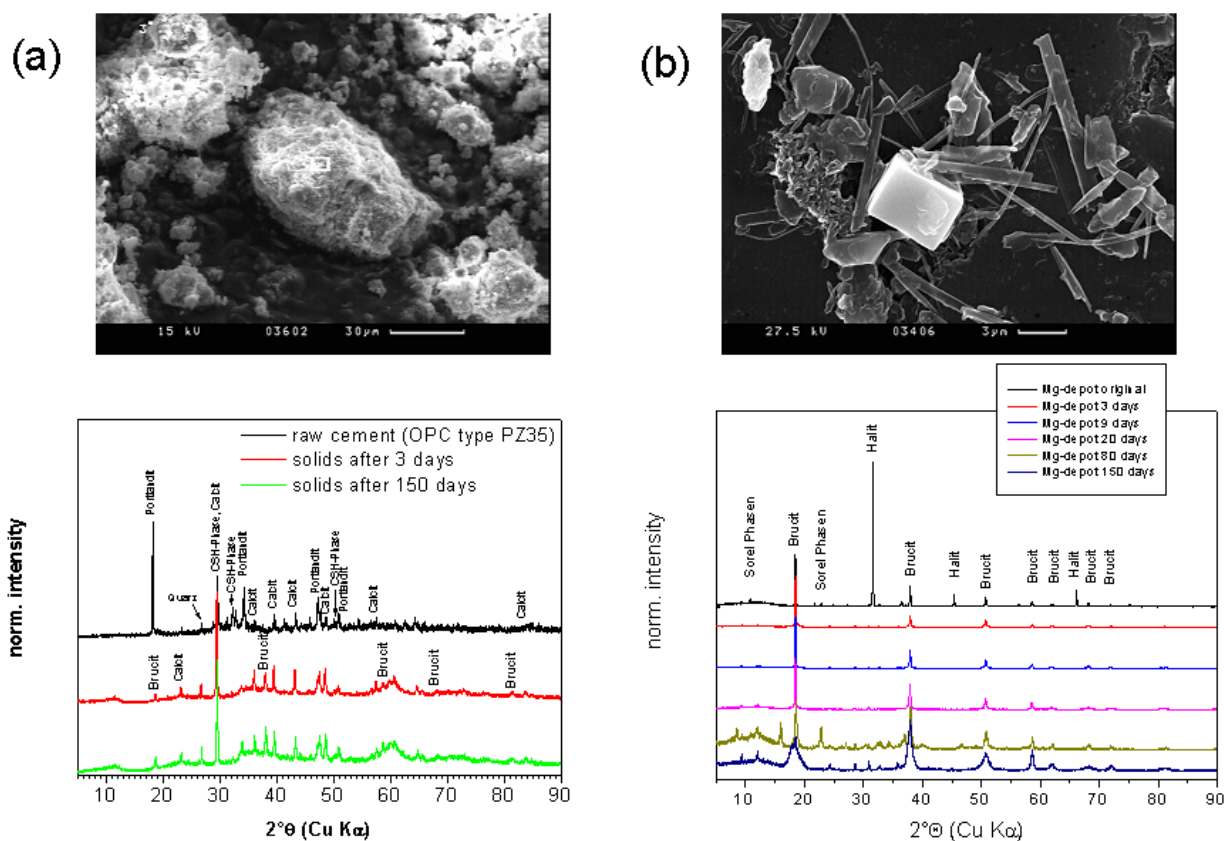


Figure 1: SEM images and XRD patterns of studied solids: (a) ordinary Portland cement and (b) *Mg-depot*.

Np-sorption experiments in equilibrated brine/solid systems

After equilibration of the binary and ternary systems, solids and solutions are separated. A stock solution of $^{237}\text{Np(V)}$ dissolved in 1 M Na_2CO_3 solution is added to the equilibrated brines to achieve a Np concentration of $6 \cdot 10^{-6}$ M. Np concentration is measured by means of LSC (Canberra, TR-2500 AIB). Then the Np doped brines are added to the preconditioned solid to achieve the target solution volume to solid mass ratios of $V/m = 9, 20$ and 100 mL g^{-1} . For each V/m ratio, three sorption experiments and one blank experiment are prepared. The experiments are started simultaneously and are sampled continuously in the course of 270 days. The variation of the Np concentration as a function of time is measured intensively in the experiments with $V/m = 20 \text{ mL g}^{-1}$. Within error, a steady state with respect to Np concentration is achieved after 200 days.

Calculation of sorption coefficients and data analysis

The experimental results at the end of the measurement period were analyzed in detail, because the long-term data are the most relevant observations for sorption coefficients to be used in performance assessment. An important issue in the calculation of the sorption coefficient is that radionuclide concentration in the blank solution may vary with time. This allows to calculate sorption coefficients with respect to the initial or final concentrations of

the blank solution. Thus in general two sorption coefficients are obtained. Additionally, the variation of V/M with sampling has to be considered. For all calculations the experimental error of the three replicates was considered both for the blank solution (3 replicates on one sample) and for the sorption samples (one measurement on three samples). Error bars shown on the experimental results originate from these data (mean and maximum and minimum value, respectively). Error bars are obtained for dissolved Np concentrations, sorption coefficients and adsorbed radionuclide amounts.

A rigorous analysis of the experimental data is proposed which considers

- plotting sorption coefficients as a function of V/M
- plotting sorption coefficients as a function of dissolved Np concentration
- plotting amount adsorbed as a function of dissolved Np concentration (isotherm plot)

With this analysis a number of criteria are checked which allow recommendations as to whether the measured sorption coefficients should be applicable with a *Kd*-concept or not. Experimental data of all solid-solution systems are checked using the 3 plotting options mentioned above. In the present communication, the isotherm presentation is discussed: Ideally, the mean experimental values can be fitted to a linear isotherm, yielding the mean sorption coefficient for the system under the conditions studied. When a constant sorption coefficient as a function of V/M is not obtained the isotherm plot may corroborate radionuclide concentration being solubility controlled. Furthermore, a statistically better fit to a non-linear isotherm may question the use of the *Kd*-concept. In the present study we used the Freundlich-isotherm to test non-linearity. This isotherm is given by the equation

$$q = K_F \cdot C^n \text{ or } \log(q) = \log(K_F) + n \cdot \log(C)$$

where q is the amount of Np adsorbed (e.g. in mol g⁻¹ also called loading), C is the dissolved Np concentration (in mol L⁻¹) and K_F and n are adjustable parameters.

Results and discussion

Sorption kinetics

It has been observed that sorption exhibits pronounced kinetics in similar solid-brine systems over an extended period of time (Kienzler et al., 2001). Typical laboratory systems are operated under conditions of lower salt concentration and liquid/solid ratios are higher. Sampling has no more than minor effects in these latter cases. In such systems a rapid adsorption step is often followed by a long-term step, which can be explained in various ways (Lützenkirchen, 2001). In site specific sorption experiments liquid/solid ratios are usually low as an attempt to mimic the expected site-specific conditions as close as possible. Sampling of the liquid phase results in significant changes in the liquid/solid ratio for the subsequent measurement. To investigate the effects of sampling exemplifying calculations on model systems are performed assuming a similar sampling procedure as in the experimental program (Lützenkirchen et al., 2003), showing that the observed kinetics may at least partly be due to the sampling procedure that reduces the V/M. In Fig. 2 the observed sorption kinetics of Np(V) is shown for the system Q-brine/cement/*Mg-depot*. There is an obvious decrease in Np concentration over time. It is not ambiguous, if sorption equilibrium is achieved by the end of the experiments (Fig. 2). The concentration in the blank sample (same solution but no sorbent) is constant within error. Calculations for the model system indicate that the observed kinetics may be due to the sampling procedure at least in part. Modifications of the experimental procedure would resolve the existing ambiguity. One might start with more samples and sample only once at the target V/M.

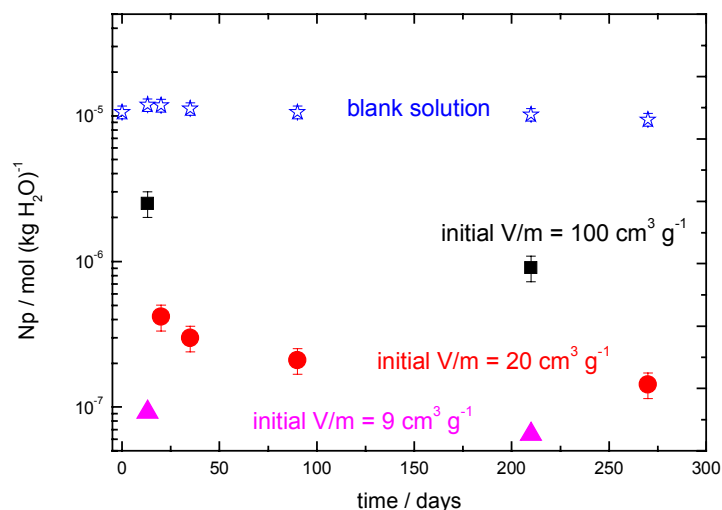


Figure 2: Observed sorption kinetics in the system Q-brine/cement/Mg-depot.

Long-term data

The long-term data obtained after more than 200 days were analyzed to estimate Np(V) sorption coefficients with respect to the studied brine/solid systems. When plotting experimental data of the system Q-brine/cement/Mg-depot as a function of V/M ratios, R_s values (apparent sorption coefficients, $R_s = q/C$ in mL g⁻¹) are obtained that are constant within the analytical error. However, deriving a Kd solely from the experimental R_s values is uncertain due to the considerable analytical error. Justification of the applicability of the Kd -concept for this system is gained by fitting a linear isotherm to the mean sorption data (data not shown). A fit to Freundlich-isotherm is obtained in a double-logarithmic isotherm plot (Fig. 3). Such a fit to the mean adsorption data yields a statistically better result ($\log q = (1.14 \pm 0.05) \cdot C + (0.8 \pm 0.3)$ with $R^2 = 0.996$) than the linear isotherm. However, within the analytical error a linear isotherm still appears to be appropriate.

The behavior of Np is essentially the same in the binary Q-brine/cement system. The variation of the mean sorption coefficients with V/M is negligible. The mean sorption coefficient obtained from the fit to the linear isotherm is $1.37 \cdot 10^3$ mL g⁻¹. A Freundlich plot yields a value for n which is very close to unity corroborating a linear isotherm. In the presence of iron the sorption of Np shows a completely different behavior (data not shown). The apparent sorption coefficients (i.e. observed R_s values) vary substantially with V/M, but the mean measured radionuclide concentrations are within a rather small range. This observation suggests that Np(V) is reduced to Np(IV) and precipitated. Although the mean values strongly suggest such an interpretation, it is known that macroscopic uptake data rarely yield conclusive mechanistic information. Therefore, laboratory uptake studies, which are intended to be used for surface complexation modeling, are more and more frequently backed up with spectroscopic investigations.

Conclusions

Model calculations suggested that the observed long-term kinetics in Np(V) sorption experiments under site specific conditions (at low liquid to solid ratios in saturated salt solutions) may at least partly be due to the sampling procedure by which the liquid to solid ratio is affected. The proposed procedure to analyze the data encompasses the calculation of sorption coefficients based on the initial and actual concentration of the blank solution. Additionally mean values and error bars were obtained from the individual measurements (replicates or parallel sorption samples). It was checked whether the calculated sorption coefficients and the error ranges would justify the application of a sorption coefficient which does not depend on liquid/solid ratio or Np concentration. A second condition was the validity of a linear isotherm.

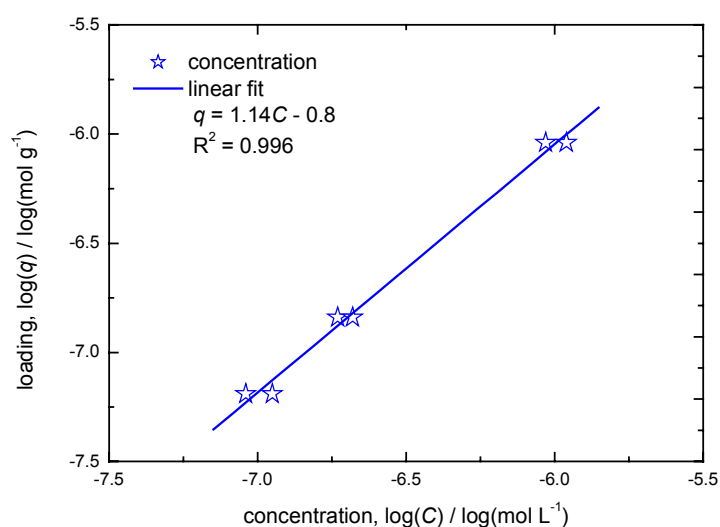


Figure 3: Isotherm plot (log Np(V) loading vs. log aqueous Np(V) concentration) for the system Q-brine/cement/Mg-depot.

The ideal case of the slope of the linear isotherm falling within the overlap range of the Np(V) sorption coefficient was found for the Q-brine/cement system. However, for the Q-brine/cement/Mg-depot system the sorption coefficient from the isotherm fit was lower than the lower bound of the overlap range. Furthermore, in this system a Freundlich-isotherm gave a statistically slightly better fit to the data. Overall, a constant sorption coefficient appeared justified even in this case, because the measured values were consistent. Addition of iron to the system caused a different behavior. Apparent sorption coefficients, R_s , as a function of dissolved radionuclide concentration coincided at nearly one dissolved Np concentration. It was suggested that Np(V), which had been added originally, is reduced to Np(IV) and the formation of an insoluble Np(IV) solid occurred. This is ideally backed up by spectroscopic investigations which can directly yield information about the redox-state of Np.

In summary for the sorption data collected for Np(V) within the experimental investigation of site-specific sorption behavior, the analysis of cement based systems showed that

- addition of the *Mg-depot* did not significantly affect the observations
- addition of iron resulted presumably in the precipitation of a Np(IV) phase due to reduction of the Np(V) by the available iron.

Acknowledgments

This study has been financially supported by Forschungsbergwerk Asse, GSF-Forschungszentrum für Umwelt und Gesundheit. The authors would like to thank Andreas Bauer, Klaus Spieler and the INE analytic team for their contributions in the experimental part.

References:

- Altmaier M., Metz V., Neck V., Müller R., and Fanghänel T. (2003) Solid-liquid equilibria of Mg(OH)₂(cr) and Mg(OH)₃Cl·4H₂O(cr) in the system Mg-Na-OH-Cl-H₂O at 25°C. *Geochimica et Cosmochimica Acta* **67**, 3595-3601.
- Harvie C. E., Møller N., and Weare J. H. (1984) The prediction of mineral solubilities in natural waters: the Na-K-Mg-Ca-H-Cl-SO₄-OH-HCO₃-CO₃-CO₂-H₂O system from zero to high concentration at 25°C. *Geochimica et Cosmochimica Acta* **48**, 723-751.
- Kienzler B., Metz V., and Vejmelka P. (2001) Near field radionuclide concentrations: Sorption or solubility constrained? *CD-ROM Proceedings of the 8th International Conference on Radioactive Waste Management and Environmental Remediation*, 44-1, 1-6.
- LLNL. (1997) EQ3/6 Software Package for Geochemical Modeling. Version 8.0. Software Produced under the Designated Unclassified Subject Area (DUSA) "Yucca". University of California, Lawrence Livermore National Laboratory.
- Lützenkirchen J. (2001) Evaluation of experimental procedures and discussion of two different modelling approaches with respect to long-term kinetics of metal cation sorption onto (hydr)oxide surfaces. *Aquatic Geochemistry* **7**, 217-235.
- Lützenkirchen J., Metz V., Kienzler B., and Vejmelka P. (2003) Site specific sorption data for the Asse salt mine. *CD-ROM Proceedings of the 9th International Conference on Radioactive Waste Management and Environmental Remediation*, 4621,1-7.
- Metz V., Schübler W., Kienzler B., and Fanghänel T. (2004) Geochemically derived non-gaseous radionuclide source term for the Asse salt mine – assessment for the use of a Mg(OH)₂-based backfill material. *Radiochimica Acta* (accepted for publication).
- Pitzer K. S. (1987) A thermodynamic model for aqueous solutions of liquid-like density. In *Thermodynamic modeling of geological materials: Minerals, fluids and melts.*, Vol. 17 (ed. I. S. E. Carmichael and H. P. Eugster), pp. 97-142. Mineralogical Society of America.
- Schübler W., Kienzler B., Wilhelm S., Neck V., and Kim J. I. (2001) Modeling of near field actinide concentrations in radioactive waste repositories in salt formations: effect of buffer materials. *Materials Research Society Symposium Proceedings* **608**, 791-798.
- Wolery T. J. (1992) EQ3/6, a software package for geochemical modeling of aqueous systems: package overview and installation guide. *UCRL-MA-110662 PT I*.

MODELLING OF ADSORPTION OF REDOX SENSITIVE OXYANIONS ON GIBBSITE

Markus Maria Miedaner, R. Weerasooriya, H.J. Tobschall

Institut für Geologie und Mineralogie
Friedrich Alexander Universität Erlangen-Nürnberg
Schlossgarten 5, 91054 Erlangen
Markus-Miedaner@web.de

The adsorptive behaviour of minerals in natural soils has been the focus of many scientific investigations for a long time. Besides mineralogical studies, geochemists are also trying to determine the filter capacity with respect to waste-waters and to understand the buffering capacity for oxyanions (As, Se, Mo, P) in soils. The present work is part of an on-going project on developing a thermodynamically consistent database for the adsorption of oxyanions onto different Al-derived oxides / hydroxides that are ubiquitous in nature. The experimental data are quantified by both 1-pK and 2-pK Surface Complexation Models using Charge Distribution Multi Site Ion Complexation- (CD-MUSIC), Double Layer- (DLM) and Triple Layer- (TLM) mechanistic models explicitly accounting for the finite size of oxyanions. With this objective the adsorption of redox-sensitive oxyanions, e.g. As and Se on gibbsite was investigated as a function of solution pH, redox state e.g. arsenite and arsenate; selenate and selenite, and adsorbate loading. All experiments were carried out in batch systems to determine adsorption edges, isotherms and proton exchange ratios ($r_{\text{anion}/\text{OH}^-}$) upon oxyanions adsorption. Initial concentration of the adsorbates and the pH were ranged 1.34 - 13.4 $\mu\text{mol/L}$ and 4 - 9.2 respectively. Possible surface configurations were examined using both vibration spectroscopy and molecular modelling methods.

When compared to arsenate and selenite, the adsorption density of arsenite and selenate was low. Therefore such experiments were practically not feasible in the latter cases. Overall trends of $\text{pH} = f(\Gamma_{\text{ads}})$ curves of arsenite have exhibited a marked deviation from typical anion adsorption edges observed for arsenate and selenite, showing a maximum Γ_{ads} around pH 8.2. Based on indirect evidence, it is observed that arsenite shows weak affinity for gibbsite forming outer-sphere complexes, whereas both arsenate and selenite showed strong bonding pointing to inner-sphere complexes. When $0.01 < \Gamma_{\text{ads}} < 0.08 \text{ mol m}^{-2}$ with $4 < \text{pH} < 7$, in the case of arsenate or selenite, the $r_{\text{As,Se}/\text{OH}^-}$ values always converged to 1.5 - 1.8 indicating release of more than one hydroxyl ion upon selenite or arsenate adsorption. In the case of arsenite, the $r_{\text{As}(3+)/\text{OH}^-}$ always converged to zero when $0.26 < \Gamma_{\text{ads}} < 7 \text{ mol m}^{-2}$ and $6.2 < \text{pH} < 8.2$. The non-integral $r_{\text{anion}/\text{OH}^-}$ values suggests the occurrence of several microstates in the surface complex formation and an arsenate - surface direct bonding, possibly an inner-sphere complex. Such data for arsenite however cannot be obtained due to its low As^{3+} values. The processing and analysing of selenite data along these lines are currently in progress.

This method as well as IR-spectroscopy suggests that As and Se are adsorbed to the gibbsite surface as bidentate complexes, which could be confirmed by molecular modelling using a cluster approach.

It was possible to reach a good agreement with published and experimental data for arsenate. Most oxyanion species converged to bidentate mononuclear complexes during optimization to lowest internal energy.

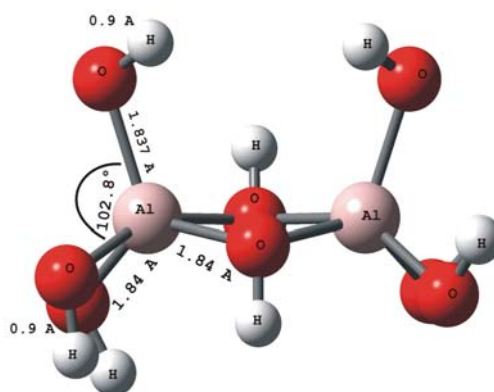


Figure 1: This gibbsite-cluster was the basis for the molecular modelling calculations. During optimization to lowest internal energy most species converged to bidentate complexes. All calculations have been performed using a RHF/6-31g parameterization. Because of the symmetry of the cluster only relevant distances and angles have been labelled.

The modelling using both 1-pK and 2-pK approaches for all data (Mo, P, As and Se) is presently in progress to account the finite size of oxyanions.

**SELECTED RESULTS OF THE NEA SORPTION FORUM:
POTENTIAL AND LIMITATIONS OF THERMODYNAMIC
SORPTION MODELS FOR THE DERIVATION OF RADIONUCLIDE
K_d VALUES FOR NUCLEAR WASTE DISPOSAL**

M. Ochs¹, J.A. Davis², M. Olin³, T.E. Payne⁴, C.J. Tweed⁵, M. Askarieh⁶ and S. Altmann⁷

¹ BMG Engineering Ltd, Ifangstr. 11, 8952 Zürich-Schlieren, Switzerland

² U. S. Geological Survey, Mail Stop 465, 345 Middlefield Rd., Menlo Park, CA 94025, USA

³ University of Helsinki, Helsinki, Finland

⁴ Environment Division, ANSTO, PMB 1 Menai 2234, Australia

⁵ Future Energy Solutions, Harwell IBC, Oxon OX11 0QJ, U.K.

⁶ United Kingdom Nirex, Ltd, Harwell, Oxon OX11 0RH, U.K.

⁷ ANDRA, Parc de la Croix Blanche, F-92298 Châtenay-Malabry, France
michael.ochs@bmgeng.ch

Background

Radionuclide sorption is an important process in safety analyses of radioactive waste disposal systems, and is typically characterised by distribution coefficients (K_d values). Because of the importance of sorption, reducing uncertainty in K_d translates directly to gaining confidence in performance assessment. The following issues contribute to uncertainty in K_d :

- Radionuclide sorption along a potential migration path is significantly influenced by the variability of the geochemical composition. Because of the conditional nature of K_d , different estimates of K_d are required for each environmental compartment.
- Often, ground- or porewater as well as solid phase composition for a given compartment cannot be determined with certainty and have to be estimated through geochemical models.
- Where very long timeframes need to be considered, it is necessary to derive K_d for estimated possible future conditions.

As it is not possible to determine K_d experimentally for each and every condition, selected values for performance assessment usually need to be derived based on data from similar and/or simplified systems, which may be supplemented with site-specific information. Thermodynamic sorption models (TSMs; i.e., surface complexation/ion exchange coupled with all relevant solution and mineral equilibria) are ideal tools for this task because they are able to integrate quantitatively the influence of all relevant geochemical parameters on K_d .

Brief summary of the NEA Sorption Project, Phase II

The present contribution presents selected results of Phase II of the NEA Sorption Project (a comprehensive documentation is in the state of a final draft for review). Phase I of this project ran from 1997 to 1998 and illustrated advances in the field of TSMs, but also the diversity in terms of thermodynamic descriptions of sorption processes. Phase II was initiated as a step towards demonstrating the consistency of TSMs and their applicability to systems relevant for radioactive waste disposal. The project was implemented in the form of a comparative modelling exercise based on carefully selected datasets from the following groups of sorbent substrates:

- Simple substrates: single oxide minerals
- Substrates of intermediate complexity: clay minerals and bentonite
- Complex substrates: soils and sediments

The value of TSMs in quantifying the geochemical factors that determine K_d was demonstrated in a variety of systems. The thermodynamic sorption models tested in this project were able to reproduce trends, and in most cases values within one order of magnitude, of measured K_d over a very wide range of simple to complex mineral substrates and aqueous chemical conditions (pH, pCO_2 , etc). Average absolute errors of model predictions in comparison to experimental data were in the range of 0.5 log K_d units or less for a number of cases. This capability demonstrates a significant system understanding and the utility of TSMs for the selection of K_d values for PA.

Often, K_d values for PA need to be derived for conditions that had not been covered as such in experiments. TSMs are the only tools that allow a direct coupling of variable solution chemistry or mineralogy with K_d in a thermodynamic framework. Therefore, TSMs represent the most traceable and defensible method to derive K_d as a function of variable conditions.

Selected critical issues for the application of TSMs to PA-relevant systems

As a contribution to a sorption workshop aimed at discussing the state of the art in this field, the focus of this presentation will not be on the performance of TSM approaches in this project and their utility for performance assessment, but on some of the open scientific questions identified in the course of this project.

Most of these questions can be related to the complexity of PA-relevant substrates, and the best use of different types of TSMs for describing sorption data and making predictions in such systems. Present approaches to sorption modelling encompass a range of mathematical simplicity and chemical correctness:

- i) The most plausible models are invariably those where the nature of surface species and/or sites is confirmed by spectroscopy, or models that use the most accurate

(detailed) description of the solid-water interface (see e.g. van Riemsdijk and Hiemstra, 1998). While these models are chemically most correct, they are typically not very useful for PA applications: They require detailed surface chemical information and are, therefore, very difficult or impossible to parameterise for PA-relevant substrates.

- ii) TSMs which contain a surface complexation model without an electrostatic correction term (SC-NEMs) form the other end of the spectrum. These approaches emphasise a good mathematical fit to experimental data, possibly at the cost of having to formulate less plausible surface species. However, these models still provide a thermodynamic framework for predicting K_d in an interpolative fashion as a function of conditions. For truly complex substrates, use of these models in a top-down approach (Generalised Composite models, cf. Davis et al., 2002) can be the only choice that actually allows parameterisation. However, top-down models are restricted to material that can be studied experimentally in a laboratory, and PA may encounter situations where a K_d is required for a material that is not directly accessible, such as a compacted bentonite, or a host rock after being altered, etc.
- iii) The traditional surface complexation models that include electrostatic corrections (DLM, BSM, TLM) make up the large middle ground between the above extremes. They can be more chemically correct than the SC-NEMs and offer a predictive capability for systems which are otherwise difficult to assess. However, they are often more difficult to parameterise. These models typically constitute the single mineral component models used in bottom-up (Component Additivity models, cf. Davis et al., 2002) approaches for complex substrates.

Thus, the best use of TSMs in bottom-up vs. top-down approaches for complex systems clearly is still a matter of uncertainty and debate. Based on the present project, it appears that bottom-up models may be suitable for some materials (e.g. natural bentonite), but are difficult to apply to a truly complex natural substrate. At present, it cannot be assessed with certainty whether this is an inherent problem of the bottom-up approach or whether this is mainly due to shortcomings in the single mineral component models or inappropriate methods of parameter transfer:

- It is possible that it is inherently incorrect to build up a sorption model by an additive process, because non-additivity of sorption may be significant in certain substrates.
- On the other hand, the present project indicates that failure of a bottom-up approach may be largely due to lack of sufficient data and appropriate models for component minerals. For example, it appeared that the choice of site densities for a given component mineral can be a major source of discrepancies in bottom-up models. This suggests that further work may be required to gain a consensus on determination or estimation of site densities.
- At the same time, there is a clear lack of data on the sorption of radionuclides in the presence of relevant groundwater anions and cations, even in studies with single

minerals, as most of the systematic sorption work to date focused on simple electrolyte solutions.

- The transfer of model parameters from independently calibrated models or from the literature to a different substrate of interest can also be identified as a critical part of predictive TSM applications. Stability constants for SC parameters cannot be used directly, even for the same mineral surface, if a different total site density is utilised in the predictive model. In particular the top-down modelling approach is semi-empirical, and surface stability constants for such models are only valid for the particular assemblage of solid phases being studied. This problem is compounded by the lack of appropriate standard states for surface complexation models. The establishment of such reference states would offer a partial solution to the problem of conditional SCM parameters (cf. Kulik, 2002; Sverjensky, 2003)

References:

- Davis, J.A., Payne, T.E., and Waite, T.D. (2002) Simulating the pH and pCO₂ dependence of uranium(VI) adsorption by a weathered schist with surface complexation models. In: *Geochemistry of Soil Radionuclides*, Soil Science Society of America, Madison, WI, Chap. 4, p. 61-86.
- Kulik, D.A. (2002) Gibbs energy minimization approach to modeling sorption equilibria at the mineral-water interface: thermodynamic relations for multi-site-surface complexation. *Am. J. Sci.*, 302, 227-279.
- Sverjensky, D.A. (2003) Standard states for the activities of mineral surface sites and species. *Geochim. Cosmochim. Acta*, 67, 17-28.
- van Riemsdijk, W.H., and Hiemstra, T. (1998). From molecular structure to ion adsorption modelling, in: Sparks, D.L., and Grundl, T.J. (eds.). *Mineral-water interfacial reactions: Am. Chem. Soc. Symp. Ser.*, vol. 715, 68-86.

Eu(III) COPRECIPITATION WITH THE TRIOCTAHEDRAL CLAY MINERAL HECTORITE

H. Pieper, D. Bosbach, P.J. Panak, K. Dardenne, J. Rothe, M. A. Denecke and T. Fanghänel

Forschungszentrum Karlsruhe
Institut für Nukleare Entsorgung (INE)
PO Box 3640
76021 Karlsruhe
Germany
pieper@ine.fzk.de

Various secondary phases form upon alteration/dissolution of HLW (**high level waste**) glass. They represent a significant retention potential for radionuclides including trivalent actinides. Hectorite $\text{Na}_{0.7}[\text{Li}_{0.7}\text{Mg}_{5.3}\text{Si}_8\text{O}_{20}(\text{OH})_4]$ is a trioctahedral smectite clay that forms within the alteration layer of corroded HLW glass (Zwicky 1989). Numerous studies have clearly demonstrated that many radionuclides tend to sorb to clay minerals via various reaction mechanisms and the migration of radionuclides into the next barrier is decelerated by complexation. Due to the structural complexity and chemical variability of smectites, sorption of trivalent actinides involves several unique sorption mechanisms: (1) adsorption via inner-sphere and outer-sphere complexation, (2) cation exchange in the interlayer and (3) incorporation into the octahedral sheet of the smectite structure. Further studies have focused on radionuclide adsorption to pre-existing clay minerals. Especially trivalent actinides are known to be adsorbed to clay minerals by an outer- and inner-sphere surface complex.

We have used a new method to synthesise an Eu- und a Cm-containing hectorite exerting Cm(III) and homologous Eu(III) coprecipitated with $\text{Mg}(\text{OH})_2$ as a precursor. Tetraethylammoniumchloride (TEA) catalysed the synthesis carried out at pH 9-10 and 100 °C (Carrado 1997 and 2000b). In the coprecipitation experiments a Mg/Eu ratio of 100 was adjusted in the Mg-hydroxide slurry.

Decanted Eu containing hectorite suspension (HecEu) was placed in a dialysis membrane in order to selectively dissolve excess Ludox SiO_2 sol at pH 4 up to 3 weeks (HecEuD1: 150 h, EuHecD2: 500 h). Sedimentation was avoided by mixing continuously. The potential precipitation of secondary phases during this procedure was excluded on the basis of hydrogeochemical calculations using PHREEQC (Nagra/PSI thermodynamic data base, Hummel et al. 2002).

The Europium containing hectorite nanoparticles were characterised by X-ray diffraction, scanning electron microscopy and atomic force microscopy. IR-spectroscopy clearly showed that the precipitated samples Hec, HecEu and HecEuD1 are hectorite with the characteristic absorption bands of the Mg_3OH units (Farmer 1974, Madejová und Komadel 2001). After 500 hours dialysis, IR measurements indicates a complete dissolution of the crystalline hectorite. The IR spectrum exhibits an additional absorption band at 968 cm^{-1} , a

common feature for impurities in this silica phase and of hydrous silica ($\text{SiO}_2 \times n \text{H}_2\text{O}$) (Farmer 1974). Apparently a new silica phase has formed during the late stage hectorite dialysis. Laser fluorescence spectroscopy clearly showed that no Eu is associated (adsorbed / incorporated) with this amorphous residue HecEuD2, in contrast to the untreated product Hec and the 150 h dialysed sample HecEuD1. Here we can deduce that Eu species are closely associated with the crystalline hectorite.

The sorption mechanisms of Cm respectively Eu associated with the synthesised hectorite were investigated by time-resolved laser fluorescence spectroscopy (TRLFS). The emission spectrum of Eu shows the $^5\text{D}_0 \rightarrow ^7\text{F}_1$ and $^5\text{D}_0 \rightarrow ^7\text{F}_2$ transition (fig. 1). The splitting of the $^5\text{D}_0 \rightarrow ^7\text{F}_2$ peak indicates a strong complexation between Eu and hectorite. The fluorescence emission decay is observed to follow a bi-exponential function, indicating the presence of at least two Eu-species.

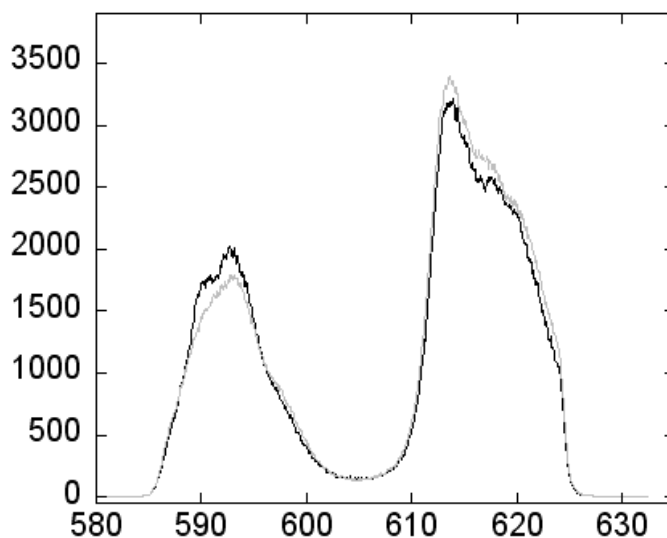


Figure 1: Eu Time-resolved laser fluorescence spectroscopy: the emission spectrum of Eu shows the $^5\text{D}_0 \rightarrow ^7\text{F}_1$ and $^5\text{D}_0 \rightarrow ^7\text{F}_2$ transition. This Eu-species remained stable under acidic conditions pH 6.5 (black) and 4 (grey).

According to the empirical equation of Kimura fluorescence lifetimes of $315 \mu\text{s} \pm 15$ corresponds to 2.8 H_2O molecules in the inner Eu-coordination sphere (Horrocks 1979, Kimura 1996). Furthermore, a lifetime of 955 μs indicates an Eu-species which has lost its entire hydration sphere. Therefore, we ascribe the Eu-species with the longer lifetime of 955 μs to an unhydrated Eu ion incorporated in the TOT-structure or into a minor amorphous silica phase remained during the hectorite synthesis. The spectra at pH 4 and pH

6.5 are identical which means this Eu-species remained stable under acidic conditions (see figure 1). In fact the very similar spectra of the Eu-Silica complex and the Eu-species incorporated into the hectorite allows not to exclude a Eu-Silica complexation during the hectorite synthesis.

The first coprecipitation experiment with Cm shows a fluorescence band at 609.3 nm due to the ${}^6D_{7/2} \rightarrow {}^8S_{7/2}$ transition of Cm (III). A strong peak shift of 15.5 nm compared to the peak position of the aquo ion at 593.8 nm is observed (fig. 2). Change of the chemical environment in the first coordination sphere of the Cm ion, like loss of H_2O or OH , leads to a red shift of the emission band.

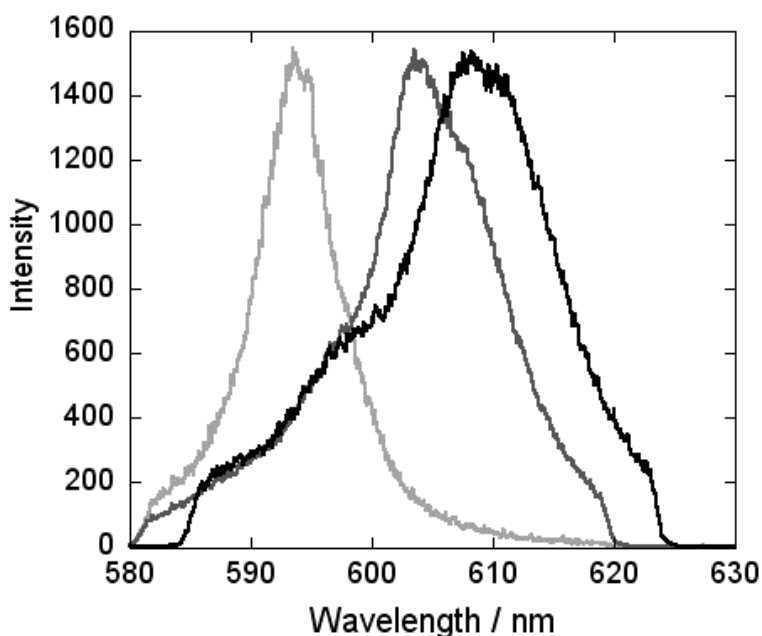


Figure 2: Cm Time-resolved laser fluorescence spectroscopy: the red shift of the Cm-Ludox emission spectrum (605.1 nm middle grey) and the Cm incorporated into the hectorite structure (609.3 nm, black) compared to the Cm aquo ion (593.8, grey)

Cm solution was also added to Ludox HS-30 in the same ratio and under the same conditions, to get a reference spectrum of the Cm species associated with silica. In the emission spectrum of Cm associated with Ludox HS 30 we find a 11.3 nm red shift to 605.1 nm compared to the Cm-aquo ion. Due to the difference in peak position of 5 nm between Cm-Silica complex and the Cm-species incorporated into the hectorite, we can differentiate unambiguously between the two mechanisms.

In order to differentiate between coprecipitated and surface sorbed Eu species, batch sorption studies were performed with synthetic Eu-free hectorite. For the surface sorbed Eu species a fluorescence lifetime of 315 μs was found, which clearly differs from the coprecipitated species with a lifetime of 955 μs .

EXAFS measurements at the Eu L3 edge are performed attempted to confirm the hypothesis that trace amounts of Cm/Eu occupy an octahedral lattice site by probing the local environment around Eu-cations in the synthetic hectorite sample. Eu L3 X-ray absorption spectra are recorded at the ANKA-XAS beamline. All spectra are recorded in fluorescence mode at room temperature. EXAFS data analysis is based on standard least-squares fitting techniques using the UWXAFS program package [Stern 1995; Newville 1993].

The Fourier transform (FT) of the k^2 -weighted EXAFS function is shown in figure 3. The FT spectrum exhibits an intense peak at about 1.8 \AA (R- Δ), corresponding to a phase-shift corrected value of about 2.3 \AA . This resonance represents backscattering from oxygen atoms comprising the first coordination sphere of Eu in the sample. Visual inspection of this FT resonance shows a rather large asymmetry, likely caused by multiple Eu-O distances. This is supported by fit results, indicating the presence of a dominant Eu-O interaction (5-6 O at 2.34 \AA , $\sigma^2=0.0125 \text{\AA}^2$) and a more distant oxygen shell (3 O at 2.42 \AA , $\sigma^2=0.0078 \text{\AA}^2$). The splitting of the oxygen neighbors into two distances could be due to the presence of the two Eu(III)-species observed by TRLFS. Detection of a second next neighbor shell (i.e., Si or Mg in the TOT-structure) would facilitate correct interpretation. However, the apparent deformation of the local environment renders detection of this shell difficult. Note that the quality of the fit is significantly improved when an additional Si/Mg-shell is included (<1 Si/Mg at 3.20 \AA , $\sigma^2=0.001 \text{\AA}^2$, σ^2 has to be fixed). Low temperature EXAFS measurements will be performed to clarify this point.

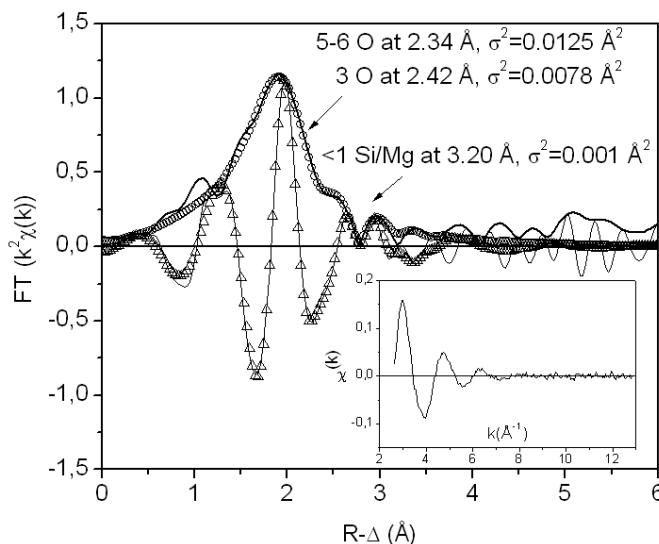


Figure 3: Eu(III)/Hectorite: Fourier transform magnitude (\blacksquare) and imaginary part (---) and R-space fit magnitude (\boxtimes) and imaginary part (ρ) of the k^2 -weighted Eu L3-EXAFS. The unweighted $\chi(k)$ is in the inset.

Combining macroscopic wet chemical techniques with laser fluorescence measurements clearly shows, that an unhydrated Eu(III) species is closely associated with the hectorite. Due to size difference between Mg/Li (0.72 Å/0.76 Å) and Cm(III) (0.97 Å) one would assume that a significant local deformation is associated to the occupation of Cm/Eu in octahedral lattice site.

References:

- Carrado K.A., Zajac G.W., Langmuir, 13, pp. 2895-2902, 1997
Carrado K.A., et al., Chem. Mater. 12, pp. 3052-3059, 2000b
Farmer V.C., The Infrared Spectra of Minerals, Mineralogical Society London, 1974
Horrocks Jr. W. DeW., Sudnick R., J. Am. Chem. Soc. 101(2), pp. 334, 1979
Hummel W., Berner, U., Curti, E. Pearson, F.J. and Thoenen, T. Nagra/PSI Chemical Thermodynamic Data Base 01/01 Universal Publishers, Parkland Florida, USA
Kimura T. et al. Radiochimica Acta 72 2 pp. 61-64, 1996
Madejová und Komadel, Clays and Clay Minerals 49, 5, pp. 410-432, 2001
Newville, M.; Livins, P.; Yacoby, Y.; Rehr, J. J.; Stern, E. A. Phys. Rev. B, 47, pp. 14126-14131, 1993
Pieper H. et al. FZK/ANKA Annual Report 2003, pp 52
Stern, E. A.; Newville, M.; Ravel, B.; Yacoby, Y.; Haskel, D. Physica B 208 – 209, pp. 117 – 120, 1995
Stumpf, T. et al. Radiochimica Acta 90(6) 345-349 2002
Zwicky H.U., Grambow B., Corrosion behaviour of british Magnox waste glass in pure water, Mat. Res. Soc. Symp. Proc., 127, pp. 129-136, 1989

GALLIUM(III) ADSORPTION ON CARBONATES AND OXIDES: X-RAY ABSORPTION FINE STRUCTURE STUDY AND SURFACE COMPLEXATION MODELING

Oleg S. Pokrovsky, Gleb S. Pokrovski and Jacques Schott

Géochimie: Transferts et Mécanismes
CNRS (UMR 5563)-OMP-Université Paul-Sabatier,
38, rue des Trente-Six Ponts
31400 Toulouse
France
oleg@lmtg.ups-tlse.fr

Abstract

Adsorption of Ga on calcite, magnesite, amorphous silica and manganese oxide was studied using batch adsorption techniques as a function of pH, $p\text{CO}_2$, and [Ga]. Adsorbed complexes of Ga on calcite, magnesite and $\delta\text{-MnO}_2$ were further characterized using XAFS spectroscopy. At high surface loadings from supersaturated solutions, Ga is likely to form polymeric network at the surface (edge and corner-sharing octahedra). At low surface loadings, Ga presents as isolated octahedra coordinated by water molecules, hydroxide groups and Me-O sites on the surface. At $\text{pH} > 6$, Ga therefore changes its coordination from 4 to 6 when adsorbing from solution ($\text{Ga}(\text{OH})_4^-(\text{aq})$) to metal surface sites ($\text{Me-O-Ga}(\text{OH})(\text{H}_2\text{O})_4^+$, Me = Ca, Mg) of carbonate minerals. A surface complexation model which assumes the formation of positively charged, neutral and negatively charged surface complexes for carbonates, manganese oxide and silica, respectively, was used to describe the dependence of adsorption equilibria on aqueous solution composition in a wide range of pH and concentration.

Introduction

In contrast to large amount of studies devoted to divalent metals, Rare Earth Elements and actinides adsorption and colloidal behavior in aquatic systems, very little is known on interface equilibria of less-common “insoluble” trivalent and tetravalent elements. Among these elements, gallium is particularly interesting because it can be used as an analog of another more environmentally important element, aluminum [1], whose structures on the mineral surfaces and in aqueous solution cannot be easily accessed by XAFS spectroscopy [2]. This paper is devoted to an experimental study of Ga adsorption on four common sorbents typical of natural waters (Ca and Mg carbonates, and Mn(IV) oxide and

amorphous silica) using a combination of batch adsorption technique, XAFS spectroscopy and surface complexation modeling.

Experimental

Synthetic calcite, natural magnesite, commercial amorphous silica and synthetic δ -MnO₂ were used in the present study. The specific B.E.T. surface areas were measured by triple-point N₂ adsorption and found to be 18.6, 0.72, 462 and 12 m²/g for calcite, magnesite, SiO₂ and δ -MnO₂, respectively. Adsorption experiments were carried out at 25±0.5°C with typical exposition time being about 1 week. No difference in adsorbed Ga concentration on calcite was detected for exposition time of 2 weeks and 6 months. Gallium concentration was measured by flame or flameless atomic absorption in a graphite furnace and by ICP-MS.

XAFS spectra (including the X-ray absorption near-edge structure region or XANES, and the extended X-ray absorption fine-structure region or EXAFS) on selected sorption samples were collected at ambient conditions (20±2°C, 1 atm) in the fluorescence mode at the Ga K-edge (~10,370 eV) over the energy range 10,200-11,800 eV on the IF BM 32 beam line (ESRF, Grenoble, France). The samples (wet mineral powders with adsorbed Ga or aqueous solutions) were placed in a Teflon cell with two 25- μ m Kapton-film windows. The spectra acquisition procedure was similar to that described in refs [2, 3]. Three to six scans (of ~50 min/scan data collection time) for each sample were collected to high energy values (up to $k \sim 14 \text{ \AA}^{-1}$, where k is the photo-electron momentum).

Results and Discussion

XAFS

Spectra of calcite samples with Ga adsorbed from aqueous solutions at initial concentrations of 1.0, 0.1 and 0.01 mM Ga and pH ~ 6-7 exhibit 1st shell signals from 5 to 6 oxygens with Ga-O distances between 1.9 and 2.1 \AA (Fig. 1). EXAFS modeling shows that the 1st shell of two more concentrated samples is splitted into 2 oxygen subshells with Ga-O distances of 1.93 and 2.09 \AA . Such 1st shell splitting is similar to that observed in Ga oxy-hydroxides (e.g., α -GaOOH) where the difference between Ga-O and Ga-OH bond lengths (1.93 and 2.08 \AA , respectively) induces significant distortions in the GaO₆ octahedron. For the most dilute sample (0.01 mM Ga), no 1st shell splitting was detected within errors: fits with two distinct Ga-O paths always converged to a single path with $R=1.94\pm0.01 \text{ \AA}$ and $N=5\pm1$. The derived average Ga-O distance is close to that corresponding to octahedral Ga in gallium oxy(hydro)xides and acid aqueous solutions (1.90-2.10 \AA , refs. [2, 4]), and it is significantly higher than that for the tetrahedral Ga as found in Ga-bearing zeolites and alkaline solutions (1.78-1.85 \AA). In contrast to the 0.01 mM sample, the 1.0 and 0.1 mM samples exhibit significant 2nd shell contributions arising from Ga-Ga pairs. Modeling of these features yields two Ga subshells with distances at ~3.05 and ~3.5 \AA . These distances are very similar to those observed for polymeric Ga hydroxide complexes formed in aqueous solution during Ga³⁺ hydrolysis at 2<pH<5, and whose structures are composed of Ga(O,OH,H₂O)₆ octahedra sharing edges and double corners.

The derived Ga-O and Ga-Ga distances and coordination numbers clearly imply the dominant formation of hexa-coordinated polymeric oxy-hydroxide complexes during the sorption of Ga on calcite surfaces from concentrated (≥ 0.1 mM) aqueous solutions at neutral pH producing high surface loading (i.e., $\sim \mu\text{mol}/\text{m}^2$). At lower aqueous metal concentrations ($< \sim 0.01$ mM), no 2nd shell contribution is detected on the calcite surface, and Ga still remains essentially hexa-coordinated. The absence of 2nd shell EXAFS signal for this dilute sample indicates that no Ga polymers are formed at the surface from such dilute solutions and low surface loadings (i.e., $\sim \text{nmol}/\text{m}^2$). The most plausible scenario of adsorbed Ga complex is an octahedra sharing one oxygen with Ca atom on the surface similar to mononuclear inner-sphere complexes of Cu(II) and Zn(II) coordinated to Ca sites at the calcite surface [5]. EXAFS spectrum of Ga sorbed at magnesite from 0.01 mM solution at $0.5 \mu\text{mol}/\text{m}^2$ surface loading exhibits a single 1st shell contribution arising from ~ 6 oxygen atoms. This shell is found to be split into 2 subshells with $R_1=1.9 \text{ \AA}$, $N_1=5.3$, and $R_2=2.12 \text{ \AA}$, $N_2=1.6$. The EXAFS spectrum of a MnO_2 sample with Ga sorbed from an aqueous solution of 0.012 mM Ga at pH 6.8 shows two distinct contributions arising from 1st Ga-O and 2nd Ga-(Mn or/and Ga) atomic shells, respectively. Modeling shows that the 1st shell corresponds to GaO_6 octahedra with an average Ga-O distance of 1.91 \AA with a relatively high DW factor, which might indicate significant distortions of the Ga octahedron. However, no 1st shell splitting could be detected.

Adsorption results

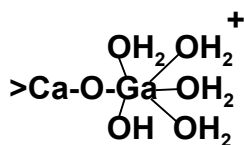
Adsorption of Ga on calcite is maximal at pH below 7 and decreases with pH at $7 \leq \text{pH} \leq 10$ for a wide range of Ga concentration (14 nM to 0.5 mM, Fig. 2a). Gallium adsorption on magnesite is very similar to that on calcite (Fig. 2b). For two different Ga concentrations in solution, a decrease of adsorbed amount starts at pH=6 and no adsorption is observed at $\text{pH} > 9$. Adsorption edge of Ga on manganese oxide is similar to that for carbonates: the adsorption is high at $2 < \text{pH} \leq 8$ but decreases to almost zero at $\text{pH} \sim 10$.

Surface Complexation Modeling

The thermodynamic model for carbonates-solution interface used in this study [6-8] postulates the formation of two primary hydration sites, $>\text{MeOH}^\circ$ (Me = Ca, Mg) and $>\text{CO}_3\text{H}^\circ$, having a 1:1 stoichiometry on the surface. The structure of surface complexes formed and the interatomic distances allow adsorption of six- coordinated Ga on positive metal centers, $>\text{CaOH}_2^+$, sharing one oxygen atom with surface Ca and undergoing protonation/deprotonation reactions. In terms of basic thermodynamic species, the adsorption of Ga on carbonate surface can be represented by



The surface complex thus formed can be schematically represented as



which reflects the presence of four water molecules, one hydroxyl group and one common oxygen with surface Ca atom.

Surface complexation model predictions of Ga adsorption on calcite and magnesite are presented as solid lines in Figure 2. For this modeling, only one adjustable parameter, the intrinsic stability constant of reaction (1), was used. All acid-base and Me^{2+} , CO_3^{2-} , HCO_3^- adsorption reaction constants, site densities and EDL capacitance were fixed during the fit [6]. This allows to estimate the reaction (1) stability constant as $\log K_1 = 7.0 \pm 0.3$ for calcite and 5.7 ± 0.1 for magnesite. Gallium adsorption on manganese dioxide was modeled within the concept of 2-pK, constant capacitance model (CCM) [9]. Only one adjustable parameter, the stability constant of Ga adsorption reaction



was varied to reproduce the experimental data. Between two independent sets of experiments, a reasonable agreement was found resulting in $\log K_2 = 0.25 \pm 0.15$. In accord with EXAFS results, the tentative structure of complex formed can therefore be represented as:

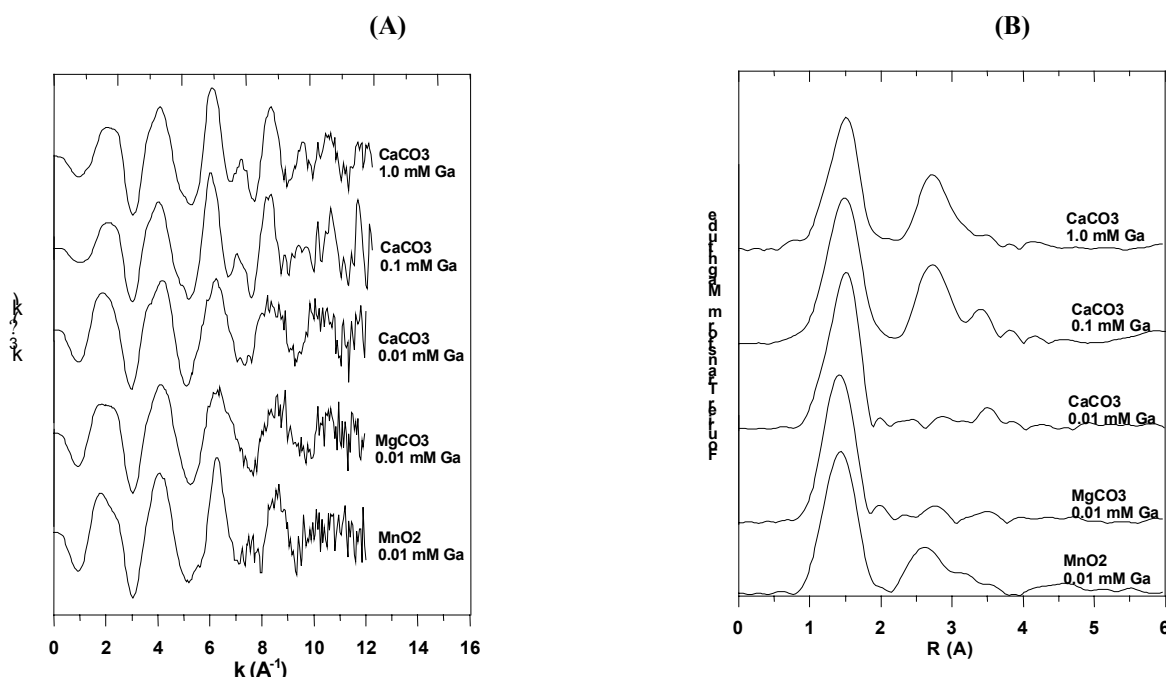
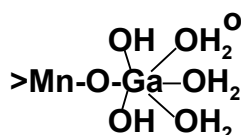


Fig. 1. (A) k^3 -weighted EXAFS spectra at Ga K-edge of selected adsorption samples, and (B) their corresponding Fourier Transform Magnitudes (not corrected for phase shift).

Gallium presents quite a different behavior compared to other metals and anions. It does not exchange with surface Ca atoms like divalent metals [5, 10] and trivalent actinides [11] or with carbonate surface groups like other oxy-anions [12, 13]. At neutral to alkaline pH, gallium changes its coordination from $\text{Ga}(\text{OH})_4^-$ anion in solution to the hexacoordinated $\text{Ga}(\text{O},\text{OH},\text{H}_2\text{O})_6$ on the surface where it binds to the metal center via octahedral corners. It can be thus hypothesized that the dominance of acid moieties on the carbonate surface ($>\text{MeOH}_2^+$) which provide extra amount of protons in comparison to the bulk aqueous solution, favors the change of Ga atomic coordination from 4 to 6 when adsorbing on a mineral surface. This is also in agreement with the known versatility of Ga to change its coordination during Ga^{3+} hydrolysis in aqueous solution and in mineral phases [2].

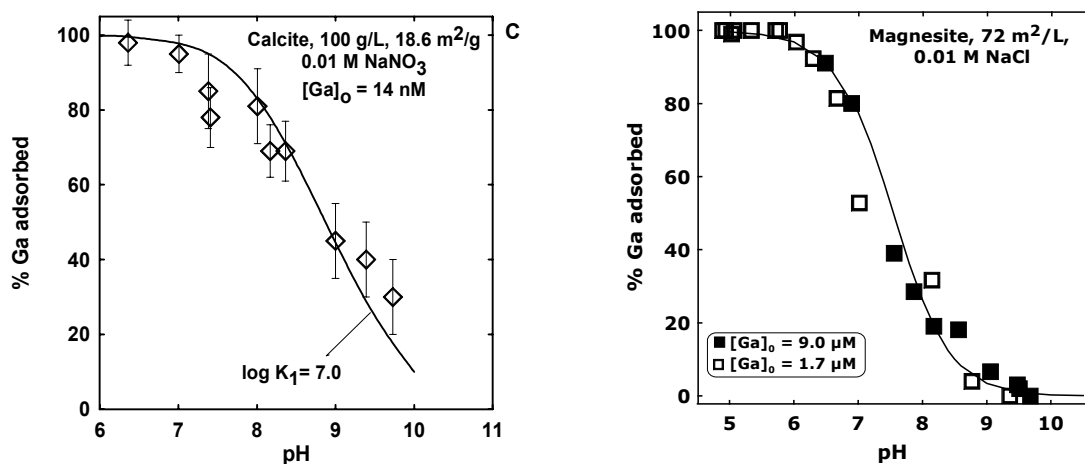


Fig. 2. Effect of pH on Ga adsorption on calcite and magnesite. Solid lines was calculated using SCM generated in this study with $\log K_1 = 7.0$ for calcite and $\log K_1 = 5.7$ for magnesite.

References:

- [1] Bénézech, P., Diakonov, I.I., Pokrovski, G.S., Dandurand, J.-L., Schott, J., Khodakovskiy, I.L., *Geochim. Cosmochim. Acta* 61 (1997) 1345.
- [2] Pokrovski, G.S., Schott, J., Hazemann, J.-L., Farges, F., Pokrovskiy, O.S., *Geochim. Cosmochim. Acta* 66 (2002) 4203.
- [3] Pokrovski, G.S., Schott, J., Farges, F., Hazemann, J.-L., *Geochim. Cosmochim. Acta* 67 (2003) 3559.
- [4] Michot, L.J., Mantargès-Pelletier, E., Lartiges, B.S., d'Espinose de la Caillerie, J.-B., Briois, V., *J. Amer. Chem. Soc.* 122 (2000) 6048.
- [5] Elzinga, E.J., Reeder, R.J., *Geochim. Cosmochim. Acta* 66 (2002) 3943.
- [6] Pokrovskiy, O.S., Schott, J., *Environ. Sci. Technol.* 36 (2002) 426.
- [7] Pokrovskiy, O.S., Mielczarski, J.A., Barres, O., Schott, J., *Langmuir* 16 (2000) 2677.
- [8] Pokrovskiy, O.S., Schott, J., Mielczarski, J., *Surface Speciation of Dolomite and Calcite in Aqueous Solutions*. In: *Encyclopedia of Surface and Colloid Science*, Marcel Dekker, 2002, p. 5081.

- [9] Sverjensky, D.A., Sahai, N., *Geochim. Cosmochim. Acta* 60 (1996) 3773.
- [10] Cheng, L., Sturchio, N.C., Woicik, J.C., Kemmer, K.M., Lyman, P.F., Bedzyk, M.J., *Surface Sci.* 415 (1998) L976.
- [11] Stumpf, Th., Fanghänel, Th., *J. Colloid Interface Sci.* 249 (2002) 119.
- [12] Cowan, Ch.E., Zachara, J.M., Resch, Ch.T., *Geochim. Cosmochim. Acta* 54 (1990) 2223.
- [13] Cheng, L., Fenter, P., Sturchio, N.C., Zhong, Z., Bedzyk, M., *Geochim. Cosmochim. Acta* 63 (1999) 3153.

ADSORPTION AND CO-PRECIPITATION OF METALS AND RADIONUCLIDES AT THE CALCITE-WATER INTERFACE: SPECTROSCOPIC OBSERVATIONS

Richard J. Reeder

Department of Geosciences and Center for Environmental Molecular Science
State University of New York at Stony Brook
Stony Brook, NY 11794-2100 USA
rjreeder@stonybrook.edu

Rapid kinetics of interfacial processes and moderate solubilities strongly coupled with solution properties allow for multiple, complex sorption mechanisms of metals and radionuclides at the surfaces of carbonate minerals. Calcite is the most abundant of the carbonate minerals and forms readily in a wide range of near-surface environments. For near-neutral and basic pH conditions, which are typical of many calcite-containing systems, the presence of significant amounts of dissolved carbonate allows competition between solution and surface-bound carbonate species for dissolved metals. Metal adsorption may dominate at low metal concentrations but overlaps with or gives way to precipitation and/or co-precipitation at higher concentrations. The presence of multiple surface sites and distinct preferences for uptake results in heterogeneous sorption and co-precipitation for many metals and radionuclides of environmental significance.

We briefly examine results from in situ spectroscopic characterization of uptake of selected metals in calcite pre-equilibrated suspensions and in calcite-supersaturated systems. As examples, Pb(II) and Zn(II) both show a high affinity for binding at the calcite surface and both readily co-precipitate to form calcite solid solutions. At low metal concentrations in calcite-saturated systems, EXAFS spectroscopy shows that Zn(II) and Pb(II) adsorb as inner-sphere surface complexes at the calcite-water interface. Observed coordination geometries differ from the octahedral coordination of Zn or Pb substituting in a Ca site in the calcite structure. Binding at steps and/or kink sites is favored over terrace sites. At higher metal concentrations, precipitation and adsorption both occur, with the precipitate phase depending on solution conditions. In calcite-supersaturated systems, Zn shows a strong preference for uptake at distinct surface sites in steps on the common growth face of calcite, similar to the preferences observed for Sr and Ba. This step-selective uptake results in heterogeneous incorporation of Zn in calcite. In contrast, Pb(II) shows weaker uptake with little preference for distinct sites.

In calcite pre-equilibrated systems (pH 7.4-8.3), U(VI) occurs in solution dominantly as carbonate complexes, which exhibit moderate to weak interaction with the calcite surface. At low U(VI) concentrations, in situ EXAFS and luminescence spectroscopies reveal the formation of multiple sorption complexes at the calcite-water interface. Coordination geometries are similar to the uranyl triscarbonate species, as observed in the mineral liebigite, but show subtle difference in equatorial coordination, possibly related to different

binding sites. At higher U(VI) concentrations, both adsorption and precipitation are observed, with the precipitate likely to be a mixed U-Ca carbonate-hydroxide.

In calcite-supersaturated systems, U(VI) shows a preference for binding at distinct step sites, resulting in heterogeneous co-precipitation patterns. EXAFS and luminescence results for U(VI) co-precipitated with calcite also reveal multiple U(VI) species in the bulk, differing primarily in equatorial coordination. It is suggested that the mechanism of co-precipitation and the availability of different surface sites influence the final form of U(VI) species incorporated into the calcite. Questions arise concerning the long-term stability of some incorporated species.

The diverse results obtained for interactions of metals and radionuclides with calcite emphasize the importance of the experimental conditions. Careful attention should be given to the procedures used for reacting carbonates with metal solutions, and particularly to the calcite saturation state over the entire duration of the experiments. The results also suggest that metals and radionuclides may be associated with carbonate minerals in multiple, complex chemical and physical states. Consequently, prediction of the long-term retention and possible release of toxic species bound with carbonates may be difficult without detailed knowledge of their state.

CAPABILITY OF SCM AND RES³T DATABASE FOR BLIND PREDICTION

A. Richter, V. Brendler

Forschungszentrum Rossendorf e.V.

Institute of Radiochemistry

P.O. Box 51 01 19

D-01314 Dresden

Germany

Anke.Richter@fz-rossendorf.de

Abstract

The paper presents the general strategy and an example for the current blind predictive capabilities of surface complexation models (SCM) and the respective database RES³T – the "Rossendorf Expert System for Surface and Sorption Thermodynamics"[1]. The approach for the elucidation of numerical data includes the collection of the mineral surface characteristics, the selection of reliable data records, the extrapolation to infinite dilution, the normalization to a reference site density and the averaging of selected thermodynamic data records.

The copper(II) sorption onto goethite was chosen as system illustrating the blind predictive capabilities. To keep the number of parameters at a minimum, the Diffuse Double Layer model was selected accounting for electrostatics. The calculations were performed with FITEQL [2]. The model prediction represents the experimental values for the adsorbed amount of Cu(II), expressed as conventional distribution coefficients K_D as required by most performance assessment software, within one order of magnitude or better.

Introduction

Still, the K_D concept of distribution coefficients is the most often utilized approach for description of sorption. The concept is wide-spread but often too simplistic, because many different basic physico-chemical phenomena are subsumed into one conditional parameter which is sensitive even to slight changes in system parameters. A K_D value used in prognostic studies is generally just a snapshot for a specific parameter combination, so there are very large uncertainties to extrapolated K_D values. Hence, from a scientific point of view the K_D concept is unsatisfactory, because empirical parameters are not able to portray complex processes on the surfaces. Surface Complexation Models (SCM) describe the sorption processes at the mineral-fluid interface on a scientific basis. The underlying assumptions are the following in brief:

- The electrical charge at the surface is determined by the chemical reactions of the mineral functional groups, including acid-base reactions and the formation of coordinative complexes.
- The equilibria of adsorption reactions can be described by mass action equations.
- Correction factors to these equations may be applied to involve electrostatic interactions.

SCM evolved over time and are now available in various versions, basing on different theoretical assumptions on the electrical double layer. The 2-pK-approaches Diffuse Double Layer Model [3,4], Constant Capacitance Model [5,6] and Triple Layer Model [7-9] are the most important and applied submodels. The individual models differ in the manner of description of the electrochemical double layer, i.e. position and hydration status of the adsorbed ion and the mechanism of protonation.

Certainly, during the next decade SCM will replace K_D only in some simple systems or systems dominated by one mineral. However, SCM can help to verify measured K_D 's, to identify the most critical sensitive experimental parameters, to assign uncertainty limits, to fill gaps difficult to access in sorption experiments, and to help to gain a better process understanding.

General strategy for the elucidation of numerical data

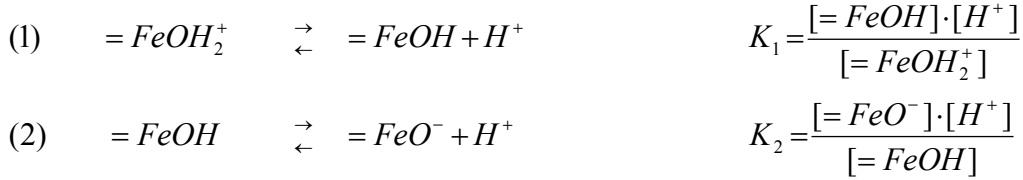
The amount of published adsorption research results using surface complexation models has increased drastically in the last decades. To overcome bias and hesitation against SCM (too complex, too few data available, not trustworthy) we think it is essential to develop a data supply strategy for modeling and to test whether SCM can already be applied successfully in prediction of K_D values for performance assessment (PA). One of the major goals of the RES³T database [1] is providing a foundation for the use of SCM in risk assessment studies. RES³T should finally be able to deliver recommended data sets for such SCM applications. Our strategy for the parameterization of the mineral-specific part of the SCM concept is shown by the following approach:

- First, a literature survey based on the RES³T database helps to define the chemical system, i.e. the mineral properties (specific surface area, site density, protolysis constants as function of ionic strength) and the set of surface species. Because the specific surface area is sample specific, the respective experimentally determined value should be used for the computations.
- The next step is the selection of reliable data records. When the data situation is sparse, also chemical analogies can be used to derive a sensible chemical model.
- The data are extrapolated to infinite dilution by the Davies equation.
- Because the reported data are related to different site densities, it is necessary to convert them to a reference state to enable comparison and averaging (normalization). The procedure according to Kulik [10] is followed, basing on a reference surface site density of 12.05 sites/nm² (20 μmol/m²). Of course this value is also used for all subsequent predictive modeling.
- After normalization, the data records applying to the same reaction (mineral surface protolysis and surface complex formation) must be compared and evaluated to identify and exclude outliers and doubtful data points. The remaining selected thermodynamic data records sets are then averaged to obtain respective model parameters.

Application example: The copper sorption onto goethite

The Diffuse Double Layer model was chosen as SCM submodel to keep the number of parameters at a minimum. The modeling was performed with the FITEQL code, version 3.2 [2].

All data collection efforts are fully based on RES³T. To keep the system as simple as possible, no distinction between strong and weak binding sites was applied. The values of K_1 and K_2 for the two protolysis steps always refer to the following deprotonation reactions:



Enquiry of RES³T resulted in 12 independent DDL data records for the goethite surface protolysis: After normalization, none of them appeared suspicious or deviated significantly from the rest. Hence, an averaging was justified leading to pK_1 of 6.49 ± 0.59 and a pK_2 of 10.41 ± 0.72 after normalization and correction to ionic strength $I=0$.

The experimental raw data for the sorption of Cu(II) onto goethite were taken from Ali and Dzombak [11]. The data sets comprised of 30 batch sorption data points with an experimental error of 4% at 2 copper concentrations for the Cu(II) sorption without admission of CO₂. Therefore, carbonate surface species had not to be considered. The following surface species have been reported in the literature: $=FeO-Cu^+$ and $=FeO-CuOH$. The ionic strength correction was performed with the Davies equation. Below the selected species are given, with their normalized reaction constants corrected to $I=0$, averaged from only 4 literature values.

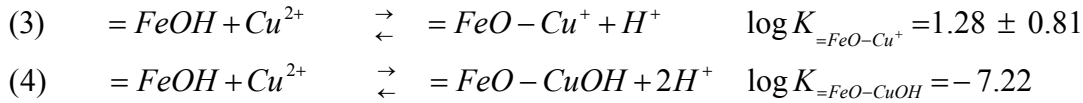


Table 1: FITEQL model conditions used for blind prediction of Cu²⁺ sorption onto goethite

Physical/chemical conditions used for prediction		Reference
Solid concentration	1.6 g/L	[11]
Site density	12.05 sites/nm ²	[10]
Surface area	79.4 m ² /g	[11]
Total site concentration	$2.54 \cdot 10^{-3}$ M	[11]
Ionic strength	0.01 M NaNO ₃	[11]
Total Cu ²⁺ concentration	$2.3 \cdot 10^{-5}/9.8 \cdot 10^{-5}$ M	[11]
Protolysis and surface complexation constants	log K¹	
$\equiv FeOH + H^+ \leftrightarrow \equiv FeOH_2^+$	-6.49	
$\equiv FeOH \leftrightarrow \equiv FeO^- + H^+$	10.41	
$\equiv FeOH + Cu^{2+} \leftrightarrow \equiv FeO-Cu^+ + H^+$	1.28	
$\equiv FeOH + Cu^{2+} + H_2O \leftrightarrow \equiv FeO-CuOH + 2H^+$	-7.22	
Aqueous speciation reactions	log K	[12]
$Cu^{2+} + H_2O \leftrightarrow CuOH^+ + H^+$	-7.29	
$Cu^{2+} + 2H_2O \leftrightarrow Cu(OH)_2 + 2H^+$	-16.2	
$2Cu^{2+} + 2H_2O \leftrightarrow Cu_2(OH)_2^{2+} + 2H^+$	-10.6	
$3Cu^{2+} + 4H_2O \leftrightarrow Cu_3(OH)_4^{2+} + 4H^+$	-20.8	
$Cu^{2+} + 2H_2O \leftrightarrow CuO_2^{2-} + 4H^+$	-39.45	

¹ log K values correspond to normalized surface site density of 12.05 sites/nm² and ionic strength $I=0$ M

The respective experimentally determined value for the specific surface area of goethite of $79.4 \text{ m}^2/\text{g}$ was used for the computations. It should be mentioned that the protolysis constants and the complexation constants derived by [11] were not taken into account for the calculation. Otherwise it would not be a proper blind prediction. In table 1 are summarized the FITEQL model conditions used for the blind prediction of Cu^{2+} sorption onto goethite (in inert atmosphere).

Involving the $\log K$ for $\text{Cu}(\text{OH})_2(\text{s})$ of -8.68 [12] a surface precipitation occurs. Because in the experiments [11] there was no evidence for that, this process seems to be kinetically inhibited and is not considered in the modeling here. Figure 1 illustrates the prediction quality of copper sorbed onto goethite for $2.3\text{E-}5 \text{ M}$ respective $9.8\text{E-}5 \text{ M}$ Cu^{2+} at an ionic strength of 0.01 M .

Figure 2 shows that the simulation congruence for the data subsets lies within one order of magnitude when focusing on the conventional distribution coefficient K_D .

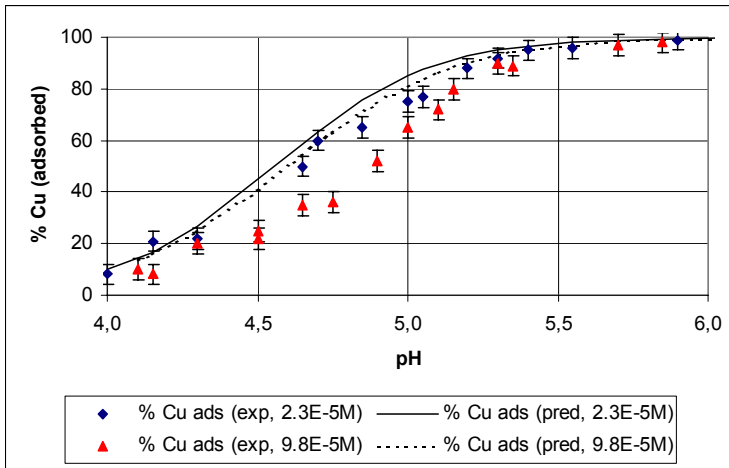


Figure 1: Predicted $[\text{Cu}(\text{II})]$ sorbed onto goethite compared with experimental values from [11]

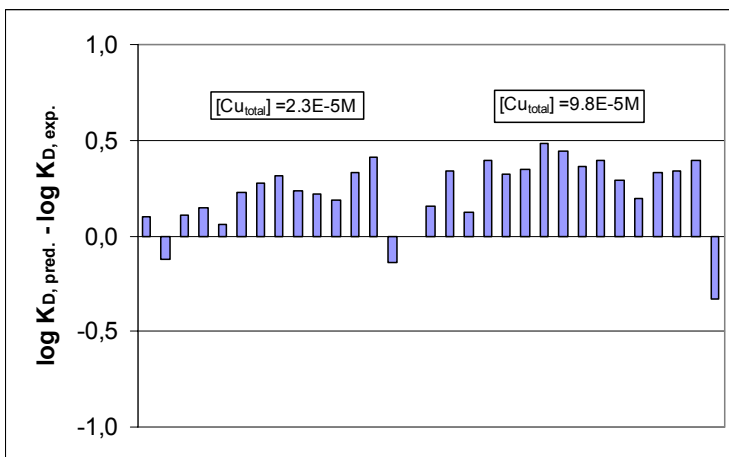


Figure 2: Difference between predicted K_D and experimental values [11]

It can be concluded, that the application of SCM can indeed be very valuable for estimating distribution coefficients for contaminants in well defined mineral systems. The SCM database so far assembled within the RES³T project is able to provide the respective parameter sets.

Acknowledgement

The development of the mineral-specific sorption database RES³T is funded by the German Federal Ministry of Economics and Labour (BMWA) under contract No. PtWt+E_02E9471, which is gratefully acknowledged.

References:

- [1] V. Brendler et al.: RES³T - Rossendorf Expert System for Surface and Sorption Thermodynamics. *J.Cont. Hydrol.*, 61(2002): 281-291
- [2] Herbelin, A.L. and Westall, J.C.: *FITEQL -Version 3.2*. Report 96-01, Department of Chemistry, Oregon State University, Corvallis, 1996
- [3] Stumm, W. et al.: Specific chemical interaction affecting the stability of dispersed systems. *Croat. Chem. Acta.* 42 (1970): 223-245
- [4] Dzombak, D.A. und Morel, F.M.M.: *Surface complexation modeling. Hydrous ferric oxide*, Wiley, New York, 1990
- [5] Schindler, P.W. und Gamsjäger, H.: Acid-base reactions of the TiO₂ (Anatase) – water interface and the point of zero charge of TiO₂ suspensions. *Kolloid-Zeitschrift – Z. Polym.* 250 (1972): 759-763
- [6] Hohl, H. und Stumm, W.: Interaction of Pb²⁺ with hydrous γ -Al₂O₃. *J. Coll. Interf. Sci.* 55 (1976): 281-286
- [7] Yates, D.E. et al.: Site-binding model of the electrical double layer at the oxide/water interface. *J. Chem. Soc. Far. Trans.* 70 (1974): 1807-1818
- [8] Davis, J.A.: Adsorption of trace metals and complexing ligands at the oxide/water interface. Ph.D. thesis, Stanford University, 1978
- [9] Hayes .K. and Leckie, J.O.: Mechanism of lead ion adsorption at the goethite-water interface, in: *ACS Symp. Ser. 323: Geochemical Processes at Mineral Surfaces.*; Davis, J.A., Hayes, K.F. (Ed.); American Chemical Society; Washington, DC
- [10] Kulik, D.A.: Gibbs energy minimization: approach to modeling sorption equilibria at the mineral-water interface: Thermodynamic relations for multi-site-surface complexations. *Am. J. Sci.*, 302 (2002): 227-279
- [11] Ali, M.A. and Dzombak, D.A.: Effects of simple organic acids on sorption of Cu²⁺ and Ca²⁺ on goethite. *Geochim. Cosmochim. Acta*, 60 (1996): 291-304
- [12] Smith, R.M. and Martell, A.E.: *NIST Critically selected stability constants of metal complexes database - Version 4.0*. Report, U.S. Department of Commerce, 1997

INFLUENCE OF HUMIC ACID ON THE NEPTUNIUM(V) SORPTION ONTO GRANITE AND ITS MINERAL CONSTITUENTS

K. Schmeide, G. Bernhard

Forschungszentrum Rossendorf e.V., Institute of Radiochemistry, P.O. Box 510119,
01314 Dresden, Germany
K.Schmeide@fz-rossendorf.de

Abstract

To evaluate the influence of humic substances upon the extent of neptunium(V) sorption by granite, the sorption of neptunium(V) on granite in the absence and presence of humic acid was studied under anaerobic conditions as a function of pH in a series of batch equilibrium experiments. The neptunium and humic acid sorption onto the mineral constituents of granite (quartz, orthoclase, albite, biotite, and muscovite) was also studied to identify the mineral component which dominates the sorption of neptunium and humic acid on granite. The study showed that the neptunium sorption on granite is effected by both the pH and the presence of humic acid. An increased mobility of neptunium was found between pH 7 and pH 11 in the presence of humic acid. The neptunium sorption onto granite is apparently controlled by the minor amount of biotite which, however, is reactive.

Introduction

Besides salt and clay formations also granitic subsurface environments are taken into account as potential host formations for the deep underground disposal of radioactive waste [1]. The sorption of Np onto different rock materials and minerals in the absence and presence of humic substances has been described in the literature [e.g., 2-6].

For this study, granite from Eibenstock (Germany) was chosen. It was already applied for uranium(VI) sorption studies [7].

In this work, the sorption of Np(V) onto granite is studied under anaerobic conditions at an ionic strength of 0.1 M as a function of pH. Furthermore, the effect of humic acid (HA) on the Np sorption is studied in order to determine whether humic material is likely to significantly influence Np sorption on granite. The minerals quartz, orthoclase, albite, biotite, and muscovite were also included in this study in order to clarify whether the Np and HA sorption on granite can be explained by Np and HA sorption on its individual main mineral constituents.

Experimental

Materials

The granite, collected in the region Eibenstock (Germany), is composed of 46.1 wt.-% quartz (SiO₂), 11.1 wt.-% orthoclase (KAlSi₃O₈), 14.6 wt.-% microcline (KAlSi₃O₈), 19.9 wt.-% plagioclase albite (NaAlSi₃O₈), 4.4 wt.-% biotite (K(Mg,Fe²⁺)₃(OH,F)₂(Al,Fe³⁺)Si₃O₁₀), 3.4 wt.-% muscovite (KAl₂(OH)₂AlSi₃O₁₀), and 0.5 wt.-% fluorapatite (Ca₅F(PO₄)₃) (determined by XRD analysis applying the Rietveld method). For the 63 to 200 μm grain size fractions of the solids, which were applied for sorption experiments, the following specific surface areas were determined: quartz - 0.033 m²/g, orthoclase - 0.58 m²/g, albite - 0.15 m²/g, biotite - 0.9 m²/g, muscovite - 1.12 m²/g and granite - 0.41 m²/g. The Np(V) stock solutions were obtained by dissolving solid ²³⁷NpO₂NO₃ in 0.1 M HNO₃. As HA the ¹⁴C-labeled synthetic HA type M42 (batch M170) with a specific activity of 2.38 MBq/g [8] was used for the experiments.

Sorption experiments

HA and Np(V) stock solutions were added simultaneously to the pre-equilibrated geomaterial (0.1 M NaClO₄) under N₂ atmosphere. ²³³Pa was separated from the Np(V) stock solutions prior to each sorption run using Dowex-50. The initial Np and HA concentration in the sample solutions was 1.3×10⁻⁶ M and 27 mg/L, respectively. The solid solution ratio was 50 mg/10 mL. The contact time was about 160 hours. After centrifugation of the samples (3500 rpm, 15 min), the equilibrium pH values were recorded. Subsequently, the supernatant was filtered (450 nm, Minisart RC 15, Sartorius). In the filtrates, the final Np and HA concentration was determined by LSC measurements (Wallac system 1414, Perkin Elmer) using α-β discrimination. The amount of Np and HA adsorbed to the mineral surface was calculated as the difference between the initial and the final Np and HA concentrations in the sample solutions and in the 450 nm filtrates, respectively. Np redox speciation in the filtrates was done by liquid-liquid extraction using TTA (4,4,4-trifluoro-1-(2-thienyl)-1,3-butane-dione).

Results and discussion

The Np sorption in the absence and presence of HA and the sorption of HA is shown for granite and its mineral constituents muscovite, orthoclase, albite, quartz, and biotite as a function of pH in Fig. 1.

The sorption experiments, carried out in the absence of HA, show that the Np sorption essentially starts between pH 7 and pH 8 and increases with increasing pH value. Comparing the percentage of Np sorption onto the minerals, biotite shows the strongest sorption, followed by muscovite, orthoclase, albite and quartz. A comparable sharp increase of the Np sorption onto biotite in the alkaline pH region was found by Nakayama and Sakamoto [9].

For the sorption experiments performed in the presence of HA the following results were obtained. As expected, the HA sorption decreases with increasing pH value. The reason for the sudden increase of the HA sorption onto biotite between pH 9.2 and pH 11, obtained in duplicate experiments, is not clear. Compared to the Np sorption in the absence of HA, the Np sorption onto granite is decreased by HA between pH 7 and pH 11. The Np sorption onto muscovite and orthoclase is somewhat increased by HA between pH 6 and pH 9 and at higher pH values relatively strongly decreased. The Np sorption onto albite and quartz is not changed by HA up to pH 10 and pH 9, respectively. At higher pH values it is again relatively strongly decreased. In case of biotite, the Np sorption is decreased by HA between pH 7 and pH 11, as was found also for granite.

The Np speciation, calculated for the experimental conditions applied in this study, is shown in Fig. 2. It was calculated with the geochemical computer code EQ3/6 [10] applying the Np(V) hydrolysis constants compiled in the NEA data base [11], the Np(V) humate complexation constant $\log \beta = 3.6$ and the pH function of the loading capacity (LC) with $LC = -0.589 + 0.101 * pH$ [8]. The results show that the free neptunyl ion predominates the Np speciation in aqueous solution both in the absence and in the presence of HA. Starting at pH 9.5, the neptunyl hydroxyl species (NpO₂OH_(aq)) is formed increasingly in solution. In the presence of HA, NpO₂HA(I) is formed between pH 6 and pH 11 with a maximum of 13.6 % near pH 10.5. For the pH region higher than 9, the formation of the mixed complex (NpO₂(OH)HA)_{coll.} is suggested by Marquardt et al. [12]. Presently, this complex cannot be quantified thermodynamically, however, this complex would explain the strong reduction of the Np sorption by HA at pH values higher than 9 and 10, respectively.

The results in Fig. 1 have shown, that both granite and biotite show a strong Np sorption in the alkaline pH region. Furthermore, compared to the Np sorption experiments in the absence of HA, the reduction of the Np sorption by HA between pH 7 and pH 11 is similar for both

materials. That means, the Np sorption onto biotite best reflects the Np sorption trend onto granite.

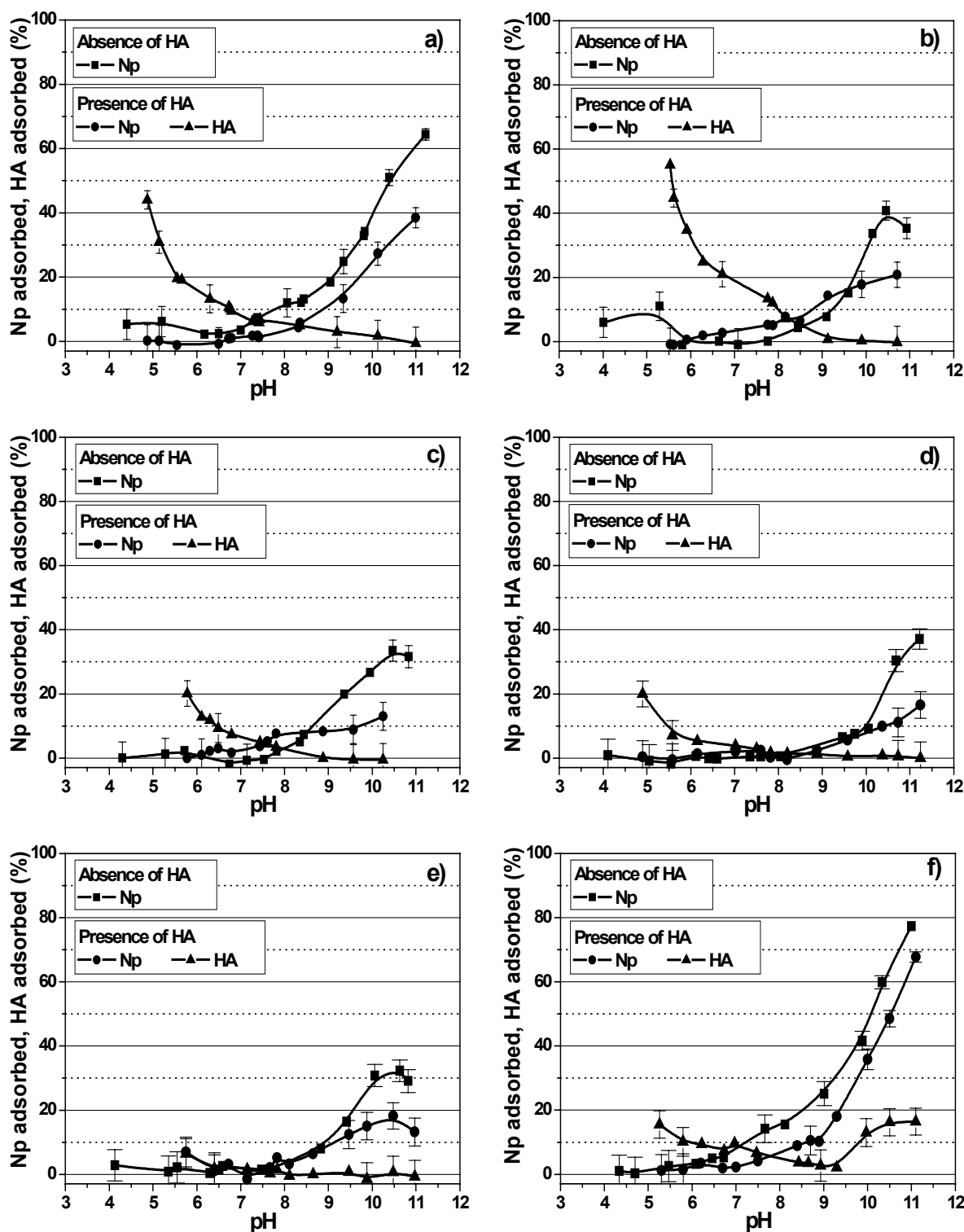


Fig. 1: Np and HA uptake by (a) granite, (b) muscovite, (c) orthoclase, (d) albite, (e) quartz, and (f) biotite ($[\text{NpO}_2^+] = 1.3 \times 10^{-6} \text{ M}$; $[\text{HA}] = 27 \text{ mg/L}$; $I = 0.1 \text{ M NaClO}_4$; CO_2 -free).

Among the minerals, the highest specific surface areas were determined for muscovite and biotite (cf. paragraph 2.1). But their content in the rock material is with 3.4 wt.-% and 4.4 wt.-%, respectively, low. It has to be noted, however, that the softer minerals biotite and muscovite in the granite 63 to 200 μm grain size fraction were, as a result of the grinding process, distinctively smaller than the harder grains quartz and albite [7]. By SEM

investigations it was estimated that the grain size of biotite and muscovite in the granite powder is $< 20 \mu\text{m}$. This is also reflected by the fact, that the specific surface area determined for granite ($0.41 \text{ m}^2/\text{g}$) is higher than calculated from the specific surface areas of the minerals taking into account their content in the rock material (about $0.3 \text{ m}^2/\text{g}$). That means, appropriate specific surface areas of the minerals biotite and muscovite have to be used in modeling the neptunium sorption onto the rock material granite.

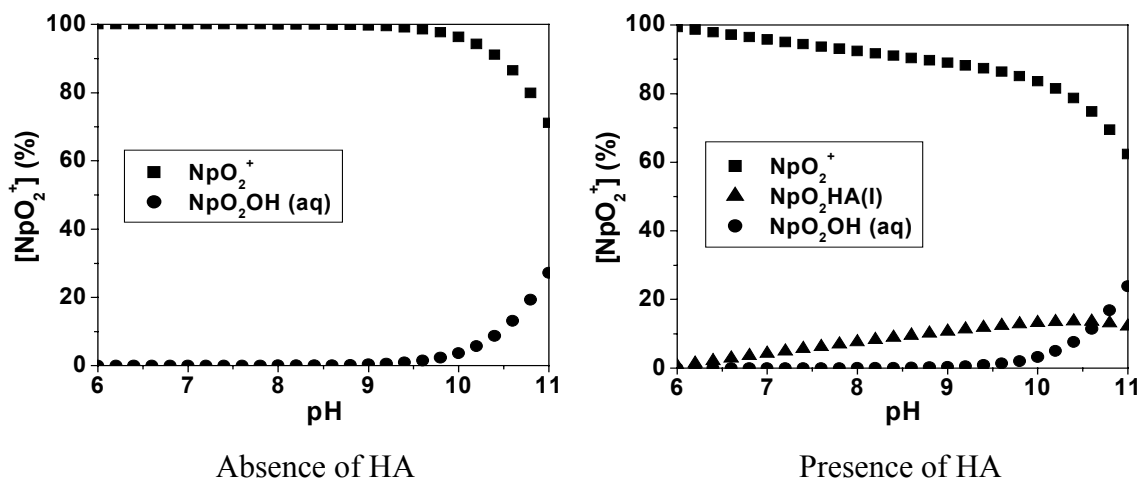


Fig. 2: Np speciation in solution ($[\text{NpO}_2^+] = 1.3 \times 10^{-6} \text{ M}$; $[\text{HA}] = 27 \text{ mg/L}$; $I = 0.1 \text{ M NaClO}_4$; CO_2 -free).

Another reason for the apparent dominance of biotite for the Np sorption onto granite could be related to its Fe(II) content. For biotite, used in this study, Mössbauer spectroscopic measurements have shown that in the unweathered mineral 84.5 % of Fe_{total} occur as Fe(II) [13]. This Fe(II) occurring in biotite and thus, also in granite could possibly lead to a reduction of Np(V) to Np(IV).

An autoradiographic study of the Np sorption onto Climax Stock granite slabs in a synthetic groundwater [14] showed a strong sorption of Np onto Fe(II)-containing minerals biotite and pyrite on the granite surface. This was attributed to a reduction of Np(V) to the less soluble Np(IV) by Fe(II) in the Fe(II)-containing minerals. Furthermore, for magnetite it was found by Nakata et al. [15] that Np(V) is reduced to Np(IV) by Fe(II) on the surface of magnetite but not by Fe(II) ions released from magnetite into solution. In contrast, Nakayama and Sakamoto [3] found no clear indication to Np(V) reduction in case of biotite since no significant difference was observed in the removal of Np by Fe(II)-containing minerals biotite and magnetite and by a ferric oxide of hematite.

A reduction of Np(V) to Np(IV) on the mineral surface would lead to an increase of the Np sorption. However, for Np batch and column experiments in the presence of HA it was found [16] that especially the combination of Fe(II), present at trace concentrations in solution, and HA could lead to a reduction of Np(V) to Np(IV). Compared to Np(V), Np(IV) is generally stronger complexed by HA [4]. The humic colloid-borne Np(IV) species is known to remain stable in groundwater and to be easily mobile in porous aquifer systems [4,16].

Thus, the decrease of the Np sorption onto granite and biotite between pH 7 and pH 11 by HA compared to the Np sorption experiments without HA, which was not observed for the other mineral constituents of granite in the neutral pH range, can be attributed to the complexation of Np(V) by HA and possibly to the complexation of Np(IV) by HA. The oxidation state of Np in the supernatant solutions of the sorption samples without and with HA was checked by liquid-liquid extraction using TTA. So far, no Np(IV) could be detected in solution.

Acknowledgements

This work was partially supported by the EC Commission under contract No. FIKW-CT-2001-00128 and by the Federal Ministry of Economics and Labour (BMWA) under contract No. 02E9299. The authors would like to thank V. Brendler for Np speciation calculations, and S. Sachs and T. Arnold for providing the HA and the rock material, respectively.

References:

- [1] Papp, R.: Gegenüberstellung von Endlagerkonzepten in Salz und Hartgestein. FZKA-PTE Nr. 3, Forschungszentrum Karlsruhe GmbH, Karlsruhe, Germany, 1997.
- [2] Kohler, M., Honeyman, B.D., Leckie, J.O.: Neptunium(V) Sorption on Hematite (α -Fe₂O₃) in Aqueous Suspension: The Effect of CO₂. *Radiochim. Acta* 85, 33 (1999).
- [3] Nakayama, S., Sakamoto, Y.: Sorption of Neptunium on Naturally-Occurring Iron-Containing Minerals. *Radiochim. Acta* 52/53, 153 (1991).
- [4] Artinger, R., Marquardt, C.M., Kim, J.I., Seibert, A., Trautmann, N., Kratz, J.V.: Humic Colloid-borne Np Migration: Influence of the Oxidation State. *Radiochim. Acta* 88, 609 (2000).
- [5] Gutierrez, M.G., Bidoglio, G., Avogadro, A., Yllera de Llano, A.: Studies on Hydro-Geochemical Controls of Neptunium and Selenium Migration in Granite Columns. *Radiochim. Acta* 58/59, 277 (1992).
- [6] Sakamoto, Y., Nagao, S., Ogawa, H., Rao, R.R.: The Migration Behavior of Np(V) in Sandy Soil and Granite Media in the Presence of Humic Substances. *Radiochim. Acta* 88, 651 (2000).
- [7] Arnold, T., Krawczyk-Bärsch, E., Bernhard, G.: Sorption of U(VI) on Granite: Comparison of Experimental and Predicted U(VI) Sorption Data. In: FZR-343, Annual Report 2001, Forschungszentrum Rossendorf, Institute of Radiochemistry, Rossendorf, Germany, 2002, p. 21.
- [8] Sachs, S., Schmeide, K., Brendler, V., Krepelová, A., Mibus, J., Geipel, G., Heise, K.H., Bernhard, G.: Investigation of the Complexation and the Migration of Actinides and Non-Radioactive Substances with Humic Acids under Geogenic Conditions. Complexation of Humic Acids with Actinides in the Oxidation State IV Th, U, Np. Final Report, BMWA Project No. 02E9299, Rossendorf, Germany, 2003.
- [9] Nakayama, S., Sakamoto, Y.: Sorption of Neptunium on Naturally-Occurring Iron-Containing Minerals. *Radiochim. Acta* 52/53, 153 (1991).
- [10] Wolery, T.J.: EQ3/6. A Software Package for the Geochemical Modeling of Aqueous Systems. Report UCRL-MA-110662 Part I. Lawrence Livermore National Laboratory, USA, 1992.
- [11] Lemire, R.J., Fuger, J., Nitsche, H., Potter, P., Rand, M.H., Rydberg, J., Spahiu, K., Sullivan, J.C., Ullmann, W.J., Vitorge, P., Wanner, H.: *Chemical Thermodynamics of Neptunium and Plutonium*. Elsevier, Amsterdam, 2001.
- [12] Marquardt, C., Kim, J.I.: Complexation of Np(V) with Humic Acid: Intercomparison of Results from Different Laboratories. *Radiochim. Acta* 80, 129 (1998).
- [13] Arnold, T., Forschungszentrum Rossendorf, personal communication.
- [14] Beall, G.W., O'Kelly, G.D., Allard, B.: An Autoradiographic Study of Actinide Sorption on Climax Stock Granite. ORNL-5617 (1980).
- [15] Nakata, K., Nagasaki, S., Tanaka, S., Sakamoto, Y., Tanaka, T., Ogawa, H.: Sorption and Reduction of Neptunium(V) on the Surface of Iron Oxides. *Radiochim. Acta* 90, 665 (2002).
- [16] Zeh, P., Kim, J.I., Marquardt, C.M., Artinger, R.: The Reduction of Np(V) in Groundwater Rich in Humic Substances. *Radiochim. Acta* 87, 23 (1999).

CHEMICAL SPECIATION OF ENVIRONMENTALLY SIGNIFICANT HEAVY METALS WITH INORGANIC LIGANDS

Staffan Sjöberg

Department of Chemistry/Inorganic Chemistry

Umeå University

S-901 87 Umeå, Sweden

Staffan.Sjoberg@chem.umu.se

Detailed knowledge of chemical speciation is essential to a full understanding of bioavailability and toxicity of heavy metal ions, and to their adsorption, sedimentation and transport phenomena in soils, rivers and aquifers. The optimisation of many industrial chemical processes, as in hydrometallurgy and pulp and paper processing, relies on a detailed understanding of speciation in often-complicated multi-component, multi-phase systems.

Chemical speciation modelling for labile systems is based on the assumption that all component and derived species are in equilibrium and that reliable equilibrium constants are available at the applicable ionic strength and temperature. The validity of these assumptions is often uncertain. Further, full details of component (stoichiometric) concentrations are required. Despite these factors, modelling has definite value in interpretation or simulation of environmental processes. It is often the only option as the necessary sensitive, selective and non-invasive analytical techniques for measuring metal ion and metal complex concentrations are still, to a great extent, missing.

Critical evaluations of thermodynamic data for a number of metal-ligand equilibria are being performed within the International Union of Pure and Applied Chemistry (IUPAC). The present work is the first in a series relevant to speciation of heavy metal ions in environmental systems of low ionic strength. The series will provide access to the best possible equilibrium data for chemical speciation modelling of reactions of heavy metal ions with the major inorganic ligands. The metal ions and ligands selected for review are: Hg^{2+} , Cd^{2+} , Cu^{2+} , Pb^{2+} , Zn^{2+} and Cl^- , OH^- , CO_3^{2-} , SO_4^{2-} and PO_4^{3-} , respectively. To enable speciation calculations on these systems recommended values for the H^+ - CO_3^{2-} and PO_4^{3-} systems are also reported.

Each contribution in this series will provide critically evaluated equilibrium data applicable to environmental waters at low ionic strength. Such values are derived from data reported in the IUPAC Stability Constants database, *SC-database* [2002PET], and extrapolated to zero ionic strength using appropriate Specific Ion Interaction Theory (SIT) functions [97GRE].

For each metal-ligand combination, the review will

- Identify the most reliable publications and stability constants.
- Identify (and reject) unreliable stability constants.
- Establish correlations between the selected data on the basis of ionic strength dependence, using the SIT functions.
- Establish recommended values of $\beta_{p,q,r}^\circ$ and K_{s0} at 25 °C and $I = 0$.
- Identify the most reliable $\Delta_r H_m$ values for each equilibrium reaction and establish recommended values at 25 °C and $I = 0$.
- Provide the user with the numerical relationships required to interpolate values of $\beta_{p,q,r}$ and $\Delta_r H_m$ at $I > 0$.
- Provide examples of SIT plots for $\beta_{p,q}$ and $\Delta_r H_m$ extrapolations, and examples of distribution diagrams for binary and multi-component systems.

Equilibrium constant and reaction enthalpy data published for 25 °C and a wide range of ionic strengths have been used in regression analyses to determine values valid at 298.15 K and $I =$

0. Literature data have been accepted as ‘reliable’ (designated ‘reported’ in relevant Tables), and thus included in the regression analysis, when all, or in some cases most, of the following requirements have been met:

- (i) full experimental details are reported (solution stoichiometry, electrode calibration method, temperature, ionic strength, error analysis),
- (ii) the equilibrium model is considered to be complete (including hydrolysis reactions)
- (iii) data are for a non-complexing medium,
- (iv) the experimental method and numerical analysis are considered to have minimal systematic errors.

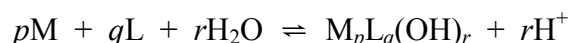
For many reactions equilibrium measurements cannot be made accurately, or at all, in dilute solutions. This is the case for reactions involving formation of weak complexes or ions of high charge. For these systems, precise equilibrium data can only be obtained in the presence of an inert electrolyte of sufficiently high concentration to ensure that reactant activity coefficients are reasonably constant. The associated short range, weak, non-electrostatic interactions between the reactant species and electrolyte anions or cations must be considered. They may be described in terms of ion pair formation (as required when the Debye-Hückel theory or the empirical Davies equation is used for activity coefficients). Alternatively they can be quantified by inclusion of specific ion interaction coefficients, $\varepsilon_{(i,k)}$, within the activity coefficient expression, as in the Brønsted-Guggenheim-Scatchard (SIT) model, which is adopted in this work:

$$\begin{aligned}\log_{10} \gamma_i &= -z_i^2 A \sqrt{I_m} (1 + a_j B \sqrt{I_m})^{-1} + \sum_k \varepsilon_{(i,k)} m_k \\ &= -z_i^2 D + \sum_k \varepsilon_{(i,k)} m_k\end{aligned}\quad (1)$$

In (1) m_k denotes the molality of ion k .

The advantage of SIT theory is that the activity coefficient expressions are valid over a very wide range of concentrations. In contrast, the Debye-Hückel and Davies equations are limited to $I < 0.03 \text{ mol kg}^{-1}$ and $< 0.1 \text{ mol kg}^{-1}$ respectively.

For a general reaction:



the formation constant $\beta_{p,q,r}$ determined in an ionic medium (containing the 1:1 electrolyte NX of ionic strength I_m) is related to the corresponding value at zero ionic strength, $\beta_{p,q,r}^\circ$, by:

$$\begin{aligned}\log_{10} \beta_{p,q,r} &= \log_{10} \beta_{p,q,r}^\circ + p \log_{10} \gamma_M + q \log_{10} \gamma_L + r \log_{10} a_{H_2O} \\ &\quad - \log_{10} \gamma_{p,q,r} - r \log_{10} \gamma_{H^+}\end{aligned}\quad (2)$$

where $\gamma_{p,q,r}$ refers to the species $M_p L_q (OH)_r$.

Substitution of (1) into (2), and the assumption that the concentration of NX is much greater than that of each reactant (such that $I_m = m_k$), gives

$$\log_{10} \beta_{p,q,r} - \Delta z^2 D - r \log_{10} a_{H_2O} = \log_{10} \beta_{p,q,r}^\circ - \Delta \varepsilon I_m \quad (3)$$

where $\Delta z^2 = (pz_M + qz_L - r)^2 + r - p(z_M)^2 - q(z_L)^2$

and $\Delta \varepsilon = \varepsilon_{(\text{complex}, N \text{ or } X)} + r\varepsilon_{(H, X)} - p\varepsilon_{(M, X)} - q\varepsilon_{(L, N)}$

The term $\log_{10} a_{\text{H}_2\text{O}}$ is near constant for most studies of equilibrium in dilute aqueous solutions where the ionic medium is in large excess; also $\log_{10} a_{\text{H}_2\text{O}} \rightarrow 0$ as $I \rightarrow 0$. For a 1:1 electrolyte (NX) this term can be calculated from the solution osmotic coefficient, Φ , if the minor electrolyte species (the reacting ions) are neglected, whence $I_m \approx m_{\text{NX}}$:

$$\log_{10} a_{\text{H}_2\text{O}} = -2m_{\text{NX}}\Phi/55.51[\ln(10)] \quad (4)$$

The application of SIT theory to the selected literature values involves graphical extrapolation of $\log_{10} \beta_{\text{p,q,r}} - \Delta z^2 D - r \log_{10} a_{\text{H}_2\text{O}}$ to $m_k = 0$ (or $I_m = 0$ for a system with a large excess of 1:1 electrolyte), using equation (3). The intercept at $I_m = 0$ gives $\log_{10} \beta_{\text{p,q,r}}^\circ$, and the slope provides the reaction ion interaction coefficient (slope = $-\Delta\varepsilon$) as defined in equation (3). If the regression line slope is negative then $\Delta\varepsilon$ is positive. Conversely, the value of $\beta_{\text{p,q,r}}$ at a specific ionic strength, I_m , can be calculated from $\beta_{\text{p,q,r}}^\circ$ if the value of the empirical parameter $\Delta\varepsilon$ is known. Thus this review reports values for both $\log_{10} \beta_{\text{p,q,r}}^\circ$ and $\Delta\varepsilon$. [It is noted that in equation (3) D is a function of I_m whereas the ion interaction term (i.e. $\sum_k \varepsilon_{(i,k)} m_k$; equation 1) is a function of m_k ; however, $m_k \approx I_m$ for a medium containing excess 1:1 electrolyte.

The presentation will focus on results obtained in the mercury(II) system. Results from some model calculations relevant to fresh water conditions will also be presented. Furthermore, modelling surface complexation of Hg(II) in mineral systems and the solubility of Hg(II) – containing solids will be discussed.

References:

- 97GRE I. Grenthe, A. V. Plyasunov, K. Spahiu. In: *Modelling in Aqueous Chemistry* (I. Grenthe and I. Puigdomenech, eds.), pp.325-426, Paris (France): Organisation for Economic Co-operation and Development, 1997.
- 2002PET L. D. Pettit and K. J. Powell. *SC-Database*, IUPAC Stability Constants Database. Release 5. IUPAC; Academic Software, Otley, UK (2001).

SPECIATION OF Cm(III) IN A QUARTZ / SILICIC ACID SYSTEM: INVESTIGATIONS BY TRLFS

S. Stumpf, Th. Stumpf and Th. Fanghänel

Forschungszentrum Karlsruhe GmbH

Institut für Nukleare Entsorgung

Postfach 36 40

76021 Karlsruhe

Germany

Silvia.stumpf@ine.fzk.de

Deep geologic formations are provided for the deposition of radioactive waste. In case of a water intrusion into a repository the release of actinides / radionuclides into the biosphere by migration with the groundwater is possible. The question arises to what extent released actinides / radionuclides migrate with the groundwater and which retardation mechanisms can inhibit the migration¹. The mobility of released radionuclides depends on sorption and desorption processes on mineral surfaces. For the working-out of a safety concept concerning the management of highly radioactive waste it is of utmost importance to know about the interaction of radionuclides with their mineral environment, to characterize the formed surface species and to elucidate the involved reaction mechanisms. Only with this information it is possible to describe the basic sorption processes generally and therefore to predict the long term performance of a repository for nuclear waste.

Trivalent actinides like americium and curium do have a great influence on the amount of radiotoxicity of radioactive waste. Because of the fluorescence spectroscopic characteristics of curium, the speciation of Cm(III) in the trace concentration range is possible by using **time-resolved laser fluorescence spectroscopy: TRLFS**².

There are some concepts concerning the future deposition of highly radioactive waste. The deposition in granite is also under discussion. One main component of granite is the framework silicate quartz. Therefore the sorption of Cm(III) – as a representative for trivalent actinides - onto quartz was investigated through TRLFS. Dependent on the pH, Cm(III) sorbs onto quartz by the formation of two sorption species with emission maxima at 601.5 nm and 603.5 nm. The lifetime of the fluorescence emission is $115 \pm 5 \mu\text{s}$ for both species and correlates with the reduction of the number of water molecules in the first coordination sphere from 9 H₂O for the aquo ion to 5 H₂O for the sorption onto quartz. In granitic groundwaters the speciation of actinides is not only influenced by the sorption onto a fixed mineral surface resulting in the retardation of the radionuclides. Moreover, actinides can be complexed in solution or can sorb onto colloids³. In both cases the actinide could be transported into the biosphere by migration with the groundwater or through colloid transport (Fig. 1). When quartz dissolves, silicic acid is formed. If the concentration is lower than the saturation, silicic acid will complex Cm(III). If the concentration is higher than the saturation, silicic acid tends to polymerize and to form colloids. Silicic acid at low concentration has no influence on the sorption of Cm(III) onto quartz (Fig. 2). At high concentration Cm(III) that is already sorbed onto the quartz surface will be complexed by polymerized silicic acid. Ternary complexes will be formed. This result was confirmed by investigations on the sorption of Cm(III) onto quartz single crystals (Fig. 3).

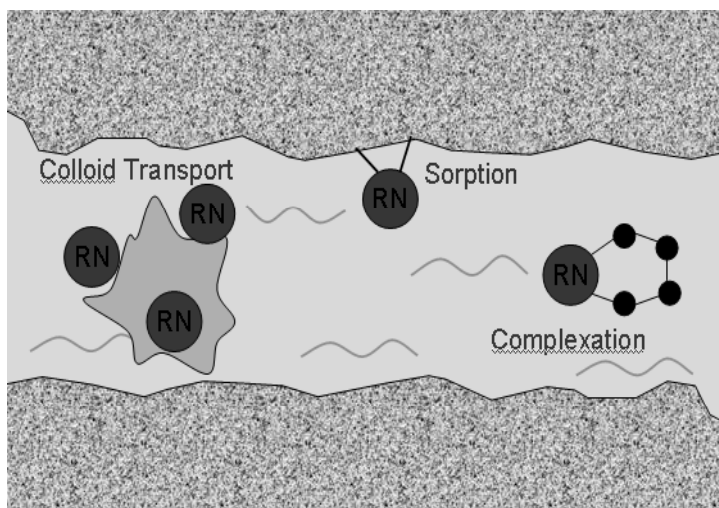


Fig. 1 Reaction Mechanisms in a Quartz / Silicic Acid System

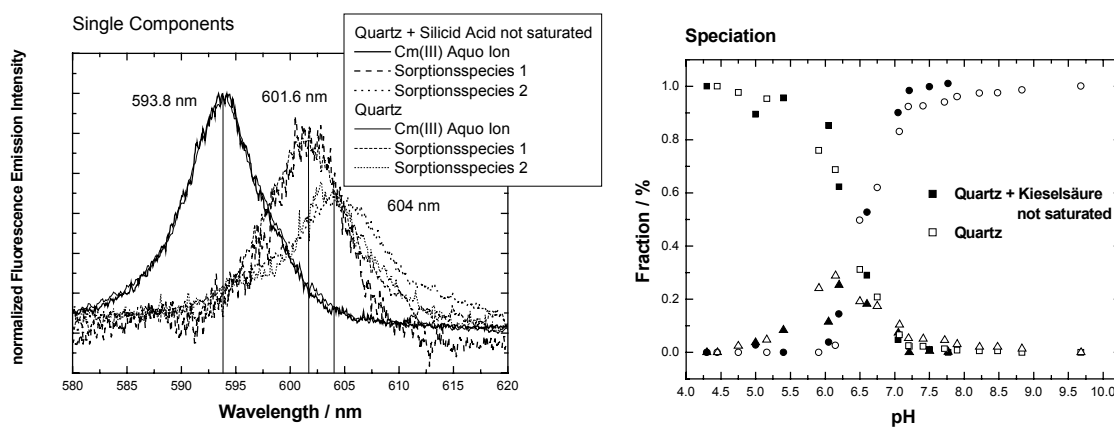


Fig. 2 Comparison of the Single Components and the Speciation of the Cm(III) Sorption onto Quartz with and without Silicic Acid (not saturated)

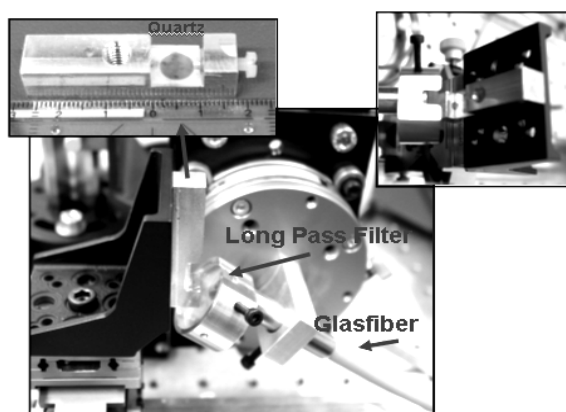


Fig. 3 Cm(III) Sorption onto Single Crystals

References:

- ¹Kohler, M; Wieland, E.; Leckie, J.O.; Water-Rock Interaction; Kharaka & Maest; **1992**; Balkema; Rotterdam
- ²Nugent, L.J.; Baybarz, R.D.; Barnett, J.L.; *J.Chem.Phys.*; 73; **1969**; 1177
- ³Silva, R.J.; Nitsche, H.; *Radiochim.Acta*; 70/71; **1995**; 377-396

INFLUENCE OF HUMIC ACID ON THE SORPTION OF Eu (III)/Am (III)/Cm(III) ONTO γ -Al₂O₃ - A TIME-RESOLVED LASER FLUORESCENCE SPECTROSCOPY STUDY -

X.K. Wang, Th. Rabung, H. Geckeis, P.J. Panak, R. Klenze, Th. Fanghänel
Forschungszentrum Karlsruhe
Institut für Nukleare Entsorgung
P.O. Box 3640
D-76021 Karlsruhe
Germany
rabung@ine.fzk.de

Introduction

Natural organic matter as humic/fulvic acids (HA/FA) are known to have strong influence on the speciation of actinides in aquifer systems (e.g. [1]). Whether HA/FA exert a mobilizing or retarding effect depends on the complex behavior of actinides in the ternary groundwater-HA/FA-mineral surface system. In general, the metal ion sorption follows the pH dependent solid/liquid distribution found for HA/FA and is enhanced at low and reduced at high pH [1,2,3,4]. Such observations suggest the predominant influence of complexation to HA/FA on the solid/liquid distribution of notably the polyvalent metal ions. In some cases, the sequence of metal ion and HA/FA addition appears to influence the solid/liquid distribution of the metal ion.

The present study is aimed to analyze the speciation of the trivalent actinide ion Cm(III) in a system containing well characterized purified humic acid (Aldrich) and γ -Al₂O₃ by TRLFS. Accompanying sorption experiments (isotherms, pH-edges) were performed with Eu(III) and Am(III) to increase the range of metal ion concentration and to clarify the similarity of sorption properties of trivalent lanthanides and actinides. In order to obtain comprehensive spectroscopic information on Cm(III) speciation, the excitation spectrum is recorded in a range from $\lambda = 370$ -400 nm. Fluorescence emission spectra obtained in an indirect excitation mode ($\lambda_{\text{ex}} = 355$ nm) are compared to spectra appearing at direct Cm(III) excitation ($\lambda_{\text{ex}} = 396.6$ nm). Only the HA bound Cm(III) is excited at $\lambda_{\text{ex}} = 355$ nm due to the energy transfer proceeding from HA to complexed Cm(III). Direct excitation provides information on all fluorescing Cm(III) species in the system.

RESULTS AND DISCUSSION

The excitation spectra for the free Cm³⁺ aquo ion (pH 1.0), Cm(III) sorbed to γ -Al₂O₃ (pH 6.3) and Cm(III) bound to HA- γ -Al₂O₃ solution (pH 6.0) in the range of $\lambda_{\text{ex}} = 370$ -400 nm are shown in Figure 1. The spectrum of the Cm³⁺ aquo ion displays the characteristic bands at 375.2, 381.2 and 396.6 nm [1]. These bands are shifted to higher wavelengths for Cm(III) sorbed to γ -Al₂O₃ indicative for the inner-sphere surface complexation. Cm(III) is quantitatively sorbed to γ -Al₂O₃ under the experimental conditions.

The spectrum obtained in presence of HA and γ -Al₂O₃ is, however, clearly different to the others. Cm(III) and HA are sorbed quantitatively to γ -Al₂O₃ under the experimental

conditions. The base line increases and absorption bands are shifted. The spectrum is poor in structure and quite flat as reported for Cm(III) humate/fulvate complexes in some humic acid containing groundwater samples [6]. Such behavior is known for Cm(III) complexes with organic ligands containing aromatic entities and notably for humate/fulvate complexes [6,2] and shows that Cm(III) is primarily excited by non-selective energy transfer from the photo-excited humic acid molecules coordinating to the metal ion.

In a first instance, we can conclude from these spectra that under the experimental conditions, Cm(III) must be coordinated at least partly to humic acid in order to enable the energy transfer.

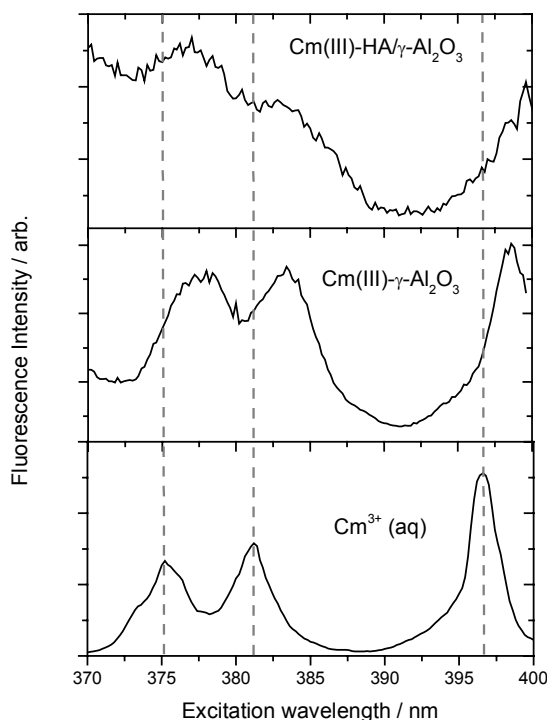


Figure 1: Excitation spectra of the Cm^{3+} -aquo ion, Cm(III) sorbed to $\gamma\text{-Al}_2\text{O}_3$ and Cm(III) bound to HA- $\gamma\text{-Al}_2\text{O}_3$.

Experimental conditions for

- the Cm^{3+} -aquo ion spectrum: $c[\text{Cm(III)}]=2.0 \times 10^{-7} \text{ mol/L}$, $\text{pH}=1.0$, 0.1 M NaClO_4
- the Cm(III)- $\gamma\text{-Al}_2\text{O}_3$ spectrum: $c[\text{Cm(III)}]=2.0 \times 10^{-7} \text{ mol/L}$, $\text{pH}=6.3$, 0.1 M NaClO_4 , $c[\gamma\text{-Al}_2\text{O}_3]=0.44 \text{ g/L}$
- the Cm(III)-HA- Al_2O_3 spectrum: $c[\text{Cm(III)}]=2.0 \times 10^{-7} \text{ mol/L}$, $\text{pH}=6.0$, 0.1 M NaClO_4 , $c[\text{Al}_2\text{O}_3]=0.44 \text{ g/L}$, $c[\text{HA}]=10 \text{ mg/L}$.

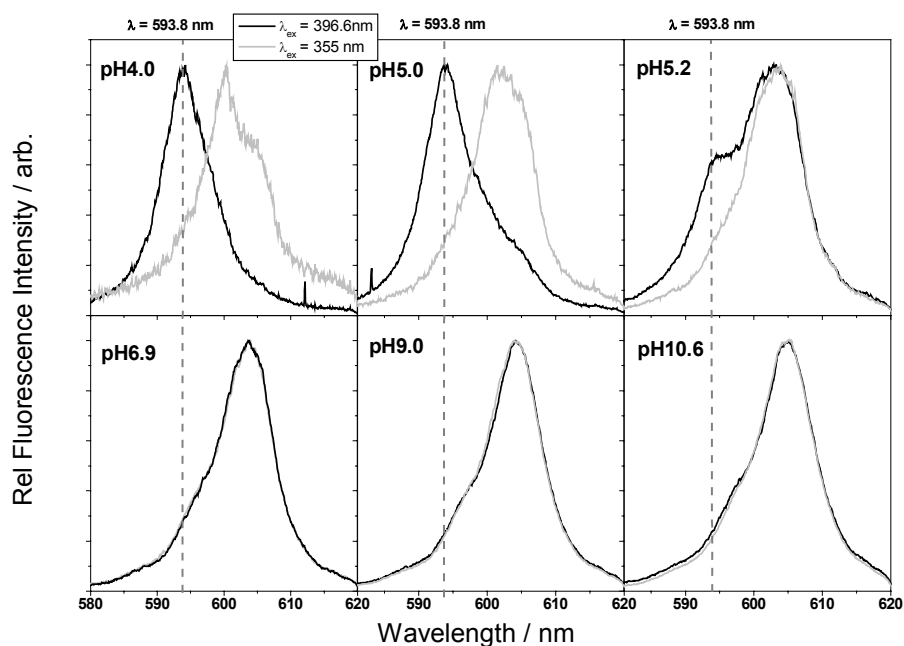


Figure 2: Comparison of emission spectra of Cm(III) in HA- Al_2O_3 solution at direct/indirect excitation measurement. $c[\text{Cm(III)}]=2.0 \times 10^{-7} \text{ mol/L}$, 0.1 M NaClO_4 , $c[\text{Al}_2\text{O}_3]=0.44 \text{ g/L}$, $c[\text{HA}]=10 \text{ mg/L}$.

Fig. 2 shows the intensity normalized fluorescence spectra obtained at two different excitation wavelengths for Cm(III) in the HA/ $\gamma\text{-Al}_2\text{O}_3$ system at different pH. Direct excitation ($\lambda = 396.6 \text{ nm}$) provides spectra of all Cm(III) species, including the aquo ion, which is recognized in samples up to $\text{pH} = 5.2$ by its band at $\lambda = 593.8 \text{ nm}$. Up to $\text{pH} 5.0$, the aquo ion should predominate the Cm(III) speciation according to batch sorption experiments. Peak maxima of the fluorescence spectra obtained by indirect excitation are shifted to 602.3 nm at $\text{pH} 4.0$ and 5.0 and then continuously increase with pH up to 604.7 nm at $\text{pH} 10.7$. At $\text{pH} \geq 6.9$ direct and indirect excitation virtually induce congruent fluorescence spectra. The congruency of spectra obtained by both excitation modes clearly points to Cm(III) species sorbed at the $\gamma\text{-Al}_2\text{O}_3$ surface which are coordinated to humic acid in this pH range. Under these pH conditions, Cm(III) is completely sorbed to the solid according to the sorption isotherm data.

Comparing peak maxima of Cm(III) in the binary systems with those in the ternary system reveals a striking difference, which is depicted explicitly in Fig. 3. Emission bands are shifted by more than 2 nm to longer wavelengths in the case of the ternary system at the same pH . The stronger shift of emission bands to higher wavelengths in the ternary system points to differences in the first coordination sphere of the Cm(III) ion. We, therefore, conclude that $>\text{Al-OH}$ groups of the $\gamma\text{-Al}_2\text{O}_3$ surface contribute to the coordination sphere of the metal ion and ternary $>\text{Al-O-Cm(HA)}$ complexes are created.

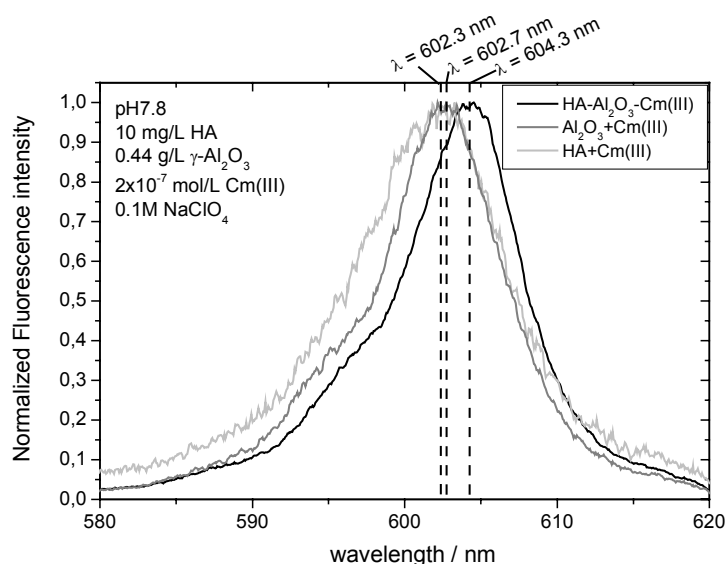


Figure 3: Comparison of emission spectra of Cm(III) in HA, Al₂O₃ and HA-Al₂O₃ solutions at pH 7.8. $c[\text{Cm(III)}]=2.0 \times 10^{-7} \text{ mol/L}$, $\text{pH}=7.8$, 0.1 M NaClO_4 , $c[\text{Al}_2\text{O}_3]=0.44 \text{ g/L}$, $c[\text{HA}]=10 \text{ mg/L}$.

Fluorescence lifetimes are frequently invoked for the derivation of the ligand number in the first coordination sphere, notably relative to the number of fluorescence quenching H₂O entities. In case of HA, this parameter is, however, obscured by intramolecular energy transfer processes exerting fluorescence quenching. In the present work, we therefore use the fluorescence decay behaviour only for comparison (Fig. 4). For the Cm(III)- γ -Al₂O₃ binary system a mono-exponential decay is derived with a lifetime $\tau=122 \mu\text{s}$ close to that found in earlier work ($\tau=110 \mu\text{s}$) [8]. For the Cm(III)-HA and the ternary system, the fluorescence decay is found to be quite congruent at short decay times. A slow lifetime component occurs for the Cm-HA complex at long delay times, which is also compatible with studies on natural HA in this pH range [9]. Lifetimes obtained by direct and indirect excitation match closely. Even though it is difficult to interpret the fluorescence lifetimes in a quantitative way due to before mentioned reasons, the experimental findings confirm that Cm(III) in the ternary system is coordinated to HA. Differences in the fluorescence decay behaviour again can be attributed to the formation of ternary complexes.

Conclusions

The present work shows that TRLFS can be applied successfully to elucidate the speciation of Cm(III) in the complex ternary solution/HA/mineral surface system. Strong evidence for the existence of $>\text{Al-O-Cm}=(\text{HA})$ ternary surface complexes can be derived from the study. Such independent spectroscopic information will be used together with sorption isotherm data to develop a mechanistic model description of the actinide behavior at the mineral/groundwater interface in presence of HA.

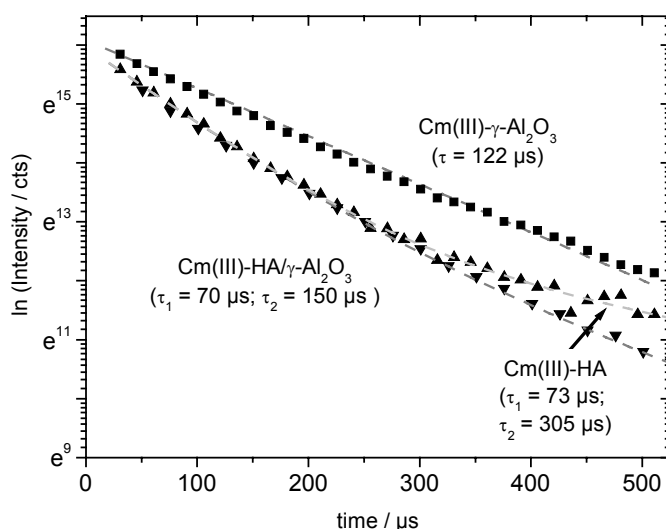


Figure 4: Time dependence of fluorescence emission decay of Cm(III) in solution containing γ - Al_2O_3 solution 0.44g/L in HA solution (10 mg/L) and in the ternary system. $c[\text{Cm(III)}]=2.0 \times 10^{-7} \text{ mol/L}$, 0.1M NaClO_4 .

References:

- [1] Kim, J.I., Rhee, D.S., Wimmer, H., Buckau, G., Klenze, R., *Radiochim. Acta*, 1993, 62, 35.
- [2] Wang, X.K., Dong, W.M., Dai, X.X., Wang, A., Du, J.Z., Tao, Z.Y., *Appl. Radiat. Iso.*, 2000, 52, 165.
- [3] Righetto, L., Bidoglio, G., Aziemonti, G., Bellodono, I.R., *Environ. Sci. Technol.*, 1991, 25, 1913.
- [4] Fairhurst, A.J., Warwick, P., Richardson, S., *Colloids Surf. A.*, 1995, 99, 187.
- [5] Y. Takahashi, Y. Minai, H. Ambe, Y. Makide, F. Ambe, *Geochim. Cosmochim. Acta* 63,1999, 815-836
- [6] J.I. Kim, H. Wimmer, R. Klenze, *Radiochim. Acta* 58/59, (1992), 165-171
- [7] P. Panak, R. Klenze, J.I. Kim, H. Wimmer, *J. Alloys and Comp.* 225 (1995), 261-266
- [8] Stumpf, Th., Rabung, Th., Klenze, R., Geckeis, H., Kim, J.I., *J. Colloid Interface Sci.*, 2001, 238, 219.
- [9] A. Morgenstern, R. Klenze, J.I. Kim, *Radiochim. Acta* 88, (2000), 7-16

THE 1-PK MECHANISTIC MODELING OF PROTON BINDING ONTO PYRITE

R. Weerasooriya¹ and H.J. Tobschall

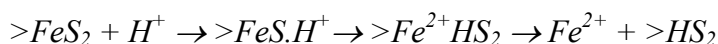
Institut für Geologie und Mineralogie, Lehrstuhl für Angewandte Geologie, Friedrich-Alexander Universität, Erlangen-Nürnberg, D 91054 Germany
rweerasooriya@hotmail.com

Pyrite surface chemistry plays an important role in many natural and technological systems, for example in low temperature geochemistry, extractive metallurgy, coal processing, geochemistry, acid-mine drainage and pollution control¹. Pyrite is also of interest as a material for solar cells due to its environmental compatibility and its very high light absorption coefficient. When compared to the investigations carried out into the interfacial properties of hydrous metal oxides, relatively few studies have been directed to probe surface properties of the pyrite – water interface^{2,3}. It was shown that the pH_{IEP} of pyrite shifted from 1.2 to even 7 (the pH_{IEP} of goethite) when experienced under different experimental conditions such as conditioning time and exposure to atmospheric conditions³. The shifting pH_{IEP} is largely ascribed to a rapid conversion of Fe^{2+} (that is released by ion exchange) iron oxy-hydroxide that covers pyrite to the extent, which the surface properties are governed by the metal hydrous oxides. The pH_{IEP} of pristine metal sulfides fall into a narrow range of 0.6 to 3.0². Compared to metal oxides, sulfides exhibit iso-electric point that is largely independent of the nature of the metal cations in the solid. An interpretation at atomic level to describe relative reactivities of pyrite sites is given using the extended Hückle molecular orbital calculations⁴. The attachment to the pyrite surface by an oxidant or a reductant requires that they have vacant orbitals (in solution phase) or a site (in solid phase) to transfer electrons between adsorbate and reaction sites in pyrite. It is evidenced that the electron transfer of pyrite (FeS_2) or iron sulfide (FeS) plays a key role in the degradation of halogenated organic pollutants in the aqueous phase⁵ and this step is essentially surface mediated that should be addressed in detail for any systematic investigations conducted on this sulfide / water interface.

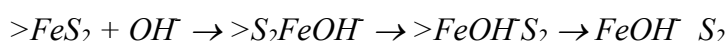
Therefore, this work aims in developing a surface complexation mechanism of the pyrite/solution systems over a range of experimental conditions that are important environmentally. Specifically, in the present part of the study, we report the variation of the surface charge as a function of potential determining ions (PDI) in the solution. The 1-pK diffuse-layer surface complexation model (1 pK-DLM) was employed to quantify experimental data. The following factors merit our justification for the use of 1-pK DLM: (i). The intrinsic acidity constants are model independent and are directly obtained from pH_{zpc} . (ii). A single plane modeling approach eliminates the estimation of several fitting parameters often associated with multi-layer models. The surface charge –potential relationship is determined by the Gouy-Chapman theory (not a fitting parameter). (c). The combination of high inner capacitance of multi-layer models indicate that the two planes are embedded in a porous mineral surface layer of finite thickness. This is in agreement with the generalized single layer representation incorporated in the DLM. The generalized DLM is capable of handling several surface sites simultaneously; hence this model provides an excellent platform for the calculation of interfacial properties of pyrite owing to its inherent simplicity.

In surface titrations of pyrite, it is required to determine the optimal experimental conditions that showed minimal solid loss. Pyrite dissolution was determined by monitoring the appearance of Fe and S species in solution. When $\text{pH} > 5$, no Fe-species were detected in solution. When $\text{pH} < 3$, both the Fe^{2+} and total Fe concentrations were almost similar. Traces of H_2S were detected at extremely acidic conditions (e.g. $\text{pH} < 2$). Similarly, the presence of

S_2^{2-} in solution (typically less than $\sim 30 \mu\text{M}$) was observed at alkaline pH (>10). Appearance of both S^{2-} or H_2S and total Fe/ Fe^{2+} is attributed to the pyrite dissolution. Neither S^{2-} nor gaseous-S products can be found when pH in solution ranged from 2.5 to 9. Production of Fe-species was, however, observed up to pH 4.5 (when $T_E < 2$ hr). This is ascribed to a surface mediated process that promotes the release of Fe^{2+} . The release of Fe^{2+} into the solution is ascribed to a surface complexation of H^+ onto $>FeSS$ sites according to the following reaction scheme:



When $pH < 2$ $>HS_2$ decomposes to form elemental sulfur ($HS_2 \rightarrow S^0 + HS^-$) and H_2S ($H^+ + HS^- \rightarrow H_2S$)⁶. Enhanced pyrite dissolution was evident under alkaline conditions indicating an effective electron transfer via OH^- (six electrons are needed to form $S_2O_3^{2-}$)⁷. The following reaction pathway is suggested to illustrate the overall process.



The surface bonded $-OH$ ion probably migrates to the S_2^{2-} sites releasing S_2^{2-} as *initial* products. Subsequently, S_2^{2-} is converted into SO_4^{2-} or $S_2O_3^{2-}$. It has been shown that O_2 serves only as an electron acceptor and does not enter the oxidative dissolution process⁸. This has been confirmed by O_2 isotope composition where the O in SO_4^{2-} and $Fe(OH)_x$ is obtained from H_2O splitting, not from dissolved oxygen⁹. The effect of equilibration time, T_E of pyrite dissolution was also examined. The Fe^{2+} showed a gradual increase with time. When $T_E < 2$ hr, both the Fe^{2+} and total Fe concentrations were always $< 0.1\text{mM}$. Afterwards, the $[Fe^{2+}]$ increased gradually yielding an apparent plateau at $Fe^{2+} = 0.30 \text{ mM}$. No S-species were detected when $T_E < 2$ hr. When $T_E = 24$ hrs, SO_4^{2-} was detected in solution. The appearance of SO_4^{2-} indicates the dissociation of water molecules when a pyrite surface is present. Therefore when $9 > pH > 2$, the pyrite dissolution rate is relatively slow. All surface titrations were conducted within 2 hr and at a pH range of 2 to 9 to minimize solid loss.

Variation of surface charge density, Γ , as a function of pH and electrolyte concentrations is shown in Figure 1. In analog to metal oxides, a common intersection point was observed at $pH = 1.5$. This point corresponds to the pH_{zpc} of pyrite (refer to Figure 2 for details). When compared to metal (hydr) oxides the surface charge values were 2 to 3 fold higher in pyrite. Extremely high charging of silica has also been reported, even much higher than can be understood assuming purely DLM. The high charging is due to the presence of pores in which part of the charge is situated. This pH_{zpc} obtained under inert conditions represents the pyrite surface under conditions which are closed to “virgin” state. Pyrite showed an iso-electric point below pH 3 when anaerobic experimental conditions are employed. In order to obtain reproducible results, the measurements should be done under consistent experimental conditions. Presently (under anaerobic conditions), we noted that following parameters should be maintained properly to reduce the noise in titrations: (i). Solid content, (ii). Equilibration time, and (iii) Initial titration pH. The H-titration data showed below are comparable to the zeta potential measurements made at 2 hrs equilibration time.

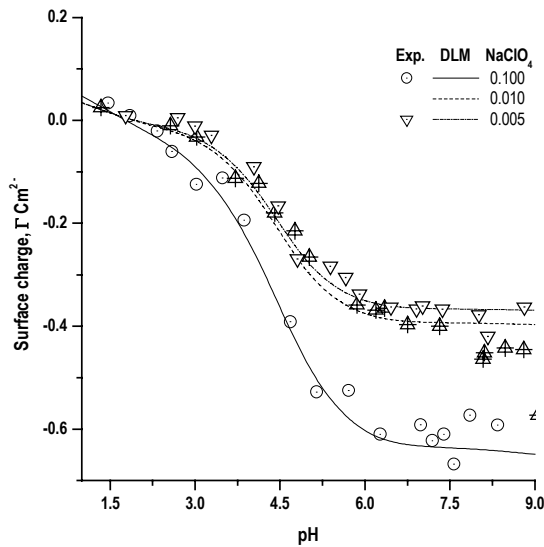
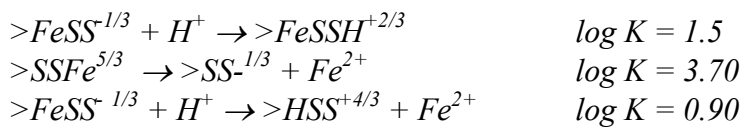


Figure 1 Variation of surface charge density, Γ , as a function of pH and background electrolyte concentration. Blank titrations were made for identical solutions without pyrite. These data were subtracted from the sample titration curves. Solid and broken lines represent Γ calculations were based on the 1-pK DLM model. Rapid titrations were carried out in a anaerobic glove box having continuous flow of Ar (purity 99.996%) using an Orion Autochemistry System (Model 960). The equilibrium pH was measured with Ross combined pH electrode.

The role played by H^+ , OH^- , Fe^{2+} and S^{2-} as potential determining ions (PDI) on surface charge development was also assessed. According to the surface titrations, the pH_{zpc} of pyrite was at 1.5. When $pH = pH_{zpc}$, the pFe_{zpc} of pyrite was estimated as 3.7.

A 1-pK diffuse layer model (1-pK DLM) quantified the proton titration data. The 1-pK DLM requires following reaction stoichiometries to quantify proton titration data:



Additionally, to model the pFe titration data, the following stoichiometry was accounted for:



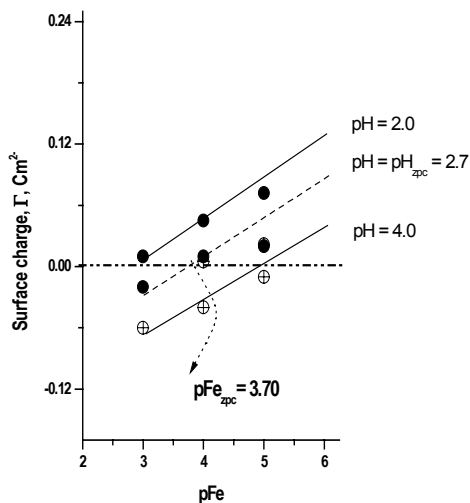


Figure 2 Variation of surface charge as a function of pFe and pH. Background electrolyte 0.1M NaClO₄. Solid and broken lines show calculated data. The stoichiometry $>FeSS^{-1/3} + Fe^{2+} \rightarrow >FeSSFe^{-5/3}$ was additionally used in data modeling. Rapid titrations were carried out at three pH conditions using pFe as a titrant in a glove box (see figure 1 caption for details). After 15 minutes, a well-stirred aliquot was taken and filtered into pre-acidified bottles for free Fe²⁺ measurements by spectrometry by 2,2'-bipyridyl method. The pFe values were calculated accordingly. During this time period, any changes in pH in the suspension were continuously monitored and adjusted either using HClO₄ or NaOH. Such titrations are not possible when pH > 5.0 due to precipitation of iron hydroxide.

References:

1. Huerla-Diaz, M.A., Morse, J.W., 1992 *Geochim. Cosmochim. Acta* 56, 2681.
2. Bebie, J., Schoonon, M.A.A., Fuhrmann, M., Strongin, D.R., 1998 *Geochim. Cosmochim. Acta* 62, 633.
3. Forenasiero, D., Eijt, V., Ralston, J., 1992 *Colloids Surf.* 62, 63.
4. Luther III, G.W., 1987 *Geochim. Cosmochim. Acta* 54, 3193.
5. Buttler, E.C., Hayes, K.Y., 1999, Effects of solution composition and pH on the reductive dechlorination of hexachloroethne by FeS, *Environ. Sci. Technol.*, 32, 1276.
6. Wei, D., Osseo-Asare, K., 1997 *J. Electrochem. Soc.*, 144, 546.
7. Brown, A.D., Jurinak, J.J., 1989, *J. Environ. Qual.*, 18, 545.
8. Moses, C.O., Nordstrom, D.K., Herman, J.S., Mills, A.L., 1987 *Geochim. Cosmochim. Acta*, 51, 1561.
9. Taylor, B.E., Wheeler, M.C., Nordstrom, D.K., 1984, *Nature*, 308, 538.

THE SURFACE CHEMISTRY OF CARBONATES

M. Wolthers^{1,2}, *L. Charlet*², *P. Van Cappellen*¹

¹Department of Earth Sciences – Geochemistry, Faculty of Geosciences, Utrecht University, PO Box 80.021, 3508 TA Utrecht, the Netherlands.

²Environmental Geochemistry Group, LGIT-OSUG, University of Grenoble, F-38041 Grenoble, Cedex 9, France

wolthers@geo.uu.nl

Abstract

The Charge Distribution-MUltiSite Ion Complexation (CD-MUSIC) model was applied to describe the calcite surface chemistry. Protonation reactions and proton affinity constants were predicted and the resulting surface model was compared to the existing Surface Complexation (SC) model. The CD-MUSIC model approach results in a surface charge pH-dependence which are consistent with the wide range of point of zero proton charge (pH_{ZPC}) values as reported from electrophoretic measurements.

Introduction

Carbonate minerals play an important role in regulating the chemistry of aquatic environments from lakes to oceans, aquifers to hydrothermal systems, and soils to sediments under oxic to anoxic conditions. Carbonates affect the biogeochemical cycles of Ca, Mg, Fe and C, major components of carbonate minerals, as well as H, P and trace elements such as radionuclides through mineral surface processes such as dissolution, precipitation and adsorption.

Van Cappellen et al. (1993) proposed a Surface Complexation model for divalent metal carbonates, in order to understand and describe the reactivity of the carbonate–water interface. This model is based on the modeling of experimentally determined surface charge curves from acid/base titrations of rhodochrosite (MnCO_3) and siderite (FeCO_3) suspensions and on data from electrokinetic and flotation studies of calcite (CaCO_3) suspensions. The model was validated by comparison to spectroscopic measurements of the surface group concentrations over a large pH range (3 to 12) (Chiarello et al. 1993, Pokrovsky et al. 2000). Table 1 summarizes the parameters from the SC model for the carbonate mineral surfaces.

However, as Van Cappellen et al. pointed out, their model represents a first-order description of the carbonate–aqueous solution interface chemistry, not taking into account surface site heterogeneities. Within the present study, an alternative model has been developed, describing the surface reactivity based on crystallographic data using the CD-MUSIC model approach (e.g. Hiemstra & Van Riemsdijk, 1996). In the CD-MUSIC model, the bond valence theory is used to describe the basic charging of mineral surfaces (Hiemstra et al. 1989a,b). Initially developed and refined for simple metal (hydr)oxides (Hiemstra et al. 1989a,b, Hiemstra & Van Riemsdijk, 1996, Hiemstra et al. 1996), it has recently been applied successfully to the more complex phyllosilicates (Tournassat C., in press). Here, it will be applied to theoretically describe the surface charge pH dependence of carbonate minerals. The CD-MUSIC model is then compared to the SC model, which shall be used to describe radionuclide sorption processes at the calcite surface.

Table 1. Surface complexation model for calcite. LogK values are at 25°C, 1 atm, $I = 0$ (Van Cappellen et al. 1993).

Surface reactions	logK
$\equiv\text{CO}_3^- + \text{H}^+ \rightleftharpoons \equiv\text{CO}_3\text{H}^0$	+4.9
$\equiv\text{CO}_3\text{Ca}^+ + \text{H}^+ \rightleftharpoons \equiv\text{CO}_3\text{H}^0 + \text{Ca}^{2+}$	+2.8
$\equiv\text{CaO}^- + \text{H}^+ \rightleftharpoons \equiv\text{CaOH}^0$	+17
$\equiv\text{CaOH}^0 + \text{H}^+ \rightleftharpoons \equiv\text{CaOH}_2^+$	+12.2
$\equiv\text{CaOH}^0 + \text{CO}_2 \rightleftharpoons \equiv\text{CaHCO}_3^0$	6.0
$\equiv\text{CaOH}^0 + \text{CO}_2 \rightleftharpoons \equiv\text{CaCO}_3^- + \text{H}^+$	-2.6

Method

To determine the surface structures, the calcite mineral structure was taken from Diamond[©]. XPS and LEED studies (Stipp & Hochella, 1991) have shown the presence of an ordered calcite surface at least 1 nm thick that is very similar to the bulk lattice. Hence, the calcite surface structure will be approximated based on the distances and bond angles present within the bulk lattices is a valid first-order approach. Koretsky et al. (1998) tested five different methods to calculate the number of surface sites on each surface of various minerals and compared the results for each method to available experimental estimates. Estimates based on the number of broken bonds gave the best agreement with site densities determined using the tritium exchange method. In this method, each broken bond on a near-surface atom was considered as a surface reactive group. This method will be followed here to calculate the site densities for carbonate surfaces. The calculated site densities and stoichiometries will be compared to experimentally determined values reported in the literature.

The orientation of cleavage and growth planes are well established experimentally (e.g., Reeder & Grams, 1987, Stipp & Hochella, 1991, Chiarello et al. 1993, Paquette & Reeder, 1995, Pokrovsky et al. 2000, Elzinga & Reeder, 2002). Additionally, atomistic simulation methods have been used to calculate and compare the surface structure and energies of various surfaces of calcite (Titiloye et al. 1998). The carbonate- and calcite-terminated $\{10\bar{1}4\}$ surface of calcite is the most stable crystal plane and will dominate the predicted equilibrium morphology. Therefore, the surface site types for calcite will be derived from an ideal cleavage rhombohedron with $\{10\bar{1}4\}$ faces and carbonate groups at the corners (Fig. 1). Surface sites present on other important faces, as shown by sector zoning, shall be explored. In the CD-MUSIC model, the site types are constrained by the crystal structure, so they are not free fitting parameters within the model. The formal charges and proton affinities of the sites have been calculated using the CD-MUSIC model (Hiemstra & Van Riemsdijk, 1996, Hiemstra et al. 1996). For the surface charge pH-dependence calculations (Fig. 2), a size of 0.04 μm for the rhombohedra was assumed.

Results and discussion

The protonation reactions and the proton affinity constants predicted using the CD-MUSIC model are listed in Table 2. The formal charges for $\equiv\text{CO}_3$ and $\equiv\text{CaO}$ vary depending on their position at the surface. This is due to a difference, with position, in coordination of the surface carbon or calcium to the bulk lattice. As can be seen in Table 2, the protonation affinities of the $\equiv\text{CO}_3$ and $\equiv\text{CaO}$ groups do not vary with position, in contrast to what has been observed, for example, for goethite (Hiemstra & Van Riemsdijk, 1996, Hiemstra et al. 1996). This is due to the constant mono-coordination of the oxygen within the $\equiv\text{CO}_3$ and $\equiv\text{CaO}$ groups to either calcium or carbon, independent of surface site position. Since the coordination of the oxygen does not change with site position, its proton affinity does not change.

Table 2. Protonation reactions and proton affinities predicted from applying the CD-MUSIC model to calcite; *values from Van Cappellen et al. (1993).

Type	Surface reactions	logK
Face	$\equiv\text{CO}_3^{-1/3} + \text{H}^+ \rightleftharpoons \text{CO}_3\text{H}^{+2/3}$	+4.4
	$\equiv\text{CO}_3\text{H}^{+2/3} + \text{Ca}^{2+} \rightleftharpoons \text{CO}_3\text{Ca}^{+5/3} + \text{H}^+$	-2.8*
	$\equiv\text{CaO}^{-5/3} + \text{H}^+ \rightleftharpoons \text{CaOH}^{-2/3}$	+25.0
	$\equiv\text{CaOH}^{-2/3} + \text{H}^+ \rightleftharpoons \text{CaOH}_2^{+1/3}$	+13.1
	$\equiv\text{CaOH}^{-2/3} + \text{CO}_2 \rightleftharpoons \text{CaHCO}_3^{-2/3}$	+6.0*
	$\equiv\text{CaOH}^{-2/3} + \text{CO}_2 \rightleftharpoons \text{CaCO}_3^{-5/3} + \text{H}^+$	-2.6*
Edge	$\equiv\text{CO}_3^{-2/3} + \text{H}^+ \rightleftharpoons \text{CO}_3\text{H}^{+1/3}$	+4.4
	$\equiv\text{CO}_3\text{H}^{+1/3} + \text{Ca}^{2+} \rightleftharpoons \text{CO}_3\text{Ca}^{+4/3} + \text{H}^+$	-2.8*
	$\equiv\text{CaO}^{-4/3} + \text{H}^+ \rightleftharpoons \text{CaOH}^{-1/3}$	+25.0
	$\equiv\text{CaOH}^{-1/3} + \text{H}^+ \rightleftharpoons \text{CaOH}_2^{+2/3}$	+13.1
	$\equiv\text{CaOH}^{-1/3} + \text{CO}_2 \rightleftharpoons \text{CaHCO}_3^{-1/3}$	+6.0*
	$\equiv\text{CaOH}^{-1/3} + \text{CO}_2 \rightleftharpoons \text{CaCO}_3^{-4/3} + \text{H}^+$	-2.6*
Corner	$\equiv\text{CO}_3^- + \text{H}^+ \rightleftharpoons \text{CO}_3\text{H}^0$	+4.4
	$\equiv\text{CO}_3\text{H}^0 + \text{H}^+ \rightleftharpoons \text{CO}_3\text{H}_2^+$	-7.5
	$\equiv\text{CO}_3\text{H}^0 + \text{Ca}^{2+} \rightleftharpoons \text{CO}_3\text{Ca}^+ + \text{H}^+$	-2.8*
	$\equiv\text{CaO}^- + \text{H}^+ \rightleftharpoons \text{CaOH}^0$	+25.0
	$\equiv\text{CaOH}^0 + \text{H}^+ \rightleftharpoons \text{CaOH}_2^+$	+13.1
	$\equiv\text{CaOH}^0 + \text{CO}_2 \rightleftharpoons \text{CaHCO}_3^0$	+6.0*
	$\equiv\text{CaOH}^0 + \text{CO}_2 \rightleftharpoons \text{CaCO}_3^- + \text{H}^+$	-2.6*

Comparison of the proton affinities from the SC model (Table 1) and the predicted proton affinities from the CD-MUSIC model (Table 2) shows that the affinities are close for the first protonation step of the $\equiv\text{CO}_3$ group and the second of the $\equiv\text{CaO}$ group. For the first protonation step of the $\equiv\text{CaO}$ group, the affinities do not agree. However, the large proton affinity of the $\equiv\text{CaO}$ group in both models indicates that, within the pH range 2–12, the deprotonated $\equiv\text{CaO}$ group is insignificant.

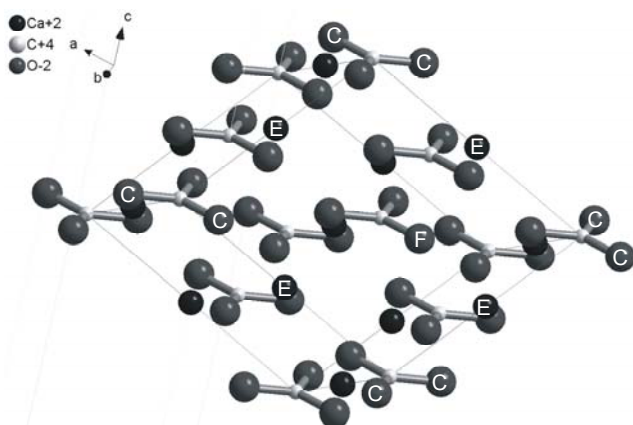


Figure 1. Sketch of a cleavage rhombohedron of calcite, consisting of $\{10\bar{1}4\}$ faces. Rib lengths are 6.399 Å. For one face, the corner (C), edge (E) and face (F) sites are indicated for the oxygen in CO_3 and the calcium in $\equiv\text{CaO}$ groups.

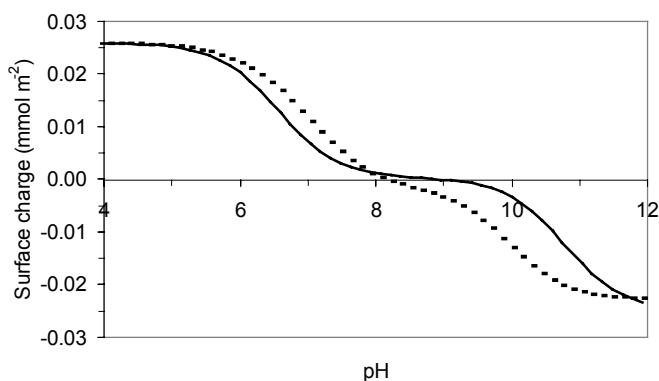


Figure 2. Preliminary surface charge pH-dependence calculated by the CD-MUSIC model (black line), compared to the surface charge pH-dependence calculated by the SC model (dashed line). The calcite surface charge was calculated using either the SC parameters or the CD-MUSIC parameters in the constant capacitance model in MINEQL+. Modeling was performed with the following conditions: specific surface area = $55 \text{ m}^2 \text{ g}^{-1}$, morphology = ideal cleavage rhombohedrons; capacitance $k = 30 \text{ F m}^{-2}$; $I = 0.032 \text{ M}$; $[\text{Ca}^{2+}] = [\text{CO}_3^{2-}] = 10^{-3} \text{ M}$. For the CD-MUSIC curve, corner sites were used as representing all sites with respect to actual charges, and for calcium and carbonate sorption, the SC reactions were used.

To facilitate comparison of the two models, the surface charge pH dependence of calcite was calculated using both models. The resulting curves are depicted in Figure 2. For calcite, no acid/base titration data are known at present. Electrophoretic measurements indicate a pH_{ZPC} varying from 7 to 10.8 (e.g. Somasundaran & Agar, 1967, Mishra, 1978, Amankonah & Somasundaran, 1985, Thompson & Pownall, 1989, Cicerone et al. 1992). The SC model was fitted to a pH_{ZPC} of 8.2 (Mishra, 1978), using the surface site density as calculated from crystallography (Van Cappellen et al. 1993). In contrast, the CD-MUSIC model gives a prediction of the surface charge, based on crystallographic information and the proton affinity calculations, which is in good agreement with the previously reported pH_{ZPC} values. In fact, the surface charge curve from the CD-MUSIC model is flat around pH_{ZPC} , which may be an explanation of the large range of pH_{ZPC} observed in electrophoretic measurements.

It must be noted that the CD-MUSIC model presented here is a preliminary model. Ongoing work on the model encompasses including the sorption reactions of carbonate and calcium, which are also potential determining ions for the pristine calcite surface. Also, the model will be applied to other carbonate minerals, such as rhodochrosite, for which surface acid/base titration data are available, to test the model approach. Furthermore, data on radionuclide adsorption onto calcite are being reviewed and shall be described using the model. The importance of specific adsorption on various faces shall be discussed.

Conclusions

The predicted proton affinities of the calcite surface by the preliminary CD-MUSIC model approach results in a surface charge pH-dependence which are consistent with the (wide) range of the pH_{ZPC} values as reported from electrophoretic measurements. The flat surface charge curve around pH_{ZPC} observed may be an explanation of the large range of pH_{ZPC} reported in literature.

The proton affinities of the surface sites do not vary with position at the surface, due to the constant mono-coordination of the surface oxygen atoms to either calcium or carbon. The formal charges of the surface $\equiv\text{CO}_3$ and $\equiv\text{CaO}$ groups do vary with position, due to the change in coordination of these groups to the bulk lattice.

Acknowledgement

This research was supported by the French national radioactive waste management agency ANDRA.

References:

- Amankonah, J.O. & Somasundaran, P. 1985. Effects of dissolved mineral species on the electrokinetic behavior of calcite and apatite. *Colloids and Surfaces* 15: 335-353.
- Chiarello, R.P. Wogelius, R.A. & Sturchio, N.C. 1993. In-situ synchrotron X-ray reflectivity measurements at the calcite-water interface. *Geochim. Cosmochim. Acta* 57(16): 4103-4110.
- Cicerone, D.S. Regazzoni, A.E. & Blesa, M.A. 1992. Electrokinetic properties of the calcite/water interface in the presence of magnesium and organic matter. *J. Coll. Interf. Sci.* 154(2): 423-433.
- Elzinga, E.J. & Reeder, R.J. 2002. X-ray absorption spectroscopy study of Cu²⁺ and Zn²⁺ adsorption complexes at the calcite surface: Implications for site-specific metal incorporation preferences during calcite crystal growth. *Geochem. Cosmochim. Acta* 66(22): 3943-3954.
- Hiemstra, T. & Van Riemsdijk, W.H. 1996. A surface structural approach to ion adsorption: the charge distribution (CD) model. *J. Colloid and Interf. Sci.* 179: 488-508.
- Hiemstra, T. De Wit, J.C.M. & Van Riemsdijk, W.H. 1989a. Multisite proton adsorption modeling at the solid/solution interface of (Hydr)oxides: a new approach. II Application to various important (Hydr)oxides. *J. Coll. Interf. Sci.* 133(1): 105-117.
- Hiemstra, T. Van Riemsdijk, W.H. & Bolt, G.H. 1989b. Multisite proton adsorption modeling at the solid/solution interface of (Hydr)oxides: a new approach. I. Model description and evaluation of intrinsic reaction constants. *J. Coll. Interf. Sci.* 133(1): 91-104.
- Hiemstra, T. Venema, P. & Van Riemsdijk, W.H. 1996. Intrinsic proton affinity of reactive surface groups of metal (hydr)oxides: the bond valence principle. *J. Colloid Interf. Sci.* 184: 680-692.
- Koretsky, C.M. Sverjensky, D.A. & Sahai, N. 1998. A model of surface site types on oxide and silicate minerals based on crystal chemistry: implications for site types and densities, multi-site adsorption, surface infrared spectroscopy, and dissolution kinetics. *Am. J. Sci.* 298: 349-438.
- Mishra, S.K. 1978. The electrokinetics of apatite and calcite in inorganic electrolyte environment. *Int. J. Min. Proc.* 5: 69-83.
- Paquette, J. & Reeder, R.J. 1995. Relationship between surface structure, growth mechanism, and trace element incorporation in calcite. *Geochim. Cosmochim. Acta* 59: 735-749.
- Pokrovsky, O. S. Mielczarski, J.A. Barres, O. & Schott J. 2000. Surface speciation models of calcite and dolomite/aqueous solution interfaces and their spectroscopic evaluation. *Langmuir* 16(6): 2677-2688.
- Reeder, R.J. & Grams, J.C. 1987. Sector zoning in calcite cement crystals: Implications for trace element distributions in carbonates. *Geochim. et Cosmochim. Acta* 51(2): 187-194.
- Somasundaran, P. & Agar, G.E. 1967. The zero point of charge of calcite. *J. Coll. Interf. Sci.* 24: 433-440.
- Stipp, S. L. & Hochella, M.F.J. 1991. Structure and bonding environments at the calcite surface as observed with X-ray photoelectron spectroscopy (XPS) and low energy electron diffraction (LEED). *Geochim. Cosmochim. Acta* 55: 1723-1736.
- Thompson, D.W. & Pownall, P.G. 1989. Surface electrocal properties of calcite. *J. Coll. Interf. Sci.* 131(1): 74-82.
- Titiloye, J.O. de Leeuw, N.H. & Parker, S.C. 1998. Atomistic simulation of the differences between calcite and dolomite surfaces. *Geochim. Cosmochim. Acta* 62(15): 2637-2641.
- Tournassat, C. Ferrage, E. Poinsignon, C. & Charlet, L. The titration of clay minerals. Part II. Structural based model and implications on clay reactivity. *J. Coll. Interf. Sci.* . *in pres.*
- Van Cappellen, P. Charlet, L. Stumm, W. & Wersin, P. 1993. A surface complexation model of the carbonate mineral-aqueous solution interface. *Geochim. Cosmochim. Acta*, 57: 3505-3518.